

**ON THE SEARCH FOR EFFICIENT CATALYSTS  
FOR OXYGEN REDUCTION REACTION**

*A THESIS*

*submitted by*

**CHITTURI VENKATESWARA RAO**

*for the award of the degree*

*of*

**DOCTOR OF PHILOSOPHY**



**DEPARTMENT OF CHEMISTRY  
INDIAN INSTITUTE OF TECHNOLOGY MADRAS  
CHENNAI - 600 036, INDIA**

**APRIL - 2008**

*Dedicated  
To  
My Parents*

## **CERTIFICATE**

This is to certify that the thesis entitled “**ON THE SEARCH FOR EFFICIENT CATALYSTS FOR OXYGEN REDUCTION REACTION**” submitted by **Ch. Venkateswara Rao** to the Indian Institute of Technology, Madras for the award of degree of **Doctor of Philosophy** is a bonafide record of research work carried out by him under my supervision. The contents of this thesis, in full or in parts, have not been submitted to any other Institute or University for the award of any degree or diploma.

Research Guides

**Prof. B. Viswanathan**

Department of Chemistry  
IIT Madras, Chennai-36

**Prof. U.V. Varadaraju**

Department of Chemistry  
IIT Madras, Chennai-36

Date:

Place:

## ACKNOWLEDGEMENTS

It is my great pleasure to express my deep and sincere gratitude to my guide **Prof. B. Viswanathan**, for his guidance, inspiration and constant encouragement throughout my research work. I am grateful to him for introducing me to the various aspects of catalysis and electrochemistry. With his enthusiasm, inspiration, and his great efforts to explain things clearly and simply, he helped to make chemistry easy for me. Throughout my research, he provided encouragement, sound advice, good teaching and lots of good ideas. The many discussions during group meetings I had with him were a major source of learning and improving my knowledge and skills. I would like to express my gratitude to his sincerity, dignity and dedication towards work. In addition, he was always accessible and willing to help his students with their research.

I am indebted to thank **Prof. U.V. Varadaraju** for his help, constant encouragement and support to carry out my research work. I was delighted to having him as my co-guide. I am grateful to him for imparting knowledge and for his suggestions during my research period.

I wish to express my sincere thanks to the Doctoral committee members, **Prof. T.K. Varadarajan, Prof. M.V. Sangaranarayanan, Prof. A. Subrahmanyam** and **Prof. S.K. Seshadri** for their fruitful discussions and suggestions during doctoral committee meetings.

I am grateful to **Prof. B. Viswanathan, Late Prof. S. Vanchesan, Prof. M.N.S. Rao, Late Prof. G. Sundararajan** (former Heads of the Department) and **Prof. R. Dhamodharan** (Head of the Department) for their kind help and for providing the necessary infrastructures to carry out the research work. I wish to acknowledge **Columbian Chemicals Company**, U.S.A for graduate fellowship. I am thankful to **DST, India** for creating National Centre for Catalysis Research, where most of my work is carried out.

I wish to thank **IIT Madras** for providing opportunity and all facilities to carry out my research.

I thank all the non-teaching staff members of the chemistry department for their timely help. I am thankful to **Mr. Narayanan** for Surface area analysis, **Mrs.**

**Kanchanamala** for TEM, Mrs. **Shanthi** for SEM, Ms. **Bhanupriya** for HRTEM, **Mr. Ram Kumar** for CHN analysis and **Mr. Mohan** for NMR. I would like to extend my thanks to present and former heads and staff of CGBS, SAIF and Department of Metallurgy, IIT Madras for providing various facilities.

I thank my seniors **Dr. Raghuv eer, Dr. R. Ganesan, Dr. V. Chidamabaram, Dr. Aulice Scibioh, Dr. Ch. Subrahmanyam, Dr. S. Shanmugam, Dr. M. Sankaran, Dr. T. Maiyalagan and Dr. Sathish** for their constant encouragement and suggestions. I must also thank them for imparting valuable laboratory skills and experimental techniques when I was new to the laboratory.

I wish to thank my lab mates **Mrs. Chandravathanam, Mr. Hima Kumar, Mr. Indra Neel, Ms. Helen, Mr. Kishore, Mr. Navaladian, Mrs. Janet, Mr. Magesh, Mrs. Rajeswari and Mr. Kuppan**, for their co-operation, fruitful discussions during group meetings and generous help throughout my research period.

I am extremely thankful to **Mr. Muthu Kumar, Dr. Arun, Dr. Leela Mohan Reddy and Dr. Krishna Kumar** for their continuous help during the experiments. I extend my thanks to my all other colleagues **Dr. B.G. Mishra, Mr. R. Prakash Babu, Mr. Justin and Mr. Sumanth Kumar Meher** for their help and encouragement.

My heart felt thanks to my dear friends **Dr. Raju, Mr. Anji Reddy, Mr. Ramana and Dr. Ram Prasad** for their motivation, constant encouragement and support through my research period. I thank all my beloved friends **Dr. Vijayakrishna, Dr. Kishore, Dr. Prabhakara Rao, Dr. Swamy, Mr. Ramakanth, Mr. Biswas, Mr. Prasanna, Mr. Hari Krishna, Mr. Asiri Naidu, Mr. Charan, Mr. Rajasekhar Reddy, Mr. Koteswaraiah, Mr. Kranthi kiran, Mr. Ranjit Kumar, Mr. Narendra, Mr. Radha Krishna, Mr. Ramesh, Mr. Sudheer, Mr. Raja, Mr. Hari, Mr. Sharma, Mr. Satheesh, Mr. Ravi and Mr. Sekhar** for encouragement and timely help in all my needs during research programme. I must also thank their companionship for making my stay here pleasant and fulfilling.

I want to express my heartfelt gratitude to my parents **Sri Ch. Arjuna Rao and Smt. Ch. Rajya Lakshmi** whose limitless love and affection has made my world beautiful

place. I thank them for all the sacrifices they have made to help me achieve my goals. My heart felt thanks to my family members **Mr. Mallikarjuna Rao, Mrs. Pushpavathi, Mr. Srinivasa Rao, Mrs. Kameswari, Mr. Purna Chandra Rao, Mrs. Vasavi, Mr. Anil Kumar, Mrs. Ratna, Mr. Madhu, Mrs. Aruna, Ms. Bhargavi, Mr. Satish, Mrs. Jyothi, Mr. Dilip** and **Ms. Shruthi** for their constant encouragement and support through my research period.

**Ch. Venkateswara Rao**

## ABSTRACT

**KEYWORDS:** Oxygen reduction reaction, Carbon supported catalysts, Platinum, Platinum alloys, Palladium alloys,  $Ru_xSe_y$  catalysts,  $MN_4C_x$  clusters

Cathodic oxygen reduction reaction (ORR) has technological importance in the development of electrochemical devices such as fuel cells, zinc-air batteries and many industrial electrolytic processes. The sluggish kinetics of oxygen reduction reaction under experimental conditions causes the deterioration of performance of the devices. In order to improve the performance with enhanced kinetics, a better electrocatalyst is necessary. Though various compositions and configurations of the electrocatalysts have been proposed, the search for an efficient electrocatalyst has always been continuing. Even though, one tends to believe that the basic principle of oxygen reduction reaction is known, the formulation of a compositional electrode, satisfying the basic requirements of the components of the overall reaction has not yet been successful. This could be due to various factors inherent in extrapolation as well as the gap existing between theoretical formulation and experimental realization.

Conventional carbon supported platinum is the best catalyst for oxygen reduction reaction. However, it is associated with several drawbacks besides the high cost. Even though it is commercially exploited, the overpotential is found to be around 300-400 mV and the kinetics is not fast enough. In addition, Pt is expensive and less abundant. The main objective of the present work is to develop both Pt and non-Pt based oxygen reduction electrocatalysts for exploitation in electrochemical devices. Conventional metals and metal alloys, chalcogenide and macrocycle based systems have been prepared in nano-size range and examined for the oxygen reduction reaction in this study.

The prepared materials are characterized by using variety of techniques such as X-ray diffraction (XRD), Transmission electron spectroscopy (TEM), Scanning electron spectroscopy (SEM), Energy dispersive X-ray analysis (EDX), X-ray photoelectron spectroscopy (XPS), Ultraviolet-Visible (UV-Vis) spectroscopy. The electrochemical measurements are carried out in aqueous media at room temperature using cyclic voltammetry. The ORR activity of the electrocatalyst was evaluated from the steady-state cyclic voltammograms and the evaluation of the performance in kinetically controlled region was measured by chronoamperometry.

In the present work, carbon supported Pt nanoparticles of different sizes were synthesized by polyol reduction method. The optimum size of Pt for maximum ORR activity is determined. To improve the ORR activity and reduce Pt loading, carbon supported Pt-M (M = Fe, Co and Cr) alloys were synthesized by polyol reduction method and the role of alloying element towards enhanced ORR activity was studied. As an alternative to Pt, carbon supported Pd, Pd-Co-M (M = Mo and Au) alloys, Ru and  $\text{Ru}_x\text{Se}_y$  ( $x = 1$  and  $y = 0-1$ ) were synthesized by reverse microemulsion (RME) method and the ORR activity was investigated. Density functional calculations were performed to study the facile reduction of oxygen on  $\text{MN}_4$  (M = Fe and Co) clusters.  $\text{MN}_x\text{C}_x$  (M = Fe and Co) clusters were prepared by pyrolyzing the corresponding metal macrocycles supported on carbon and the ORR activity was investigated.



# TABLE OF CONTENTS

	Page No.
<b>ACKNOWLEDGEMENTS</b> .....	<b>i</b>
<b>ABSTRACT</b> .....	<b>iv</b>
<b>TABLE OF CONTENTS</b> .....	<b>vi</b>
<b>LIST OF TABLES</b> .....	<b>xii</b>
<b>LIST OF FIGURES</b> .....	<b>xiv</b>
<b>LIST OF SCHEMES</b> .....	<b>xix</b>
<b>ABBREVIATIONS</b> .....	<b>xx</b>
<b>NOTATIONS</b> .....	<b>xxi</b>
 <b>CHAPTER 1 INTRODUCTION</b>	
1.1 Mechanistic Aspects of Oxygen Reduction.....	7
1.2. Electrocatalysts for Oxygen Reduction .....	11
1.3 Pt Metal Electrocatalysts .....	11
1.3.1 ORR Mechanism .....	14
1.4 Pt Alloy Electrocatalysts .....	15
1.4.1 ORR Mechanism .....	21
1.5 Pd and Pd Alloy Electrocatalysts .....	24
1.5.1 ORR Mechanism .....	29
1.6 Transition Metal Chalcogenides .....	30
1.6.1 ORR Mechanism .....	39
1.7 Transition Metal Macrocycles .....	40
1.7.1 ORR Mechanism .....	47
1.8 Other Electrocatalysts .....	51

## **Table of contents (contd.)**

1.9	Nanomaterials and Electrocatalysis .....	53
1.10	Methods for the Preparation of Supported Metal Nanoparticles .....	55
1.11	Motivation and Objective of the Present Investigation .....	58

## **CHAPTER 2 EXPERIMENTAL METHODOLOGY**

2.1	Chemicals and Materials Used .....	60
2.2	Purification of Gases .....	61
2.2.1	Purification of Argon .....	61
2.2.2	Purification of Oxygen .....	61
2.3	Electrochemical Measurements .....	61
2.4	Characterization of the Catalysts .....	61
2.4.1	X-ray Diffraction (XRD) .....	61
2.4.2	X-ray Photoelectron Spectroscopy .....	62
2.4.3	Estimation of Metal(s) Loading .....	63
2.4.4	Scanning Electron Microscopy (SEM).....	63
2.4.5	Transmission Electron Microscopy (TEM) .....	63
2.4.6	UV-Visible Spectroscopic Analysis .....	64
2.4.7	Elemental Analysis .....	64
2.4.8	Surface Area Measurements .....	64

## **CHAPTER 3 SYNTHESIS, CHARACTERIZATION AND ELECTROCHEMICAL STUDIES OF CARBON SUPPORTED Pt CATALYSTS FOR OXYGEN REDUCTION**

3.1	Introduction .....	65
3.2	Synthesis of Pt Nanoparticles of Different Sizes.....	68
3.3	Preparation of the Carbon Supported Pt Catalysts .....	70
3.4	Characterization of the Carbon Supported Pt Catalysts.....	71

## **Table of contents (contd.)**

3.4.1	Salient Features of Carbon Black Support (CDX975).....	71
3.4.2	X-ray Diffraction Analysis .....	72
3.4.3	TEM and EDX Analysis .....	73
3.4.4	X-ray Photoelectron Spectroscopy (XPS) Analysis .....	78
3.4.5	Estimation of Pt Loading on the Carbon Support .....	78
3.5	Electrochemical Performances of Pt/C Catalysts .....	79
3.5.1	Electrode Fabrication .....	79
3.5.2	Electrochemical Reduction of Oxygen .....	80

## **CHAPTER 4 SYNTHESIS, CHARACTERIZATION AND ELECTROCHEMICAL STUDIES OF CARBON SUPPORTED Pt-M (M = Fe, Co and Cr) ALLOY CATALYSTS FOR OXYGEN REDUCTION**

4.1	Introduction .....	87
4.2	Synthesis of Pt-M (M = Fe, Co and Cr) Alloy Nanoparticles .....	90
4.3	Preparation of the Carbon Supported Pt-M Alloy Catalysts .....	91
4.4	Characterization of The Carbon Supported Pt-M Alloy Catalysts .....	92
4.4.1	X-ray Diffraction Analysis .....	92
4.4.2	TEM and EDX Analysis.....	93
4.4.3	Estimation of Pt in the Catalysts .....	96
4.4.4	Estimation of Iron (Fe) in the Catalysts .....	96
4.4.5	Estimation of Cobalt (Co) in the Catalysts .....	97
4.4.6	Estimation of Chromium (Cr) in the Catalysts .....	97
4.5	Electrochemical Performance of Pt-M(1:1)/CDX975 (M = Fe, Co And Cr) Catalysts .....	98
4.5.1	Electrode Fabrication .....	98
4.5.2	Electrochemical Reduction of Oxygen .....	99

## Table of contents (contd.)

4.5.3	Chronoamperometric Response .....	102
-------	-----------------------------------	-----

### **CHAPTER 5 SYNTHESIS, CHARACTERIZATION AND ELECTROCHEMICAL STUDIES OF CARBON SUPPORTED Pd AND Pd-Co-M (M = Mo and Au) ALLOY CATALYSTS FOR OXYGEN REDUCTION**

5.1	Introduction .....	104
5.2	Preparation of 20 wt.% Pd/CDX975 and Pd-Co-M/CDX975 (M = Mo and Au) Catalysts .....	106
5.3	Characterization of the Catalysts .....	108
5.3.1	X-ray Diffraction Analysis .....	108
5.3.2	TEM and EDX Analysis .....	112
5.4	Electrochemical Performance of Carbon Supported Pd and Pd-Co-M (M = Mo And Au) Alloy Catalysts .....	112
5.4.1	Electrode Fabrication.....	112
5.4.2	Electrochemical Reduction of Oxygen .....	115
5.4.3	Chronoamperometric Response.....	122

### **CHAPTER 6 Ru<sub>x</sub>Se<sub>y</sub>/C CATALYSTS FOR OXYGEN REDUCTION – A REVERSE MICROEMULSION METHOD OF FABRICATION OF ELECTRODE MATERIAL**

6.1	Introduction .....	124
6.2	Synthesis of 20 wt.% Ru <sub>x</sub> Se <sub>y</sub> /CDX975 Catalysts.....	127
6.3	Characterization of the Ru <sub>x</sub> Se <sub>y</sub> /CDX975 Catalysts .....	128
6.3.1	X-ray Diffraction Analysis .....	128
6.3.2	SEM, EDX and TEM Analysis .....	132
6.4	Electrochemical Performance of Ru <sub>x</sub> Se <sub>y</sub> /CDX975 Catalysts .....	134
6.4.1	Electrode Fabrication .....	134

## **Table of contents (contd.)**

6.4.2	Electrochemical Reduction of Oxygen .....	135
6.4.3	Chronoamperometric Response .....	140

## **CHAPTER 7 MN<sub>4</sub>C<sub>x</sub> CLUSTERS (M = Fe and Co) – POTENTIAL OXYGEN REDUCTION ELECTRODES FOR PROTON EXCHANGE MEMBRANE FUEL CELL (PEMFC) APPLICATIONS**

7.1	Introduction .....	142
7.2	Theoretical Studies on MN <sub>4</sub> Clusters for Oxygen Reduction .....	144
7.3	Experimental Section .....	149
7.3.1	Synthesis of Iron Tetraphenylporphyrin (FeTPP).....	149
7.3.2	Synthesis of Iron Phthalocyanine (FePc).....	150
7.3.3	Synthesis of Iron and Cobalt Tetramethoxyphenylporphyrin Complexes (FeTMPP-Cl and CoTMPP) .....	150
7.3.4	Preparation of FeTPP/CDX975 and FePc/CDX975.....	151
7.3.5	Modification of Carbon Black (CDX975) Support .....	151
7.3.6	Preparation of FeTMPP/CDX975, CoTMPP/CDX975 and MN <sub>4</sub> C <sub>x</sub> Clusters .....	152
7.3.7	Estimation of Iron in the Catalysts .....	152
7.3.8	Estimation of Cobalt in the Catalysts .....	152
7.3.9	Estimation of Nitrogen in the Catalysts .....	152
7.4	Characterization of the Iron and Cobalt based Catalysts .....	153
7.5	Electrochemical Performance of Iron and Cobalt based Catalysts .....	156
7.5.1	Electrode Fabrication .....	156
7.5.2	Electrochemical Reduction of Oxygen .....	156
7.5.3	Chronoamperometric Response .....	165
7.5.4	Single-Cell PEMFC Measurements .....	167

**Table of contents (contd.)**

**CHAPTER 8 SUMMARY AND CONCLUSIONS .....170**

**REFERENCES .....174**

**LIST OF PUBLICATIONS .....199**

## LIST OF TABLES

Table	Title	Page
1.1	Characteristic features of various electrochemical devices	3
1.2	Mechanistic ORR pathways in acidic and basic media	9
1.3	Preparation methods, electrocatalytic activity and selectivity towards oxygen reduction of Pt alloys compared to Pt	17
1.4	Preparation methods, electrocatalytic activity and selectivity towards oxygen reduction of Pd based electrocatalysts compared to Pt	27
1.5	Preparation methods, electrocatalytic activity and selectivity towards oxygen reduction of transition metal chalcogenides compared to Pt	37
1.6	Electrocatalytic activity and selectivity towards oxygen reduction of transition metal macrocycles compared to Pt	48
3.1	Reactants and conditions employed for the preparation of Pt/CDX975 catalysts	68
3.2	Size of Pt (from XRD and TEM), Pt loading, onset potential and ORR activity of Pt/CDX975 catalysts	82
4.1	Metal loading, particle size, onset potential for oxygen reduction and ORR activity of carbon supported Pt alloys and commercial Pt/C catalysts	102
5.1	Compositions of microemulsion system used for the synthesis	108
5.2	Structural parameters of Pd/CDX975 and Pd-Co-M/CDX975 catalysts	111
5.3	EDX composition, onset potential for oxygen reduction and ORR activity of Pd/CDX975, Pd-Co-M/CDX975 (M = Mo and Au) and commercial Pt/C catalysts	119
6.1	Lattice parameters (a, c) and cell volume of Ru <sub>x</sub> Se <sub>y</sub> /CDX975 catalysts	129
6.2	Elemental composition, Se/Ru atomic ratio, crystallite size, onset potential for oxygen reduction and ORR activity of 20 wt.% Ru <sub>x</sub> Se <sub>y</sub> /CDX975 (x = 1 and commercial 20 wt.% Pt/C (E-TEK) catalysts	131
7.1	Percentage atomic orbital contributions to HOMO and LUMO of MN <sub>4</sub> and O <sub>2</sub> by DFT method using Gaussian 98	147
7.2	Elemental composition of the synthesized complexes	153
7.3	Estimated iron loading, nitrogen content and ORR activity of untreated and heat-treated FeTPP/CDX975 catalysts	157

## List of Tables Contd.

---

7.4	Estimated iron loading, nitrogen content and ORR activity of untreated and heat-treated FePc/CDX975 catalysts	157
7.5	Estimated metal loading, nitrogen content, onset potential for oxygen reduction and ORR activity of Fe- and Co-based catalysts as well as commercial Pt catalysts	161
7.6	Single-cell PEM fuel cell performance of Fe- and Co-based catalysts as well as commercial Pt catalysts at +0.7 V vs. NHE	169



## LIST OF FIGURES

Figure	Title	Page
1.1	Typical polarization curve for a fuel cell: voltage drops due to: (i) surface reaction kinetics; (ii) electrolyte resistance; and (iii) reactant/product diffusion rates	5
1.2	Molecular Orbital diagram of oxygen molecule	7
1.3	Possible configurations of dioxygen interaction with a metal in a complex	8
1.4	Schematic presentation of ORR pathway	10
1.5	Schematic explanation of the proposed enhancement mechanism of the ORR by alloying Pt with Fe-group metals	23
1.6	Dependence of the overpotential, at a current density of $10^{-2}$ mA/cm <sup>2</sup> , as a function of valence electron counting (VEC) per cluster for Chevrel phases	32
1.7	Schematic representation of the energy diagram and crystal structure of Mo <sub>x</sub> Ru <sub>y</sub> Se <sub>z</sub> indicating that electron exchange occurs via the mixed metal clusters	39
3.1	(a) SEM image, (b) TEM image, (c) XRD pattern and (d) pore size distribution of the carbon black (CDX975) support	72
3.2	Powder XRD patterns of the as-synthesized Pt/CDX975 catalysts; (a) Pt1C (b) Pt2C (c) Pt3C (d) Pt4C (e) Pt5C and (f) Pt6C	73
3.3	TEM images of the as-synthesized Pt/CDX975 catalysts (a) Pt1C (b) Pt2C (c) Pt3C (d) Pt4C (e) Pt5C and (f) Pt6C (First and second rows corresponds to the low and high magnification images respectively)	74
3.4	Histogram of the Pt particles supported on carbon catalysts (a) Pt1C (b) Pt2C (c) Pt3C (d) Pt4C (e) Pt5C and (f) Pt6C	75
3.5	EDX of the as-synthesized Pt/CDX975 catalysts (a) Pt1C (b) Pt2C (c) Pt3C (d) Pt4C (e) Pt5C and (f) Pt6C	76
3.6	(a and b) low and high magnification TEM images, (c) histogram of particle size distribution and (d) EDX spectrum of the commercial Pt/C catalyst	77
3.7	XPS spectrum of Pt4C catalyst	78

**List of figures (contd.)**

<b>Figure</b>	<b>Title</b>	<b>Page</b>
3.8	Linear sweep voltammograms of the carbon supported Pt catalysts in Ar- and O <sub>2</sub> - saturated 0.5 M H <sub>2</sub> SO <sub>4</sub> ; Scan rate – 5 mV s <sup>-1</sup> (Empty and full symbols corresponding to the LSVs in Ar- and O <sub>2</sub> - saturated 0.5 M H <sub>2</sub> SO <sub>4</sub> respectively)	81
4.1	Powder X-ray diffraction patterns of (a) commercial Pt/C (E-TEK) (b) Pt-Co(1:1)/CDX975 (c) Pt-Cr(1:1)/CDX975 and (d) Pt-Fe(1:1)/CDX975 catalysts	93
4.2	Transmission electron microscopic (TEM) images of carbon supported Pt alloy catalysts; (a) Pt-Fe(1:1)/CDX975 (b) Pt-Co(1:1)/CDX975 and (c) Pt-Cr(1:1)/CDX975	94
4.3	Histograms of Pt alloy particle size distribution in carbon supported catalysts; (a) Pt-Fe(1:1)/CDX975 (b) Pt-Co(1:1)/CDX975 (c) Pt-Cr(1:1)/CDX975	95
4.4	EDX spectra of carbon supported Pt alloy catalysts; (a) Pt-Fe(1:1)/CDX975 (b) Pt-Co(1:1)/CDX975 and (c) Pt-Cr(1:1)/CDX975	96
4.5	Cyclic voltammograms (CVs) of Pt-M(1:1)/CDX975 (M = Fe, Co and Cr) and commercial Pt/C (E-TEK) catalysts in Ar-saturated 0.5 M H <sub>2</sub> SO <sub>4</sub> ; Scan rate – 25 mV s <sup>-1</sup>	100
4.6	Linear sweep voltammograms (LSVs) of Pt-M(1:1)/CDX975 (M = Fe, Co and Cr) and commercial Pt/C (E-TEK) catalysts in Ar- and O <sub>2</sub> - saturated 0.5 M H <sub>2</sub> SO <sub>4</sub> ; Scan rate – 5 mV s <sup>-1</sup> (Empty and full symbols corresponding to the LSVs in Ar- and O <sub>2</sub> -saturated 0.5 M H <sub>2</sub> SO <sub>4</sub> )	101
4.7	Current density-time plots of (a) commercial Pt/C (E-TEK) (b) Pt-Fe(1:1)/CDX975 (c) Pt-Co(1:1)/CDX975 (d) Pt-Cr(1:1)/CDX975 catalysts in oxygen saturated 0.5 M H <sub>2</sub> SO <sub>4</sub> at +0.7 V vs NHE for 3 h	103
5.1	Powder X-ray diffraction patterns of (a) Pd/CDX975 (b) as-synthesized Pd-Co-Mo(7:2:1)/CDX975; heat-treated Pd-Co-Mo(7:2:1)/CDX975 at (c) 973 K (d) 1073 K and (e) 1173 K respectively	109
5.2	Powder X-ray diffraction patterns of (a) Pd/CDX975 (b) as-synthesized Pd-Co-Au(7:2:1)/CDX975; heat-treated Pd-Co-Au(7:2:1)/CDX975 at (c) 973 K (d) 1073 K and (e) 1173 K respectively	109
5.3	(a) TEM image and (b) EDX spectrum of heat-treated Pd-Co-Mo(7:2:1)/CDX975 at 973 K	113

## List of figures (contd.)

Figure	Title	
5.4	(a) TEM image and (b) EDX spectrum of heat-treated Pd-Co-Au(7:2:1)/CDX975 at 1073 K	114
5.5	Cyclic voltammograms (CVs) of carbon supported Pd and Pd-Co-Mo catalysts in Ar-saturated 0.5 M H <sub>2</sub> SO <sub>4</sub> ; Scan rate – 25 mV s <sup>-1</sup>	116
5.6	Cyclic voltammograms (CVs) of carbon supported Pd and Pd-Co-Au catalysts in Ar-saturated 0.5 M H <sub>2</sub> SO <sub>4</sub> ; Scan rate – 25 mV s <sup>-1</sup>	116
5.7	Linear sweep voltammograms (LSVs) of O <sub>2</sub> reduction on carbon supported Pd, Pd-Co-Mo and commercial Pt/C (E-TEK) catalysts in 0.5 M H <sub>2</sub> SO <sub>4</sub> ; Scan rate - 5 mV s <sup>-1</sup> (Empty and full symbols corresponding to the LSVs in Ar- and O <sub>2</sub> -saturated 0.5 M H <sub>2</sub> SO <sub>4</sub> )	118
5.8	Linear sweep voltammograms (LSVs) of O <sub>2</sub> reduction on carbon supported Pd, Pd-Co-Au and commercial Pt/C (E-TEK) catalysts in 0.5 M H <sub>2</sub> SO <sub>4</sub> ; Scan rate - 5 mV s <sup>-1</sup> (Empty and full symbols corresponding to the LSVs in Ar- and O <sub>2</sub> -saturated 0.5 M H <sub>2</sub> SO <sub>4</sub> )	118
5.9	Effect of heat-treatment temperature on the ORR activity and surface area of the carbon supported Pd–Co–Mo (Pd:Co:Mo = 70:20:10 atom%) catalysts prepared by the reverse microemulsion method	120
5.10	Effect of heat treatment temperature on the (a) degree of alloying and surface area and (b) catalytic activity for ORR of the carbon supported Pd–Co–Au (Pd:Co:Au = 70:20:10 atom%) catalysts prepared by the reverse microemulsion method	121
5.11	Current density-time plot of (a) Pd/CDX975; heat-treated Pd-Co-Mo(7:2:1)/CDX975 at (b) 973 K (c) 1073 K and (d) 1173 K respectively in oxygen saturated 0.5 M H <sub>2</sub> SO <sub>4</sub> at +0.7 V vs NHE for 3 h	122
5.12	Current density-time plot of (a) Pd/CDX975; heat-treated Pd-Co-Au(7:2:1)/CDX975 at (b) 973 K (c) 1073 K and (d) 1173 K respectively in oxygen saturated 0.5 M H <sub>2</sub> SO <sub>4</sub> at +0.7 V vs NHE for 3 h	123
6.1	Powder X-ray diffraction patterns of as-synthesized Ru <sub>x</sub> Se <sub>y</sub> /CDX975 catalysts; (a) Ru/CDX975 (b) Ru <sub>1</sub> Se <sub>0.2</sub> /CDX975 (c) Ru <sub>1</sub> Se <sub>0.4</sub> /CDX975 (d) Ru <sub>1</sub> Se <sub>0.6</sub> /CDX975 (e) Ru <sub>1</sub> Se <sub>0.8</sub> /CDX975 and (f) Ru <sub>1</sub> Se <sub>1</sub> /CDX975	129

**List of figures (contd.)**

<b>Figure</b>	<b>Title</b>	
6.2	Variation of lattice parameters and cell volume with Se content in Ru <sub>x</sub> Se <sub>y</sub> /CDX975 catalysts	130
6.3	Slow scan XRD spectra for the (110) peak of Ru <sub>x</sub> Se <sub>y</sub> /CDX975 catalysts; (a) Ru/CDX975 (b) Ru <sub>1</sub> Se <sub>0.2</sub> /CDX975 (c) Ru <sub>1</sub> Se <sub>0.4</sub> /CDX975 (d) Ru <sub>1</sub> Se <sub>0.6</sub> /CDX975 (e) Ru <sub>1</sub> Se <sub>0.8</sub> /CDX975 and (f) Ru <sub>1</sub> Se <sub>1</sub> /CDX975	131
6.4	SEM image (inset shows the high magnification image) and (b) EDX spectrum of Ru <sub>1</sub> Se <sub>0.6</sub> /CDX975	133
6.5	TEM images of (a) Ru <sub>1</sub> Se <sub>0.6</sub> /CDX975 at low magnification (b) Ru <sub>1</sub> Se <sub>0.6</sub> /CDX975 at high magnification. (c) Histogram of Ru <sub>1</sub> Se <sub>0.6</sub> particles on CDX975	134
6.6	Linear sweep voltammograms (LSVs) of O <sub>2</sub> reduction on 20 wt% Ru <sub>x</sub> Se <sub>y</sub> /CDX975 and commercial Pt/C (E-TEK) catalysts in 0.5 H <sub>2</sub> SO <sub>4</sub> ; Scan rate – 5 mV s <sup>-1</sup> (Empty and full symbols corresponding to the LSVs in Ar- and O <sub>2</sub> - saturated 0.5 M H <sub>2</sub> SO <sub>4</sub> respectively)	137
6.7	Se/Ru atomic ratio vs. ORR current density of as-synthesized Ru <sub>x</sub> Se <sub>y</sub> /CDX975 catalysts	138
6.8	Cyclic voltammograms (CVs) of (■) Ru/CDX975 and (●) Ru <sub>1</sub> Se <sub>0.6</sub> /CDX975 catalysts in Ar-saturated 0.5 H <sub>2</sub> SO <sub>4</sub> ; Scan rate – 20 mV s <sup>-1</sup>	139
6.9	Current density vs. time curves of as-synthesized 20 wt.% Ru <sub>x</sub> Se <sub>y</sub> /CDX975 catalysts; (a) Ru/CDX975 (b) Ru <sub>1</sub> Se <sub>0.2</sub> /CDX975 (c) Ru <sub>1</sub> Se <sub>0.4</sub> /CDX975 (d) Ru <sub>1</sub> Se <sub>0.6</sub> /CDX975 (e) Ru <sub>1</sub> Se <sub>0.8</sub> /CDX975 (f) Ru <sub>1</sub> Se <sub>1</sub> /CDX975 and (g) commercial Pt/C (E-TEK) measured in oxygen saturated 0.5 M H <sub>2</sub> SO <sub>4</sub> at +0.65 V vs. NHE	141
7.1	Model systems with geometric parameters	146
7.2	Electron density maps of (a) HOMO of FeN <sub>4</sub> (b) HOMO of CoN <sub>4</sub> and (c) π* orbital of O <sub>2</sub>	148
7.3	Mode of activation of O <sub>2</sub> on MN <sub>4</sub> (M = Fe and Co) species	149
7.4	TEM images of (a) CDX1-FeTMPPCl(HT), (b) CDX2-FeTMPPCl(HT), (c) CDX1-CoTMPP(HT) and (d) CDX2-CoTMPP(HT)	154
7.5	EDX spectra of (a) CDX1-FeTMPPCl(HT), (b) CDX2-FeTMPPCl(HT), (c) CDX1-CoTMPP(HT) and (d) CDX2-CoTMPP(HT)	155

**List of figures (contd.)**

<b>Figure</b>	<b>Title</b>	<b>Page</b>
7.6	Cyclic voltammograms of (○) CDX1 and (●) CDX2 in Ar-saturated 0.5 M H <sub>2</sub> SO <sub>4</sub> ; Scan rate - 10 mV s <sup>-1</sup>	158
7.7	Linear sweep voltammograms (LSVs) of untreated and heat-treated Fe(III)TMPP-Cl supported on as-received and oxidized carbon catalysts (a) CDX1-FeTMPPCl(UT), (b) CDX2-FeTMPPCl(UT), (c) CDX1-FeTMPPCl(HT) and (d) CDX2-FeTMPPCl(HT) in Ar- and O <sub>2</sub> - saturated 0.5 M H <sub>2</sub> SO <sub>4</sub> ; Scan rate – 10 mV s <sup>-1</sup>	160
7.8	Linear sweep voltammograms (LSVs) of untreated and heat-treated CoTMPP supported on as-received and oxidized carbon catalysts (a) CDX1-CoTMPP(UT), (b) CDX2-CoTMPP(UT), (c) CDX1-CoTMPP(HT) and (d) CDX2-CoTMPP(HT) in Ar- and O <sub>2</sub> - saturated 0.5 M H <sub>2</sub> SO <sub>4</sub> ; Scan rate -10 mV s <sup>-1</sup>	162
7.9	Polarization curve of heat-treated MTMPP (M = Fe and Co) supported on as-received and oxidized carbon catalysts: (a) CDX1-FeTMPPCl(HT), (b) CDX2-FeTMPPCl(HT), (c) CDX1-CoTMPP(HT) and (d) CDX2-CoTMPP(HT) in O <sub>2</sub> -saturated 0.5 M H <sub>2</sub> SO <sub>4</sub> ; Scan rate – 10 mV s <sup>-1</sup>	163
7.10	Linear sweep Voltammograms (LSVs) of commercial 2 wt.% Pt/Vulcan XC72R (E-TEK) in Ar- and O <sub>2</sub> - saturated 0.5 M H <sub>2</sub> SO <sub>4</sub> ; Scan rate - 10 mV s <sup>-1</sup>	165
7.11	Current density vs. time plots of (a) CDX1-FeTMPPCl(HT), (b) CDX2-FeTMPPCl(HT) and (c) commercial Pt/C (E-TEK) measured in oxygen saturated 0.5 M H <sub>2</sub> SO <sub>4</sub> at +0.7 V vs. NHE	166
7.12	Current density vs. time plots of (a) CDX1-CoTMPP(HT) and (b) CDX2-CoTMPP(HT) and (c) commercial Pt/C (E-TEK) measured in oxygen saturated 0.5 M H <sub>2</sub> SO <sub>4</sub> at +0.7 V vs. NHE	166
7.13	H <sub>2</sub> /O <sub>2</sub> PEM fuel cell polarization curves with (Δ) CDX1-FeTMPPCl(HT), (▲) CDX2-FeTMPPCl(HT), (□) CDX1-CoTMPP(HT) and (■) CDX2-CoTMPP(HT) and (●) commercial Pt/C (E-TEK) for oxygen reduction at 353 K	168

## LIST OF SCHEMES

<b>Scheme</b>	<b>Title</b>	<b>Page</b>
1.1	Schematic representation of molecular oxygen reduction on the Ru <sub>x</sub> Se <sub>y</sub> species	40
3.1	Preparation of carbon supported Pt catalysts	69

## ABBREVIATIONS

Au - Gold  
Co – Cobalt  
Cr - Chromium  
CV - Cyclic Voltammetry  
DMFC - Direct Methanol Fuel Cell  
EDX - Energy Dispersive X-ray Analysis  
Fe – Iron  
FWHM – Full Width Half Maximum  
HOMO – Highest Occupied Molecular Orbital  
LSV – Linear Sweep Voltammetry  
LUMO – Lowest Unoccupied Molecular Orbital  
Mo - Molybdenum  
NHE – Normal Hydrogen Electrode  
ORR – Oxygen Reduction Reaction  
PEMFC – Proton Exchange Membrane Fuel Cell  
Pt – Platinum  
Pd – Palladium  
RDE – Rotating Disk Electrode  
RME – Reverse Microemulsion Method  
RRDE - Rotating Ring Disk Electrode  
Ru - Ruthenium  
SEM - Scanning Electron Microscopy  
TEM - Transmission Electron Microscopy  
TGA - Thermogravimetric Analysis  
UV-Vis - Ultraviolet – Visible Spectroscopy  
VEC – Valence Electron Count  
XRD - X-ray Diffraction

## NOTATIONS

Å - Angstrom

$\theta$  - Angle

$\lambda$  - Wavelength

h - Hour

K - Degree Kelvin

°C - Degree Celsius

T - Temperature

V - Volume

A – Absorbance

cm - centimeter

eV - Electron Volt

mV - Milli Volt

mA – Milli ampere

E - Potential (V)

I - Current

t - Time



# CHAPTER 1

## INTRODUCTION

The electrochemical reduction of molecular oxygen on the electrode surface is important especially for devices such as fuel cells, metal-air batteries (e.g., Zinc-Air batteries) and air cathodes in many industrial electrocatalytic processes (e.g., chlor-alkali cells). An understanding of oxygen reduction is important because it is often the counter electrode reaction that controls even the desired reaction process.

During the past decade, fuel cells received considerable attention from both energy and environmental stand points. Fuel cells appear to be one of the alternate energy sources that can cater to the needs of future world. A fuel cell consists of an anode to which a fuel is supplied and a cathode to which an oxidant, commonly oxygen, is supplied. The oxygen needed by a fuel cell is generally supplied in the form of air. The two electrodes of a fuel cell are separated by an ion-conducting electrolyte. All fuel cells have similar basic operating principle. The input fuel is catalytically reacted (electrons removed from the fuel) in the fuel cell to create an electric current. The input fuel passes over the anode is catalytically split into electrons and ions. Oxygen passes over the cathode is reduced by the electrons which are generated at anode and passed on to the cathode by external circuit. At cathode, the ions which are formed at anode and transported to cathode, combine with the oxide ions and generate the oxidized product. If the fuel happens to be hydrogen, then water is formed. Depending on the input fuel and electrolyte, different chemical reactions will occur (Vielstitch, 1965; Viswanathan and Aulice Scibioh, 2006).

Among the various types of batteries, because of its steady performance, source of raw material and low-cost, the study and development of Zinc–Air battery has

received much attention. Because of their high specific energy ( $100 \text{ Wh kg}^{-1}$ ) and environmentally benign materials, Zn–Air batteries are promising energy storage devices. It is a special feature of the zinc–air system that only the active component of the negative electrode (zinc) needs to be stored in the battery, while the reactant for the positive electrode (oxygen) during discharge is drawn from air. This is the basis for the system's high specific energy—distinctly higher than that of conventional battery systems (Lead–Acid, Ni/Cd, and Ni/MH). The key problem in the development of Zn–Air batteries is the oxygen-diffusion electrode (Deiss *et al.*, 2002).

Industrial electrochemical processes such as the chlor-alkali process based on the electrolysis of brine for the production of chlorine and caustic soda is capital-intensive process. It also consumes significant power. This is true for today's existing process formulations, where chlorine is produced at the anode and NaOH and  $\text{H}_2$  are obtained at the cathode. The hydrogen-evolving reaction has the penalty of working at a decomposition voltage of more than 1.2 V including the overvoltages and ohmic drops. Replacing the hydrogen-evolving cathode by an oxygen reduction (consuming) electrode in a membrane brine electrolysis cell reduces the total energy input to the cell by approximately 30% (Hoare, 1968). Active electrocatalysts are needed to reduce oxygen in order to get high cell efficiency. The characteristic features of various types of fuel cells, metal-air batteries and chlor-alkali cells are given in Table 1.1.

Oxygen reduction reaction (ORR) has been studied over the years because of its fundamental complexity, sensitivity to the electrode surface, and sluggish kinetics. The sluggish kinetics of ORR under the conditions employed in electrochemical

Table 1.1 Characteristic features of various electrochemical devices (Viswanathan and Aulice Scibioh, 2006; Deiss *et al.*, 2002)

Electrochemical device	Operating temp (K)	Electrolyte	Charge carrier	Electrolyte state	Oxidant	Cathodic reaction
Alkaline fuel cell (AFC)	333-423	45% KOH	OH <sup>-</sup>	Immobilized liquid	O <sub>2</sub> /Air	O <sub>2</sub> + 2H <sub>2</sub> O + 4e <sup>-</sup> → 4OH <sup>-</sup>
Phosphoric acid fuel cell (PAFC)	453-493	H <sub>3</sub> PO <sub>4</sub>	H <sup>+</sup>	„	O <sub>2</sub> /Air	O <sub>2</sub> + 4H <sup>+</sup> + 4e <sup>-</sup> → 2H <sub>2</sub> O
Proton exchange membrane fuel cell (PEMFC)	333-353	Ion exchange membrane (e.g., Nafion)	H <sup>+</sup>	Solid	O <sub>2</sub> /Air	O <sub>2</sub> + 4H <sup>+</sup> + 4e <sup>-</sup> → 2H <sub>2</sub> O
Direct methanol fuel cell (DMFC)	333-353	Ion exchange membrane (e.g., Nafion)	H <sup>+</sup>	Solid	O <sub>2</sub> /Air	O <sub>2</sub> + 4H <sup>+</sup> + 4e <sup>-</sup> → 2H <sub>2</sub> O
Molten carbonate fuel cell (MCFC)	923-973	Alkali carbonate mixture	CO <sub>3</sub> <sup>2-</sup>	Immobilized liquid	O <sub>2</sub> /Air	O <sub>2</sub> + 2CO <sub>2</sub> + 4e <sup>-</sup> → 2CO <sub>3</sub> <sup>2-</sup>
Solid oxide fuel cell (SOFC)	1073-1273	Yttria-stabilized zirconia	O <sup>2-</sup>	Solid	O <sub>2</sub> /Air	O <sub>2</sub> + 4e <sup>-</sup> → 2O <sup>2-</sup>
Zinc-air batteries	298	Alkali	OH <sup>-</sup>	Liquid	Air	O <sub>2</sub> + 2H <sub>2</sub> O + 4e <sup>-</sup> → 4OH <sup>-</sup>
Chlor-alkali cells	298	Alkali	OH <sup>-</sup>	Liquid	Air	O <sub>2</sub> + 2H <sub>2</sub> O + 4e <sup>-</sup> → 4OH <sup>-</sup>

devices is due to the low partial pressure of oxygen in air, slow flow rate of oxygen i.e., low residence time for oxygen molecules on active sites) under ambient conditions. The main disadvantage in this important electrode reaction is the exchange current density ( $j_0$ ) value in the region of  $10^{-10}$  A/cm<sup>2</sup> in acidic medium and  $10^{-8}$  A/cm<sup>2</sup> at 298 K in alkaline solution which is lower than the  $j_0$  value of anodic reaction ( $10^{-3}$  A/cm<sup>2</sup>) in all the electrochemical devices (Bockris and Reddy, 1970). Hence (from the equation  $\eta = RT/nF \ln(j/j_0)$ ) the oxygen reduction reaction usually contributes considerably to the overpotential and therefore results in a low efficiency in the functioning electrochemical energy devices using air as oxidant. Understanding and exploitation of electrocatalysis for this reaction is needed more than any other reactions in electrochemical devices.

Fig. 1.1 shows a typical voltage-current ( $E - I$ ) discharge curve for a fuel cell with an open-circuit voltage  $E_{oc}$ . The overpotential  $\eta = (E_{oc} - E)$  reflects the resistive IR losses due to the surface reaction kinetics, the resistance to transport of the working ion, H<sup>+</sup> or O<sup>2-</sup> between the reductant and the oxidant reactive sites, and the resistance to diffusion of the oxidant and/or reductant to the catalytic sites and their products away from these sites. At low currents, the performance of a fuel cell is dominated by kinetic losses. These losses mainly stem from the high overpotential of the oxygen reduction reaction (ORR). At intermediate currents, ohmic losses arise from ionic losses in the electrodes and separator, although contact and electronic resistances can be important under certain operating conditions. At high currents, mass transport limitations become increasingly important. These losses are due to reactants not being able to reach the electrocatalytic sites. Typically, oxygen is the problem due to flooding of the cathode by liquid water, but protons and electrons can also cause mass-transfer limitations.

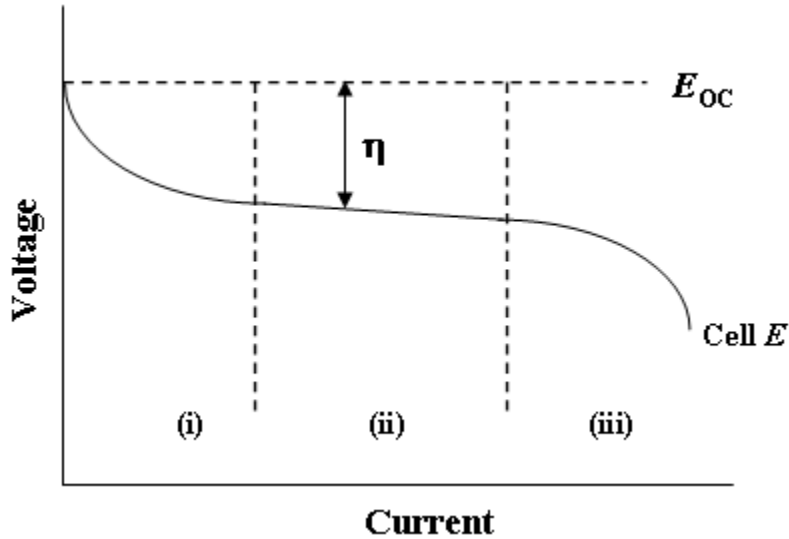


Fig. 1.1 Typical polarization curve for a fuel cell: voltage drops due to: (i) surface reaction kinetics; (ii) electrolyte resistance; and (iii) reactant/product diffusion rates (Vielstitch, 1965)

At any potential, both oxidation and reduction reactions can occur; at the rest potential  $\phi_{oc}$ , the two reactions occur at equal rates. The net current density for an outer sphere reaction at a metallic electrode is given by the Butler-Volmer equation (Bockries and Reddy, 1970)

$$j = j_0 [\exp(\alpha_A n F \eta / RT) - \exp(-\alpha_C n F \eta / RT)] \quad \dots\dots\dots (1.1)$$

where  $n$  is the number of electrons transferred in the reaction,  $F$  is the Faraday constant,  $\eta$  is the overpotential for the charge-transfer reaction at the surface,  $j_0$  is the exchange current density and  $\alpha_A$  and  $\alpha_C$  are the anodic and cathodic transfer coefficients respectively. For a concentration  $C_{ox}$  of the oxidizing species  $O_2$  at the surface, the exchange current density of the cathodic ORR is

$$j_0 = n F C_{ox} k_{ox} \quad \dots\dots\dots (1.2)$$

where  $k_{ox} = k_{o,ox} \exp(-\Delta G(\phi_{oc}) / RT)$  is the electrochemical rate constant and  $\Delta G(\phi_{oc})$  is the activation energy for electron transfer to the oxidant at the rest potential  $\phi_{oc}$ . At small current densities, the exponents of the Butler-Volmer equation are small and the expansion of  $\exp(x)$  can be approximated as  $(1+x)$  thus giving the expression

$$j \sim j_o (nF\eta/RT) = \eta/R_{tr} \dots\dots\dots (1.3)$$

where the electron transfer resistance  $R_{tr} = RT/j_o n F$  is independent of  $\alpha_A$  and  $\alpha_C$ . At low current densities ( $i_o < 1 \text{ mA cm}^{-2}$ ), electrodes give a larger  $R_{tr}$  and therefore overpotential,  $\eta$  should be greater than 400 mV (at room temperature) (Appleby, 1993). An extremely active electrocatalyst is needed to overcome this initial voltage drop in the  $E$  versus current *discharge* curve.

To obtain a high performance cathode, a macroscopic dimensioning of the porous cathode layer has to be made with regard to cell design and to the composition of cathode materials. In general, oxygen reduction takes place at a three phase boundary (TPB). A gas diffusion electrode of high performance is required to reduce oxygen effectively at the cathode. The gas diffusion electrode should not only comprise of sufficient amount of electrode catalyst having low overvoltage for oxygen reduction reaction, but also should have a carrier on which highly dispersed electrocatalysts are supported. Moreover, the gas diffusion electrode should have a pore structure and hydrophobic nature of pore surface so as to enable the formation of a highly reactive three phase boundary to form an interface where electrode catalyst, catholyte and oxygen contact effectively with each other. Its structure must satisfy two conflicting criteria, high gas permeability and low liquid permeability in order to achieve high performance required for commercial production (Kinoshita, 1992; Zhou and Poorten, 1995; Maja *et al.*, 2000). Maintaining a stable interface between liquid and gas within the active layer of the gas-diffusion cathode is the key to long-term operation.

## 1.1 Mechanistic Aspects of Oxygen Reduction

Even though oxygen reduction reaction (ORR) appears to be simple, it is quite complex. The molecular orbital diagram of oxygen molecule is shown in Fig. 1.2 (Taube, 1965). According to Hund's rule, in the ground-state,  $O_2$  possesses two unpaired electrons located in a doubly degenerate  $\pi^*$  antibonding orbital. This corresponds to a triplet state. The bonding orbitals of oxygen molecule can be ascribed to the  $3\sigma_g$  orbital with two electrons, the doubly degenerate  $1\pi_u$  and  $1\pi_g^*$  orbitals, where the  $1\pi_u$  orbital has double occupancy while the  $1\pi_g^*$  orbital has single occupancy. The resulting bond order is two. When  $O_2$  undergoes reduction, the electrons added occupy anti-bonding orbitals, decreasing the bond order of O-O. This increases the O-O bond distance and the vibrational frequency decreases. This explains the high stability of the  $O_2$  molecule and its relatively low reactivity, in spite of its high oxidizing power (Valentine, 1973).

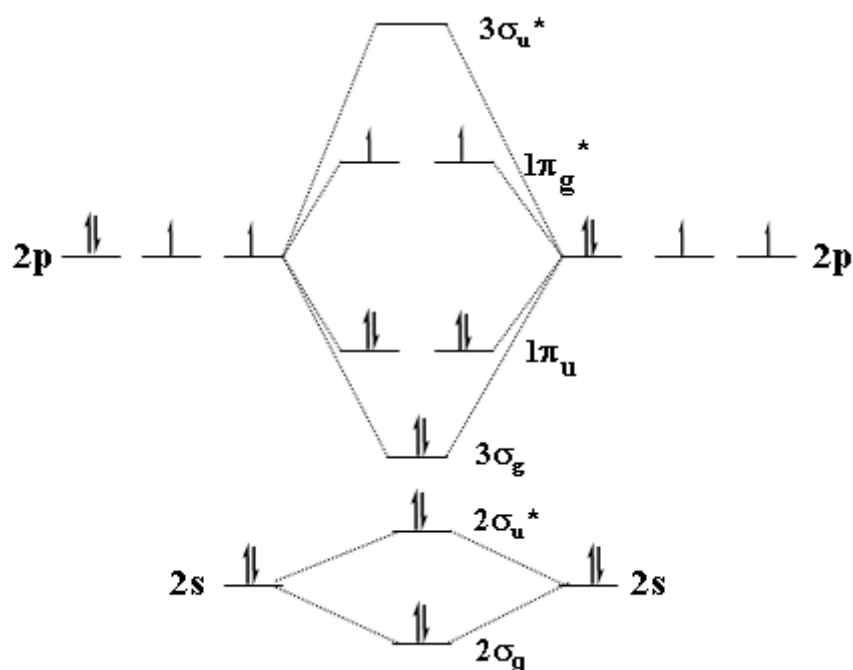


Fig. 1.2 Molecular Orbital diagram of oxygen molecule (Taube, 1965)

The plausible 1:1 and 2:1 metal-dioxygen complex structures are given in Fig. 1.3. Geometries 1 and 2 have been shown to give similar bonding patterns: each exhibits one  $\sigma$  and one  $\pi$  interaction. The Griffiths model (Griffith, 1956) (1), involves a side-on interaction of  $O_2$  with the metal. The bonding can be viewed as arising from two contributions:  $\sigma$  type of bond formed by the overlap between mainly  $\pi$  orbital of oxygen and  $d_z^2$  (and s) orbital on the metal and a  $\pi$  backbond interaction between the metal d  $\pi$  orbitals and the partially occupied  $\pi^*$  antibonding orbital on  $O_2$ . In the Pauling model (Pauling, 1964) (2) which involves an end-on interaction of  $O_2$  with the metal, a  $\sigma$ -bond is formed by the donation of electron density from the  $\sigma$ -rich orbital of dioxygen to an acceptor orbital  $d_z^2$  on the metal whereas the  $\pi$  interaction is produced between the metal d-orbitals ( $d_{xz}$ ,  $d_{yz}$ ) and  $\pi^*$  orbital of dioxygen, with charge transfer from the metal to the  $O_2$  molecule. It indicates that the preference of geometries (1) and (2) is determined by the relative donating abilities of the filled  $\pi$  and  $\sigma$  orbitals of dioxygen molecule respectively.

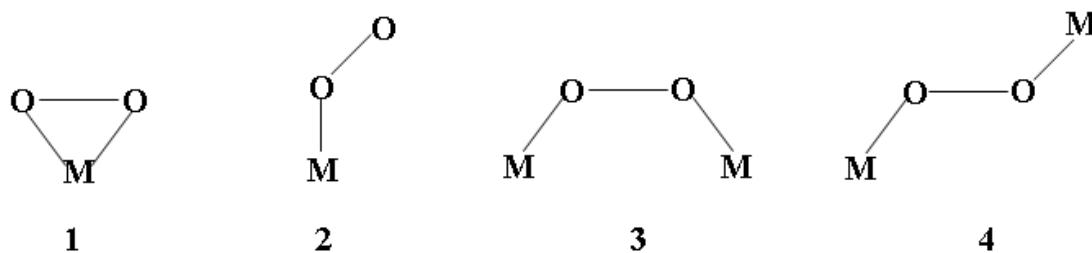


Fig. 1.3 Possible configurations of dioxygen interaction with a metal in a complex

In 2:1 complexes of metal-dioxygen, the bonding arises from the interaction between the d-orbitals on the metal with  $\pi^*$  and  $\pi$  orbitals combination on  $O_2$  (Tatsumi and Hoffman, 1981). It means that the singlet or triplet nature of dioxygen orbitals determines the bridge or trans mode of interaction of dioxygen with metal. The bridge interaction was proposed by Yeager (1981) and it is likely to occur on noble metals such as Pt, face-to-face porphyrins (Collman *et al.*, 1979) where  $O_2$  is reduced to



water with little or no peroxide formed. A trans configuration is likely to occur on metal porphyrins, metal phthalocyanines, dimeric metal complexes (Smith and Pilbrow, 1981). Griffith type of interaction could also lead to the rupture of the O-O bond. Some organometallic complexes (Vaska, 1976) are known to form adducts with O<sub>2</sub> with a side-on interaction. However, these compounds do not exhibit any catalytic activity for O<sub>2</sub> reduction, probably because the interaction leads to a stable adduct. Depending on the mode of adsorption of oxygen molecule on metal surface, different mechanistic steps will occur. The ORR pathways in both acidic and alkaline medium are given in Table 1.2.

Table 1.2 Mechanistic ORR pathways in acidic and basic media (Appleby, 1993)

Mode of interaction	ORR pathways	
	Acidic medium	Basic medium
Bridge (or) Trans	$O_2 + 2e^- + 2H^+ \rightarrow 2OH_{ads}$	$O_2 + 2e^- + 2H_2O \rightarrow 2OH_{ads} + 2OH^-$
	$2OH_{ads} + 2H^+ + 2e^- \rightarrow 2H_2O$	$2OH_{ads} + 2e^- \rightarrow 2OH^-$
End-on	Overall direct reaction: $O_2 + 4H^+ + 4e^- \rightarrow 2H_2O$ ; $E^o = 1.23 \text{ V vs. NHE}$	Overall direct reaction: $O_2 + 2H_2O + 4e^- \rightarrow 4OH^-$ ; $E^o = 0.401 \text{ V vs. NHE}$
	$O_2 + e^- + H^+ \rightarrow HO_{2,ads}$	$O_2 + H_2O + e^- \rightarrow HO_{2,ads} + OH^-$
	$HO_{2,ads} + e^- + H^+ \rightarrow H_2O$	$HO_{2,ads} + e^- \rightarrow HO_2^-$
	Overall indirect reaction: $O_2 + 2H^+ + 2e^- \rightarrow H_2O_2$ ; $E^o = 0.682 \text{ V vs. NHE}$	Overall indirect reaction: $O_2 + H_2O + 2e^- \rightarrow HO_2^- + OH^-$ ; $E^o = -0.076 \text{ V vs. NHE}$
	with	with
	$H_2O_2 + 2H^+ + 2e^- \rightarrow 2H_2O$ ; $E^o = 1.77 \text{ V vs. NHE}$	$HO_2^- + H_2O + 2e^- \rightarrow 3OH^-$ ; $E^o = 0.88 \text{ V vs. NHE}$

Based on all these facts, various authors proposed different schemes for ORR pathway (Damjanovic *et al.*, 1966; Wroblowa *et al.*, 1976; Anastasijevic *et al.*, 1987).

Of various schemes proposed for ORR, a modified scheme proposed by Wroblowa *et al.* (1976) appears to be the appropriate one to describe the complicated reaction pathway for the reduction of  $O_2$  at the metal surface (refer to Fig. 1.4).

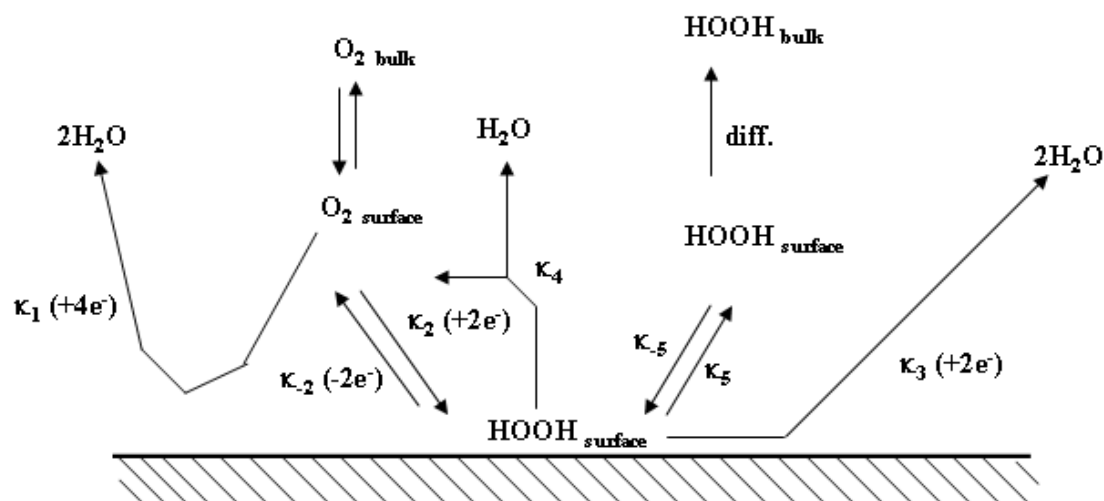


Fig. 1.4 Schematic presentation of ORR pathway (Wroblowa *et al.*, 1976)

At high potentials  $k_1/k_2$  is constant with  $k_1 > k_2$  indicating a direct reduction of oxygen to water than the two-electron reduction to peroxide. At intermediate potentials,  $k_1/k_2$  ratio decreases indicating an increase in the two-electron reduction to peroxide. At lower potentials  $k_1/k_2$  becomes lower than 1. However,  $k_3$  increases resulting in a further reduction of peroxide to water before it escapes into solution.

On most of the electrocatalysts, oxygen reduction takes place by the formation of high energy intermediate,  $H_2O_2$  followed by further reduction to  $H_2O$ . It is probably a consequence of the high stability of the O-O bond, which has a dissociation energy of  $494 \text{ kJ mol}^{-1}$ . In contrast, the dissociation energy of the O-O bond in  $H_2O_2$  is only  $146 \text{ kJ mol}^{-1}$  (Zagal, 1992). In order to obtain maximum efficiency and to avoid corrosion of carbon supports and other materials by peroxide, it is desired to achieve a four electron reduction. The two electron reduction is of practical interest for the

production of hydrogen peroxide. Finding suitable electrocatalysts that can promote the direct four electron reduction of oxygen molecule is an important task.

## **1.2 Electrocatalysts for Oxygen Reduction**

The essential criteria for a better oxygen reduction electrocatalysts are: high electronic conductivity, chemical and structural stability under the conditions namely; operating temperature, wide range of oxygen partial pressure and concentration of electrolyte, ability to decompose the intermediate species formed during the reduction process, chemical and thermomechanical compatibility to electrolyte and interconnector materials, tolerant to contaminants e.g., halide ions, methanol, NO<sub>x</sub>, CO<sub>x</sub>, SO<sub>x</sub> and low cost.

Both noble and non-noble metal based electrodes were investigated for oxygen reduction. In the case of noble metal electrocatalysts, platinum and palladium based materials appear to be the best, whereas in the case of non-noble metal electrocatalysts, transition metal chalcogenides and pyrolyzed macrocyclic compounds are two of the most widely studied.

## **1.3. Pt Metal Electrocatalysts**

The most promising electrocatalysts for oxygen reduction are based on platinum since they exhibit good activity and chemical stability under the operating conditions. But Pt is expensive and less abundant. The ORR consists of an oxygen diffusion process, adsorption process, charge transfer process, desorption process, and back diffusion process. The work function would be one of the key factors of the charge transfer process, because the work function is the minimum energy needed to remove an electron from the material surface. However, the work function of platinum with high catalytic activity for the ORR is higher than other transition metals (Trasatti, 1971).

In general, oxygen reduction takes place at high positive potentials. At such potentials most of the metals will dissolve and give rise to a similar situation to that prevailing at the cathode i.e., only noble metals and some of their alloys offer possibilities among metallic systems. The most familiar oxygen reduction catalysts are based on noble metals, particularly platinum. These have been investigated extensively as pure metals, as nanoparticles (Geins *et al.*, 1998) and as polycrystalline and single crystal surfaces (Perez *et al.*, 1997; Markovic *et al.*, 1977). They show a wide variety of behaviour, reflecting both the surface structure (Damjanovic, 1991) and the presence or absence of oxide films (King *et al.*, 1995). To date, conventional carbon supported platinum is the efficient electrocatalyst for oxygen reduction. But the cost of the Pt/C electrocatalysts is the main hurdle for the commercialization of electrochemical devices. To reduce the amount of Pt loading at the cathode side, thereby reducing cost, various synthetic approaches are adopted to disperse Pt on suitable support. Among the various support materials, carbon is the most attractive one because of its unique features like good electronic conductivity, chemical stability, surface area, mechanical stability, abundance and low cost.

The methods adopted for the preparation of supported Pt catalysts include impregnation method (Rajesh *et al.*, 2003; Vračar *et al.*, 2006), electrodeposition (Antoine *et al.*, 2001; Rajesh *et al.*, 2004; Wei *et al.*, 2005), chemical reduction of Pt metal salts by using reducing agents, such as borohydride (Ma *et al.*, 2006; Guo *et al.*, 2005), formaldehyde (Hou *et al.*, 2003; Viswanathan *et al.*, 2004) and formic acid (Zhang *et al.*, 2004), sputtering technique (Makino *et al.*, 2005), colloidal route (Bönnemann *et al.*, 1996), polyol reduction (Liu *et al.*, 2005; Wang *et al.* 2007; Nisha Shukla *et al.*, 2006; Liu *et al.*, 2007), microwave-assisted polyol reduction method (Liu *et al.*, 2005), supercritical deposition technique (Bayrakceken *et al.*, 2008).

Recently, Pt supported on conducting polymers (Qi and Pickup, 1998), carbon nanotubes (Cui *et al.*, 2005; Saha *et al.*, 2008; Leela Mohana Reddy and Ramaprabhu, 2007), carbon nanofibers (Zheng *et al.*, 2008; Lee *et al.*, 2006) have received enormous attention in order to develop efficient electrocatalytic system by enhanced metal-support interaction leading to activation of both dispersed metal and a matrix towards oxygen reduction reaction. But the preparation of CNTs and CNFs in bulk quantities and stability of polymers at high potentials are drawbacks for commercialization.

The observations made from the ORR measurements on the carbon supported Pt catalysts are:

(i) Sluggish kinetics of oxygen reduction reaction on Pt (Liang and Juliard, 1965). It was observed that the formation of  $-OH$  species at  $+0.8$  V (from the water oxidation as well as corrosion under acidic conditions) on the Pt surface hinder the oxygen reduction in such a way the kinetics is not facile. The  $-OH$  species also causes the less availability of molecular oxygen species and thereby reduce ORR activity.

(ii) Oxygen reduction is a structure sensitive reaction. Literature reports suggest that the optimum size of Pt for oxygen reduction is 3-5 nm (Kinoshita, 1990; Gamez *et al.*, 1996; Tamizhmani *et al.*, 1996; Min *et al.*, 2000; Maillard *et al.*, 2002). Still debate exists in the literature regarding the optimum particle size. Of the several factors which influence electrocatalytic activity of carbon-supported Pt catalysts, particle size, dispersion and structural effects are of crucial importance.

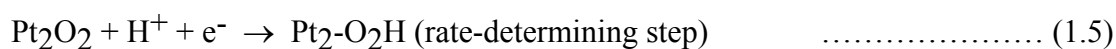
(iii) Hydrogen peroxide formation during oxygen reduction on Pt (Gouerec *et al.*, 1998). It was known that the oxygen reduction reaction is a complex process that includes many electrochemical (chemical) steps with different intermediates. The hydrogen peroxide radicals produced by the two-electron reduction of  $O_2$  can also

attack the active sites and also carbon layer, resulting in significant degradation of electrochemical device, and even cause the failure of the device (Gupta *et al.*, 1998).

(iv) Pt catalysts are sensitive to contaminants (Schmidt *et al.*, 2001). For example, strongly adsorbing halides (i.e., Cl<sup>-</sup>, Br<sup>-</sup>, I<sup>-</sup>), air borne contaminants of both organic (benzene, propane) and inorganic (CO, NO<sub>2</sub>, SO<sub>2</sub>, NH<sub>3</sub>, dust) nature significantly reduce the activity of Pt catalysts in the operational potential range. While H<sub>2</sub>O is the exclusive reaction product of the ORR on Pt at typical cathode potentials (0.6-1.0 V), the presence of strongly adsorbing halides changes the ORR pathway and substantial amounts of H<sub>2</sub>O<sub>2</sub> are formed. This product degrades the Pt sites and it leads to the reduction in cell voltage and also its life span.

### 1.3.1 ORR Mechanism

In terms of electrocatalysis, O<sub>2</sub>-reduction on Pt crystallites occurs by a parallel mechanism with direct four-electron reduction as the dominant step. However due to large number of possible steps within this ambit, a detailed mechanism still defies formulation. The main steps in the mechanism of oxygen reduction on Pt are shown below (Sidik *et al.*, 2002):



It was demonstrated that there was a relationship between oxygen reduction activity and the binding ability of O and OH. Accordingly, Pt and Pd are at the top of the volcano plot (Nørskov *et al.*, 2004). It was further elucidated that at high potentials,

adsorbed oxygen is stable and that proton and electron transfer was impossible. They proposed that the origin of the overpotential for Pt was the O and OH adsorption, and both dissociative and associative reaction paths may contribute to the oxygen reduction reaction depending on the metal and the electrode potential.

Pure Pt shows two Tafel slope regions in agreement with the report by Yeager (1981). Langmuirian kinetics was used to explain the Tafel slope of 120 mV decade<sup>-1</sup> below 0.8 V, while the 60 mV decade<sup>-1</sup> Tafel slope beyond 0.8 V was explained assuming oxygen adsorption under Temkin conditions in the presence of surface Pt-OH, a surface poison to the O<sub>2</sub> adsorption (Danjanovic and Bockris, 1966). Literature reports have shown that the formation of Pt-OH beyond +0.8 V is derived not from the interaction of O<sub>2</sub> with Pt, but rather from reaction of H<sub>2</sub>O with Pt causing inhibition of the O<sub>2</sub> reduction resulting in a low Tafel slope of 60 mV decade<sup>-1</sup> (Yeager, 1981; Panchenko *et al.*, 2004; Teliska *et al.*, 2005). In electrolytes containing phosphate or bisulfate anions a low Tafel slope was not observed on Pt(111) due to the surface poisoning by these anions which shift the Pt-OH formation to a more positive potential. However, for the other low index planes Pt(100) and Pt(110) a change of slope was observed since the anion adsorption on these planes is minimal (Markovic *et al.*, 1995; Markovic *et al.*, 1997). Significant improvement of ORR electrocatalysis could therefore be afforded by, first inhibiting the formation of adsorbed oxygenated species (primarily Pt-OH) beyond 0.8 V, a known surface poison, and, second, changing the electronic and short-range atomic order around Pt to induce alternative lower energy pathways for improved ORR kinetics.

#### **1.4 Pt Alloy Electrocatalysts**

Quite a lot of promising approaches and results have been reported to enhance the oxygen reduction activity of carbon supported Pt catalysts, the overpotential still

remains about 300-400 mV. Furthermore, a series of aspects, such as effective Pt catalyst layer utilization, the durability and reliability of such a supported catalyst component, are still problematic. If much more of the 200 mV available at the cathode is to be recovered, then a fundamentally different approach is required. The focus of the continued search for oxygen reduction catalysts is on the development Pt alloys with the required stability, and greater activity than Pt.

A variety of Pt-alloy systems have been investigated as oxygen reduction electrocatalysts for their use in various fuel cells. Various preparation methods and ORR activity of Pt alloys are given in Table 1.3. The results obtained throughout these studies are not consistent. Luczak and Landsman (1984 and 1987) found an increase in mass activity of a factor of 1.5 to 2.5 (at 0.9 V) whereas Beard and Ross (1990) and Glass *et al.* (1987) could not find an increased activity for Pt-Co and Pt-Cr alloys. Half cell studies in phosphoric acid revealed an enhancement factor of 2 to 5 when using Pt-M (M = Cr, Co and Ni) versus pure Pt (Min *et al.*, 2000). When comparing different alloy catalysts in proton exchange membrane fuel cells (PEMFCs), Mukerjee and Srinivasan (1993), Mukerjee *et al.* (1995a) and Tamizhmani and Capuano (1994) found similar activity enhancement factors (of 2 to 4) when using Pt-Mn, Pt-Cr, Pt-Fe, Pt-Co and Pt-Ni alloys or Pt-Cr and Pt-Cr-Cu alloys, respectively, versus pure Pt. Toda *et al.* (1999) reported enhancement factors of up to 10 for sputtered Pt-Fe, Pt-Co and Pt-Ni films in comparison to Pt films in 0.1 M HClO<sub>4</sub> at room temperature. On the other hand, ORR measurements on carbon supported Pt-Co and Pt-Ni catalysts revealed an activity enhancement of at most a factor of 3 in comparison to a supported Pt catalyst (Paulus *et al.*, 2002).



Table 1.3 Preparation methods, electrocatalytic activity and selectivity towards oxygen reduction of Pt alloys compared to Pt

Catalyst	Preparation method	Electrolyte medium	No. of electrons transferred	Catalytic activity towards O <sub>2</sub> reduction vs. Pt	Reference
Pt <sub>70</sub> Co <sub>30</sub> /C	Formic acid reduction method	Acid (fuel cell)	--	Comparable	Salgado <i>et al.</i> , 2005a
Pt <sub>75</sub> M <sub>25</sub> /C (M = Co and Ni)	Commercial E-TEK catalysts	Acid (fuel cell)	--	Comparable	Antolini <i>et al.</i> , 2005b
Pt <sub>75</sub> Co <sub>25</sub> /C	Alloying method	Acid	n. r	Comparable	Salgado <i>et al.</i> , 2005b
Pt <sub>85</sub> Co <sub>15</sub> /C	Borohydride reduction method	Acid	n. r	Comparable	Salgado <i>et al.</i> , 2005b
Pt-Cr(1:1)/C, Pt-Cr(3:1)/C, Pt-Cr(9:1)/C	Borohydride reduction method	Acid	n. r	Excellent	Antolini <i>et al.</i> , 2006
Pt-Co(1:1)/C, Pt-Co(3:2)/C and Pt-Co(2:1)/C	Carbonyl complex route followed by hydrogen reduction method	Acid	n. r	Comparable	Yang <i>et al.</i> , 2005
Pt <sub>32</sub> V <sub>14</sub> Fe <sub>54</sub> /C	Polyol reduction method	Acid	n. r	Comparable	Luo <i>et al.</i> , 2006
Pt <sub>(100-x)</sub> Ni <sub>x</sub> (x = 11-	Sputtering method	Acid	n. r	Excellent	Toda <i>et al.</i> , 1999

80 atom %), Pt <sub>(100-x)</sub> Co <sub>x</sub> (x = 10-78 atom %), Pt <sub>(100-2x)</sub> Fe <sub>x</sub> (x = 18-75 atom %) thin films					
Pt-Fe/C; Pt/Fe = 1:1, 3:1 and 9:1	Colloidal method	Acid	n. r	Excellent	Gong <i>et al.</i> , 2007
Pt-Au(2:1)/C	Microemulsion method, colloidal method and impregnation method	Acid	4	Comparable	Hernández-Fernández <i>et al.</i> , 2007
Pt-M(3:1)/C; M = Fe, Co and Cu	Sulfite complex route followed by incipient wetness method	Acid	n. r	Comparable	Baglio <i>et al.</i> , 2007
Pt-Fe(1:1)/C	Alloying method	Acid	n. r	Comparable	Shukla <i>et al.</i> , 2004
Pt-Cr(1:1)/C	Carbonyl route	Acid	n. r	Good	Yang <i>et al.</i> , 2005
Pt-Fe(3:1)/C	Polyol reduction method	Acid	n. r	Excellent	Li <i>et al.</i> , 2004
Pt <sub>(100-2x)</sub> Cr <sub>x</sub> /C (x =	Colloidal route	Acid	4	Excellent	Koffi <i>et al.</i> , 2005

10-30 atom%) Pt <sub>70</sub> Ni <sub>30</sub> /C	NaBH <sub>4</sub> reduction	Acid	n. r	Comparable	Antolini <i>et al.</i> , 2005c;
Pt-M/C; M = Fe, Co and Cr	Reverse microemulsion method	Acid	4	Excellent	Qian <i>et al.</i> , 2008
Pt-M(3:1)/C; M = Ni, Co and Cr	Incipient wetness method	Acid	4	Excellent	Min <i>et al.</i> , 2000
Pt-Co/C; Pt/Co = 1:1, 2:1, 3:1 and 5:1	Carbonyl complex route followed by hydrogen reduction	Acid	n. r	Excellent (1.2-2.2 times high activity)	Huang <i>et al.</i> , 2006
Pt-M(1:1)/C; M = Cr and Co	Decomposition of organometallic complexes	Acid	n. r	Excellent	Grinberg <i>et al.</i> , 2007
Pt <sub>50</sub> M <sub>50</sub> /C, Pt <sub>75</sub> M <sub>25</sub> /C; M = Co and Ni	Commercial catalysts	Acid	4	Excellent (1.5-3 times high activity)	Paulus <i>et al.</i> , 2002
Pt-Cr/C; Pt/Cr – 1:1, 2:1 and 3:1	Carbonyl complex route followed by hydrogen reduction method	Acid	n. r	Excellent (1.5-3 times high activity)	Yang <i>et al.</i> , 2004

Pt-M(3:1)/C; M = Fe and Co	Reverse microemulsion method and NaBH <sub>4</sub> reduction method	Acid	n. r	Excellent	Xiong and Manthiram, 2005
Pt-Ni(1:1)/C, Pt-Fe(1:5) and Pt-Co(1:7)/C	Sodium formatted reduction method	Acid	n. r	Comparable	Xiong <i>et al.</i> , 2002
Pt-Ni/C; Pt/Ni = 1:1, 2:1, 3:1 and 5:1	Carbonyl complex route followed by hydrogen reduction method	Acid	n. r	Excellent (1.5-4 times high activity)	Yang <i>et al.</i> , 2004
Pt-Ni/C; Pt/Ni = 3:1, 3:2 and 9:1	Microemulsion method	Acid	4	Comparable	Santos <i>et al.</i> , 2006
Pt-Co(1 :1)/C	Incipient wetness method	Acid	n. r	Comparable	Hwang <i>et al.</i> , 2007

(n.r = not reported)

### 1.4.1 ORR Mechanism

The possible mechanisms given by various authors for the enhancement of the ORR kinetics on Pt alloys than pure Pt are: (i) Jalan and Taylor (1983) extensively studied the ORR on Pt alloys supported on carbon black and claimed the role of shortening of Pt-Pt interatomic distances by alloying in the enhancement. (ii) Appleby (1986) claimed that the lattice contractions due to alloying resulted in a more favorable Pt-Pt distance for the dissociative adsorption of O<sub>2</sub>, while maintaining the favorable Pt electronic property. (iii) Paffet *et al.* (1988) reported that the enhancement could be attributed to a simple surface roughening brought about by the enhanced corrosion. However, the data of electrocatalytic activity normalized with electrochemically measured surface areas indicates that the enhancement does not result from such a surface roughening. (iv) Beard and Ross (1990) claimed a particle termination with particular vicinal planes on dispersed catalyst surfaces as a reason for the enhanced electrocatalysis. Later it was disproved by Toda *et al.* (1999) based on the peak ratio  $\langle 200 \rangle / \langle 111 \rangle$  for all the alloys. (v) In a recent work with *in-situ* X-ray absorption spectroscopy (XAS) studies, Mukerjee *et al.* (1995a and 1995b) explained the enhanced electrocatalysis on the basis of the interplay between the electronic (Pt d-vacancy) and geometric factors (Pt-Pt interatomic distance and Pt coordination number) and their effect on the chemisorption behavior of OH species from the electrolyte. They observed volcano-type behavior from the plots of electrocatalytic activity vs. the electronic and geometric parameters. They demonstrated that Pt-Cr located at the top of the curve than the other investigated alloy catalysts (Pt-Co, Pt-Fe, Pt-Ni), based on the best combination of both the Pt d-band vacancies and the Pt-Pt bond distances, *i.e.*, 0.36 (based on XANES data) for the former and 2.71 Å (based on EXAFS data) or 2.73 Å (based on XRD data) for the latter, respectively. It was

reported that the optimum distance between Pt-Pt (determined by XRD) corresponding to the maximum performance lies between 2.71 and 2.75 Å.

The proposed mechanism for the enhancement of ORR on  $\text{Pt}_{(100-x)}\text{Fe}_x$  alloys is schematically shown in Fig. 1.5. By addition of Fe up to 30-50 atom %, the 5d vacancies of the surface increase, because Fe has more 5d vacancies than Pt. Such an increase of 5d vacancies led to an increased  $2\pi$  electron donation from  $\text{O}_2$  to the surface Pt, resulting in an increased  $\text{O}_2$  adsorption and a weakening of the O–O bond. As a result, scission of the bond must occur instantaneously as electrons are back donated from 5d orbitals of the surface Pt to  $2\pi^*$  orbitals of the adsorbed  $\text{O}_2$ , that is, the first one-electron transfer accompanied by  $\text{H}^+$  binding, followed by the additional back donation of three residual electrons and by the additional introduction of three  $\text{H}^+$  ions. When the 5d vacancy of the electrode increases or the Fermi level further lowers by addition of the Fe beyond optimum content, the Pt–O bonding becomes stronger and the back donation becomes difficult, resulting in the lowered  $\text{O}_2$  reaction rate. When the content of the second element becomes too large, the resulting large d-band vacancy may contribute just to the enhancement of O–O bond scission *i.e.*, the surface oxide formation. Consequently, the suppression against the ORR at the large d-band vacancies region may be the same phenomenon as a previous claim (Grgur *et al.*, 1997) that  $\text{OH}_{\text{ads}}$  impeded the ORR on a single-crystal Pt. Thus, the volcano-type electrocatalytic behavior of Pt alloys with increasing the second element content can be explained.

However, all these authors did not consider the differences of combinations, compositions, or crystallographic structures among the alloys. As seen by these studies, the role of morphology or crystallographic changes and of the electronic

structure change brought by alloying on the electrocatalysis for the ORR still remains elusive.

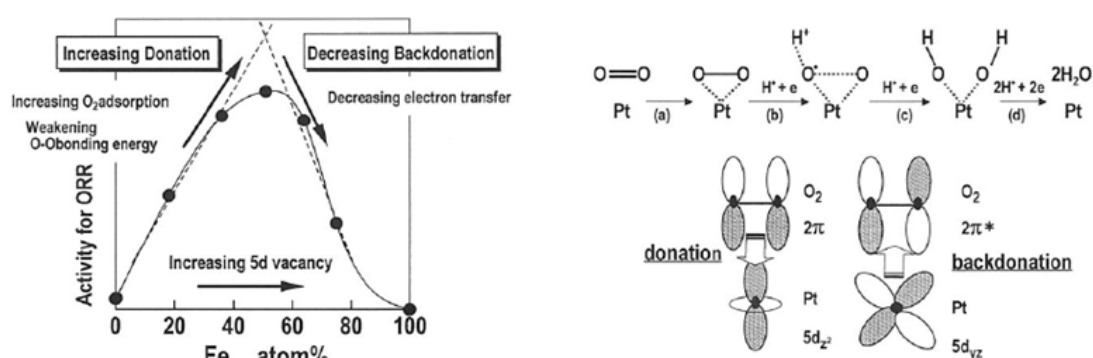


Fig. 1.5 Schematic explanation of the proposed enhancement mechanism of the ORR by alloying Pt with Fe-group metals (Toda *et al.*, 1999)

By careful analysis of both the theoretical and experimental data on Pt alloys for oxygen reduction, it can be concluded that the Pt-Cr, Pt-Co, Pt-Fe and Pt-Ni have shown good activities among the various investigated bimetallic Pt alloys compared to Pt. Changes in short-range atomic order, particle size, Pt d-band vacancy, Pt skin effects, and Pt-OH inhibition have been advanced as some of the reasons attributed for the observed enhanced performance by these alloys. Inhibiting or shifting the onset potential (approximately 800 mV vs RHE for Pt) of Pt-OH formation, providing free sites for molecular oxygen adsorption, is generally expected to lower the overpotential losses. A number of prior reports have provided indirect evidence to the possibility of inhibiting the formation of anodic activation of water for Pt-OH formation. Shifting the onset potential of OH formation on Pt is dependent on (a) the ability of the alloying elements to modify the Pt electronic and short-range atomic order for inhibiting activation of H<sub>2</sub>O and (b) the ability of the alloying element to attract and hold H<sub>2</sub>O<sub>ads</sub> more strongly than the surrounding surface Pt atoms.

## 1.5 Pd and Pd Alloy Electrocatalysts

Palladium has a similar valence shell electronic configuration and lattice constant to platinum. Moreover, it is more abundant than Pt. Considering both aspects of performance and price, palladium based materials can be one of the alternative material for oxygen reduction. It was also reported that the oxygen reduction takes place in the same manner as that on Pt (Sepa *et al.*, 1981; Vračar *et al.*, 1987; Vračar *et al.*, 1989). But the less ORR activity than Pt and poor stability of Pd at high potentials about +0.8 V vs. NHE hinders its commercial exploitation. To improve the catalytic ORR activity of Pd, various bimetallic Pd alloys such as Pd–Co, Pd–Fe, Pd–Ni, Pd–Ta and Pd–Cr have been investigated. It was found that their activities toward ORR were significantly enhanced (Savadogo *et al.*, 2004). Later Fernandez *et al.* (2005a) designed bimetallic electrocatalysts for oxygen reduction based on thermodynamic principles. They assumed a simple mechanism where one metal breaks the oxygen-oxygen bond of molecular O<sub>2</sub> ( $2M + O_2 \rightarrow 2MO$ ) and the other metal acts to reduce the resulting adsorbed atomic oxygen ( $2MO + 4H^+ + 4e^- \rightarrow 2M + 2H_2O$ ). Analysis of the Gibbs free energies of these two reactions on various metal combinations revealed that Pd-Co, Pd-Ti, Pd-Co-Au and Pd-Co-Mo appear to be good. The electrocatalytic activity of these materials for the ORR in acidic medium was examined using scanning electrochemical microscopy (SECM) in a new rapid-imaging mode. This was used to rapidly screen arrays covering a wide range of catalyst compositions for their activity for the ORR in 0.5 M H<sub>2</sub>SO<sub>4</sub>. Using the SECM technique, they have identified combinations of metals with enhanced electrocatalytic activities when compared with the constituent, pure metals. Addition of Co to Pd clearly decreases the ORR overpotential, in agreement with the proposed model. Catalyst spots that exhibited enhanced electrocatalytic activity in the SECM screening technique were then examined using classical rotating disk electrode (RDE)



experiments. The measurements revealed that the C/Pd-Co electrodes (10-30% Co) exhibited remarkable activity for ORR catalysis, close to that of carbon-supported Pt. However, the good performance of Pd-Co was lost after approximately 3 h of continuous operation, as evidenced by a noticeable increase of the ORR overpotential. Upon addition of 10% Au or Mo to the Pd-Co mixture, the stability was greatly improved and the electrode retained its high electrocatalytic activity. Significantly, the agreement between RDE and SECM results is excellent. By comparing the activities determined by both techniques, they have attributed the apparent high electrocatalytic activity of Pd-Co-Au or Pd-Co-Mo observed in the SECM imaging to a stabilizing effect of Au and Mo. Investigation of Pd-Co-Mo(7:2:1)/C and Pd-Co-Au(7:2:1)/C catalysts as cathode materials in PEMFCs by Fernandez *et al.*, (2005b) and Raghhuveer *et al.*, (2005 and 2006) showed the comparable performance to that of the state-of-art commercial Pt/C catalysts.

Wang and Balbuena (2005) also attempted to design bimetallic catalysts for oxygen reduction. They have performed density functional calculations to calculate the Gibbs free energies of key elementary steps for the electrocatalytic oxygen reduction reaction (ORR):  $O_2 + M + H^+ + e^- \rightarrow HOO-M$  ( $\Delta G_1$ ),  $HOO-M + M \rightarrow HO-M + O-M$  ( $\Delta G_2$ ),  $O_2 + 2M + H^+ + e^- \rightarrow O-M + HO-M$  ( $\Delta G_3$ ), and  $HO-M + O-M + 3H^+ + 3e^- \rightarrow 2H_2O + 2M$  ( $\Delta G_4$ ), where M stands for the adsorption site of a metal catalyst modeled by a single metal atom as well as by an  $M_3$  cluster. Taking Pt as a reference,  $\Delta G_4$  is plotted against  $\Delta G_1$  for metals from groups V to XII. It is found that no single metal has both  $\Delta G_1$  and  $\Delta G_4$  more negative than that of Pt, although some of them have either more negative  $\Delta G_1$  or more negative  $\Delta G_4$ . This enables to explain thermodynamically why no other single metal catalyzes the ORR as effectively as Pt does. Moreover, a thermodynamic analysis reveals that the signs of  $\Delta\Delta G$  (the

difference between  $\Delta G$  of other metals and  $\Delta G$  of Pt) strongly correlate with the valence electronic structure of metals, i.e.,  $\Delta\Delta G_1 < 0$  and  $\Delta\Delta G_4 > 0$  for metals M with vacant valence d orbitals, whereas  $\Delta\Delta G_1 > 0$  and  $\Delta\Delta G_4 < 0$  for metals M' with fully occupied valence d orbitals. Thus, a simple thermodynamic rule for the design of bimetallic catalysts for the ORR is proposed: couple a metal M ( $\Delta\Delta G_1 < 0$ ) with a second metal M' ( $\Delta\Delta G_4 < 0$ ) to form an alloy catalyst  $MM'_3$ . The rationale behind this selection is based on M being more efficient for the rate-determining step, i.e., for the formation of the adsorbed species M-OOH, while M' can enhance the reductions of O and OH in the last three electron-transfer steps. They concluded that the Pd<sub>2</sub>Co bimetallic system thermodynamically has similar performance to Pt to catalyze the ORR.

Recently, Shao *et al.* (2006 and 2007) demonstrated that ORR activity of Pd<sub>3</sub>Fe/C was comparable to that of the carbon-supported Pt electrocatalysts. In the continuing effort to improve ORR catalytic activity of Pd-Fe catalyst, Wang *et al.* (2008) prepared Pd-Fe-Ir/C by colloidal route and investigated the ORR activity in terms of half-cell and PEMFC measurements. They observed comparable performance to that of the state-of-art carbon-supported Pt electrocatalysts. The preparation methods and ORR activity of various Pd based electrocatalysts are given in Table 1.4. Literature reports indicated that binary Pd-M (M = Co, Fe) and ternary Pd-Co-M (M = Au, Mo and Fe) alloys were comparable to, or slightly better than, that of commercial Pt catalysts. An understanding of the origin of their high activities may help us in designing inexpensive and more active catalysts.

Table 1.4 Preparation methods, electrocatalytic activity and selectivity towards oxygen reduction of Pd based electrocatalysts compared to Pt

Catalyst	Preparation method	Electrolyte medium	No. of electrons transferred	Catalytic activity towards O <sub>2</sub> reduction vs. Pt	Methanol tolerance vs. Pt	Reference
Pd-Ti/C and Pd-Co-Au/C	Reverse microemulsion method (RME)	Acid	n. r	Comparable	n. r	Fernández <i>et al.</i> , 2005
Pd-Co-Mo/C	Borohydride reduction method	Acid	n. r	Comparable	Excellent	Raghuveer <i>et al.</i> , 2005
Pd-Co-Au/C	Borohydride reduction method and RME	Acid	n. r	Comparable	n. r	Raghuveer <i>et al.</i> , 2006
Pd and Pd-Fe nanoparticles	Hydrogen reduction method	Acid	n. r	n. r	n. r	Shao <i>et al.</i> , 2006
Pd <sub>x</sub> Fe <sub>y</sub> /C (x = 1, 2, 3 and 4) and y = 0 and 1)	Pulse-microwave assisted polyol synthesis	Acid	4	Comparable	Excellent	Song <i>et al.</i> , 2008
Pd <sub>3</sub> Pt <sub>1</sub> /C	Polyol reduction method	Acid	n. r	Excellent	Excellent	Li <i>et al.</i> , 2004
Pd <sub>x</sub> Co <sub>y</sub> /C (x = 1, 2, 3 and	Polyol reduction method	Acid	4	Comparable	Excellent	Wang <i>et al.</i> , 2007

4) and y = 0 and 1)						
Pd <sub>75</sub> Co <sub>25</sub>	Electrodeposition method	Acid	n. r	Comparable	Excellent	Tominaka <i>et al.</i> , 2008
Pd	Borohydride reduction method	Acid	4	Less	n. r	Salvador-Pascual <i>et al.</i> , 2007
Pd-M (M = Co, Ni and Cr)	rf sputtering method	Acid	n. r	Less	Excellent	Lee <i>et al.</i> , 2006
Carbon supported Pd, Pd-Fe and Pd <sub>3</sub> Fe	Underpotential deposition method	Acid	n. r	Comparable	n. r	Shao <i>et al.</i> , 2007
Pd-Co/C and Pd- Co-M/C (M = Pt, Ag and Au)	RME	Acid	4	Comparable	Excellent	Mathiyarasu and Phani, 2007
Pd <sub>3</sub> Fe <sub>1</sub> Ir <sub>1</sub> /C	Colloidal method	Acid	n. r	Comparable	Excellent	Wang <i>et al.</i> , 2008
Pd <sub>3</sub> Pt <sub>1</sub> /C	Polyol reduction method	Acid	n. r	Comparable	n. r	Li <i>et al.</i> , 2007
Pd-Co/C	Formaldehyde, borohydride and polyol reduction	Acid	n. r	Less	n. r	Zhang <i>et al.</i> , 2007

### 1.5.1 ORR Mechanism

Considerable research towards the fundamental understanding of the ORR catalytic activity of Pd alloys has been undertaken. The possible reasons for enhanced activity of Pd alloys than Pd metal given by various authors are:

(i) Induced change in the density of states (DOS) at the Fermi level of Pd sites by alloy formation. Lee *et al.* (2006) considered that the decreased DOS induced by the electron transfer from Co, Ni, or Cr to Pd may weaken the chemisorption bonds between Pd and reactants such as O<sub>2</sub>, O/OH, O<sub>2</sub><sup>-</sup>, and H<sub>2</sub>O<sub>2</sub>, reducing their blocking effect in the O<sub>2</sub> reduction process. As a result, the ORR kinetics may be enhanced. For example, an alloyed Pd showed a reduced ORR overpotential by ~50 mV at 0.2 mA cm<sup>-2</sup> compared to that catalyzed by pure Pd.

(ii) Induced change in ORR Gibbs free energy. Wang and Balbuena (2005) explained that if a catalyst consists of two metals, one with a low occupancy of d-orbitals (such as Co, Ni, Cr, or V) and the other with fully occupied d-orbitals (such as Pd, Au, and Ag), the d-orbital coupling effect between them can significantly decrease the Gibbs free energy of the electron transfer steps in ORR, resulting in an enhancement in ORR kinetics.

(iii) Pd lattice compression induced by alloy formation. A metal d-band center can be altered by orbital overlap. The formation of the alloy can induce Pd lattice compression (or reduction of bond lengths between metals) through the modification of the electronic structure and orbital overlap. This will cause the shift of the d-band center, resulting in a change in the surface activity of Pd sites. The density functional calculations made by Hammer and Nørskov (2000) confirmed that the compression of a Pd lattice in alloys could downshift the d-band center energy. The Pd lattice compression can enhance the catalyzed ORR.

(iv) Facilitated  $O_2$  dissociation by alloy formation. Fernandez *et al.* (2005a) interpreted the enhanced activity upon alloying through a simple thermodynamic model. They thought that an incorporation of more active metals into Pd, such as Co, could facilitate the dissociative adsorption of  $O_2$  to form dissociated oxygen atoms ( $O_{ads}$ ), and that these  $O_{ads}$  could migrate from the Co site to the Pd site where the electroreduction could occur with less polarization. The RDE experiments showed a clear onset potential shift of  $\sim 200$  mV in the positive direction for ORR when Pd was alloyed by Co; and the Pd–Co alloy with an atomic ratio of 80:20 could give a optimum activity, which was very close to the activity exhibited by Pt catalysts.

(v) Formation of the desirable “Pd shell and alloy core” structure. Guo *et al.* (2007) in their recent paper on the first principles consideration in the design of Pd alloy catalysts for ORR, proposed that the key to improving the ORR activity of Pd-based catalysts is to alloy Pd with elements of smaller atomic size to form a “Pd shell and alloy core” structure, so as to take advantage of the lattice strain effect (lattice contraction induced by the incorporation of smaller atoms, such as Co, into the Pd lattice). This lattice strain effect can cause a downshift in the metal d-band center, weakening the interaction between the catalyst and the adsorbate (such as  $O_2$ ). Three catalysts such as Pd, Pd–Co, and Pt experimentally showed an ORR activity order of  $Pt > Pd-Co > Pd$ , which is consistent with the theoretical interpretation.

## 1.6 Transition Metal Chalcogenides

Chevrel phase based on metal clusters constitute one class of materials that show activity for oxygen reduction. Ternary chalcogenides of the formula  $M_xMo_6X_8$  ( $M = Cu, Ag, Ni, Fe, Pb, \text{rare earth, etc.}$  and  $X = S, Se, \text{ or } Te$ ) have been first synthesized by Chevrel *et al.* (1971) and therefore are often referred to as Chevrel compounds. These are characterized by a central octahedral metal cluster in which the

delocalization of electrons leads to high electronic conductivity and also these clusters act as a reservoir for electronic charge carriers while maintaining a stable electrochemical potential. These clusters have the ability to provide neighboring binding sites for reactants and intermediates and also have the ability to change its volume and bonding distances during electron transfer. The rhombohedral Chevrel phase consists of a stacking of  $\text{Mo}_6\text{X}_8$  units and contains channels where additional metal atoms can be inserted, forming  $\text{M}_x\text{Mo}_6\text{X}_8$  compounds where M can be a variety of atoms from small to large ones (M= Ag, Sn, Ca, Sr, Pb, Ba, Ni, Co, Fe, Cr, Mn etc). Electrochemical properties of ternary Chevrel phases depend on the size and electronic configuration of the filling atoms. For example, substitution of two or four of the Mo atoms by Ru or Re gives rise to the mixed cluster compounds e.g.,  $\text{Mo}_4\text{Ru}_2\text{X}_8$  and  $\text{Mo}_2\text{Re}_4\text{X}_8$ . It leads to a contraction of the cluster which then becomes regular. According to molecular orbital calculations, the number of electrons in the intracluster bonding (Valence electron count, VEC) for  $\text{Mo}_6\text{X}_8$  is  $(6 \times 6) - (2 \times 8) = 20$  or  $3.33e^-$  per molybdenum atom whereas for  $\text{Mo}_4\text{Ru}_2\text{X}_8$ :  $(4 \times 6) + (2 \times 8) - (2 \times 8) = 24$  or  $4e^-$  per cluster atom. These electrons are essentially derived from the transition metal d-states and available at the Fermi level,  $E_F$ . By substitution of Mo atoms by suitable transition metal atoms, the position of the Fermi level will alter in such a way it is suitable to the redox potential of the  $\text{O}_2/\text{H}_2\text{O}$  couple (Alonso-Vante *et al.*, 1987).

Electrocatalysis of the ORR on some Chevrel phases was reported for the first time by Alonso-Vante and Tributsch (1986). They investigated the ORR activity of various Chevrel type chalcogenides and observed the increment in activity from the samples containing nonsubstituted Mo octahedra showing metallic behaviour to samples containing Ru substituted Mo octahedra ( $\text{Mo}_{6-x}\text{M}_x\text{X}_8$ , where X = S, Se, Te) showing semiconducting behaviour (Alonso-Vante *et al.*, 1987). Moreover, significant changes

in the overpotential for oxygen reduction was observed on metal, metal cluster and mixed metal clusters. This could be explained in terms of geometric/electronic factors through electrochemical measurements, which is supported by the density of states (DOS) at the Fermi level. Fig.1.6 summarizes the electrocatalytic activity of Chevrel phases in terms of the overpotential,  $\eta$  (at  $-0.01 \text{ mA/cm}^2$ ) as a function of VEC per cluster unit. It is observed that the overpotential for ORR on the metal cluster ( $\text{Mo}_6$ ) is decreased by 0.4 V in comparison to that of the metal.

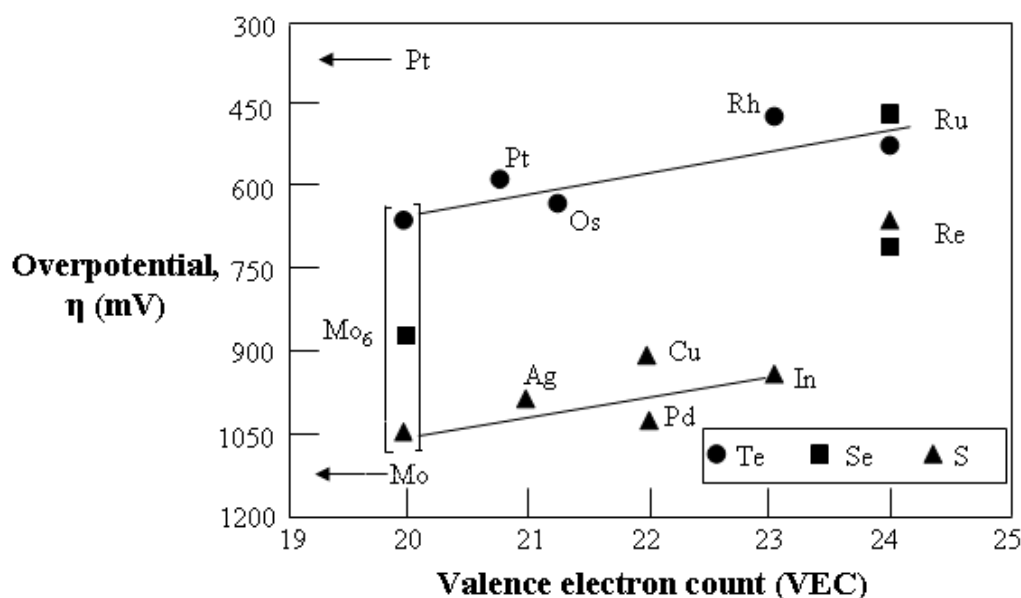
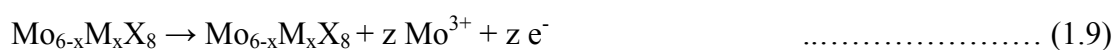


Fig. 1.6 Dependence of the overpotential, at a current density of  $10^{-2} \text{ mA/cm}^2$ , as a function of valence electron counting (VEC) per cluster for Chevrel phases (Alonso-Vante *et al.*, 2003).

When the catalytic center is enriched by electrons (3.3 to  $4 e^-$  per metal atom in the cluster) the overpotential is further decreased (0.76 V for  $\text{Mo}_4\text{Ru}_2\text{Se}_8$  and 0.6 V for  $\text{Mo}_4\text{Ru}_2\text{Te}_8$ ). On the binary series  $\text{Mo}_6\text{X}_8$ , the trend in the overpotential is as follows:  $\text{Te} < \text{Se} < \text{S}$  (Alonso-Vante *et al.*, 1989; Fischer *et al.*, 1995). It means that the VEC plays an important role in the ORR activity of chalcogenides. The cluster material with highest ORR activity is  $\text{Mo}_4\text{Ru}_2\text{Se}_8$ . This material has high DOS at the Fermi



level compared to the simple metal cluster and other chalcogen contained mixed metal clusters. Its current-potential characteristics have the same shape as that of platinum electrodes. The overpotential compared to Pt is still high. The origin of this phenomenon is due to the fact that the open circuit potential becomes limited by the presence of a mixed potential (corrosion potential). The corrosion process is complex and the suggested mechanism is



The formation of MoO<sub>3</sub> is dependent on the stabilization of metal clusters by the chalcogen atom (Alonso-Vante *et al.*, 1987). The *in situ* EXAFS analysis (Alonso-Vante *et al.*, 2002; Malakhov *et al.*, 2002) of the Ru and Mo k-edges as a function of the electrode potential indicated that the coordination distance between Ru-Ru was sensitive in the oxygen saturated electrolyte than the coordination distance between Mo-Mo. The consequence of this is that it leads to a distortion of the framework due to a change in the co-ordination distance between Ru and chalcogen. It revealed that dynamics of the ruthenium centers during electrocatalysis was preferentially modified by the presence of oxygen in the electrolyte. Furthermore, there was no change in the coordination distance between Mo and Mo ( $R_{\text{Mo-Mo}}$ ) observed in the potential range of electrocatalytic current in Ar and oxygen atmospheres. However, change in the coordination distance between Ru and Ru ( $R_{\text{Ru-Ru}}$ ) was evident and attained a value of ca.1 %.  $R_{\text{Ru-Se}}$  followed the same trend as that of  $R_{\text{Ru-Ru}}$ , thus, assessing a certain dynamics of the cluster unit for ORR and led to the identification of the electrocatalytic center, namely the ruthenium.

Although the compounds ( $\text{Mo}_{6-x}\text{M}_x\text{X}_8$ ) synthesized by Alonso-Vante and Tributsch (1986) was thought to be related to Chevrel phases, studies by Trapp *et al.* (1996) on

MoRuS showed evidence for the formation of a stable  $\text{RuS}_x$  phase together with an initially unstable  $\text{MoO}_x$  phase. This composition relates to an approximate composition  $\text{Mo}_2\text{Ru}_2\text{S}_5$ . Based on these observations, Reeve *et al.* (1998a and 1998b) prepared a variety of compounds  $\text{Mo}_x\text{Ru}_y\text{S}_z$ ,  $\text{Mo}_x\text{Os}_y\text{S}_z$ ,  $\text{W}_x\text{Ru}_y\text{S}_z$ ,  $\text{Rh}_x\text{Ru}_y\text{S}_z$  and  $\text{Re}_x\text{Ru}_y\text{S}_z$  supported on various surface functionalized carbon blacks and observed the best oxygen reduction activities with  $\text{Rh}_x\text{Ru}_y\text{S}_z$ ,  $\text{Re}_x\text{Ru}_y\text{S}_z$  and  $\text{Mo}_x\text{Ru}_y\text{S}_z$ . Even though the ORR activity of these materials was lower than that of platinum, their activity relative to Pt increased significantly in methanol containing electrolytes. Under the DMFC conditions, the cell utilizing  $\text{Re}_x\text{Ru}_y\text{S}_z/\text{C}$  cathode gave working cell voltages at  $100 \text{ mA cm}^{-2}$  within 100 and 80 mV of that obtained using a Pt cathode for 2 and 4 M methanol feed concentrations, respectively, where methanol permeation gave rise to appreciable degradation in Pt performance.

Later Schmidt *et al.* (2000) adopted the low temperature chemical precipitation method to prepare the Mo-Ru-Se and their studies showed that a carbon-supported  $\text{Ru}_x\text{Mo}_y\text{SeO}_z$  had similar catalytic activity to a carbon supported Ru catalyst, suggesting only ruthenium formed the catalytic site and both Mo and Se probably did not participate in the electrocatalysis process. However, Bron *et al.* (2001) demonstrated that the presence of selenium may have acted as a bridge to facilitate efficient electron transfer between the Ru-complexes and the colloids, while protecting the catalysts from the electrochemical oxidation through surface modification of the catalyst by carbonyl and carbide-carbonyl complexes or carbon compounds, which led to an enhanced stability.

The experience gained with the  $\text{Mo}_x\text{Ru}_y\text{Se}_z$  clusters opened the possibility to examine a family of ruthenium based chalcogenide compounds  $\text{Ru}_x\text{X}_y$  where X = S, Se, and Te. The ORR measurements performed by Solorza-Feria *et al.* (1994 and 1997)

showed higher electrocatalytic ORR activity and chemical stability than those of Chevrel phase materials. The ORR activity follows the order of  $Ru_xS_y < Ru_xTe_y < Ru_xSe_y \approx Mo_xRu_ySe_z$ . Structural analysis of the active centers of  $Ru_xX_y$  ( $X = S, Se$  and  $Te$ ) species by *in situ* EXAFS studies performed by Alonso-Vante *et al.* (2002) suggests that the catalysts have a core of ruthenium atoms, which has triangular coordination and a direct metal-metal bond. Depending on the chalcogen, the Ru-cluster consists of two or three metal layers of different size and mutual coordination with chalcogen atoms coordinated to the periphery of the metal cluster. Variation of the chalcogen type affects the size of the Ru-cluster and the strength of its interaction with the chalcogen. This influences the interaction of Ru-clusters with oxygen and thus their activity in the reduction of molecular oxygen.

In order to probe active centers of Ru chalcogenide electrocatalysts during oxygen reduction, Malakhov *et al.* (2002) examined the materials by *in situ* EXAFS technique. The important observations are: (i) comparison of  $Ru_xSe_y$  and  $Ru_xTe_y$  electrocatalysts shows that for the later, the Ru-O coordination numbers (CNs) are significantly higher while Ru-Ru coordination numbers are lower. Furthermore, oxygen has a stronger bond to the catalytic center in  $Ru_xTe_y$  with the bond length in the range of 2.01-2.07 Å. This is apparently due to the weaker interaction of Te with Ru in  $Ru_xTe_y$  in comparison to  $Ru_xSe_y$ . As a result, oxygen binds Ru strongly and produces  $RuO_x$ , whose catalytic activity decreases as a function of exposure of the sample to air. (ii) Comparison of  $Ru_xSe_y$  and  $Ru_xS_y$  electrocatalysts shows that the coordination number (CN) of Ru to S is higher than to Se in  $Ru_xSe_y$  clusters. It means that the chalcogen S is blocking the Ru active site against molecular oxygen adsorption. This is apparently the reason for the observed lower catalytic activity of  $Ru_xS_y$ . These facts supported the experimental results of Bron *et al.* (2001) who

observed high current density, inhibition of formation of ruthenium oxide, negligible amount of H<sub>2</sub>O<sub>2</sub> production and enhanced stability in the case of Ru<sub>x</sub>Se<sub>y</sub> cluster compounds. All these facts indicate that the presence of selenium alters the electronic factors of the active center and facilitates the electron transfer.

Based on the above observations, Ru<sub>x</sub>Se<sub>y</sub>/C material was tested as cathode material under DMFC conditions. The important observations are the selective ORR on the chalcogenide material in the presence of methanol, as verified with half-cell measurements and the similar electrochemical behavior between Ru<sub>x</sub>Se<sub>y</sub>/C and Pt/C in the real DMFC mode (Shukla *et al.*, 2002; Scott *et al.*, 2004). Because of the high tolerance of the chalcogenide material to methanol, this measurement proves that platinum is depolarized by the methanol crossed over the electrolyte Nafion 117 membrane. Recently, Campbell (2004) claimed the electrocatalytic activity of carbon-supported Ru<sub>x</sub>Se<sub>y</sub> catalyst prepared by the NaBH<sub>4</sub> reduction method was very close to that of carbon-supported platinum catalysts. Various methods used to prepare most of the investigated systems for oxygen reduction and the corresponding ORR activity are given in Table 1.5. From the data given in this Table, one arrives at the conclusion that there is still a margin to optimize the distribution of the supported chalcogenide catalyst particles to obtain higher current densities and also to obtain the open circuit voltage near to that at equilibrium.

Table 1.5 Preparation methods, electrocatalytic activity and selectivity towards oxygen reduction of transition metal chalcogenides compared to Pt

Catalyst	Preparation method	Electrolyte medium	No. of electrons transferred	Catalytic activity towards O <sub>2</sub> reduction vs. Pt	Reference
Chevrel phases Mo <sub>6-x</sub> Ru <sub>x</sub> Se <sub>8</sub> where x = 1.8	High temperature solid state reaction	Acid	4	Low	Alonso-Vante <i>et al.</i> , 1987; Alonso-Vante <i>et al.</i> , 1989
Mo <sub>x</sub> Ru <sub>y</sub> S <sub>z</sub> , Mo <sub>x</sub> Os <sub>y</sub> S <sub>z</sub> , W <sub>x</sub> Ru <sub>y</sub> S <sub>z</sub> , Re <sub>x</sub> Ru <sub>y</sub> S <sub>z</sub>	„	Acid	n. r	Low	Reeve <i>et al.</i> , 1998a; Reeve <i>et al.</i> , 1998b
Amorphous phases Mo <sub>x</sub> Ru <sub>y</sub> SeO <sub>z</sub>	Low temperature chemical precipitation	Acid	4	Low	Schimdt <i>et al.</i> , 2000; Bron <i>et al.</i> , 2001
Amorphous phases Ru <sub>x</sub> S <sub>y</sub> (CO) <sub>n</sub>	Low temperature pyrolysis method	Acid	4	Low	Duron <i>et al.</i> , 2000
Amorphous phases Ru <sub>x</sub> Se	Low temperature aqueous medium method	Acid	4	Comparable	Campbell, 2004
Amorphous phases Ru <sub>x</sub> Se <sub>y</sub>	Impregnation method	Acid	4	Comparable	Hilgendorff <i>et al.</i> , 2003
Amorphous phases Ru <sub>x</sub> Se <sub>y</sub> O <sub>z</sub>	Colloidal method	Acid	4	Comparable	Tributsch <i>et al.</i> , 2001

$Ru_xS_y, Ru_xTe_y$	High temperature solid state reaction	Acid	4	Low	Alonso-Vante <i>et al.</i> , 2002
$Ru_xCr_ySe_z,$ $Ru_xFe_ySe_z,$	Low temperature chemical precipitation method	Acid	4	n. r	Gonzalez-Cruz and Solorza-Feria, 2003
$Mo_xOs_ySe_z(CO)_n$ $W_xOs_ySe_z(CO)_n$	„	Acid	4	n. r	Solorza-Feria <i>et al.</i> , 1999
$M_xMo_6S_8$ (M = Ag, Ba, Cd, Zn, Sn, Pb, In, Pd)	„	Acid	<4	n. r	Schubert <i>et al.</i> , 1996
$M_xMo_{6-x}Te_8$ (M = Pt, Ru, Os, Rh)	„	Acid	<4	n. r	Fischer <i>et al.</i> , 1995
$Ru_{85}Se_{15}/C$	Microwave assisted polyol reduction	Acid	n. r	Comparable	Liu <i>et al.</i> , 2007
$Ru_xSe_y/C$	Colloidal method followed by hydrogen reduction	Acid	n. r	Comparable	Colmenares <i>et al.</i> , 2006
$Ru_xSe_y/C$	Thermolysis	Acid	n. r	Low	Fiechter <i>et al.</i> , 2007

### 1.6.1 ORR Mechanism

Since  $\text{Mo}_x\text{Ru}_y\text{Se}_z \approx \text{Ru}_x\text{Se}_y$  material provides a four-electron reduction pathway for the oxygen reduction, it has been studied thoroughly in literature. The complex formation between the reduced oxygen molecule and the cluster must be the key to these systems with favourable catalytic behaviour. As a consequence of electron transfer from the transition metal cluster to the chemisorbed oxygen molecule, two distinct phenomena were to be expected.

(i) The expected upward shift of electronic levels is due to a positive charging of the cluster. Due to the semiconducting properties of the material with a Fermi level above the edge of the valence band, a complete refilling of the cluster with electrons (e.g., by tunneling) is to be expected so that the metal cluster can donate electrons easily to the redox couple ( $\text{O}_2/\text{H}_2\text{O}$ ) which is just below the Fermi level of the electrode (Alonso-Vante *et al.*, 1987). This is schematically shown in Fig. 1.7.

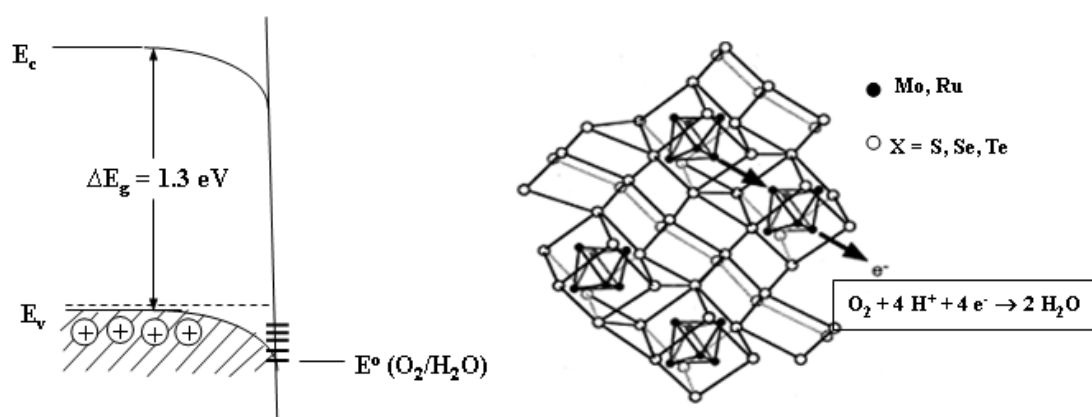
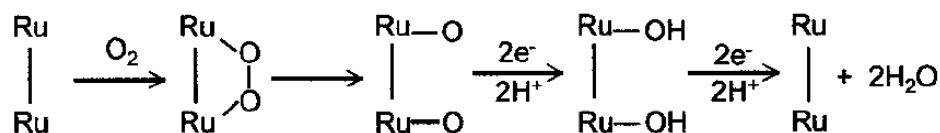


Fig. 1.7 Schematic representation of the energy diagram and crystal structure of  $\text{Mo}_x\text{Ru}_y\text{Se}_z$  indicating that electron exchange occurs via the mixed metal clusters (Alonso-Vante *et al.*, 1987; Tributsch *et al.*, 2001)

(ii) There is a correlation between the formal number of the valence electrons in the cluster and the metal-metal bonding distances in the cluster. Since no cooperative

reaction between neighboring atoms is possible in chalcogenides due to the large interatomic distance (2.7 Å), the breaking of the –O-O- bond is facilitated and leads to the formation of water (Alonso-Vante *et al.*, 1987). This is schematically shown in Scheme 1.1.



Scheme 1.1 Schematic representation of molecular oxygen reduction on the  $\text{Ru}_x\text{Se}_y$  species (Alonso-Vante *et al.*, 1987)

### 1.7 Transition Metal Macrocycles

Macrocyclic derivatives of transition metals constitute a unique class of electrocatalyst for oxygen reduction. One of the characteristics of an oxygen electrode is that it chemisorbs oxygen without degradation of the catalytically active surface. Reversible adsorption has been observed in aqueous solution for some metal chelates e.g., bis(salicylal) ethylene diamine cobalt(II), heme, and Co(II) histidine. The possible application of these soluble compounds as cathode catalysts would lead to a complicated engineering system, even if the kinetics was favourable. A number of insoluble metal chelates will also chemisorb oxygen; the most chemically stable of these are metal porphyrins, metal phthalocyanines and metal tetraazannulenes to some extent (Vasudevan *et al.*, 1990). The reason for exploiting these materials as oxygen reduction catalysts is due to their analogous structures of enzyme catalase, which decomposes oxygen in living cells. These molecules are having square planar structures with the metal atom symmetrically surrounded by four nitrogen atoms. These nitrogen atoms are each members of ring systems, which in turn are connected by carbon atoms (porphyrins) or nitrogen atoms (phthalocyanines). A number of these are insoluble and stable in acids (8 M  $\text{H}_2\text{SO}_4$ ) and bases (7 M KOH). Catalytic



activity for oxygen reduction is found only with a macrocyclic ligand, which has a cyclic conjugation of ' $\pi$ ' electrons (Zagal *et al.*, 1992).

Jasinski (1964) first reported oxygen electrocatalysis with an adsorbed transition metal macrocycle, the CoPc, adsorbed on carbon and nickel structures. Shortly thereafter, Jahnke *et al.* (1976) examined polymeric metal phthalocyanines and Kozawa *et al.* (1970) extensively studied the adsorbed Fe and Co phthalocyanines on pyrolytic graphite electrodes. In recent years, the desires for a low cost, catalytic oxygen electrode for fuel cells have accelerated the examination of various transition metal macrocycles as potential catalysts. Metal phthalocyanines, porphyrines, Schiff bases and related derivatives are frequently investigated. All these materials display an activity for the electroreduction of oxygen. Metal porphyrins and phthalocyanines have the advantage, in comparison to Schiff bases, that their chemical properties can be manipulated through substituents in the  $\beta$ - or meso-positions. Also, electrocatalytic activity and stability in acidic media appear to be enhanced for metal porphyrins and metallophthalocyanines with respect to the Schiff bases. Macrocyclic M-N<sub>4</sub> complexes of a great variety of metals have been tested, including Fe, Co, Ru, Pd, Pt, Ir, Cr, Ni, Cu, Zn, vanadyl ion, Mo, Al, Sn, uranyl ion, Sb, Ga, Na, Ag. All experimental evidences accumulated over the years have demonstrated that macrocyclic complexes of Fe and Co appear to be the best. For some particular complexes Fe is better, for others Co is better. Oxygen reduction on most Co chelates gives hydrogen peroxide as the main product of the reaction (Zagal *et al.*, 1980; Zagal *et al.*, 1992). Studies conducted on substituted Co chelates have shown that even though the activity varies for each individual complex depending on the substituent, the mechanism remains the same and peroxide is always the product (Elzing *et al.*, 1987; Zagal *et al.*, 1992). The activity of Fe phthalocyanine is lower than that of Co

phthalocyanine. The reverse is true for porphyrins. However, they suffer from low electrochemical stability, and they decompose either via hydrolysis in the electrolyte or attack of the macrocycle ring by peroxy intermediates generated during oxygen reduction. Collman *et al.* (1980) and Steiger *et al.* (1993) investigated the oxygen reduction activity of dicobalt face-to-face porphyrins, other binuclear and polynuclear Co phthalocyanines and found the direct reduction to water in acidic medium. In alkali only reduction to peroxide was observed (Durand *et al.*, 1983). Oxygen reduction on planar dicobalt chelates (van der Putten *et al.*, 1988) gives water in alkaline solutions and peroxide in acid, which is exactly opposite of what is observed with face-to-face Co porphyrins. This could be explained by assuming that  $O_2^-$  is the intermediate: in acid it will be rapidly attacked by protons, forming hydrogen peroxide. In alkaline solution it is more stable, enabling bridge adsorption and leading to water formation. The difference in behaviour observed for cofacial and planar dicobalt complexes is due to the binding of oxygen molecule in a trans- and cis-manner respectively. They have also reported on the behaviour of a set of cobalt porphyrines having  $\pi$ -acid ligands pendant to the porphyrin ring as electrocatalysts for the reduction of  $O_2$ . Four electron reduction of  $O_2$  to water can also be achieved by using two different metal centres, as proposed by Bettelheim *et al.* (1990) and Steiger *et al.* (1993) for electropolymerized layers of Co and Mn tetra(o-aminephenyl)porphyrins and multilayers of Co tetra-4-pyridyl porphyrin. Tse *et al.* (1997) have found that electropolymerized Co tetraaminophthalocyanines (CoTAPc) also promotes the four electron reduction mechanism. However, it was only observed at high polarizations. At low polarization, peroxide is formed on poly-CoTAPc.

From the studies on oxygen reduction activity of various Fe chelates it has been found that the nature of ligand is also an important in hydrogen peroxide reduction or

decomposition. When comparing the activity of FeTPP-Cl (Bouwkamp-Wijnoltz *et al.*, 1998) and FeTPyPz, the latter does not promote the reduction of peroxide. Tanaka *et al.* (1989) found the formation of water at low overpotentials whereas peroxide at high overpotentials on FeTPyPz (iron tetrapyrrolineporphyrine). A relation exists between an increasing hydrogen peroxide decomposition rate constant and increasing oxygen reduction activity in acid solution. All the experimental results show that iron porphyrin and phthalocyanine derivatives exhibited highest oxygen reduction activity with single site for O<sub>2</sub> adsorption. In order to increase the activity and stability, metal chelates were adsorbed on carbon and investigated the oxygen reduction measurements. It has been shown that the carbon with basic functional groups is the most effective type of support. However, the activity and stability of these Co and Fe chelates was far less compared to the Pt electrocatalysts.

Later it was reported (Bagotzky *et al.*, 1977; van Veen *et al.*, 1981; Scherson *et al.*, 1983; Scherson *et al.*, 1986; Sawaguchi *et al.*, 1990; Widelov and Larson, 1992; Ladouceur *et al.*, 1993; Jiang and Chu, 2000; Faubert *et al.*, 1996; Lalande *et al.*, 1996; Gojkovic *et al.*, 1998; Gojkovic *et al.*, 1999; Schulenburg *et al.*, 2003) that the heat-treatment of macrocycles supported on carbon supports improves their stability as electrocatalysts for oxygen reduction and, in some instances, enhancing their oxygen reduction activity. Usually heat treatment is carried out in argon or nitrogen atmosphere at temperatures between 673–1273 K. The maximum activity has been observed in the range of 773-1073 K for most of the chelates adsorbed on carbon support. The optimum temperature for maximum activity depends on the metal, the ligand, and nature of support. What is left on the electrode surface after the heat treatment consists largely of the metal atoms of the porphyrin. The distances between such metal atoms will correspond to the diameter of the adsorbed organic.

Correspondingly, the high temperature will have bound the atom to the carbon surface. Thus, the individual atoms would be acting catalytically; they would not be able to lose catalytic power by aggregating to form clusters in which most of the atoms are hidden from reactants inside the clusters. The composition and the structure of the electrocatalytic center formed upon pyrolysis were not clear. Still some controversies exist. But it was accepted that the creation of M-N<sub>4</sub> moiety on carbon matrix or simply MN<sub>4</sub>C<sub>x</sub> species are the active species for oxygen reduction.

Studies on iron and cobalt macrocycles adsorbed on carbon support had shown that the reduction of oxygen is enhanced by the presence of MN<sub>4</sub>C<sub>x</sub> (where M= Fe and Co) species. At first Joyner *et al.* (1982) proved the existence of CoN<sub>4</sub> with Co-N distance as  $\approx 1.95$  Å at medium temperatures by using EXAFS in the case of cobalt porphyrins (CoTPP, CoTBP). Later XAS measurements performed on Co chelates by van Wingerden *et al.* (1988), Martin Alves *et al.* (1992) also identified the existence of CoN<sub>4</sub> species. XRD, XPS, TEM and ToF-SIMS studies on heat-treated FeTPP/C and CoTPP/C catalysts by Faubert *et al.* (1996) had shown the presence of metal-N<sub>4</sub> part in the temperature range of 773-973 K, where the ORR activity is maximum and disappearance of metal-N<sub>4</sub> moiety and presence of metal particles, metal oxides and metal carbides at higher temperatures ( $>1073$  K). Mossbauer spectral studies (Nath *et al.*, 1993) of unsupported FePc and CoPc heat-treated at 773-973 K also indicate that the N<sub>4</sub>-M moiety is mainly retained. Lalande *et al.* (1996 and 1997) also observed the ions containing the metal bound to nitrogen using ToF-SIMS for Co and Fe phthalocyanines pyrolyzed at temperatures upto 973 K and porphyrins pyrolyzed upto 1073 K. Several authors (Faubert *et al.*, 1996; Lalande *et al.*, 1996; Wang *et al.*, 1999) reported the generation of active sites by using independent metal, nitrogen and carbon precursors. Even though the results were satisfactory, valuable information

was obtained. Choi *et al.* (2002) also reported the presence of Fe-N<sub>4</sub> at medium temperatures and iron oxides and carbides at higher temperatures based on EXAFS measurements. ToF-SIMS measurements studied by Lefevre *et al.* (2000, 2002 and 2003) on FeTMPP on carbon also proved the existence of FeN<sub>4</sub> at medium temperatures (873 K) and FeN<sub>2</sub> at high temperatures (1073 K). Recently, the same authors (2005) performed ToF-SIMS studies on CoTMPP adsorbed on carbon and proved the existence of CoN<sub>4</sub> moiety alone where the ORR activity is maximum but not observed the CoN<sub>2</sub> moiety at any heat treatment temperature.

In literature, oxygen reduction activity was measured in terms of current density at a potential where the oxygen reduction kinetics is more favorable and/or potential at which maximum reduction current occurs. But in commercial point of view, one requires a catalyst, which has the ability to reduce oxygen at higher potentials with high current densities. Among the various substituted Fe and Co macrocycles, iron and cobalt tetra methoxy- phenylporphyrins exhibited higher activity and stability. Most of the authors concentrated on Fe-based catalysts because of their high activity towards oxygen reduction compared to Co-based catalysts. The results obtained by fabricating the electrodes with CoTcPc/C for different temperature treatments show that the activity of the electrodes increases with temperature up to 1173 K whereas activity was lost at 1273 K. The catalyst that is more active is comparable with that of Pt/C. Life time tests conducted on the same catalysts show the better stability up to 20 h of cell operation and also comparable with that of Pt/C (Lalande *et al.*, 1995). Stability of the active sites generated by employing ployvinylferrocene as iron precursor and acetonitrile as a source of nitrogen exhibited the stable currents upto 300 h under fuel cell conditions. The recorded current density per mg of metal is about 1/3 of a comparable Pt containing catalyst (Lalande *et al.*, 1997). Impressive

activities for oxygen reduction was obtained using catalysts prepared via the pyrolysis of nitrogen containing polymers such as polypyrrole, polyacrylonitrile on carbon containing transition metal ions (Gupta *et al.*, 1989). This behaviour is presumably analogous to that of the metal chelate systems. Jiang and Chu (2000) have investigated methanol tolerance for the performance of the oxygen cathode for a series of heat-treated metalloporphyrins. The heat-treated CoTPP/FeTPP mixture at 873 K exhibits optimum catalytic activity for the reduction of oxygen with an onset potential of 0.9 V vs. NHE, which is comparable with that of platinum black (1.0 V vs. NHE). The catalytic activity for oxygen reduction on the heat-treated metalloporphyrin is not affected by the presence of methanol in an acidic electrolytic solution. Under similar conditions, platinum catalysts are severely affected by the presence of the same amount of methanol. No long-term life tests were reported but a loss of activity during the first 20 h of operation probably occurs as reported for other similar catalysts (Lalande *et al.*, 1995). Convert *et al.* (2001) investigated the catalytic activity of cobalt tetrazannulene (CoTAA) in half-cell conditions. The activity for the reduction of oxygen of this electrode is not affected when methanol is present in the electrolyte, whereas a noticeable decrease in activity is observed on Pt-based cathodes under the same conditions. Moreover, stability of it was comparable with that of Pt-based electrodes over a period of 90 min. Gupta *et al.* (1998) and Sun *et al.* (2001) have studied heat-treated  $\mu$ -oxo-iron(III)tetramethoxy phenyl porphyrin, iron tetramethoxy phenyl porphyrin and iron(III)octaethylporphyrin adsorbed on high surface area carbons and found high stability for oxygen reduction and insensitivity to the presence of methanol. The activity of these electrodes is not modified after periods of 24 h. the activity of these catalysts tested in a mini-fuel cell similar to that of supported platinum (E-tek). The electrolyte was 85% H<sub>3</sub>PO<sub>4</sub> equilibrated Nafion 117 membrane at 398 K and hydrated Nafion membrane at 333 K. However, supported

platinum in the presence of methanol under the same conditions of the supported macrocycles showed decreased activity. RDE measurements show that the ORR activity of heat-treated (at 1073 K) FeTMPP-Cl/BP catalysts is about 1 order of magnitude lower than that of commercial platinum catalysts (20% Pt/C from E-TEK) (Lefevre *et al.*, 2000). The percentage H<sub>2</sub>O<sub>2</sub> measured at their maximum catalytic activity is quite low (<5%) and comparable with that observed on commercial catalyst (Lefevre *et al.*, 2003). ORR activity of various metal macrocyclic complexes and pyrolyzed macrocycles is summarized in Table 1.6. The negligible amount of hydrogen peroxide formed as an intermediate in these pyrolyzed catalysts reflects the stability. It can be concluded that heat-treated macrocycles supported on carbon are promising for applications in low temperature fuel cells, if the decrease in activity with time of operation can be overcome.

### **1.7.1 ORR Mechanism**

For a qualitative explanation of the activity of these systems, different concepts were developed. Application of the MO theory (Jahnke *et al.*, 1976) to these systems has shown that the highest interaction of O<sub>2</sub> with the central metal ion is obtained with Fe(II) and Co(II). The higher this interaction, the more the O-O bond is weakened and the more easily the molecule is reduced. Another approach has been given by Ulstrup (1977). If the electronic levels of the electrode and reactant lie too far apart, the transition of electrons is improbable. The catalysts should then act as a mediator supplying intermediate levels thus increasing the probability of electron transport. A third concept is that of redox catalysis developed by Beck (1977).

Table 1.6 Electrocatalytic activity and selectivity towards oxygen reduction of transition metal macrocycles compared to Pt

Catalyst	Electrolyte medium	No. of electrons transferred	Catalytic activity towards O <sub>2</sub> reduction vs. Pt	Reference
CoPc	Alakli/Acid	2	n. r	Zagal, 1992 Zagal <i>et al.</i> , 1980
CoTPP	Acid	2	n. r	Zagal, 1992
Co-Co (face-to-face porphyrins)	Acid	4	n. r	Collman <i>et al.</i> , 1980
Pillared dicobalt porphyrins	Acid	4	n. r	Chang <i>et al.</i> , 1984
Planar dicobalt porphyrins	Alkali	4	n. r	van der Putten <i>et al.</i> , 1988
Poly-CoTAPc	pH: 1.65-13	4	n. r	Tse <i>et al.</i> , 1997
FePc	Alkali	4	n. r	Faubert <i>et al.</i> , 1996; Lalande <i>et al.</i> , 1996
FeTSPc	Alkali	4	n. r	Zagal, 1992
FeTPyPz	Alkali	4	n. r	Tanaka <i>et al.</i> , 1989
HT-FeTPPCl at 873 K	Acid	4	n. r	Bouwkamp-Wijnoltz <i>et al.</i> , 1998



FeAc/pyrrole black at 1073 K	Acid	3.9	n. r	Gupta <i>et al.</i> , 1998
FeTMPy/VulcanXC72R at 1073 K	Acid	2.7	n. r	Sawaguchi <i>et al.</i> , 1990
FeTPPS/VulcanXC72R at 1073 K	Acid	2.7	n. r	Sawaguchi <i>et al.</i> , 1990
FeNPc/PrintexXE2 at 773 K	Acid	3.5	n. r	Biloul <i>et al.</i> , 1994
Fe(phen) <sub>3</sub> /VulcanXC72R at 1073 K	Acid	3.7	n. r	Bron <i>et al.</i> , 2002
HT-CoTPP/FeTPP at 873 K	Acid	4	Comparable	Jiang and Chu, 2000
HT-FeTMPP-Cl at 1073 K	Acid	4	Comparable	Gupta <i>et al.</i> , 1998; Lefevre <i>et al.</i> , 2000
CoTAA	Acid	2	Comparable	Convert <i>et al.</i> , 2001
CoTcPc/VulcanXC72R at 973 K	Acid	n. r	Comparable	Lalande <i>et al.</i> , 1995
FePc/VulcanXC72R at 1173 K	Acid	4	Comparable	Lalande <i>et al.</i> , 1995

In this concept the redox potential of the central metal ion is crucial. In this concept, the interaction of O<sub>2</sub> molecule with metal center in the macrocycle causes a partial electron transfer from the frontier orbitals of metal to the frontier orbitals of the O<sub>2</sub>. The precursor or adduct formed, undergoes further reduction to give intermediate species like peroxide which can be the product or decomposed/reduced further to give water. The crucial steps in the catalytic cycle are given as follows:



According to this redox mechanism, the redox potential of M(III)/M(II) must be located within an appropriate, rather narrow window of potential values to obtain maximum activity. When the activity for the oxygen reduction is compared with the redox potential of the M(III)/M(II) transition of different metal chelates a volcano shaped curve is obtained (Trasatti, 1980). However, recent studies of different substituted Pc's have revealed that the lower the electron density on the metal center, the higher the catalytic activity for O<sub>2</sub> reduction. For studies conducted with substituted Co phthalocyanines, when the logarithm of the rate constant (taken at constant potential) of the electroreduction of O<sub>2</sub> is plotted versus the Co(III)/Co(II) redox potential of different substituted phthalocyanines (Co-Pcs), for graphite electrodes modified with these complexes, a straight line is obtained. Log k decreases as the driving force of the phthalocyanines increases (the driving force is represented by the Co(III)/Co(II) redox potential) so the greater the reducing power of the CoPcs, the less is the activity for O<sub>2</sub> reduction. This was explained in terms of the chemical intermolecular hardness of the system, i.e., the more the separation between the energy of the frontier orbitals of the donor (Co-Pc) and the acceptor (O<sub>2</sub>), the less the reactivity. These studies reveal that questions still remain open on the role of the

redox potential in determining the catalytic activity. However, most authors agree that the redox mechanism requires the stability of the 3+ and 2+ oxidation states of the metal, needed for oxygen activation in the potential region of interest for O<sub>2</sub> reduction. It has been found that Co and Fe porphyrins are active as long as the 3+ oxidation state is accessible at a given potential. However, for some Co complexes, O<sub>2</sub> reduction takes place at potentials far removed from the potential of the Co(III)/Co(II) (Collman *et al.*, 1980). Most authors also agree that the Fe(II)/Fe(I) redox couple is the one that plays the crucial role in the activation of the O<sub>2</sub> molecule (Zagal, 1992). Collman *et al.* (1980) established the mechanistic details of the oxygen reduction process on dicobalt face-to-face porphyrins by bridge mode of adsorption of O-O on two cobalt metal centres followed by cleavage to form water as the main product. Since the structure of MN<sub>4</sub>C<sub>x</sub> species generated by the pyrolysis of the carbon supported macrocycles was not known in literature, mechanism was not well established.

### **1.8 Other Electrocatalysts**

Transition metal ions in oxides, precisely because of their ability to switch between different valencies, possess appreciable chemical and/or electrocatalytic activity, which make them versatile materials for chemical and electrochemical reactions (Trasatti, 1980). Transition metal ions in oxides, which can exist in various valency states, exhibit metal-like conductivity if half-filled d-bands are present. Many oxides have been investigated but it has been mainly focused on perovskites, spinels and pyrochlores since these materials can be expected to provide reversible pathway for oxygen reduction. Alternate to platinum based catalysts, various simple metal oxides such as RuO<sub>2</sub>, IrO<sub>2</sub>, Fe<sub>3</sub>O<sub>4</sub>, PbO<sub>2</sub>, NiO, TiO<sub>2-δ</sub>, CrO<sub>2</sub>, PdO<sub>x</sub>, CeO<sub>2</sub>, ZrO<sub>2</sub>, SnO<sub>2</sub>, Ta<sub>2</sub>O<sub>5</sub>, TiO<sub>2</sub>, WO<sub>3-δ</sub> and MnO<sub>2</sub> [Matsuki and Kamada, 1986; Chang *et al.*, 1997; Vago and

Calvo, 1995; Manoharan and Goodenough, 1995; Kim *et al.*, 2007; Liu *et al.*, 2005) were investigated for oxygen reduction. Comparison of electrocatalytic activities towards oxygen reduction has led to the following order: RuO<sub>2</sub> and IrO<sub>2</sub>>Co and Ni containing oxides>Fe, Pb and Mn containing oxides. MnO<sub>2</sub> shows some promise due to its low cost and its high catalytic activity for the oxygen reduction for metal-air battery applications (Yang and Xu, 2003). Oxygen reduction studies on various Perovskites (Matsumoto *et al.*, 1977), spinels (Hays *et al.*, 1993, Nissinen *et al.*, 2002) and pyrochlores (Horowitz *et al.*, 1983; Raghuvver *et al.*, 2002) indicates that the intrinsic activity as well as stability of these metal oxides in acidic medium is less compared to that of the Pt based materials. Even though these materials do not exhibit significant activity, the experience gained from the studies led to the search of new fascinating materials for oxygen reduction.

Owing to the good electrical conductivity, corrosion resistance and eventual catalytic activity, metal nitrides (Mazza and S. Trasatti, 1963; Giner and Swette, 1966; Zhong *et al.*, 2006; Zhong *et al.*, 2007), metal carbides (Mazza and Trasatti, 1963; Voinov *et al.*, 1971) and metal oxynitrides (Ishihara *et al.*, 2005; Liu *et al.*, 2007) were exploited for oxygen reduction in aqueous solutions. Mazza and Trasatti (1963) investigated the oxygen reduction activity of TiN, TiC, TaC and WC in acidic solutions. They observed superior activity of WC than other investigated systems. The order of activity is, TaC<TiC<TiN<WC. Later Giner and Swette (1966) evaluated the oxygen reduction activity of TiC and TiN in alkaline solutions and observed higher activity of TiN than TiC followed by Ti. Even though WC exhibited good catalytic activity, it is far less compared to the Pt catalysts and also not stable for long time. Recently, Lee *et al.* (2004) examined the Ta-added WC in acid electrolyte and observed the reduction current of the WC+Ta catalyst for the ORR at a potential of 0.8 V vs. dynamic

hydrogen electrode higher than that of WC (0.35 V). The enhanced electrocatalytic activity for the ORR might be caused by the presence of W carbide, which exists on the surface and/or sub-surface. The stability of the WC was significantly increased by the addition of Ta compared to the pure WC. Recently, Mo<sub>2</sub>N (Zhong *et al.*, 2006), W<sub>2</sub>N (Zhong *et al.*, 2007), TaO<sub>x</sub>N<sub>y</sub>/C (Ishihara *et al.*, 2005) and ZrO<sub>x</sub>N<sub>y</sub>/C (Liu *et al.*, 2007) were investigated for oxygen reduction and tested them as a cathodes for PEMFCs. But the performance of these materials was 15-20 times less compared to the commercial Pt electrocatalysts.

### **1.9 Nanomaterials and Electrocatalysis**

Nanomaterials are believed to exhibit unique science. The interest in nanomaterials arises from the fact that their physico-chemical properties are a function of their dimensions. Nanomaterials are materials whose characteristic length scale lies in nanometric range i.e., 1-100 nm. These materials display properties intermediate between quantum and bulk materials because of their size and large surface area-to-volume ratios. In comparison to bulk, materials in nano regime possess several advantageous properties like short range ordering, enhanced interaction with environments due to the high number of dangling bonds, great variety of the valence band electron structure and self-structuring for optimum performance in adsorption and electrocatalysis (Cao, 2004). The unusual physicochemical properties of nanomaterials are due to the comparable size of nanomaterials to the Bohr radius of the excitons as well as with the size of molecules.

(i) As a consequence of the size reduction, larger the portion of their constituent atoms located at the surface (surface to volume ratio) and higher the surface area (Klabunde *et al.*, 1996). In general, increases in the surface area provide more adsorption of reactant molecules on its surface, which results the higher catalytic

activity. Similarly, the increase in the number of surface atoms creates more number of active site, which ultimately results higher catalytic activity. In metallic nanoparticles, a large surface area to volume ratio permits effective charge-transfer.

(ii) Nanomaterials are characterized by a very high number of low coordination number atoms at edge and corner sites which can provide a large number of catalytically active sites (Bell, 2003). Such materials exhibit chemical and physical properties characteristic of neither the isolated atoms nor of the bulk material. The excess surface free energy makes the particles more reactive and structurally sensitive towards their environment. Modern surface science studies indicate that, during chemisorption and catalytic reaction, these particles restructure, and the adsorbed molecules also possess a high degree of surface mobility. Since the atoms in the nanoparticles have low coordination, such adsorbate-induced restructuring is facile (Hammer and Nørskov, 2000). As any materials interact with their environment through solid/gas, solid/liquid, and solid/solid interfaces, the nanometer scale surface created can be modified to perform certain functions.

(iii) As we go down in particle size, more will be surface unsaturation, defects and the proportion of edge/corner ions to the total surface ions (Klabunde *et al.*, 1996). During size reduction the surface/volume ratio is enlarged and an interface is formed which is transformed into a metastable system through a series of quasi equilibrium states. The key issue in the field of nanomaterials is the easy functionalization of the interface due to its high excess free energy acquired. The surface irregularities, i.e. the presence of steps, kinks, terraces, as well as the "dangling" bonds of the atoms located at these-sites, make it possible to create highly reactive species.

(iv) Nanosize metal particles play a crucial role in surface reactivity, chemisorption and electrocatalysis (Hammer and Nørskov, 2000; Lima *et al.*, 2007; van Bokhoven and Miller, 2007). The small size significantly affects the electrochemical behavior of

the nanocrystal materials. While going from bulk to nano size, the semiconductor energy levels (higher and lower are the positions of CB and VB respectively) become more separated from each other and the effective band gap increases. In the case of metals also, the valence and conduction band energy levels are separated to certain extent when the size of the particle is reduced. In this situation the metal does not exhibit bulk metallic or semiconducting behavior. As a result of increase in band gap, the conductivity as well as the density of states in the conduction and valence band will be reduced. Because of this unusual behaviour of metals and semiconductors while going from bulk to nano, the Fermi level and density of states at the interface will alter. Since the Fermi level is associated with the redox ability of the system, there will be a considerable change in the rate of redox processes. It would therefore be possible to control the electrocatalytic activity of metals and semiconductors by changing their size.

### **1.10 Methods for the Preparation of Supported Metal Nanoparticles**

One of the paths in the field of electrocatalysis is the preparation of metal catalysts on suitable support materials. It is well known that the electrocatalytic activity of a catalyst strongly depends on particle size, morphology and particle distribution. So in the preparation of supported metal nanoparticles, control of the metal particle size with size distribution as narrow as possible is needed; furthermore, stability of the originally metastable dispersion must be assured. The importance of the narrow size distribution in nanosize range is emphasized by the fact, that in the 1-10 nm region relatively small changes in the size can be accompanied by significant morphological changes (viz. change in the fraction of the coordinatively unsaturated corner, kink and edge atoms) and seriously influence redistribution in the valence band density of states (van Bokhoven and Miller, 2007).

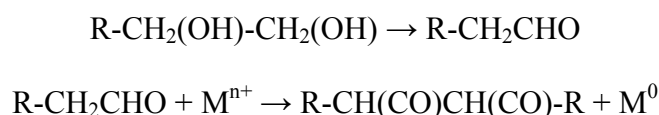
In terms of experimental approaches, different synthetic methods have been used in the synthesis of supported metal catalysts. The major focus has been the effect of synthesis conditions on catalyst morphology and catalytic activity. In the conventional impregnation approaches, a solution of metal salt(s) is prepared and mixed with the carbon support. The resulting slurry is dried to remove the solvent and then usually heat-treated and/or reduced to decompose the salt to give the desired form of the catalyst. This is a simple and one-step preparation method, but it provides a poor control over the particle size and size distribution, especially for the preparation of 20-60 wt.% metal loading on supports (Chan *et al.*, 2004). A variation of this method is incipient-wetness impregnation. In this method, volume of the impregnating metal solution is chosen to match the pore volume of the carbon. This method has the advantage that metal is only deposited within the pore structure of the carbon. But the particle size cannot be controlled. In addition, various synthesis procedures were adopted for the preparation of support metal catalysts. It is observed that both geometric as well as electronic factors will vary depending on the method of preparation. The geometric factors (interatomic distance, the crystal structure, its grain size, and concentration and types of defects and irregularities) and electronic factors ( $d$  character,  $d$ -band vacancies, and more general characteristic features such as work function and latent heat of sublimation) are known to influence the electrochemical behaviour of the prepared catalysts (Antolini *et al.*, 2003). So the development of techniques in order to control the size (monodisperse nanoparticles are preferred) and composition of the supported catalyst has been a major area of research.

In the last few years, polyol reduction method and reverse microemulsion method (RME) have been chosen as versatile methods to generate metal colloids and/or



clusters on the nanoscale with greater uniformity and controllable composition. Subsequently, the prepared nanoparticles will be added to the dispersed support and dry/activate under different conditions to prepare the supported metal nanoparticles.

Polyol reduction method (Sun *et al.*, 2000) involves the preparation of metal colloids by the reduction of metal precursor by polyol in the presence of capping agents. This method also has been used to prepare bimetallic catalysts with narrow particle size distributions, controllable composition and alloy structures. The reduction of metal precursor by polyol is represented below.



where R – alkyl chain and M – metal.

Binary metallic alloys can be prepared either by the reduction of corresponding metal precursors with polyol (like ethylene glycol or glycerol or hexadecanediol or octanediol) or reduction of one metal precursor with polyol and decomposition of second metal in high temperature solutions.

The size and shape of the nanoparticles can be controlled by varying the reducing agent (polyol), capping agents, reaction temperature, metal precursors (Li *et al.*, 2001; Shevchenko *et al.*, 2003). This method has been employed to prepare a variety of nanomaterials, include metal alloys (Sun *et al.*, 2000), metal oxides (Hyeon *et al.*, 2001) and metal sulfides (Liu *et al.*, 2007).

Reverse micellar solutions are transparent, isotropic, thermodynamically stable water-in-oil microemulsions with nanosized water droplets which are dispersed in a continuous oil phase and stabilized by surfactant molecules at the water/oil interface (Hoar and Schulman, 1943). The surfactant-stabilized water pools not only act as

nanoreactors for processing reactions but also inhibit the excess aggregation of particles because the surfactants could adsorb on the particle surface when the particle size approaches that of water pool. Consequently, the particles obtained in such a medium are generally very fine and uniform. Spherical reverse micelles, which minimize surface energy, are the most common form (Capek, 2004; Eriksson *et al.*, 2004).

This method involves the preparation of two separate microemulsions, incorporating the different reactants. Upon mixing, nucleation occurs on the micelle edges as the water inside them becomes supersaturated with reactants. Growth then occurs around this nucleation point, with the arrival of more reactant fed via intermicellar exchange. It would appear that growth initially begins at the interface and then moves into the core of the micelle. The rate limiting step for particle growth is intermicellar exchange (Capek, 2004). Control of this exchange via interfacial fluidity of the surfactant is believed to be a significant factor. Particle growth has shown to be strongly dependent on intermicellar exchange rates. The resultant particle size appears to be dependent on dominant parameters: type of solvent, type of surfactant/co-surfactant, concentration of the reagents, ionic additives and composition via [water]:[surfactant] ratio, W (Eastoe *et al.*, 2006). A number of nanoparticle systems have been prepared in reverse micelles, including metals (Taleb *et al.*, 1997), metal alloys (Raghuveer *et al.*, 2006), metal oxides (Raghuveer *et al.*, 2002) and metal chalcogenides (Haram *et al.*, 1996).

### **1.11 Motivation and Objective of the Present Investigation**

At present, carbon supported platinum is the best and commercially exploited electrocatalyst for oxygen reduction. But the overpotential of 300-400 mV under typical experimental conditions, corrosion at high potentials of +0.8 V vs. NHE and sluggish kinetics for oxygen reduction on Pt, limit its practical application. Moreover,

Pt is expensive and less abundant. One of the possible ways to overcome these difficulties is the dispersion of Pt on carbon support or alloying it with suitable metal and supported on carbon. Another way is the replacement of Pt by possible Pd or Ru or Fe or Co- based electrocatalysts.

The main objective of the present work is to develop carbon supported Pt and non-Pt electrocatalysts for oxygen reduction reaction. Conventional metals and metal alloys, chalcogenide and macro-cycle based systems have been examined for the oxygen reduction reaction in this study. The thesis work is focused on the following aspects.

- Synthesis of carbon supported Pt nanoparticles of different sizes by polyol reduction method and evaluation of the optimum size of Pt for oxygen reduction.
- Synthesis of carbon supported Pt alloy (Pt-Cr, Pt-Co and Pt-Fe) nanoparticles by polyol reduction method and examining the role of the alloying element on the enhanced oxygen reduction activity.
- Synthesis of carbon supported Pd and Pd alloys (Pd-Co-M; M = Mo and Au) by reverse microemulsion method and identifying the role of the alloying element on the enhanced oxygen reduction activity.
- Synthesis of carbon supported  $Ru_xSe_y$  ( $x = 1$  and  $y = 0, 0.2, 0.4, 0.6, 0.8$  and  $1.0$ ) catalysts by reverse microemulsion method and study of the optimum composition of Ru/Se for maximum oxygen reduction activity.
- Studies on the facile reduction of oxygen on  $MN_4$  (M = Fe and Co) clusters using Density Functional Theory (DFT).
- Preparation of  $MN_4C_x$  (M = Fe and Co) clusters in nano-size range by pyrolyzing macrocyclic complexes supported carbon and study of the oxygen reduction activity.

## CHAPTER 2

### EXPERIMENTAL METHODOLOGY

#### 2.1 CHEMICALS AND MATERIALS USED

The chemicals used for the preparation of Pt, Pt-Fe, Pt-Co and Pt-Cr nanoparticles are Platinum(II) acetylacetonate, Fe(II) chloride,  $\text{Co}_2(\text{CO})_8$ ,  $\text{Cr}(\text{CO})_6$ , diphenyl ether (99%), Octyl ether (99%), 1,2-hexadecanediol (97%), Oleic acid (99%), Oleylamine (98%), nonanoic acid (96%) and nonylamine (98%) which were obtained from Sigma-Aldrich.

$\text{H}_2\text{PdCl}_4$ ,  $\text{HAuCl}_4$  and  $\text{MoCl}_5$  from Sigma-Aldrich,  $\text{CoCl}_2$ , Triton-X-100 and hydrazine from Merck were used as received for the preparation of carbon supported Pd-Co-M (M = Au and Mo) alloys. Ruthenium(III) chloride and selenous acid obtained from Sigma-Aldrich, AOT obtained from Acros Organics and sodium borohydride obtained from Merck were used as received for the preparation of carbon supported  $\text{Ru}_x\text{Se}_y$  ( $x = 1$  and  $y = 0-1$ ).

Fe(II)chloride, Co(II)acetate and pyrrole (99%) from Sigma-Aldrich, anisaldehyde and benzaldehyde from Merck were used as received for the preparation of Fe and Co macrocyclic complexes.

Water purified by a Milli-Q water purification system was used through out the experimental work. Carbon black (CDX975), received from Columbian Chemicals Company, USA was used as the support for the catalysts. Glassy Carbon (GC) disc ( $0.07 \text{ cm}^2$ ) and polishing kit were purchased from Bio Analytical System, USA. 5 wt% Nafion solution was purchased from Aldrich. All other chemicals and solvents used in the investigation were of analytical (AR) grade and were obtained from S. D. Fine chemicals, India. These chemicals were used as such without further purification.

## **2.2 PURIFICATION OF GASES**

### **2.2.1 Purification of Argon**

High pure argon from M/s. Karnataka Oxygen Ltd., was bubbled through a series of gas washing bottles. The first two of the wash bottles contained 50 g of amalgamated zinc and 200 ml of 0.1 M ammonium metavanadate in hydrochloric acid. The next two traps had distilled water and concentrated sulphuric acid respectively to remove vanadium and moisture from the gas stream. Finally, the gas was passed through a silica gel column to absorb traces of moisture and thus dry argon gas free of oxygen was obtained.

### **2.2.2 Purification of Oxygen**

Oxygen gas used for the electrochemical reduction of oxygen reaction was obtained from M/s Indian Oxygen Ltd. and the gas was used as-received.

## **2.3 ELECTROCHEMICAL MEASUREMENTS**

Electrochemical activity of the catalysts was determined by cyclic voltammetry using a potentiostat (BAS 100 electrochemical analyzer). All experiments were performed at room temperature in a conventional one-compartment electrochemical glass cell assembled with glassy carbon (GC) disk as the working electrode, Ag/AgCl, 3.5 M KCl (+0.205 V vs. NHE) as the reference and Pt foil as the counter electrodes, respectively.

## **2.4 CHARACTERIZATION OF THE CATALYSTS**

### **2.4.1 X-Ray Diffraction Study**

X-ray diffraction (XRD) patterns for the powder samples were recorded on a Rigaku Miniflex X-ray diffractometer using a Ni filtered Cu K $\alpha$  source operated at 30 kV at a scan rate of 0.05° s<sup>-1</sup>. Calculation of the lattice constants and the metal crystallite

sizes were based on the angle position and on the full width at half maximum (FWHM) of the peaks, respectively. The values of the lattice constants were determined by means of the least-square method.

For crystallite size measurements, X-ray diffraction patterns were recorded at scan rate of  $0.025^\circ \text{ s}^{-1}$  and metal crystallite size was calculated by X-ray line broadening technique employing Debye-Scherrer equation (Patterson, 1939).

$$L = \frac{0.9\lambda}{\beta_{1/2} \cos \theta} \dots\dots\dots (2.1)$$

where L is the crystallite size,  $\lambda$  is the wavelength of the X-ray (1.5406 Å),  $\theta$  is the angle at the position of the peak maximum and  $\beta_{1/2}$  is the width (in radians) of the diffraction peak at half height.

#### **2.4.2 X-ray Photoelectron Spectroscopy**

X-ray photoelectron spectroscopy (XPS) measurements of the as-synthesized Pt/CDX975 was carried out with Omicron nanotechnology instrument using an Mg monochromatic X-ray ( $h\nu = 1253.6 \text{ eV}$ ) at a power of 350 W operated under the base pressure of  $\leq 2 \times 10^{-9}$  mbar. The spectra were referenced to Cu  $2p_{3/2}$  (932.7 eV), Ag  $3d_{5/2}$  (368.2 eV), and Au  $4f_{7/2}$  (84.0 eV) lines. The powder samples were mounted onto the holder using the conductive double-side adhesive tape. The catalyst surface was scraped *in situ* to remove any surface contamination that could arise from atmospheric components like water and  $\text{CO}_2$ . Due to the conductive nature of the samples, charging effects were not observed. The energy resolution of the spectrometer was set at 1.1 eV at pass energy of 50 eV. The binding energy (BE) was calibrated with respect to Ag  $3d_{5/2}$  core level at 368.2 eV.

### **2.4.3 Estimation of Metal(s) Loading**

Platinum in carbon supported Pt or Pt alloys, cobalt in carbon supported Pt-Co alloy or  $\text{CoN}_4\text{C}_x$  clusters and Chromium in carbon supported Pt-Cr alloy catalysts were extracted from the catalyst by suitable extracting method and analyzed by UV-Vis spectrophotometer (Perkin-Elmer spectrophotometer) calibrated with standard solutions containing known metal contents.

Iron content in carbon supported Pt-Fe alloy or  $\text{FeN}_4\text{C}_x$  clusters were extracted from the catalyst by suitable extracting method and analyzed by standard titration procedure.

### **2.4.4 Scanning Electron Microscopy (SEM)**

Scanning electron microscope with EDX (FEI, Model: Quanta 200) was used to observe the surface morphology and composition of the catalysts. The sample powders were dispersed on a carbon tape before mounting on a sample holder. In order to reduce the charge developed on the sample, gold sputtering was done for 3 min on all the samples. Elemental analysis was performed with the energy dispersive X-ray (EDX) method on the energy-dispersive X-ray spectrometer equipped with Si (Li) detector with energy resolution 130 eV.

### **2.4.5 Transmission Electron Microscopy (TEM)**

Transmission electron microscope (TEM) images were obtained by using a high-resolution JEOL 2010 TEM system with lattice resolution 1.4 Å and accelerating voltage 200 kV. The sample for TEM analysis was prepared by placing a drop of dispersed catalyst onto the carbon coated copper grid and drying it in air at room temperature.

#### **2.4.6 UV-Visible Spectroscopic Analysis**

UV-Visible absorption spectra were recorded using a Perkin-Elmer spectrophotometer in the spectral range of 200-800 nm. The absorption spectra for macrocyclic complexes were recorded in appropriate solvent using 4 cm quartz cell at room temperature. Prior to that, background correction was done with the same solvent.

#### **2.4.7 Elemental Analysis**

The C, H and N analysis was done using the Heraeus CHN analyzer.

#### **2.4.8 Surface Area Measurements**

Surface area and pore size distribution of carbon black (CDX975) were investigated by Brunauer–Emmett–Teller (BET) analyses with nitrogen adsorption–desorption isotherms on a Carlo–Erba sorptometer (Model 1800) instrument at 77 K. The samples were outgassed at 423 K and  $10^{-3}$  torr vacuum for 12 h. For adsorption experiments, ultrahigh pure nitrogen was used at liquid nitrogen temperature. BET method was used to evaluate the surface area and pore volume evaluated at the  $p/p_0$  of 0.999.



## CHAPTER 3

# SYNTHESIS, CHARACTERIZATION AND ELECTROCHEMICAL STUDIES OF CARBON SUPPORTED Pt CATALYSTS FOR OXYGEN REDUCTION

### 3.1 INTRODUCTION

Conventional carbon supported platinum is the active, efficient, applicable and successful catalyst for oxygen reduction (Ralph and Hogarth, 2002; Gasteiger *et al.*, 2005). But Pt is expensive and less abundant. So research efforts are concentrated on the reduction of the amount of Pt in the electrodes by preparing Pt in nanosize range on suitable support material (e.g., carbon) to enhance the oxygen reduction activity as well as to reduce the cost.

There has been great interest in the relationship between the activity of carbon supported Pt catalysts toward ORR and the size of the supported Pt particles. Although efforts were made, the conclusions varied among the different researchers. One of the first investigations towards elucidating particle size and structural dependence was by Zeliger (1967) and Bett *et al.* (1973). Zeliger's work involved Pt deposited on asbestos (Pt crystallite sizes around 5-10 nm), while Bett's study was on commercial Pt blacks and Pt supported on graphitized carbon (Pt crystallite sizes around 3-40 nm). The ORR measurements performed in sulphuric acid electrolyte showed that the specific activity for oxygen reduction was independent of Pt crystallite size. Further support to this conclusion was provided by Kunz and Gruver (1975) and Vogel and Baris (1977) who showed a similar independence of particle size on ORR activity. On the other hand, Blurton *et al.* (1972) and Bregoli (1978) found a decrease in the specific activity for oxygen reduction with diminishing particle size from 12 nm to 3 nm and 2 nm, respectively. The studies reported by Blurton *et al.* (1972) involved highly dispersed Pt on carbon in 20% H<sub>2</sub>SO<sub>4</sub> at 343 K.

He found a 20-fold decrease in activity with a particle size range of 2-12 nm and attributed the results to either a particle size effect or an effect of the support interaction or a combination of both these factors. The study by Bregoli (1978) involved highly dispersed catalysts in 99% H<sub>3</sub>PO<sub>4</sub> at 450 K. He found the specific activity for oxygen reduction to vary by a factor of two in the range of particle size studied (12-2 nm). Peuckert *et al.* (1986) in their investigations with highly dispersed 5, 10, 20 and 30 wt% Pt on carbon catalysts (particle sizes in the range 12-1 nm) in 0.5 M H<sub>2</sub>SO<sub>4</sub> found the maximum ORR activity in the case of 3-4 nm sized Pt particles on carbon. However, a 20-fold decrease in ORR activity as the particle size decreased from 3 to 1 nm is observed, which was in contrast to expectations based on changes in surface area (or dispersion). Sattler and Ross (1986) also observed the same phenomenon in their investigations with dispersed Pt catalysts of crystallite size range 2.8-11.2 nm in 97% H<sub>3</sub>PO<sub>4</sub>. Later, ORR measurements were performed on carbon supported Pt catalysts with different Pt loading by several research groups (Giordano *et al.*, 1991; Giordano *et al.*, 1994; Gamez *et al.*, 1996; Tamizhmani *et al.*, 1996; Antoine *et al.*, 2001; Min *et al.*, 2000; Maillard *et al.*, 2002) also observed the decrease in specific activity (mA cm<sup>-2</sup> of Pt) with a decrease in particle size ( $d < 3$  nm) while specific activity for large ( $d \geq 5$  nm) particles is approximately the same as for bulk platinum. In all the reports, the authors prepared a series of catalysts with 5, 10, 15, 20 and 30 wt.% Pt on carbon and studied the effect of particle size on oxygen reduction based on potentiodynamic rotating ring disk electrode (RRDE) measurements. Usually, supported catalysts contain a wide distribution of particle sizes, so experimental evidence for a particle size effect is often difficult to obtain. Hence, the inconsistent results and conclusions are most probably caused by the

existence of Pt particles in different sizes and uncontrollable shapes by the procedures adopted for the preparation of catalysts. These studies also suggest that the kinetics of oxygen reduction on Pt is not only affected by the particle size but also by the particle shape which may modify the distribution of oxygen adsorption sites on the Pt surface. So if one were able to prepare monodispersed Pt nanoparticles of different sized nanoparticles on carbon and investigate the ORR activity under potentiostatic measurements, it will provide information on the optimum size of Pt for maximum ORR activity.

By means of conventional preparation techniques, namely wet impregnation method and chemical reduction of the metal precursors using reducing agents, achieving desired sizes of Pt nanoparticles (2-5 nm) with homogeneous dispersion on the carbon support appears to be difficult (Cushing *et al.*, 2004). Hence, in order to produce desired sizes of Pt nanoparticles with uniform dispersion on the carbon support, some kind of stabilizing agents, such as surfactants, ligands or polymers, are usually employed during the preparation process (Bönnemann *et al.*, 1996; Prabhuram *et al.*, 2003). Polyol reduction method is one of the suitable methods to generate metal colloids and/or clusters on the nanoscale with greater uniformity (Sun *et al.*, 2000; Liu *et al.*, 2004, Nisha Shukla *et al.*, 2006).

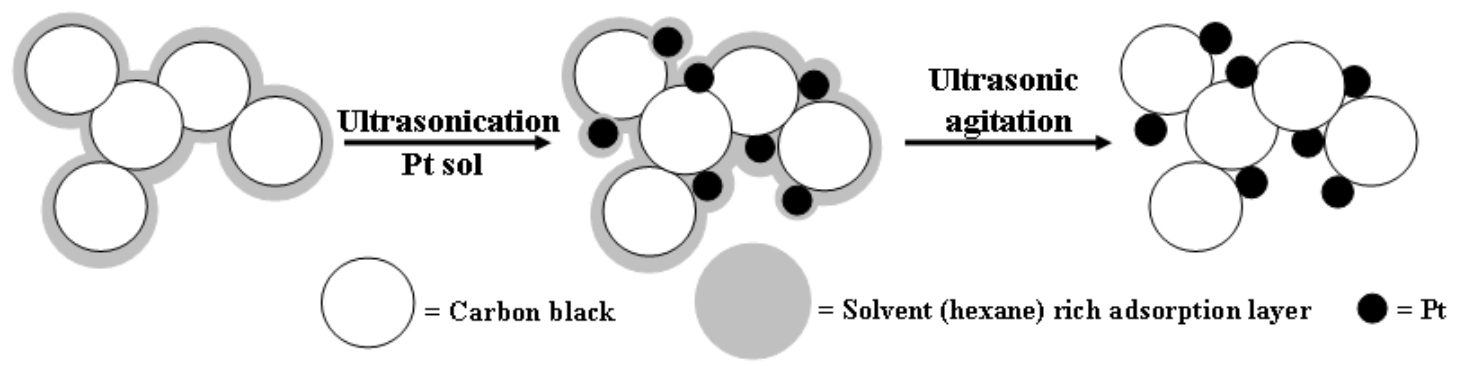
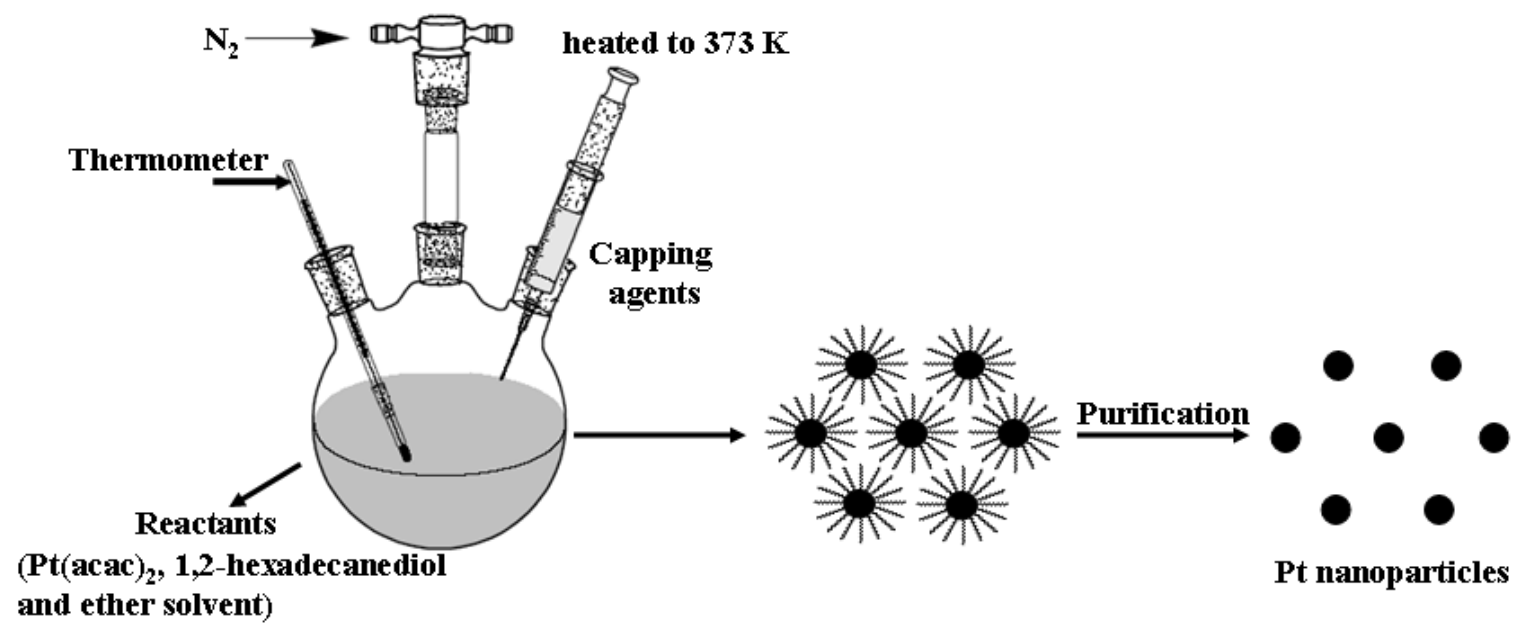
In the present study, monodispersed Pt nanoparticles of different sizes 2-6 nm are synthesized by employing polyol reduction method and loaded onto carbon support to achieve 20 wt.% Pt. The prepared catalysts are characterized by XRD, TEM, EDX and XPS. Steady-state linear sweep voltammetric measurements are performed to investigate the optimum size of Pt for maximum ORR activity.

### 3.2 SYNTHESIS OF Pt NANOPARTICLES OF DIFFERENT SIZES

Monodispersed Pt nanoparticles of different sizes (around 2.0, 2.5, 3.5, 4.0, 5.0 and 6.0 nm) are synthesized by reduction of platinum(II)acetylacetonate with 1,2-hexadecanediol in the presence of long chain carboxylic acid and long chain alkyl amine as protecting agents. To prepare different sized Pt nanoparticles, either the combination of oleic acid and oleylamine or nonanoic acid and nonylamine are used. The used reactants and conditions employed for the preparation of Pt nanoparticles are given in Table 3.1. The synthesis was carried out using standard Schlenk line technique under dry nitrogen. Scheme 3.1 represents the synthesis of Pt nanoparticles and preparation of carbon supported Pt nanoparticles.

Table 3.1 Reactants and conditions employed for the preparation of Pt/CDX975 catalysts

Catalyst	Reactants	Temperature and time	Reference
Pt1C	Pt(acac) <sub>2</sub> , 1,2-hexadecanediol, oleic acid, oleylamine, octyl ether	563-573 K 30 min	Nisha Shukla <i>et al.</i> , 2006
Pt2C	„	563-573 K 45 min	This work
Pt3C	„	563-573 K 60 min	This work
Pt4C	Pt(acac) <sub>2</sub> , 1,2-hexadecanediol, nonanoic acid, nonylamine, diphenylether	523-533 K 30 min	This work
Pt5C	„	523-533 K 45 min	This work
Pt6C	„	523-533 K 60 min	This work



Scheme 3.1 Preparation of carbon supported Pt catalysts

In a typical synthesis, a mixture of 0.5 mmol of Pt(acac)<sub>2</sub> and 2 mmol of 1,2-hexadecanediol were taken under nitrogen atmosphere into a 100 ml three-necked round-bottom flask equipped with a N<sub>2</sub> in/outlet, PTFE coated magnetic stir bar, septa rubber and a thermal probe. Ether solvent (25 ml) was then transferred into the flask and the contents stirred while purging with N<sub>2</sub> at room temperature. The flask was then heated to 373 K and held at 373 K for 20 min. During this hold, 0.5 mmol of long chain alkylamine and 0.5 mmol of long chain carboxylic acid are injected drop wise with syringe into the flask while continuing the N<sub>2</sub> gas purge. Then the suspension was refluxed for different time intervals before cooling down to room temperature under the N<sub>2</sub> atmosphere. Afterwards, all handlings are performed under atmospheric conditions.

The Pt nanoparticles obtained are purified as follows: 25 ml of the suspension taken from the flask is added to 100 ml of ethanol (EtOH) and the mixture was centrifuged for 15 min. The supernatant was discarded and the precipitate is dispersed in 40 ml of hexane and 20 ml of EtOH. Additional small amount of capping agents is added to aid in dispersing the nanoparticles. This suspension is centrifuged for 15 min. The supernatant is transferred to a new centrifuge tube, discarding any precipitate that separated. An additional 50 ml of EtOH is added to this suspension and centrifuged again. The supernatant was discarded and the remaining black precipitate dispersed in hexane is used for further work.

### **3.3 PREPARATION OF THE CARBON SUPPORTED Pt CATALYSTS**

The purified nanoparticles are loaded onto carbon support by scheme 3.1. To make carbon-supported 2.0 nm, 2.5 nm, 3.5 nm, 4.0 nm, 5.0 nm and 6.0 nm Pt catalysts with 20% loading, 100 mg of as-prepared Pt particles dispersed in hexane are mixed

with 400 mg of dispersed carbon black (CDX975). Particles are deposited on carbon support by ultrasonication agitation for 2 h. Finally it is dried at room temperature in vacuum to avoid the oxidation of Pt nanoparticles.

### **3.4 CHARACTERIZATION OF THE CARBON SUPPORTED Pt CATALYSTS**

#### **3.4.1 Salient Features of Carbon Black Support (CDX975)**

The features of the carbon black (CDX975) particles used for electrode support were characterized by SEM, TEM and XRD. Specific surface area and pore size distribution were investigated by Brunauer–Emmett–Teller (BET) analysis. SEM and TEM images of carbon black particles (CDX975) are shown in Fig. 3.1. SEM images show that the carbon black is made of spherical aggregates about 150–200 nm in size (Fig. 3.1(a)) and TEM image reveal that each aggregate being made of elementary particles of about 50-80 nm (Fig. 3.1(b)). Fig. 3.1(c) shows the XRD pattern of carbon black (CDX975) particles. The carbon particles exhibit polyaromatic, turbostratic structural features with (002) and (101) peaks. The broad diffraction peak (002) with large FWHM (full width at half maximum) and low intensity indicates the amorphous nature of carbon black. The fact that the (004) peak is nearly absent relates to the poor crystallinity of the material and specifically to the low average number of graphenes stacked within the coherent domains. The BET specific surface area of the carbon sample is about 260 m<sup>2</sup> g<sup>-1</sup>. The pore diameter distribution is shown in Fig. 3.1(d) and shows that the dominant pore diameter of the carbon particles is in the range of 2–50 nm, which is in the mesopore range. In fact, a mesoporous structure is a key factor contributing to the feasibility of carbon supports in electrocatalysis (Pietron *et al.*, 2002).

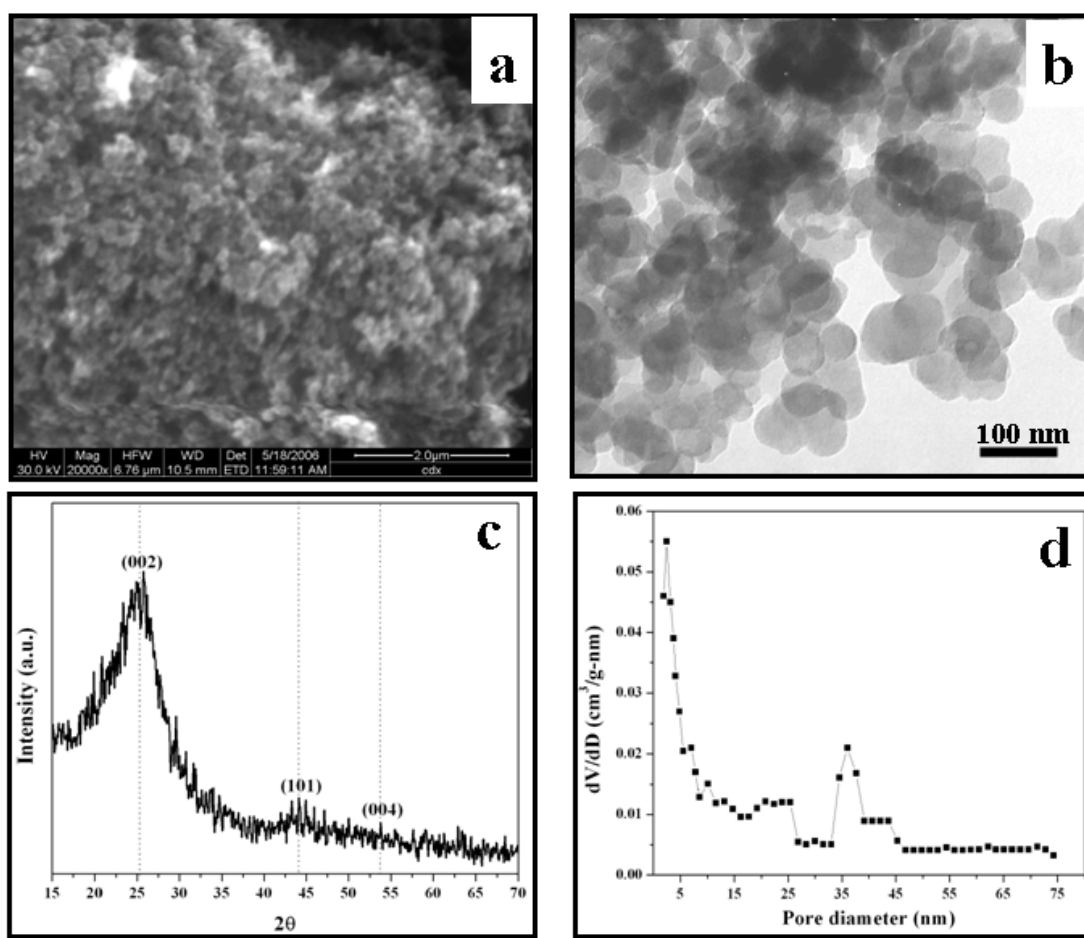


Fig. 3.1 (a) SEM image, (b) TEM image, (c) XRD pattern and (d) pore size distribution of the carbon black (CDX975) support

### 3.4.2 X-ray Diffraction Analysis

Powder X-ray diffraction patterns of the as-synthesized and commercial Pt/C catalysts recorded at a scan rate of  $0.025^\circ \text{ s}^{-1}$  in the  $2\theta$  range of  $10^\circ$ - $90^\circ$  are shown in Fig. 3.2(a)-(e). All the catalysts exhibited five characteristic diffraction peaks at  $2\theta$  values around  $40^\circ$ ,  $46^\circ$ ,  $68^\circ$ ,  $81^\circ$  and  $87^\circ$  corresponding to the (111), (200), (220), (311) and (222) planes respectively. These peaks indicated that the Pt is present in the face-centered cubic (fcc) structure (JCPDS card 4-802). The broad diffraction peaks of Pt in the Pt/C catalysts are indicative of the nano-sized Pt. The gradual increase of full width half maximum (FWHM) from (a) to (e) indicates the decrease of Pt crystallite size. The diffraction peak at around  $2\theta$  value of  $25^\circ$  corresponds to the (002)



diffraction peak of the hexagonal structure of the carbon support. The average crystallite sizes of Pt particles supported on carbon are calculated from line broadening of the (220) diffraction peak (Gaussian-Lorentzian peak) according to Scherrer's equation (Patterson, 1939) and the values are given in Table 3.2.

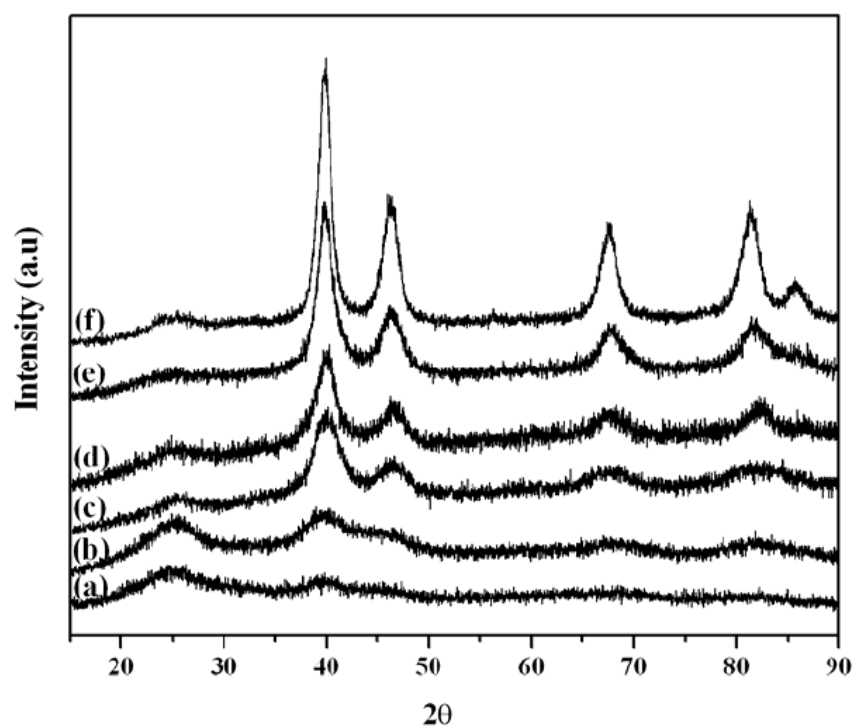


Fig. 3.2 Powder XRD patterns of the as-synthesized Pt/CDX975 catalysts; (a) Pt1C (b) Pt2C (c) Pt3C (d) Pt4C (e) Pt5C and (f) Pt6C

### 3.4.3 TEM and EDX Analysis

Fig. 3.3 presents the low- and high-magnification TEM images of the as-synthesized Pt/CDX975 catalysts. Uniform size and spherical shaped Pt nanoparticles on the carbon support can be seen in all the prepared Pt/CDX975 catalysts. The particle sizes obtained by TEM are given in Table 3.2. Well dispersed and well-separated spherical shapes of Pt fringes of 2.0 nm, 2.5 nm, 3.5 nm, 4.0 nm, 5.0 nm and 6.0 nm in size were observed in the Pt1C, Pt2C, Pt3C, Pt4C, Pt5C and Pt6C catalysts respectively. The similarity of the particle sizes and the crystallite sizes suggest that most of the existing particles are single crystallites.

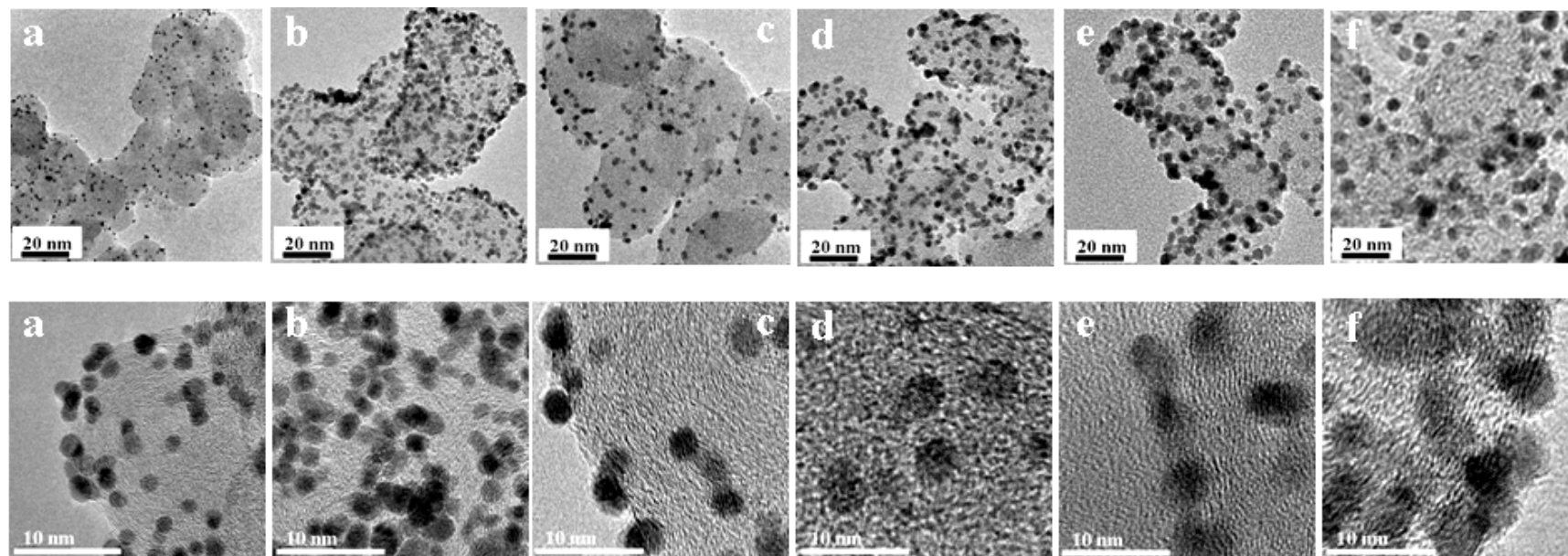


Fig. 3.3 TEM images of the as-synthesized Pt/CDX975 catalysts (a) Pt1C (b) Pt2C (c) Pt3C (d) Pt4C (e) Pt5C and (f) Pt6C (First and second rows corresponds to the low and high magnification images respectively)

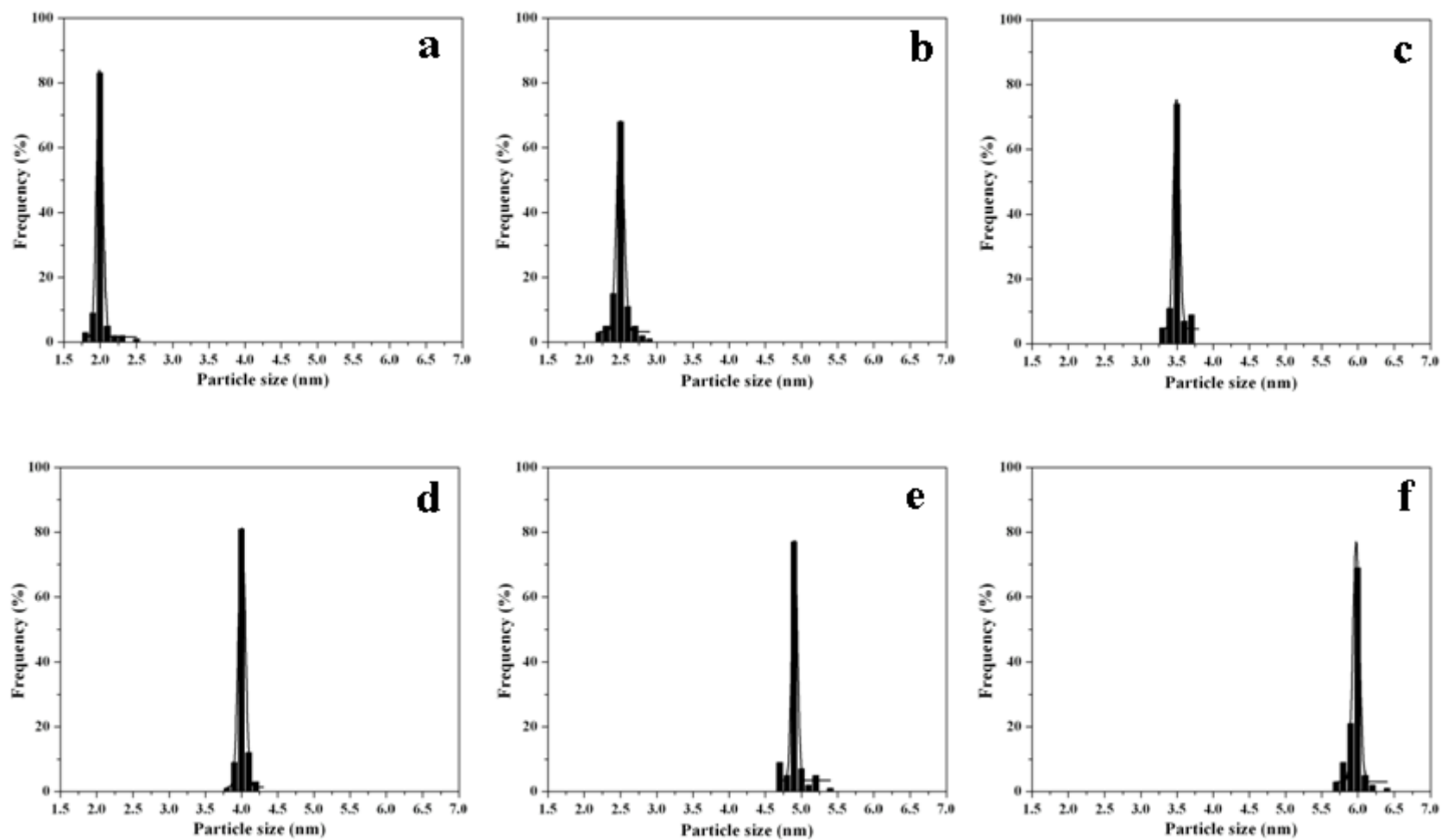


Fig. 3.4 Histogram of the Pt particles supported on carbon catalysts (a) Pt1C (b) Pt2C (c) Pt3C (d) Pt4C (e) Pt5C and (f) Pt6C

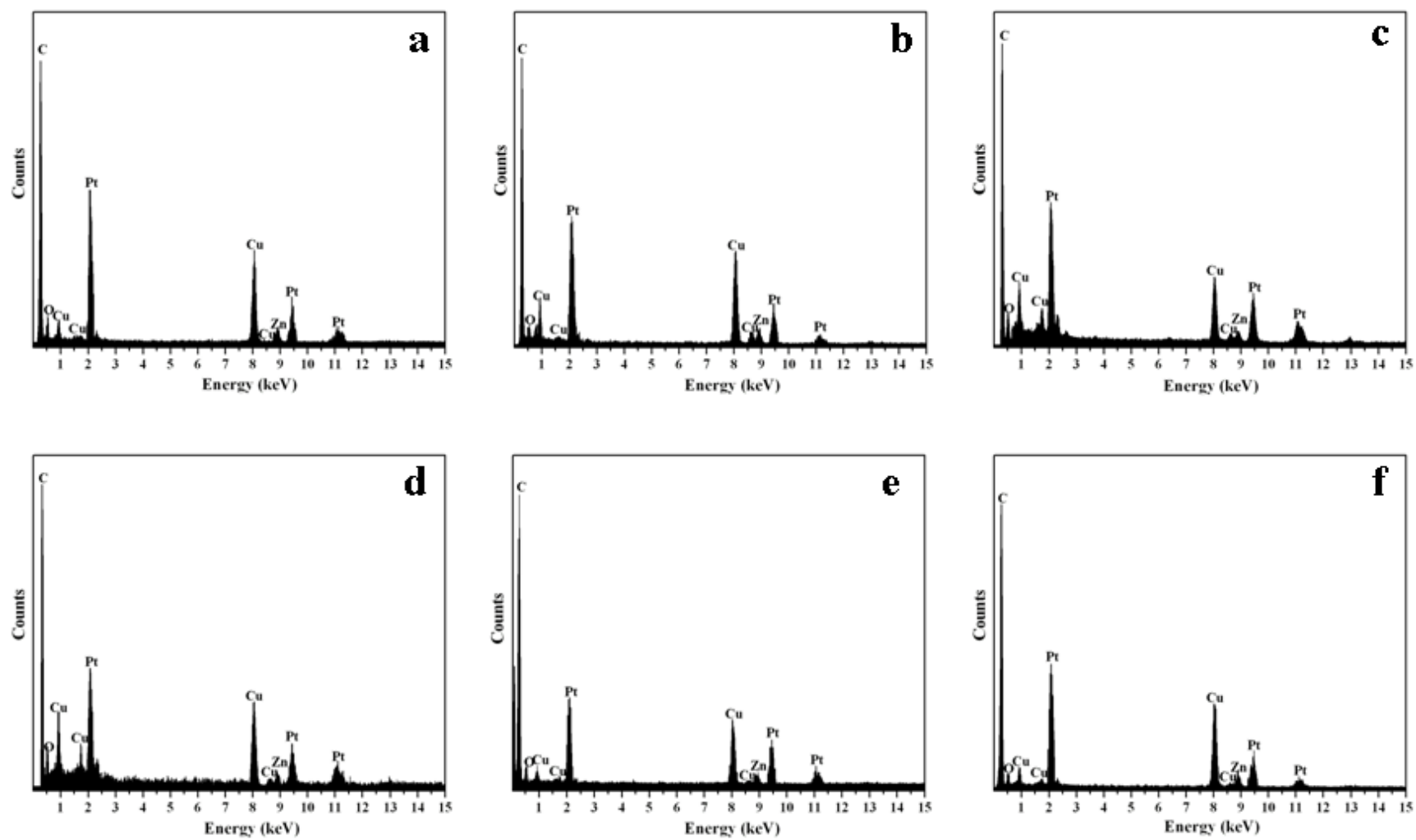


Fig. 3.5 EDX of the as-synthesized Pt/CDX975 catalysts (a) Pt1C (b) Pt2C (c) Pt3C (d) Pt4C (e) Pt5C and (f) Pt6C

The particle size distributions obtained by random counting from the HRTEM micrographs are shown in Fig. 3.4. As can be seen, around 60-70% of the Pt particles have a size 2.0 nm, 2.5 nm, 3.5 nm, 4.0 nm, 5.0 nm and 6.0 nm for Pt1C, Pt2C, Pt3C, Pt4C, Pt5C and Pt6C catalysts respectively. EDX spectra of the Pt1C, Pt2C, Pt3C, Pt4C, Pt5C and Pt6C catalysts are shown in Fig. 3.5. It confirms the presence of Pt and C with a small amount of oxygen in all the catalysts. TEM image, histogram of Pt particles on carbon and EDX spectrum of commercial (E-TEK) catalyst are shown in Fig. 3.6. Both dispersion as well as agglomeration of Pt particles on carbon support can be seen from the TEM images (Fig. 3.6(a) and 6(b)). The average particle size of Pt in commercial catalyst is 3.7 nm with a standard deviation of 0.4 nm. EDX spectrum shows the presence of Pt and C (Fig. 3.6(d)).

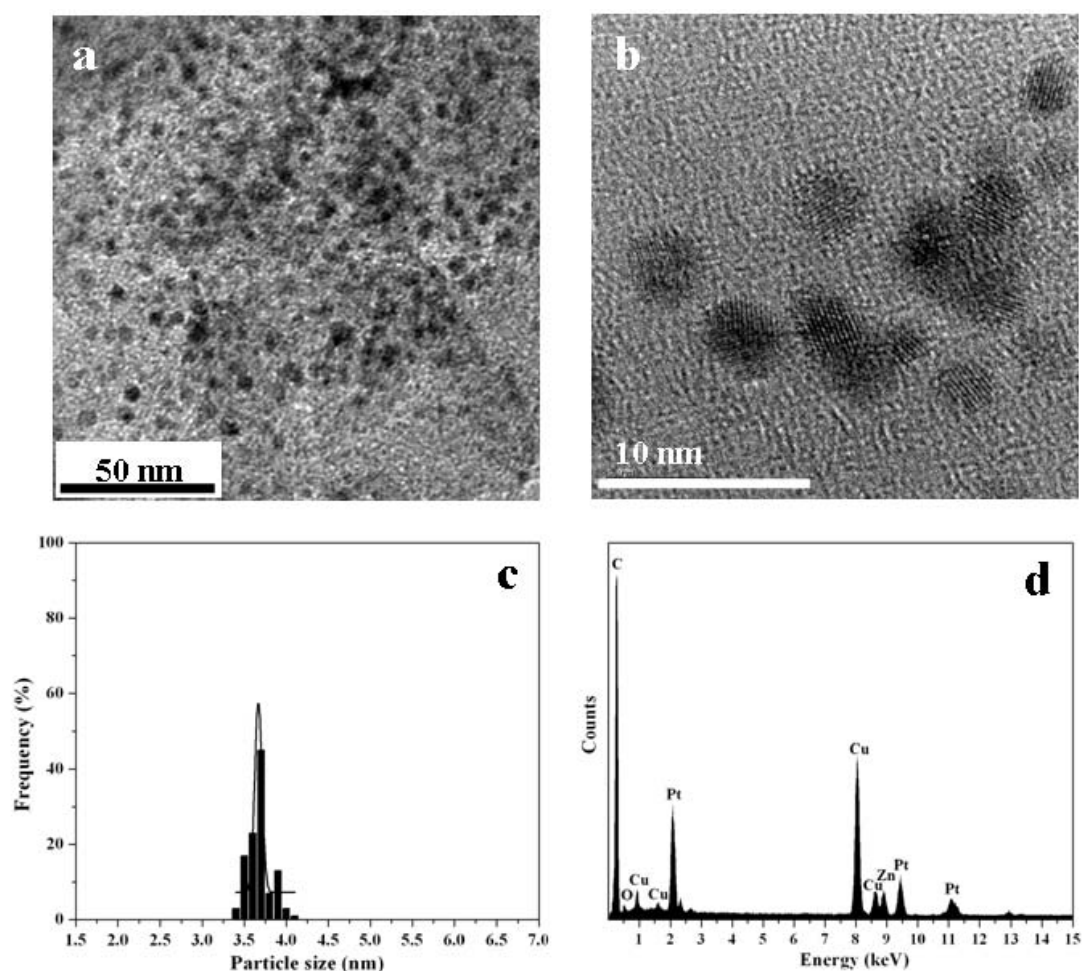


Fig. 3.6 (a and b) low and high magnification TEM images, (c) histogram of particle size distribution and (d) EDX spectrum of the commercial Pt/C catalyst

### 3.4.4 X-ray Photoelectron Spectroscopy (XPS) Analysis

Fig. 3.7 shows the XPS of Pt 4f spectrum for the Pt4C catalyst prepared by polyol reduction method. The Pt 4f spectrum shows a doublet containing a low-energy band (Pt 4f<sub>7/2</sub>) and a high-energy band (Pt 4f<sub>5/2</sub>) at 71.2 and 74.6 eV, respectively. These binding energy values are in good agreement with the literature data for Pt (Hufner and Wertheim, 1975). These peaks indicated that Pt is present in metallic state, Pt(0).

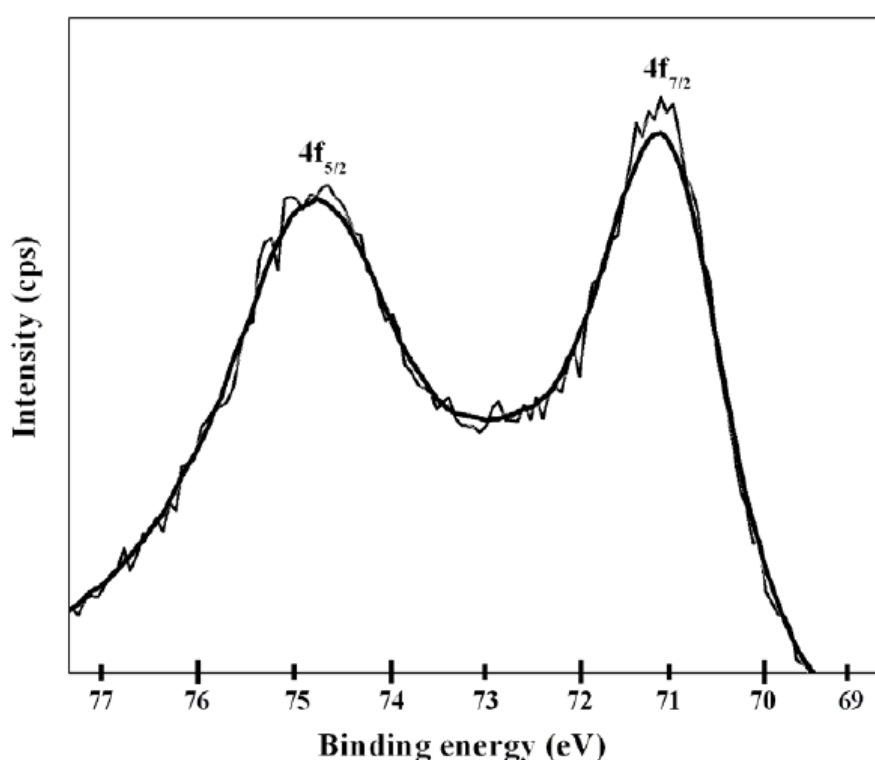


Fig. 3.7 XPS spectrum of Pt4C catalyst

### 3.4.5 Estimation of Pt Loading on the Carbon Support

Platinum in carbon supported Pt catalysts was determined by spectrophotometric method (Balcerzak *et al.*, 1999). In this method, a known weight (20 mg) of the Pt/C catalyst was placed in a quartz crucible and calcined at 1173 K for 12 h to remove carbon. The residue was treated with hot aqua regia and evaporated to dryness. Then conc. HCl was added to convert platinum into soluble chloride complexes and the

solution was evaporated almost to dryness. This process is repeated 3-4 times for the complete extraction of Pt. Finally the solution was made up to known volume with 2 M HCl (25 ml). To the 5 ml of this solution, 5 ml of freshly prepared 10% SnCl<sub>2</sub> solution was added to form yellow complex, [PtCl<sub>2</sub>(SnCl<sub>3</sub>)<sub>2</sub>]<sup>2-</sup> and the solution was made up to 25 ml with 2 M HCl. The absorbance of the solution was measured at 403 nm against the blank. The amount of platinum was calculated by comparing the measured absorbance value to the absorbance of standard solutions. The estimated amount of Pt in the as-prepared Pt/C catalysts is given in Table 3.2.

### **3.5 ELECTROCHEMICAL PERFORMANCES OF Pt/C CATALYSTS**

#### **3.5.1 Electrode Fabrication**

The electrode was fabricated as described by Schmidt *et al.* (1998). In this process, 5 mg of Pt/C catalyst was dispersed in 5 ml of isopropanol by ultrasonication for 20 min. Subsequently, 20 µl of the catalyst suspension was pipetted on a mirror-finished glassy carbon electrode with 3 mm diameter. It was dried at room temperature under argon stream to avoid the oxidation of Pt nanoparticles. Then the catalyst was covered with 10 µl of a diluted Nafion<sup>®</sup> solution (Aldrich, 5 wt.% in 15-20% water/low aliphatic alcohols) and dried at room temperature. The glassy carbon disk was polished with slurry of 0.5 and 0.03 µm alumina successively and washed ultrasonically in distilled water prior to use. The apparent surface area of the glassy carbon disk was 0.07 cm<sup>2</sup>; thus, the Pt metal loading was 56 µg cm<sup>-2</sup>. The metal loading was found to be reproducible within ±5% based on a series of experiments in which cyclic voltammograms are evaluated. Current densities are normalized to the geometric area of the glassy carbon substrate (0.07 cm<sup>2</sup>).

### 3.5.2 Electrochemical Reduction of Oxygen

Electrochemical oxygen reduction measurements are performed at room temperature in a three electrode; one compartment cell containing 0.5 M H<sub>2</sub>SO<sub>4</sub> as the electrolyte. After fabrication, the electrode is immersed in 0.5 M H<sub>2</sub>SO<sub>4</sub> and purged with Ar gas for 30 min to deaerate the solution. Owing to slight contamination from the Nafion<sup>®</sup> solution, the electrode potential was cycled 2-3 times between +0.0 and +1.2 V vs NHE in order to produce a clean electrode surface. Then the linear sweep voltammogram (LSV) was recorded between +0.2 V and +1.2 V vs NHE at a scan rate of 5 mV s<sup>-1</sup>. For the oxygen reduction experiments, the electrolyte was saturated with pure oxygen and the linear sweep voltammogram (LSV) were recorded between +0.2 and +1.2 V vs NHE at a scan rate of 5 mV s<sup>-1</sup>. Current densities are normalized to the geometric area of the glassy carbon substrate (0.07 cm<sup>2</sup>).

Fig. 3.8 shows the linear sweep voltammograms (LSVs) of Pt1C, Pt2C, Pt3C, Pt4C, Pt5C and Pt6C catalysts in Ar- and O<sub>2</sub>-saturated 0.5 M H<sub>2</sub>SO<sub>4</sub> between +0.2 and +1.2 V vs NHE at a scan rate of 5 mV s<sup>-1</sup>. For comparison, LSVs of commercial Pt/C (E-TEK) are also shown in figure. It shows that the ORR on all the catalysts is diffusion-controlled when the potential is less than +0.65 V and is under mixed diffusion-kinetic control (or surface reaction control region) in the potential region between +0.65 and +0.95 V vs NHE. For all the Pt/C catalysts, when the potential was swept from +1.2 to +0.2 V single oxygen reduction peak is observed in the potential region of ca. 1.0–0.7 V. Moreover, the steep increase in peak current at +0.7 V indicates the facile kinetics of ORR. The activity obtained in O<sub>2</sub> atmosphere is a sum of oxygen reduction current, current due to Pt oxide formation or reduction, and double layer charging current. So in order to eliminate the back ground currents, oxygen reduction activity was calculated by taking the difference in activity at +0.7 V vs. NHE in Ar-



and O<sub>2</sub>- saturated 0.5 M H<sub>2</sub>SO<sub>4</sub>. This method of determination of background current assumes that currents for Pt oxide formation and reduction are the same in Ar and O<sub>2</sub> atmosphere. It is evident from Fig. 3.8 that the Pt3C and Pt4C catalysts exhibited higher oxygen reduction activity than other Pt1C, Pt2C, Pt5C and Pt6C catalysts. Moreover, their ORR activity is comparable to that of commercial Pt/C (E-TEK).

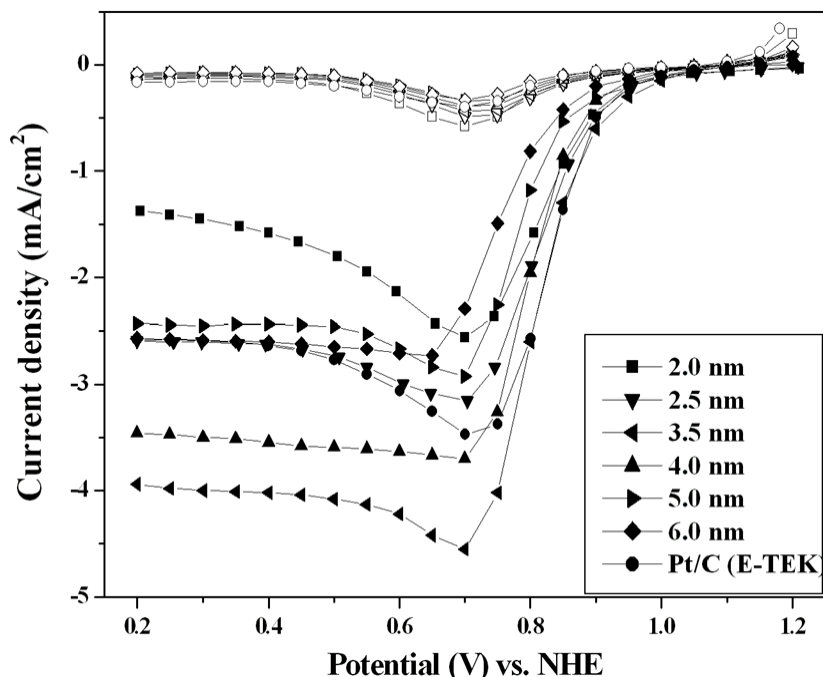


Fig. 3.8 Linear sweep voltammograms of the carbon supported Pt catalysts in Ar- and O<sub>2</sub>- saturated 0.5 M H<sub>2</sub>SO<sub>4</sub>; Scan rate – 5 mV s<sup>-1</sup> (Empty and full symbols corresponding to the LSVs in Ar- and O<sub>2</sub>- saturated 0.5 M H<sub>2</sub>SO<sub>4</sub> respectively)

The onset potential for oxygen reduction and ORR activity of the as-prepared catalysts are given in Table 3.2. The onset potential for oxygen reduction on Pt1C is about 930 mV and Pt6C is about 870 mV. A gradual reduction of onset potential for ORR is observed when going from Pt1C to Pt6C. It is believed that the differences in ORR onset reduction potentials are caused by the differences in the surface activation of various catalysts, which are related to the size and distribution of the metal nanoparticles (Sattler and Ross, 1986; Kinoshita, 1990).

Table 3.2 Size of Pt (from XRD and TEM), Pt loading, onset potential and ORR activity of Pt/CDX975 catalysts

Catalyst	Pt crystallite size from XRD (nm)	Size of Pt from TEM (nm)	Pt metal loading (wt.%)	Onset potential for oxygen reduction (mV vs. NHE)	ORR activity at +0.7 V vs. NHE (mA cm <sup>-2</sup> )
Pt1C	1.8	2.0±0.1	19.3	+930	1.9
Pt2C	2.3	2.5±0.2	19.5	+930	2.5
Pt3C	3.4	3.5±0.1	19.3	+925	4.3
Pt4C	3.8	4.0±0.1	19.1	+915	3.4
Pt5C	4.7	5.0±0.2	19.3	+880	2.8
Pt6C	5.8	6.0±0.2	19.6	+865	2.2
Pt/C (E-TEK)	--	3.7±0.4	19.8	+915	3.1

These results obtained agreed with those reported in literature (Peuckert *et al.*, 1986; Giordano *et al.*, 1991; Giordano *et al.*, 1994; Gamez *et al.*, 1996; Antoine *et al.*, 2001; Maillard *et al.*, 2002). 3-5 nm is the optimum size of Pt for obtaining maximum ORR activity. The relatively higher oxygen reduction activity of the Pt3C and Pt4C catalysts can be correlated with the homogeneous distribution of Pt particles and orientation of surface atoms in the crystal planes, alteration of redox energy levels as a function of Pt particle size and anion (sulphate) effect.

The oxygen reduction reaction (ORR) on Pt surfaces has been widely studied in electrochemistry, but the details of the mechanism still remain elusive. The overall ORR is a multistep process involving four-electron transfer during which bonds are broken and formed. Oxygen reduction on the platinum surface is a structure sensitive reaction due to structure-sensitive adsorption of spectator species, such as O<sub>2,ads</sub>,

$\text{OH}_{\text{ads}}$ , and  $\text{OOH}_{\text{ads}}$ . The OH radical is one of the important intermediates of the ORR and is formed in large amounts during the processes of oxygen reduction and water oxidation (Teliska *et al.*, 2005). It is shown that oxygen reduction generally increases as the surface area decreases and this effect is explained by variation of the different Pt crystal planes exposed to the electrolyte as a function of the particle size. The crystal planes of Pt(110), Pt(111) and Pt(100) can facilitate adsorption of oxygen molecules via the bridge model on the surface of the Pt particles and favour dissociation of adsorbed oxygen during the ORR (Markovic *et al.*, 1997; Panchenko *et al.*, 2004). In general, oxygen reduction activity on different low-index Pt surfaces increases in the sequence (100) < (110) < (111) in the potential range ( $E > 0.75$  V) where  $\text{O}_2$  reduction is under kinetic diffusion control. But in aqueous  $\text{H}_2\text{SO}_4$  solutions, the ORR rate increases in the sequence Pt(111) < Pt(100) < Pt(110) (Markovic *et al.*, 1997). An exceptionally large deactivation is observed at the (111) surface probably due to competition of the strongly adsorbing (bi)sulfate anion (Markovic *et al.*, 1995; Markovic *et al.*, 1997). The decrease of the activity on (100) surface is related to a high affinity of (100) sites for the adsorption of hydroxyl species, leading to a lack of active centers for  $\text{O}_2$  adsorption on Pt(100) as it is covered with  $\text{OH}_{\text{ads}}$ . It was proposed that the bridge mode of adsorption of oxygen molecule on the (110) surface is the most favorable one for the oxygen molecule among the three low-index planes of platinum, suggesting that it is the preferred adsorption site on a polycrystalline Pt substrate (Panchenko *et al.*, 2004). In spherical shaped Pt particles, there should be the probable distribution of all planes. It means that all the planes have the same probability to react with oxygen molecular species. Kinoshita (1990) has correlated the specific activity ( $\text{mA cm}^{-2}$  of Pt) of highly dispersed Pt electrocatalysts based on the change in the fraction of surface atoms on

the crystal facets of Pt particles, which results from the change in surface coordination number with a change in the average particle size. Under the operating conditions, especially in the presence of electric potential there should be a drastic change in the geometries, charges, and adsorption energies of the species on a catalyst surface and preferential exposure of Pt in particular orientation (Panchenko *et al.*, 2004). As a result, population of the anti-bonding  $\pi^*$  orbitals in oxygen molecule increases and facilitates the reduction of oxygen to water. All these reports support the higher performance of the Pt3C and Pt4C catalysts where there should be a optimum number of Pt atoms on various crystal facets and separated with optimum interatomic distance than the other catalysts.

The observed low ORR activity of Pt1C and Pt2C at +0.9 V vs NHE (kinetically controlled region) compared to the other catalysts implies the strong adsorption of (hydr)oxy species on small sized (<3 nm) Pt nanoparticles. Takasu *et al.* (1996) also observed the same phenomenon and attributed the particle size effect in ORR to a stronger interaction of oxygen with smaller Pt particles. Density functional calculations performed by Xu *et al.* (2006) on a series of  $Pt_x$ ,  $Pt_xO_x$  and  $Pt_xO_{2x}$  clusters ( $x = 1, 2, 3, 4, 5$ , and 10) reveal that the discrete Pt clusters are more readily oxidized than bulk Pt and smaller the Pt cluster, the more readily it is oxidized. So it is believed that the small sized Pt nanoparticles, below 3 nm oxidize more readily than other sized (>3 nm) Pt nanoparticles. As a result, the surface may be covered with more (hydr)oxy species and leads to low ORR activity. The most widely accepted rate limiting step in oxygen reduction is: active site +  $O_2 + H^+ + e^- \rightarrow [HO_2]_{ads}$ , the strength and susceptibility of the surface oxygenated species play an important role in determining the overall ORR activity. As a result of the strong Pt-OH bonds with high coverage on smaller particles (<3nm), there should be less availability of oxygen to

the Pt sites so that low ORR activity was observed. The results obtained are also supported by in-situ XAS measurements performed on Pt/C catalysts which indicate the stronger adsorption of H and OH on small particles of size  $<3$  nm in the kinetically controlled potential region (0.55 to 0.9 V) and account for the decline in specific activity for oxygen reduction (Mukerjee and McBreen, 1999).

The high catalytic activity could be explained, too, taking into consideration the concept of Hammer and Nørskov (2000) of the metal reactivity changes, through the changes in adsorbate–surface interaction energy due to the attraction of the local d-band position relative to the Fermi level. Since the Pt particles are anchored on the surface of carbon in the case of as-synthesized catalyst (evident from TEM images), restructuring of particles which can induce steric and electronic differences among the catalytic sites was more favorable and facilitates the oxygen reduction. As a result, there should be a better interaction between the adsorbate valence states and the metal d-orbitals and consequent electron transfer from the metal d-orbital to the antibonding  $2\pi^*$  orbital of molecular oxygen.

The high ORR activity of 3-5 nm sized particles than other sized Pt particles can be viewed from the alteration of redox energy levels as a function of Pt particles size. Adsorption and dissociation of  $O_2$  occurs only when there exists a resonance (energetically and symmetrically) between metal cluster HOMO orbital and the acceptor orbital of oxygen molecule. In one of the reports, Heiz *et al.* (1999) investigated the chemical interaction of Pt clusters with oxygen in terms of the frontier orbitals. It is believed that the d-band position is the most decisive parameter, when describing molecule-surface bonding. The HOMOs (or d-band centers) of Pt clusters are found to be between the atomic limit (-9.00 eV, IP of the Pt) and the bulk

limit (-5.32 eV) and the acceptor orbital of molecular oxygen is -6.16 eV. It was proposed that the energy of the highest occupied orbitals (HOMO) of the clusters, associated with the energy of the center of the d-band, can be tuned from -9.0 eV, the ionization potential (IP) of the atom, to -5.32 eV, the Fermi energy of bulk platinum by changing the cluster size. Based on these observations, the high ORR catalytic activity of Pt3C and Pt4C catalysts can be assigned with the suitable energy of HOMOs (or position of the center of the d-band) and the concomitant enhanced resonance with the anti-bonding  $\pi^*$  state of O<sub>2</sub>. As a result, there should be facile transfer of electrons from the HOMO to the anti-bonding  $\pi^*$  state of O<sub>2</sub> and causes the dissociation of O<sub>2</sub> molecule. For the small particles (<3 nm), the energies of the frontier orbitals may not match to cause the dissociation of O<sub>2</sub> molecule. So the alteration of the position of d-band center as a function of Pt particles size may be one of the reasons for the observed different kinetic behaviour of investigated carbon supported Pt catalysts.

In addition, the anion (sulfate) effect on the specific activity at a given potential is comparatively stronger for the smaller (d<3 nm) Pt nanoparticles (Gamez *et al.*, 1996; Gojkovic *et al.*, 1998; Paulus *et al.*, 2001). This effect is generally ascribed to the impeding effect of specific anion adsorption on different crystal faces, the distribution of which changes with Pt particle size. As a result, there should be a less availability of oxygen at the surface Pt atoms (mass transfer limitations) and consequently lower oxygen reduction activity on small size Pt particles present in the Pt1C and Pt2C catalysts compared to that of the Pt3C and Pt4C catalysts.

## CHAPTER 4

# SYNTHESIS, CHARACTERIZATION AND ELECTROCHEMICAL STUDIES OF CARBON SUPPORTED Pt-M (M = Fe, Co and Cr) ALLOY CATALYSTS FOR OXYGEN REDUCTION

### 4.1 INTRODUCTION

Even though conventional carbon supported Pt is the commercially exploited electrocatalyst for oxygen reduction reaction (ORR) in electrochemical devices; it is associated with several drawbacks besides the cost issue. The main drawback is the high overpotential (0.3-0.4 V) as a result of sluggish kinetics of ORR on Pt surface (Ralph and Hogarth, 2002; Gasteiger *et al.*, 2005). In order to lower the overpotential, to increase the oxygen reduction activity and to reduce the amount of Pt in the electrodes, significant research has been focused on platinum alloys. Pt has been alloyed with a variety of elements including V, Cr, Ti, Mn, Fe, Co, Ni, W, Mo, Ir, Pd, Zn. An enhancement in activity (1.5 - 5 times) for ORR on the alloy catalysts in comparison to pure Pt has been reported using potentiodynamic RRDE measurements (Mukerjee and Srinivasan, 1993; Mukerjee *et al.*, 1995; Toda *et al.*, 1999; Paulus *et al.*, 2002a and 2002b; Xiong *et al.*, 2002; Antolini *et al.*, 2002; Shukla *et al.*, 2004; Yang *et al.*, 2004; Li *et al.*, 2004; Antolini *et al.*, 2006; Ioroi and Yasuda *et al.*, 2005; Sode *et al.*, 2006; Huang *et al.*, 2006; Gong *et al.*, 2007; Grinberg *et al.*, 2007; Li *et al.*, 2007; Qian *et al.*, 2008;). It was also reported that the overpotential for the ORR on Pt alloys is 20-40 mV less compared to Pt. The improvement in the ORR electrocatalysis on Pt alloys has been explained by several factors, such as geometric and electronic effects (Jalan and Taylor, 1983; Paffet *et al.*, 1988; Beard and Ross, 1990; Watanabe *et al.*, 1994; Mukerjee *et al.*, 1995; Toda *et al.*, 1998; Toda *et al.*,

1999; Antolini *et al.*, 2005a). Based on these investigations and in the context of the ORR mechanisms, the principle explanations for the enhanced ORR activity could be attributed due to (i) modification of the electronic structure of Pt (5d-band vacancies); (ii) changes in the physical structure of Pt (Pt-Pt bond distance and coordination number); (iii) adsorption of oxygen containing species (oxy or hydroxy species) from the electrolyte on to the Pt or alloying element; and/or (iv) redox type processes involving the first row transition alloying element. Still, what aspect of the ORR mechanism is affected by Pt-M alloy catalysts remains unclear. It is certainly true that the move toward Pt alloys as the catalyst for ORR is necessary, but many issues still need to be resolved.

Among the various Pt bimetallic alloys, Pt-Cr, Pt-Co and Pt-Fe appear to be good. Usually, the carbon-supported Pt alloy catalysts were prepared by the impregnation of the second metal on Pt/C and then alloying at temperatures above 973 K under reducing Ar-H<sub>2</sub> gas atmosphere (Salgado *et al.*, 2005b). But the heat-treatment at high temperatures gives rise to an undesired particle growth of the alloy; induce the sintering of particles and causes the loss of surface area, which results in the decrease in specific activity for ORR. Another issue is the change in the hydrophilic nature of the catalyst particles, making them more susceptible to flooding due to the increased hydroxide content on the surface. It is known that the particle size, dispersion, differences in surface characteristics (e.g., crystallographic plane) and compositional homogeneity of the alloy clusters resulting from the conditions employed in the synthesis procedures play an important role in the ORR catalysis. Therefore, it is of significance to prepare uniform size and shape with controllable composition of Pt-M alloys by a low temperature chemical reduction method and investigate the ORR



activity. In this context, polyol reduction method (Sun *et al.*, 2000) appears to be one of the choices for the preparation of Pt bimetallic nanoparticles.

The formation potential of  $\text{OH}_{\text{ads}}$  and maximum ORR activity was found to depend significantly on the sub-surface composition. Various authors reported that the bimetallic Pt-M in 1:1 or 2:1 or 3:1 as optimum for good performance. For example, Mukerjee *et al.* (1993) reported bulk Pt-Co, Pt-Ni and Pt-Fe alloys with atomic ratio 1:1 exhibited good ORR activity. According to Xiong *et al.* (2002), who prepared various carbon supported Pt-M electrocatalysts by a low temperature reduction procedure with sodium formate, reported that the Pt-Co electrocatalyst showed the best performance with the maximum catalytic activity and minimum polarization at a Pt:Co atomic ratio of around 1:7. Toda *et al.* (1999) investigated the electrocatalytic ORR activity of Pt alloys with Co, Fe and Ni, formed by sputtering, and observed maximum activity at *ca.* 40, 50 and 30% content of Co, Fe and Ni, respectively. They also observed an increase in kinetic current densities by which 10, 15 and 20 times larger than that of pure Pt. Kinetic analysis of the data in comparison to pure Pt, revealed an activity enhancement of a factor of 2 to 3 for the 50 at.% Co-catalyst (Paulus *et al.*, 2002a; Paulus *et al.*, 2002b). Huang *et al.* (2006) prepared carbon supported Pt-Co alloy catalysts with different Pt/Co atomic ratios, 1:1, 2:1, 3:1, 4:1 and 5:1 by the carbonyl complex route followed by  $\text{H}_2$  reduction in the temperature range of 423-573 K and reported the maximum activity with a Pt/Co atomic ratio of 2:1. Shukla *et al.* (2004) prepared Pt-Fe(1:1)/C by alloying method and found the better ORR activity than Pt/C. Gong *et al.* (2007) synthesized Fe-modified carbon-supported platinum electrocatalysts by colloidal route and observed good catalytic activity at atomic compositions of Pt/Fe = 9:1 and Pt/Fe = 1:1 than the Pt/Fe = 3:1. Yang *et al.* (2004) prepared carbon-supported Pt-Cr alloy catalysts with different

Pt/Cr atomic ratios (1:1, 2:1 and 3:1) by Pt-carbonyl route and observed the good performance in the case of Pt-Cr (1:1). Antolini *et al.* (2005) prepared carbon supported Pt-Cr alloy nanoparticles in 1:1, 3:1 and 9:1 atomic ratios by NaBH<sub>4</sub> reduction method and observed good performance in the case of 1:1 and 3:1. Grinberg *et al.* (2007) prepared carbon supported Pt-Co and Pt-Cr alloys in 1:1 atomic ratio by the thermal decomposition of organometallic complexes of Pt and Co or Cr and found good ORR activity than Pt alone. The inconsistency is due to the variation of geometric factors (degree of alloying and Pt-Pt interatomic distance) and electronic factors (Pt d-band vacancies) resulting from the preparation methods and heat-treatments.

In this study, Pt-M (M = Fe, Co and Cr) alloy nanoparticles of atomic ratio 1:1 are prepared by polyol reduction method and supported on carbon black (CDX975) to achieve 20 wt% metal loading.. The prepared catalysts are characterized by XRD, TEM and EDX. Electrochemical measurements are performed to investigate the role of alloying elements towards the enhancement of ORR activity.

#### **4.2 SYNTHESIS OF Pt-M (M = Fe, Co and Cr) ALLOY NANOPARTICLES**

Uniform size and shaped Pt-M (50:50 atom%) alloy nanoparticles are synthesized by polyol reduction method by employing platinum(II)acetylacetonate as Pt precursor, FeCl<sub>2</sub> as Fe precursor, Cr(CO)<sub>6</sub> as Cr precursor, Co<sub>2</sub>(CO)<sub>8</sub> as Co precursor, 1,2-hexadecanediol as reducing agent and nonylamine and nonanoic acid as stabilizing agents. The synthesis is carried out using standard Schlenk line technique under dry nitrogen.

In a typical synthesis of Pt-Fe alloy nanoparticles, a mixture of 0.5 mmol of Pt(acac)<sub>2</sub>, 0.5 mmol of FeCl<sub>2</sub> and 2 mmol of 1,2-hexadecanediol were taken under nitrogen

atmosphere in a 100 ml three-necked round-bottom flask equipped with a N<sub>2</sub> in/outlet, PTFE coated magnetic stir bar, septa rubber and a thermal probe. 25 ml of diphenyl ether (DPE) solvent is then transferred into the flask and the contents stirred while purging with N<sub>2</sub> at room temperature. The flask is then heated to 373 K and held at 373 K for 20 min. During this hold, 0.5 mmol of nonylamine and 0.5 mmol of nonanoic acid are injected into the flask while continuing the N<sub>2</sub> gas purge. Then the dark brown suspension is heated to 523 K. The flask is maintained at the refluxing temperature of 523-533 K for 30 min before cooling down to room temperature under the N<sub>2</sub> atmosphere. Afterwards, all handling are performed under atmospheric conditions. Similarly, Pt-Co and Pt-Cr alloy nanoparticles are synthesized.

Following synthesis, the nanoparticles are subjected to additional washing cycles to remove excess surfactant from the synthesis solution. The 'excess surfactant' is the fraction of surfactant in solution that is not bonded to the Pt-M alloy nanoparticles. The original mixture of surfactant coated nanoparticles in diphenylether solvent is first mixed with 10 parts of ethanol causing the particles to precipitate. The mixture is centrifuged to separate the particles from the solution. The supernatant solvent consisting of diphenylether was then discarded and the nanoparticles are redispersed in non-polar solvent, hexane. This sequence of precipitation in ethanol, centrifuging to separate the solvent and redispersion in hexane was then repeated three times. Finally, the nanoparticles are dispersed in hexane and used for further work.

### **4.3 PREPARATION OF THE CARBON SUPPORTED Pt-M ALLOY CATALYSTS**

To make carbon-supported Pt-M (M = Fe, Co and Cr) alloy catalysts with 20 wt.% metal loading, 100 mg of as-prepared Pt alloy nanoparticles dispersed in hexane are

mixed with 400 mg of dispersed carbon black (CDX975). Particles are deposited on carbon support by ultrasonication agitation for 2 h. Finally it is dried at room temperature in vacuum to avoid the oxidation of nanoparticles.

## **4.4 CHARACTERIZATION OF THE CARBON SUPPORTED Pt-M ALLOY CATALYSTS**

### **4.4.1 X-ray Diffraction Analysis**

Fig. 4.1 shows the XRD patterns of the carbon-supported Pt-M (50:50 atom%) alloy catalysts (with a metal loading of 20 wt.%) recorded in the range of  $10^{\circ}$ - $90^{\circ}$  at a scan rate  $0.025^{\circ} \text{ s}^{-1}$ . For the sake of comparison, the commercial Pt/C catalyst (E-TEK) with 20 wt.% metal loading is also shown in the figure. As indicated in Fig. 4.1, all the catalysts exhibited five characteristic peaks at  $2\theta$  values around  $40^{\circ}$ ,  $47^{\circ}$ ,  $68^{\circ}$ ,  $82^{\circ}$  and  $87^{\circ}$  corresponding to the (111), (200), (220), (311) and (222) planes of face-centered cubic (fcc) structure of Pt (JCPDS No. 87-0640). In the case of Pt-M/CDX975 catalysts, these five diffraction peaks are shifted to higher  $2\theta$  values with respect to the corresponding peaks in the Pt/C (E-TEK) catalyst. It indicates the contraction of lattice by the incorporation of base metal (Cr or Co or Fe) in the fcc structure of Pt due to alloy formation. This shift also suggests that the interatomic distance of Pt is decreased due to the substitution of a smaller atom, such as a transition metal, Fe, Co or Cr. (Hwang and Chung, 1993; Mukerjee *et al.*, 1995). No peaks for pure base metal or its oxides are observed, but their presence cannot be discarded because they may be present in a small amount or even in an amorphous form. The broad peak observed at around  $2\theta = 24\text{--}26^{\circ}$  is due to the hexagonal structure of carbon support.

It is known that oxygen is adsorbed on Pt surface by dual site mode, therefore the Pt-Pt nearest-neighbor distance plays the key role to determine the adsorption behavior.

Jalan and Taylor (1983) have studied the effect of Pt–Pt nearest-neighbor distance and oxygen reduction activity of various platinum alloys. They claimed that the short Pt–Pt nearest-neighbor distance in alloys compared to that of the pure Pt causes the facile reduction of oxygen. So the contraction of Pt lattice observed in the case of as-prepared catalysts may be favourable for dissociation of oxygen and enhance the kinetics.

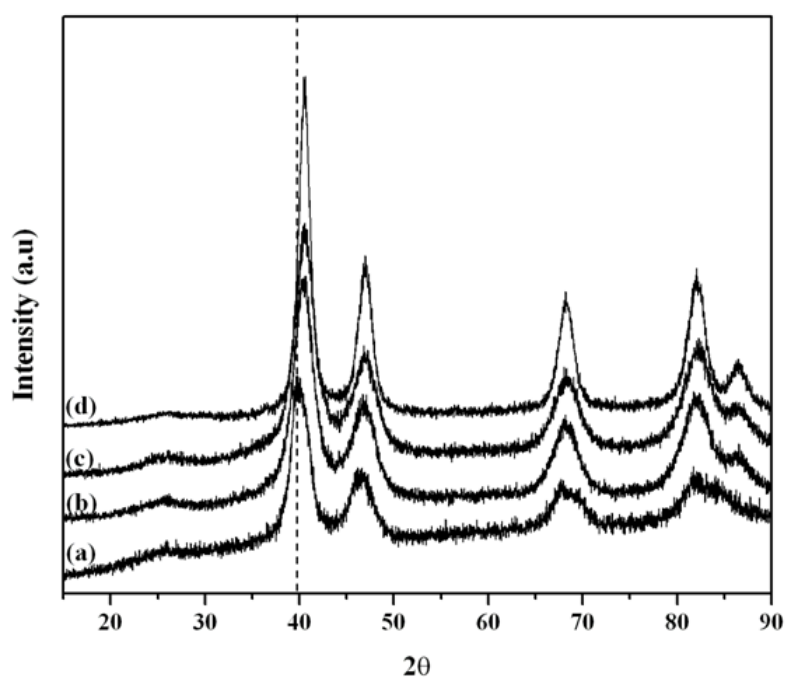


Fig. 4.1 Powder X-ray diffraction patterns of (a) commercial Pt/C (E-TEK) (b) Pt-Co(1:1)/CDX975 (c) Pt-Cr(1:1)/CDX975 and (d) Pt-Fe(1:1)/CDX975 catalysts

#### 4.4.2 TEM and EDX Analysis

Fig. 4.2 shows the TEM images of the carbon-supported Pt-M alloy catalysts. A good spatial distribution of spherical shaped Pt alloy particles over the carbon support with a narrow particle size distribution is observed. Particle size around 5 nm in the case of Pt-Cr/CDX975 and Pt-Co/CDX975 and 6 nm in the case of Pt-Fe/CDX975 catalysts is observed.

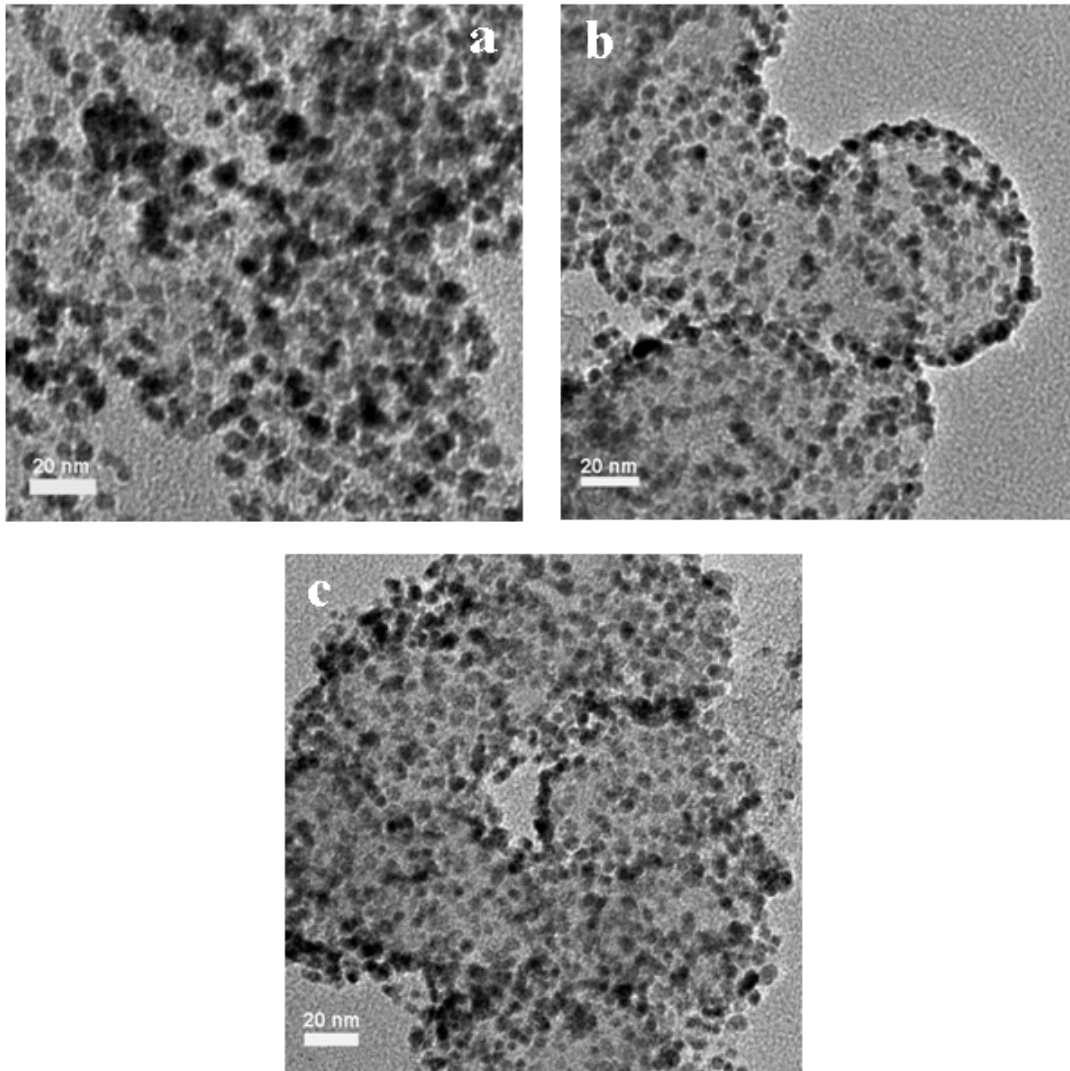


Fig. 4.2 Transmission electron microscopic (TEM) images of carbon supported Pt alloy catalysts; (a) Pt-Fe(1:1)/CDX975 (b) Pt-Co(1:1)/CDX975 and (c) Pt-Cr(1:1)/CDX975

Fig. 4.3 shows the particle size distribution histograms of the carbon-supported Pt-M alloy catalysts. These histograms are based on the observation of 500 nanoparticles. The mean particle diameter ( $d$ ) is calculated according to the equation (4.1),

$$d = \frac{\sum_i n_i d_i}{n_i} \dots\dots\dots (4.1)$$

where  $n_i$  is the frequency of occurrence of particles of the size  $d_i$ .

TEM analysis reveals that the as-prepared carbon supported Pt-Fe, Pt-Co and Pt-Cr alloy nanoparticles have a mean diameter of 5, 5 and 6.5 nm with a standard deviation of 0.1-0.2 nm respectively.

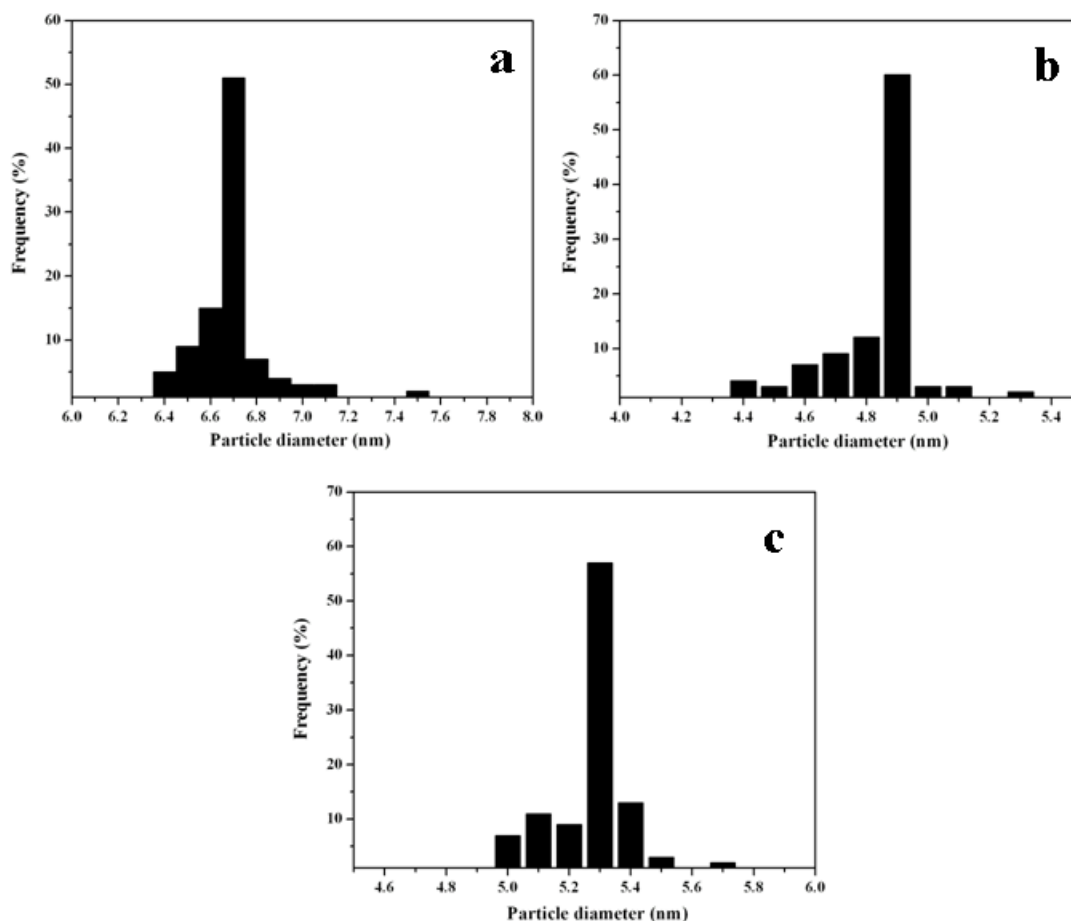


Fig. 4.3 Histograms of Pt alloy particle size distribution in carbon supported catalysts; (a) Pt-Fe(1:1)/CDX975 (b) Pt-Co(1:1)/CDX975 (c) Pt-Cr(1:1)/CDX975

Fig. 4.4 shows the EDX spectra of the carbon-supported Pt-M alloy catalysts. It confirms the presence of respective elements and a small amount of oxygen in the catalysts. Average composition of the catalysts obtained by EDX analysis by the collection of data for 50 nanoparticles is found to be approximately 1:1 in all the catalysts.

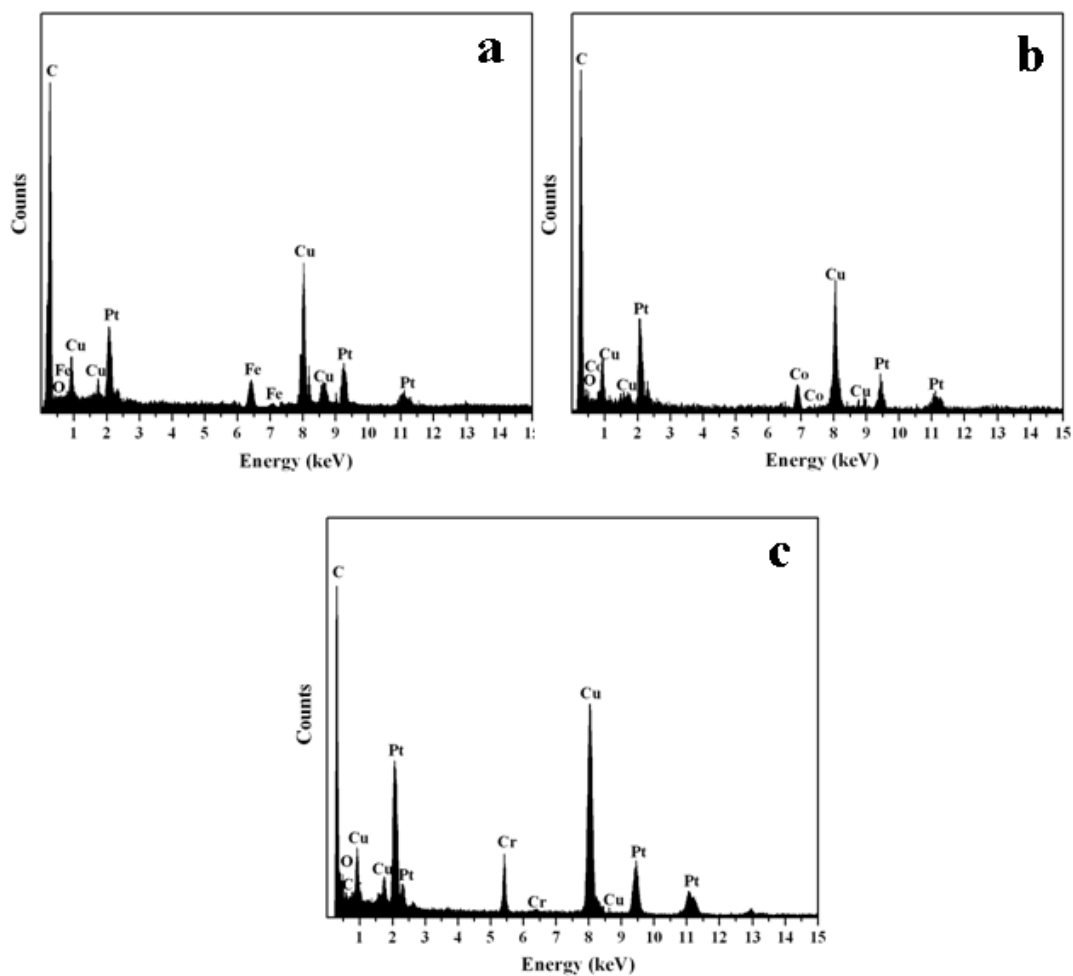


Fig. 4.4 EDX spectra of carbon supported Pt alloy catalysts; (a) Pt-Fe(1:1)/CDX975 (b) Pt-Co(1:1)/CDX975 and (c) Pt-Cr(1:1)/CDX975

#### 4.4.3 Estimation of Pt in the Catalysts

The amount platinum in carbon supported Pt-M alloy catalysts is determined by spectrophotometric method (Balcerzak *et al.*, 1999) described in section 3.4.5. The estimated amount of Pt in the as-synthesized Pt/CDX975 catalysts is given in Table 4.1.

#### 4.4.4 Estimation of Iron (Fe) in the Catalysts

The presence of iron in the carbon supported Pt-Fe catalyst was estimated by following a standard redox titration procedure (Vogel, 1985). A known weight of sample is dissolved in hot conc. HCl to release the iron as  $\text{Fe}^{+3}$  ions. After that it is



cooled, filtered and made up to a known volume with de-ionized water (stock solution). Then 10% SnCl<sub>2</sub> solution was added to reduce the Fe<sup>+3</sup> in the solution to Fe<sup>+2</sup>. Finally, the Fe<sup>+2</sup> solution was titrated against K<sub>2</sub>Cr<sub>2</sub>O<sub>7</sub> using 1% diphenylamine as indicator until the colourless solution becomes bluish violet. In this process, excess SnCl<sub>2</sub> was destroyed by adding mercuric chloride so that the reducing agent SnCl<sub>2</sub> does not react with K<sub>2</sub>Cr<sub>2</sub>O<sub>7</sub>. From the burette reading, concentration and weight of iron present in the stock solution was calculated. Finally, the weight (%) of iron in the sample was calculated by dividing the weight of iron with weight of sample taken for measurements. Estimated amount of iron is given in Table 4.1.

#### **4.4.5 Estimation of Cobalt (Co) in the Catalysts**

Cobalt content in carbon supported Pt-Co catalyst was estimated using absorption spectroscopy (Faubert *et al.*, 1996). This technique involves a nitric acid digestion of the catalyst to release the cobalt as Co<sup>2+</sup> ions. After that it is cooled, filtered and made up to a known volume with de-ionized water. Then, the addition of ammonium thiocyanate (NH<sub>4</sub>SCN) to this solution causes the formation of a blue complex, Co(SCN)<sub>2</sub>. This complex is then extracted with methyl isobutyl ketone and its absorbance was measured at 620 nm. By comparing the measured absorbance value to the absorbance of standard solutions, the amount of cobalt in the original sample was calculated. Estimated amount of cobalt is given in Table 4.1.

#### **4.4.6 Estimation of Chromium (Cr) in the Catalysts**

Chromium content in carbon supported Pt-Cr catalyst was estimated by spectrophotometric method (Malik and Ramesh, 1975). In this method, a known weight of sample is dissolved in hot concentrated HCl to release chromium as Cr<sup>+3</sup> ions. For the spectrophotometric determination of Cr(III), potassium

hexacyanoferrate(II) is used as a complexing agent to form brown coloured complex,  $\text{KCr}^{\text{III}} [\text{Fe}(\text{CN})_5\text{OH}]$ . To 5 ml of sample (contain approximately 10 ppm Cr(III)), 1 ml of 0.001 M  $\text{K}_4\text{Fe}(\text{CN})_6$  solution and 4 ml of HCl-acetate buffer of pH 4.0 are added and allowed to stand in the dark for 24 h at room temperature. The absorbance is measured at 235 nm. The amount of chromium in the sample is calculated by comparing the measured absorbance value to the absorbance of standard solutions prepared using  $\text{K}_4\text{Fe}(\text{CN})_6$  and  $\text{CrCl}_3$ . Estimated amount of chromium in the catalyst is given in Table 4.1.

#### **4.5 ELECTROCHEMICAL PERFORMANCE OF Pt-M(1:1)/CDX975 (M = Fe, Co and Cr) CATALYSTS**

##### **4.5.1 Electrode Fabrication**

The electrode is fabricated as described by Schmidt *et al.* (1998). 5 mg of the catalyst was dispersed in 5 ml of isopropanol by ultrasonication for 20 min. Glassy carbon disk electrode (Bas electrode,  $0.07 \text{ cm}^2$ ) was polished to a mirror finish with  $0.05 \mu\text{m}$  alumina suspensions before each experiment and served as an underlying substrate of the working electrode. An aliquot of  $20 \mu\text{l}$  catalyst suspension was pipetted onto the carbon substrate. After evaporation of the isopropanol in an argon stream, the deposited catalyst was then covered with  $10 \mu\text{l}$  of a diluted Nafion<sup>®</sup> solution (Aldrich, 5 wt.% in 15-20% water/low aliphatic alcohols) and dried at room temperature. Each electrode contained about  $56 \mu\text{g cm}^{-2}$  of the metal. The metal loading was found to be reproducible within  $\pm 5 \%$  based on a series of experiments in which cyclic voltammograms are evaluated. Current densities are normalized to the geometric area of the glassy carbon substrate ( $0.07 \text{ cm}^2$ ).

#### 4.5.2 Electrochemical Reduction of Oxygen

Electrochemical measurements are performed at room temperature in a three electrode; one compartment cell containing 0.5 M H<sub>2</sub>SO<sub>4</sub> (or) oxygen saturated 0.5 M H<sub>2</sub>SO<sub>4</sub> as the electrolyte. After fabrication, the electrodes are immersed in deaerated 0.5 M H<sub>2</sub>SO<sub>4</sub>. Owing to slight contamination from the Nafion<sup>®</sup> solution, the electrode potential was cycled 2-3 times between 0.0 and 1.0 V vs NHE in order to produce a clean electrode surface. The catalysts are first characterized electrochemically by cyclic voltammetry. Fig. 4.5 shows the cyclic voltammograms of Pt-M/CDX975 (M = Fe, Co and Cr) and commercial Pt/C (E-TEK) catalysts in deaerated 0.5 M H<sub>2</sub>SO<sub>4</sub> at the scan rate of 25 mV s<sup>-1</sup>. In the case of Pt/C catalyst, well-defined reversible hydrogen desorption/adsorption peaks and irreversible preoxidation/reduction peaks are observed. During the anodic scan, hydrogen is desorbed between -0.05 and +0.3 V vs NHE and surface platinum oxides are formed beyond +0.8 V vs NHE. During the cathodic scan, the surface platinum oxides are reduced between +1.0 and +0.5 V vs NHE and hydrogen is adsorbed at potentials more cathodic than +0.3 V vs NHE. It is thought that, in acid solution, OH<sub>ads</sub> is formed from oxidation of water on platinum surfaces at around +0.8 V and blocks surface sites for O<sub>2</sub> adsorption; thus resulting in low ORR activity (Murthi *et al.*, 2004). However, not well-defined hydrogen adsorption/desorption peaks on the carbon supported Pt-M alloy catalysts is observed, suggesting the high dispersion of the catalysts with the disordered surface structure.

A comparison of the voltammetry of carbon supported Pt and Pt-M alloy catalyst shows the difference in the onset of oxide formation on Pt (accepted as Pt-OH). Pt-M/CDX975 catalysts exhibit a significantly lower extent of oxide formation. For Pt/C, oxide formation starts at +0.8 V and for Pt-M/CDX975 the onset can be observed at around +0.85-+0.90 V. It indicates that the alloying of Pt with base metal inhibits the

chemisorption of (hydr)oxy species on the Pt sites at high potentials (above 0.8 V) by the change in electronic structure. This may have a beneficial effect on the oxygen adsorption at low overpotentials and thus may lead to an enhancement of the ORR kinetics (Mukerjee *et al.*, 1995b; Murthi *et al.*, 2004).

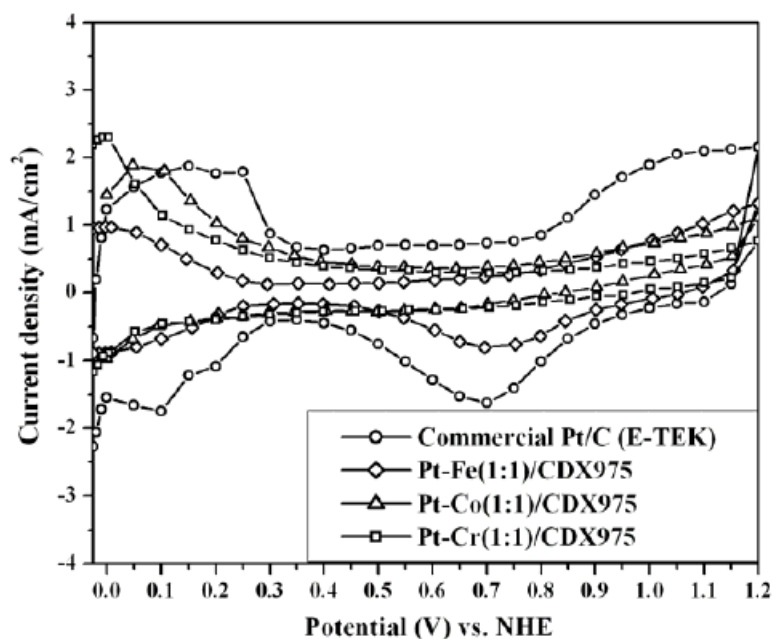


Fig. 4.5 Cyclic voltammograms (CVs) of Pt-M(1:1)/CDX975 (M = Fe, Co and Cr) and commercial Pt/C (E-TEK) catalysts in Ar-saturated 0.5 M H<sub>2</sub>SO<sub>4</sub>; Scan rate – 25 mV s<sup>-1</sup>

Fig. 4.6 shows the linear sweep voltammograms (LSVs) of Pt-M/CDX975 (M = Fe, Co and Cr) and commercial Pt/C (E-TEK) catalysts in Ar- and O<sub>2</sub>- saturated 0.5 M H<sub>2</sub>SO<sub>4</sub> between +0.2 and +1.2 V vs NHE at a scan rate of 5 mV s<sup>-1</sup>. It is evident that the oxygen reduction on all the catalysts is diffusion-controlled when the potential is less than +0.7 V and is under mixed diffusion-kinetic control in the potential region between +0.7 and +1.0 V vs NHE. For all catalysts, when the potential was swept from +1.2 to +0.2 V, single oxygen reduction peak is observed in the potential region of ca. 1.0–0.7 V. The steep increase in peak current at +0.7 V indicates the facile

kinetics of ORR. Oxygen reduction activity of the catalysts is calculated by taking the difference in activity at +0.7 V vs. NHE in Ar- and O<sub>2</sub>- saturated 0.5 M H<sub>2</sub>SO<sub>4</sub> and given in Table 4.1.

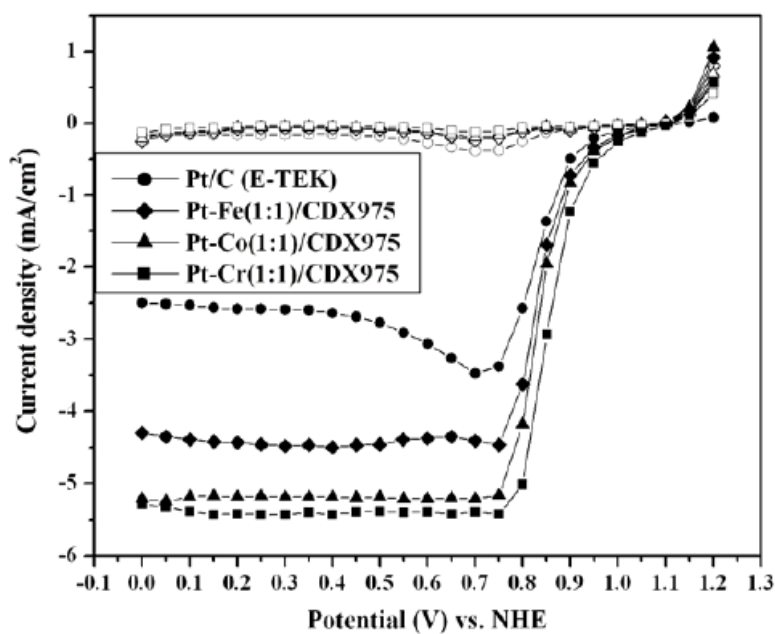


Fig. 4.6 Linear sweep voltammograms (LSVs) of Pt-M(1:1)/CDX975 (M = Fe, Co and Cr) and commercial Pt/C (E-TEK) catalysts in Ar- and O<sub>2</sub>- saturated 0.5 M H<sub>2</sub>SO<sub>4</sub>; Scan rate – 5 mV s<sup>-1</sup> (Empty and full symbols corresponding to the LSVs in Ar- and O<sub>2</sub>-saturated 0.5 M H<sub>2</sub>SO<sub>4</sub>)

The results of linear sweep voltammetry indicate that the Pt-M/CDX975 (M = Fe, Co and Cr) catalysts exhibited 1.5-1.7 times higher ORR activity than the commercial Pt/C (E-TEK) catalyst. The high ORR activity is attributed to the inhibition of formation of (hydr)oxy species on Pt surface. Among the investigated Pt-M/CDX975 catalysts (M = Fe, Co and Cr), maximum ORR activity is observed for the Pt-Cr(1:1)/CDX975 and Pt-Co(1:1)/CDX975.

Moreover, oxygen reduction proceeded in a relatively positive potential region for the Pt-M/CDX975 (M = Cr, Co and Fe) catalysts compared to the Pt/C (E-TEK). The

overpotential for ORR of the Pt alloys is about 40-70 mV less compared to that of Pt. This may be due to differences in the surface activation which is related to the size and distribution of the metallic nanoparticles. Similar shape of LSVs and high current density of Pt alloy catalysts to that of Pt/C catalyst indicate that the oxygen reduction takes place in the same manner on the catalysts but with facile kinetics on Pt alloys.

Table 4.1 Metal loading, particle size, onset potential for oxygen reduction and ORR activity of carbon supported Pt alloys and commercial Pt/C catalysts

Catalyst	Metal loading (wt.%)	Particle size (nm)	Onset potential for oxygen reduction (mV vs. NHE)	ORR activity at +0.7 V vs NHE ( $\text{mA cm}^{-2}$ )
20% Pt-Cr(1:1)/CDX975	Pt – 15.3 Cr – 4.1	5.0±0.2	+990	5.2
20% Pt-Co(1:1)/CDX975	Pt – 15.1 Co – 4.5	5.0±0.1	+975	5.0
20% Pt-Fe(1:1)/CDX975	Pt – 15.4 Fe – 4.4	6.5±0.2	+955	4.2
Commercial 20% Pt/C (E-TEK)	Pt – 19.8	3.7±0.4	+915	3.1

#### 4.5.3 Chronoamperometric Response

Fig. 4.7 shows the current density–time plots of Pt-M(1:1)/CDX975 (M = Fe, Co and Cr) and commercial Pt/C (E-TEK) catalysts in oxygen saturated 0.5 M  $\text{H}_2\text{SO}_4$  at +0.7 V vs NHE. The percentage degradation of activity for the carbon supported Pt-Cr, Pt-Co, Pt-Fe after 3 h are calculated to be 10, 22 and 24, respectively, which are less than the commercial Pt/C (E-TEK) catalyst (35%). It indicates the better performance of carbon supported Pt alloys compared to that of Pt/C (E-TEK).

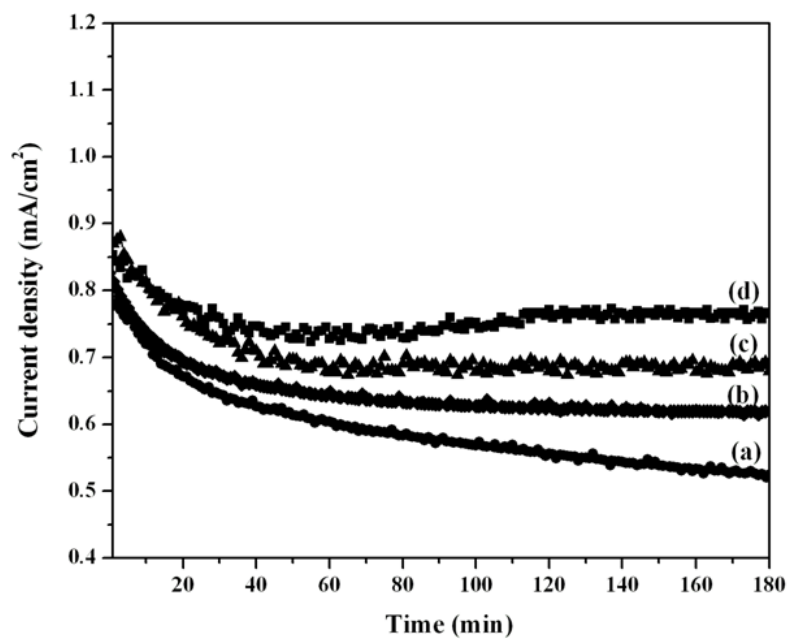


Fig. 4.7 Current density-time plots of (a) commercial Pt/C (E-TEK) (b) Pt-Fe(1:1)/CDX975 (c) Pt-Co(1:1)/CDX975 (d) Pt-Cr(1:1)/CDX975 catalysts in oxygen saturated 0.5 M H<sub>2</sub>SO<sub>4</sub> at +0.7 V vs NHE for 3 h

## CHAPTER 5

# SYNTHESIS, CHARACTERIZATION AND ELECTROCHEMICAL STUDIES OF CARBON SUPPORTED Pd AND Pd-Co-M (M = Mo and Au) ALLOY CATALYSTS FOR OXYGEN REDUCTION

### 5.1 INTRODUCTION

In the effort to reduce the cost of platinum based catalysts, there has been increasing interest in developing alternative electrocatalysts for oxygen reduction reaction (ORR). Next to Pt, Pd appears to be one of the choices. Moreover, Pd is more abundant and cheaper than Pt. But the intrinsic catalytic activity of Pd for the reduction of oxygen is lower than that of Pt and the long-term stability at high potentials is also not as good as that of Pt. It has been proven that the oxygen reduction takes place in the same manner as that on Pt (Sepa *et al.*, 1981; Vračar *et al.*, 1987; Vračar *et al.*, 1989). As like Pt, intermediate oxygen species will be covered on Pd surface at technically relevant potential region of 0.7-0.9 V vs. NHE and hinders oxygen reduction (Will and Knorr, 1960a; Will and Knorr, 1960b; Kinoshita, 1992). So the development of Pd alloy electrocatalysts that inhibits the adsorption of oxy species and enhances the ORR activity has been of interest. Recent reports have shown that the ORR activity of Pd-based catalysts can be improved significantly by adding elements like Co, Ni, Cr and Fe (Fernández *et al.*, 2005a; Wang and Balbuena, 2005; Shao *et al.*, 2006; Lee *et al.*, 2006). Considerable research towards the fundamental understanding of the ORR catalytic activity of Pd alloys has been undertaken and hypotheses have been put forward to explain the enhanced ORR activity of Pd alloys compared to that of Pd (Hammer and Nørskov, 1990; Fernández *et al.*, 2005a; Lee *et al.*, 2006; Shao *et al.*, 2007; Guo *et al.*, 2007). It is assumed that



the observed enhancement in the ORR activity for the Pd alloys might be related to the electronic property of Pd like the Pt alloys. But still the reason for enhanced ORR activity of Pd-Co-M (M = Mo and Au) alloys is not clear.

Among the various bimetallic Pd alloy systems, Pd-Co appears to be best. The ORR activity of the Pd-Co/C catalysts with a Co content of 10–30% was found to be close to that of Pt/C. Even though the ORR activity was comparable, the overpotential on Pd-Co alloy is 70-80 mV high compared to the Pt/C catalyst (Fernández *et al.*, 2005a; Wang *et al.*, 2007). Moreover, the long-term stability of Pd-Co alloy catalysts is an anticipated fundamental issue since dissolution of non-noble metal components would result in a significant decrease in ORR activity (Zhang *et al.*, 2007a; Zhang *et al.*, 2007b). In recent years, Fernández *et al.* (2005a and 2006) proposed suitable Pd metal combinations with optimum compositions that exhibit good activity for ORR using a scanning electrochemical microscope (SECM)-based combinatorial approach. Rapid screening of various Pd metal combinations over a wide range of compositions in 0.5 M H<sub>2</sub>SO<sub>4</sub> by SECM led to the identification of Pd-based compositions, Pd-Ti (50:50 atom %), Pd-Co-Au (70:20:10 atom%) and Pd-Co-Mo (70:20:10 atom%) as good catalysts for oxygen reduction. Subsequently, Fernández *et al.* (2005b) and Raghuveer *et al.* (2005 and 2006) prepared the identified compositions on carbon support and investigated them as cathode materials for PEMFC applications. They observed comparable activity of Pd alloys with that of commercial Pt/C for ORR in proton exchange membrane fuel cells (PEMFCs) at 333 K. In view of high ORR activity, Pd-Co-Mo(7:2:1)/C and Pd-Co-Au(7:2:1)/C appears to be promising. Raghuveer *et al.* (2005) prepared 20 wt.% Pd-Co-Mo(7:2:1)/C by three step procedure: (i) preparation of Pd-Co/C by NaBH<sub>4</sub> reduction method, (ii) Mo incorporation by an impregnation method, and (iii) heat-treatment in reducing atmosphere at high temperature. As a

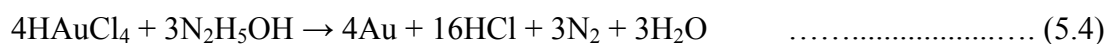
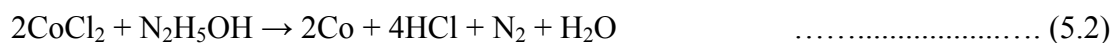
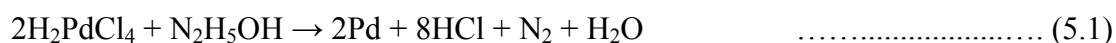
result, the size of Pd-Co-Mo particles on carbon support was found to be around 20 nm. Raghuveer *et al.* (2006) prepared carbon supported Pd-Co-Au alloy catalysts by reverse microemulsion method using sodium bis(2-ethylhexylsulfosuccinate (AOT) as the surfactant and NaBH<sub>4</sub> as the reducing agent followed by heat-treatment in reducing atmosphere at high temperature. It was reported that the heat-treated Pd-Co-Au/C at 773 K exhibited comparable activity with that of Pt/C but the stability was not good. It may be due to the poor degree of alloying. The size of Pd-Co-Au particles on carbon support was reported to be around 15-30 nm. Thus the synthesis procedures that can give catalysts with desirable composition and small particle size have the possibility of improving the ORR activity further.

In the present study, 20 wt.% Pd/CDX975 and Pd-Co-M(7:2:1)/CDX975 (M = Mo and Au) catalysts are prepared by reverse microemulsion method (RME) using non-ionic Triton-X-100 as a surfactant and investigated the role of alloying elements toward the increment of oxygen reduction activity by cyclic voltammetry. Finally, ORR activity of the prepared catalysts is compared with that of commercial Pt/C (E-TEK) catalyst.

## **5.2 PREPARATION OF 20 wt.% Pd/CDX975 AND Pd-Co-M/CDX975 (M = Mo and Au) CATALYSTS**

Carbon supported Pd and Pd-Co-M (M = Mo and Au) alloy catalysts were prepared by water-in-oil reverse microemulsion technique. The microemulsion system used in this study consisted of non-ionic Triton-X-100 as a surfactant, propanol-2 as a co-surfactant, cyclohexane as the continuous oil phase, and either the Pt-Co-M (M = Mo and Au) precursor solution or hydrazine solution as the dispersed aqueous phase. Composition of the microemulsions used for the preparation colloidal Pd-Co-M

(7:2:1) nanoparticles is indicated in Table 5.1. Microemulsion 1 and 2 were prepared separately by mixing by volume 10% surfactant, 35% cyclohexane, 40% propanol-2 and 15% of the aqueous phase. The amount of hydrazine is in stoichiometric excess compared with the equal volume of Pd–Co–M precursor solution in microemulsion I. A small additional amount of propanol-2 is then titrated slowly into each of the microemulsion system with stirring until the microemulsion system turned transparent. The two stable microemulsions are then mixed together and ultrasonicated for 2 h. Pd–Co–M nanoparticles are formed upon contact between the precursor containing droplets and the hydrazine containing droplets. The reductions of  $\text{H}_2\text{PdCl}_4$ ,  $\text{CoCl}_2$ ,  $\text{MoCl}_5$  and  $\text{HAuCl}_4$  are as follows:



Subsequently, an appropriate amount of carbon black (CDX975) is added to the mixture to give a metal(s):C weight ratio of 20:80. The resultant slurry is kept under constant stirring for 2 h, filtered, washed with acetone followed by deionized water and finally dried in an air oven at 348 K for 2 h. The powder samples thus obtained are heat-treated at different temperatures 973, 1073 and 1173 K in a flowing mixture of 10%  $\text{H}_2$ –90% Ar for 1 h and cooled to room temperature. Similarly, 20 wt.% Pd/CDX975 was prepared to investigate the effect of alloying elements of Pd towards the oxygen reduction activity.

Table 5.1 Compositions of microemulsion system used for the synthesis

	Microemulsion 1	Microemulsion 2	Vol%
Aqueous phase	7 mM H <sub>2</sub> PdCl <sub>4</sub> + 2 mM CoCl <sub>2</sub> + 1 mM MoCl <sub>5</sub> or HAuCl <sub>4</sub>	Hydrazine	15
Surfactant	Triton-X-100	Triton-X-100	10
Co-surfactant	Propanol-2	Propanol-2	40
Oil phase	Cyclohexane	Cyclohexane	35

### 5.3 CHARACTERIZATION OF THE CATALYSTS

#### 5.3.1 X-ray Diffraction Analysis

X-ray diffraction (XRD) patterns for the carbon supported Pd and Pd-Co-M (M = Mo and Au) alloy catalysts are recorded at a scan rate of  $0.025^\circ \text{ s}^{-1}$  over the  $2\theta$  range of  $10^\circ$ - $90^\circ$ . The corresponding XRD patterns are shown in Fig. 5.1 and 5.2. Both Pd/CDX975 and as-synthesized Pd-Co-M/CDX975 (M = Mo and Au) catalysts show peaks at  $2\theta$  values around  $40^\circ$ ,  $47^\circ$ ,  $68^\circ$ ,  $82^\circ$  and  $87^\circ$  corresponding to the (111), (200), (220), (311) and (222) planes of face-centered cubic (fcc) structure of Pd (JCPDS No. 88-2335). The broad peaks indicate that the particles are in nanocrystalline range. The diffraction peak at  $2\theta$  value of  $25^\circ$  corresponds to the (002) plane of the hexagonal structure of the carbon support. No appreciable change in the X-ray diffraction pattern of the as-synthesized Pd-Co-M/CDX975 (M = Mo and Au) compared to the Pd/CDX975 is observed. It indicates that the metal nanoparticles are not transformed into alloy. In order to improve alloying, it is heat-treated at different temperatures from 973 to 1173 K. As evidenced from XRD, with increasing temperature, the diffraction peaks are shifted to higher angles compared to the Pd/CDX975 catalyst indicating the contraction of lattice due to alloy formation.

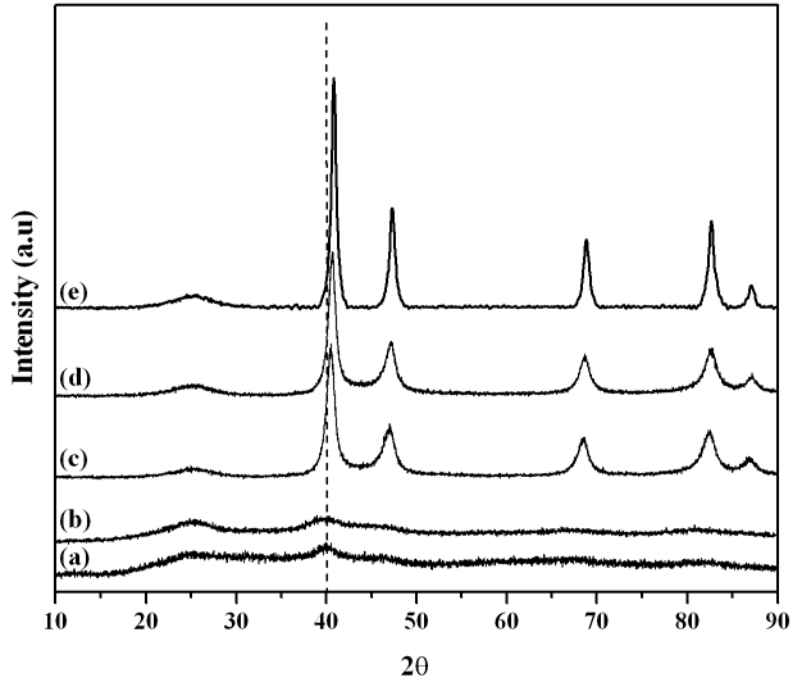


Fig. 5.1 Powder X-ray diffraction patterns of (a) Pd/CDX975 (b) as-synthesized Pd-Co-Mo(7:2:1)/CDX975; heat-treated Pd-Co-Mo(7:2:1)/CDX975 at (c) 973 K (d) 1073 K and (e) 1173 K respectively

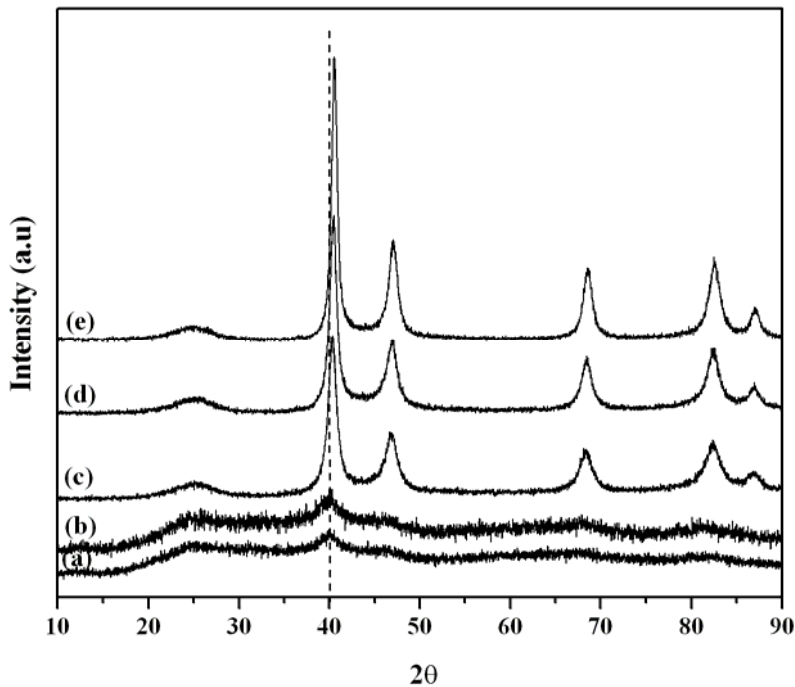


Fig. 5.2 Powder X-ray diffraction patterns of (a) Pd/CDX975 (b) as-synthesized Pd-Co-Au(7:2:1)/CDX975; heat-treated Pd-Co-Au(7:2:1)/CDX975 at (c) 973 K (d) 1073 K and (e) 1173 K respectively

The extent of shift increases and the lattice parameter decreases with increasing heat-treatment temperature (Table 5.2), suggesting an increase in the degree of alloying. By using lattice parameter values, degree of alloying  $D_A$  is calculated by using the equation (5.5),

$$D_A = \frac{\{a_{Pd} - a_{alloy(T)}\}}{\{a_{Pd} - a_{alloy(900)}\}} \times 100 \quad \dots\dots\dots (5.5)$$

where  $a_{Pd}$ ,  $a_{alloy(T)}$ , and  $a_{alloy(900)}$  refer to the cell parameter values of Pd, Pd–Co–M alloy heat-treated at various temperatures ( $T = 973, 1073$  and  $1173$  K), and Pd–Co–M alloy heat-treated at  $1173$  K, respectively (Cullity, 1978; Raghuveer *et al.*, 2006). The calculated values are given in Table 5.2. The crystallite size for all the catalysts is calculated from broadening of the (220) diffraction peak using Scherrer’s equation (Patterson, 1939).

Surface area of the catalysts is calculated by using the equation (5.6),

$$A_{sp} = \frac{6000}{\rho d} \quad \dots\dots\dots (5.6)$$

where  $\rho$  is the metal density,  $d$  is the particle size (in nm) with  $A_{sp}$  given in  $m^2 g^{-1}$  (Raghuveer *et al.*, 2005). The density values used for Pd, Pd-Co-Mo (70:20:10 atom %) and Pd-Co-Au (70:20:10 atom %) are 21.5, 11.2 and 12.2  $g cm^{-3}$  respectively. The results obtained are given in Table 5.2. It shows that surface area decreases with increasing heat-treatment temperature for the Pd-Co-M (M = Mo and Au) alloys due to the increase in crystallite size.

Table 5.2 Structural parameters of Pd/CDX975 and Pd-Co-M/CDX975 catalysts

Catalyst	Heat-treatment temp (K)	Lattice parameter (nm)	Degree of alloying (%)	Crystallite size (nm)	Surface area (m <sup>2</sup> g <sup>-1</sup> )
Pd/CDX975	As-syn	0.3898	--	1.2	232
Pd-Co-Mo(7:2:1)/CDX975	As-syn	0.3897	--	1.6	--
Pd-Co-Mo (7:2:1)/CDX975	973	0.3858	66	7.1	75
Pd-Co-Mo (7:2:1)/CDX975	1073	0.3847	85	9.4	57
Pd-Co-Mo(7:2:1)/CDX975	1173	0.3838	100	13.5	39
Pd-Co-Au(7:2:1)/CDX975	As-syn	0.3896	--	2.1	--
Pd-Co- Au (7:2:1)/CDX975	973	0.3854	59	6.3	78
Pd-Co- Au (7:2:1)/CDX975	1073	0.3839	79	8.7	56
Pd-Co- Au (7:2:1)/CDX975	1173	0.3824	100	10.4	47

### 5.3.2 TEM and EDX Analysis

Transmission electron microscopic (TEM) image and EDX spectrum of heat-treated Pd-Co-M(7:2:1)/CDX975 (M = Mo and Au) catalysts are shown in Fig. 5.3 and 5.4. Broad distribution of metallic nanoparticles of average size 9 nm (in the case of heat-treated Pd-Co-Mo(7:2:1)/CDX975 at 973 K) and 8 nm (in the case of heat-treated Pd-Co-Au(7:2:1)/CDX975 at 1073 K) on the carbon support can be seen from the TEM images (Fig. 5.3(a) and 5.4(a)) respectively. Elemental analysis performed by EDX confirms the presence of respective elements Pd, Co, Mo (or Au), C and a very small quantity of oxygen (Fig. 5.3(b) & 5.4(b)). Elemental composition (Pd:Co:Mo) in heat-treated Pd-Co-Mo(7:2:1)/CDX975 at 973 K is about (wt.%) 77.7:12.3:10.0 corresponding to approximate atomic ratio of 7:2:1. Elemental composition (Pd:Co:Au) in heat-treated Pd-Co-Au (7:2:1)/CDX975 at 1073 K is about (wt.%) 71.3:11.6:17.1 corresponding to approximate atomic ratio of 7:2:1. The calculated elemental composition (Pd:Co:M) in all the catalysts is given in Table 5.3. It is observed that the average compositions are nearly in agreement with those of the initial metal salt solutions.

## 5.4 ELECTROCHEMICAL PERFORMANCE OF CARBON SUPPORTED Pd AND Pd-Co-M (M = Mo and Au) ALLOY CATALYSTS

### 5.4.1 Electrode Fabrication

The electrode is fabricated as follows: 5 mg of catalyst is dispersed in 5 ml of isopropanol by ultrasonication for 15 min. Glassy carbon (GC) disk polished to a mirror finish with 0.05  $\mu\text{m}$  alumina suspensions before each experiment and served as an underlying substrate of the working electrode. An aliquot of 20  $\mu\text{l}$  catalyst suspension was then transferred onto the mirror polished glassy carbon substrate,



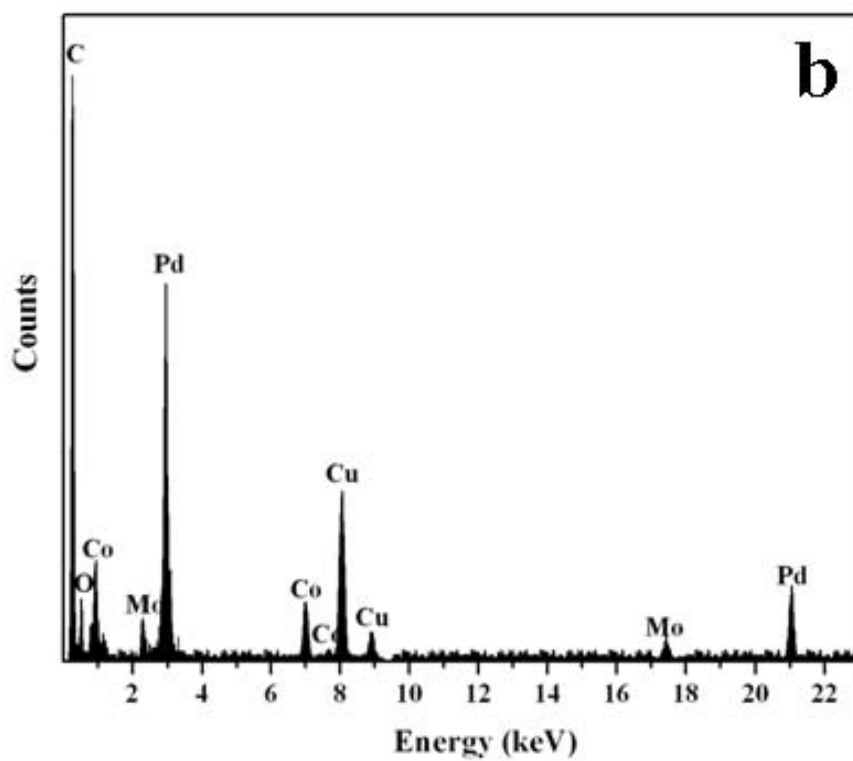
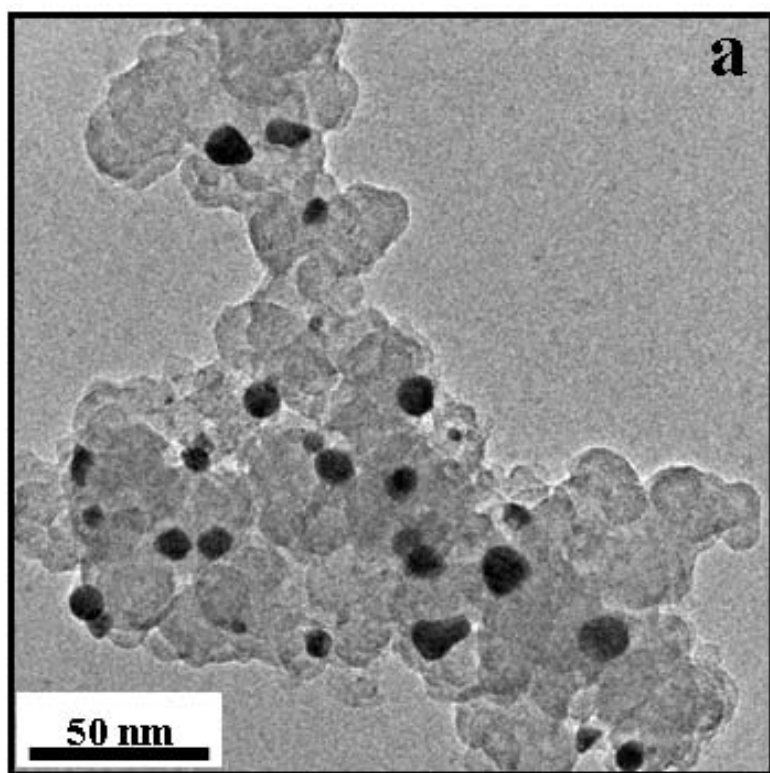


Fig. 5.3 (a) TEM image and (b) EDX spectrum of heat-treated Pd-Co-Mo(7:2:1)/CDX975 at 973 K

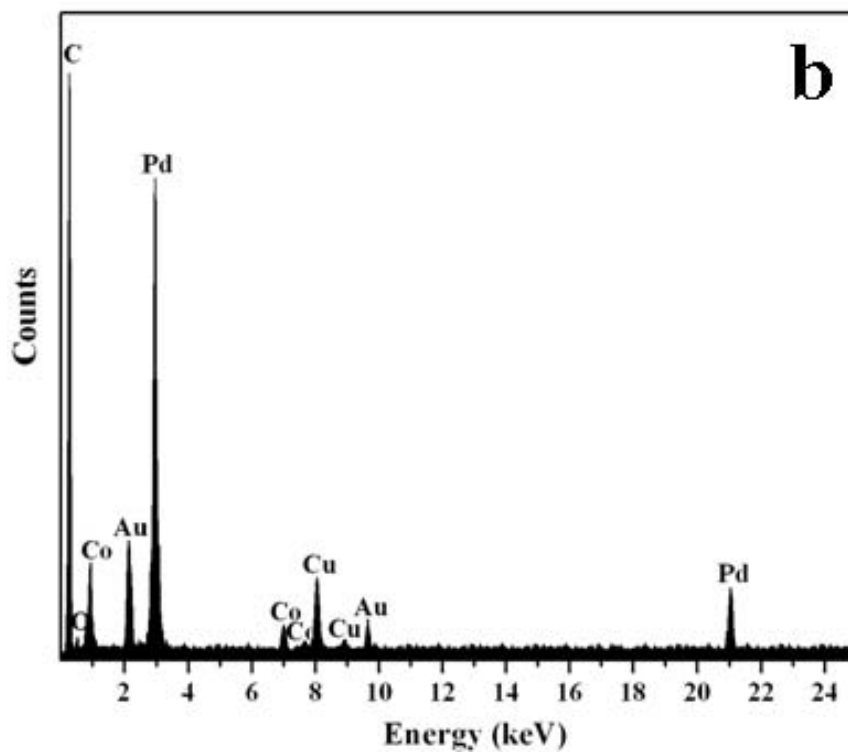
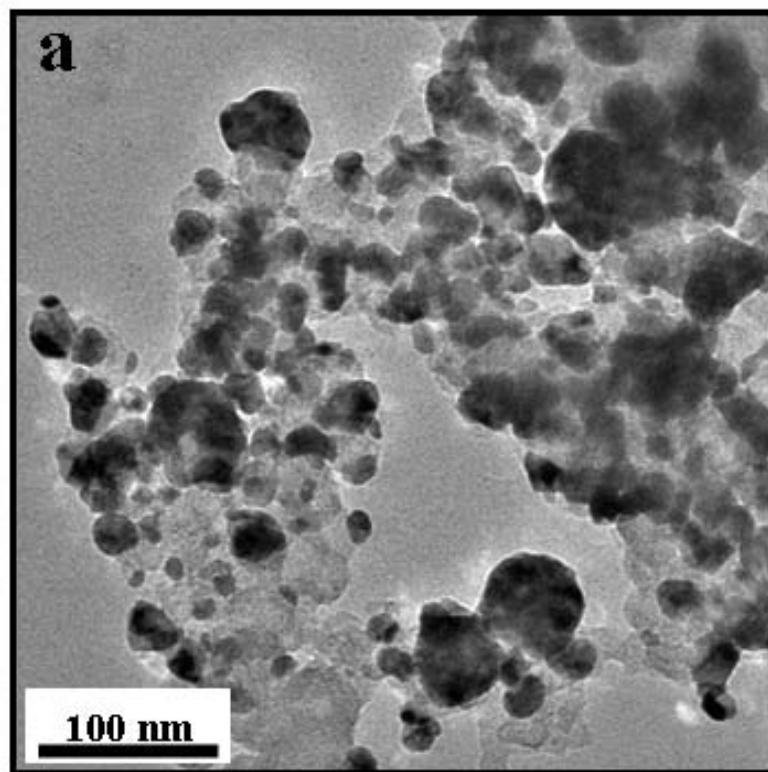


Fig. 5.4 (a) TEM image and (b) EDX spectrum of heat-treated Pd-Co-Au(7:2:1)/CDX975 at 1073 K

leading to a metal loading of  $56 \mu\text{g}_{\text{metal}} \text{cm}^{-2}$  and dried in flowing argon at room temperature. Then 10  $\mu\text{l}$  of a diluted Nafion<sup>®</sup> (Aldrich, 5 wt.% in 15-20% water/low aliphatic alcohols) was pipetted on the electrode surface in order to attach the catalyst particles onto the GC disk. The current densities are referenced to the geometric area of the glassy carbon substrate ( $0.07 \text{ cm}^2$ ).

#### 5.4.2 Electrochemical Reduction of Oxygen

Fig. 5.5 shows the cyclic voltammograms (CVs) of the carbon black (CDX975) supported Pd and Pd-Co-Mo alloys in deaerated 0.5 M  $\text{H}_2\text{SO}_4$  solution at a scan rate of  $25 \text{ mV s}^{-1}$ . The Pd/CDX975 electrocatalyst exhibited a large anodic peak at +0.25 V vs NHE. This is caused by dissolution of the adsorbed hydrogen into the bulk of the Pd catalyst (Bard, 1976; Enyo *et al.*, 1983). As in the case of Pd, the formation of surface palladium oxides (Pd-OH or  $\text{PdO}_x$  species) at the potentials of +0.8 V vs NHE during anodic scan and the corresponding reduction peaks of surface palladium oxides are observed at around +0.7 V vs NHE during the cathodic scan. With increasing  $\text{OH}_{\text{ad}}$  formation/surface oxidation, the ORR activity decreases and also it has been reported that the  $\text{PdO}_x$  species at the metallic Pd surface is inactive towards oxygen reduction (Lipkowski and Ross, 1998). For the as-synthesized Pd-Co-Mo/CDX975 catalyst anodic peak is shifted to lower potentials ca. 0.15 V vs NHE compared to the Pd/CDX975. It shows that the modification of the electronic structure of Pd by the presence of Co and Mo. In the case of heat-treated Pd-Co-Mo/CDX975 catalysts at different temperatures, the hydrogen adsorption/desorption peaks on the surface of the Pd alloys are observed at potentials of +0.04 V vs NHE showing a similar behavior to that of Pt (Lee *et al.*, 2006). This result is due to the interruption of the dissolution of hydrogen into the Pd lattice by alloying elements (Hoare and Schuldiner, 1958; Enyo

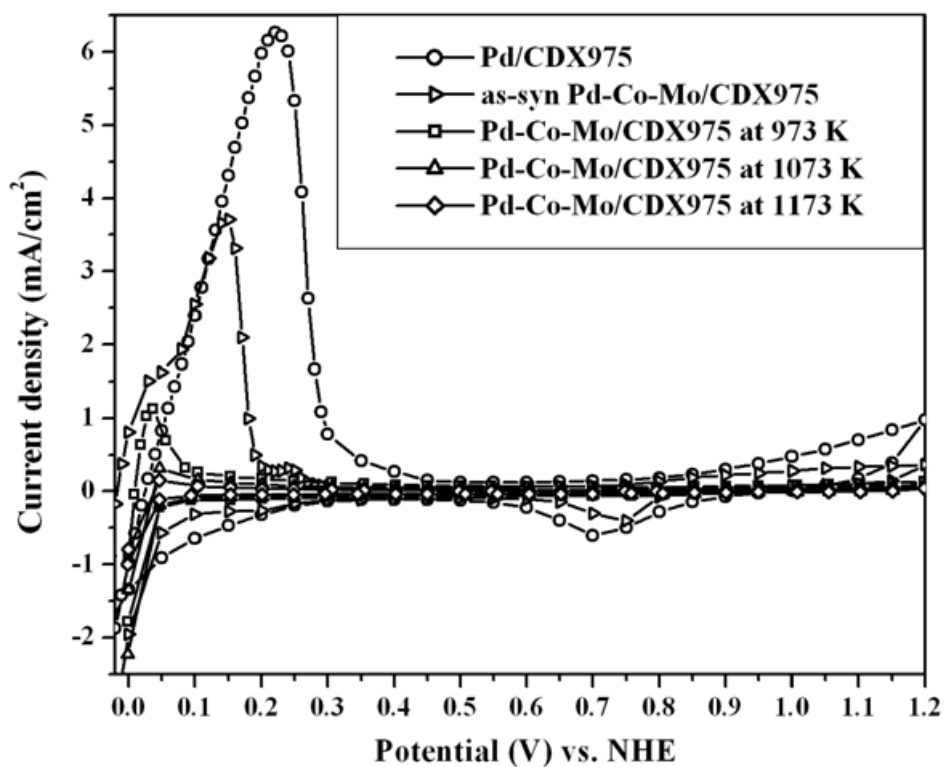


Fig. 5.5 Cyclic voltammograms (CVs) of carbon supported Pd and Pd-Co-Mo catalysts in Ar-saturated 0.5 M H<sub>2</sub>SO<sub>4</sub>; Scan rate – 25 mV s<sup>-1</sup>

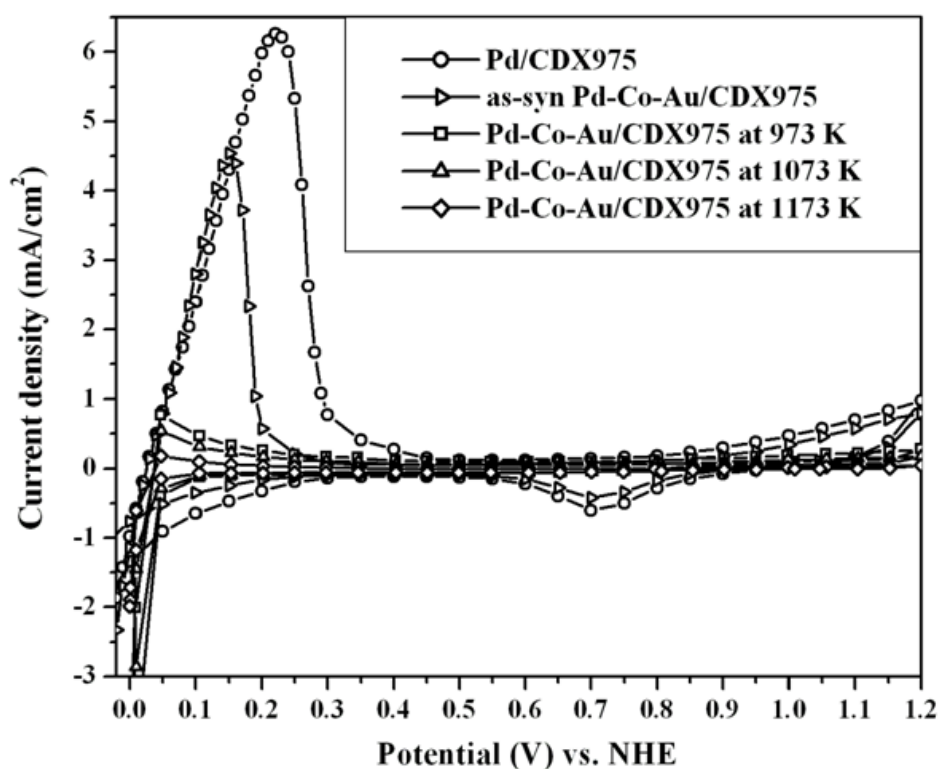


Fig. 5.6 Cyclic voltammograms (CVs) of carbon supported Pd and Pd-Co-Au catalysts in Ar-saturated 0.5 M H<sub>2</sub>SO<sub>4</sub>; Scan rate – 25 mV s<sup>-1</sup>

*et al.*, 1983). Moreover, the formation of surface oxy species which are the poisoning species for oxygen reduction are not observed and this may be beneficial to the oxygen adsorption at low overpotential and thus the ORR kinetic enhancement. A similar phenomenon is observed in the case of Pd-Co-Au/CDX975 catalysts also (Fig. 5.6).

For oxygen reduction measurements, linear sweep voltammograms (LSVs) are recorded between +0.2 V and +1.2 V vs. NHE at a scan rate of  $5 \text{ mV s}^{-1}$  in both Ar- and  $\text{O}_2$ -saturated  $0.5 \text{ M H}_2\text{SO}_4$ . Fig. 5.7 and 5.8 shows the linear sweep voltammograms (LSVs) of Pd-Co-Mo/CDX975 and Pd-Co-Au/CDX975 catalysts inrespectively. For comparison, LSVs of as-synthesized Pd/CDX975 and Pt/C (E-TEK) are also shown. As can be seen, at the applied potential lower than ca. 0.6 V, the ORR is under diffusion-controlled regime where mass transfer of  $\text{O}_2$  to the electrode determines the ultimate current density. The ORR falls into the kinetics-controlled regime at the potential at or above +0.7 V at which the catalytic activity of the catalysts will be benchmarked. When the potential is swept from +1.2 to +0.2 V vs NHE, single oxygen reduction peak is observed in the potential region of ca. 1.0–0.6 V in all the catalysts. The steep increase in peak current indicates the facile kinetics of oxygen reduction. Oxygen reduction activity of the catalysts is calculated by taking the difference in activity at +0.7 V vs. NHE in Ar- and  $\text{O}_2$ - saturated  $0.5 \text{ M H}_2\text{SO}_4$  and given in Table 5.3.

The important points emerged from LSV results are, (i) Pd-Co-M/CDX975 (M = Mo and Au) catalysts exhibited the good activity to oxygen reduction compared to the Pd/CDX975. The propensity of Pd to form  $\text{PdO}_x$  species, the reaction inhibitor that does not take part in the reaction, may be the reason of its low activity for the ORR.

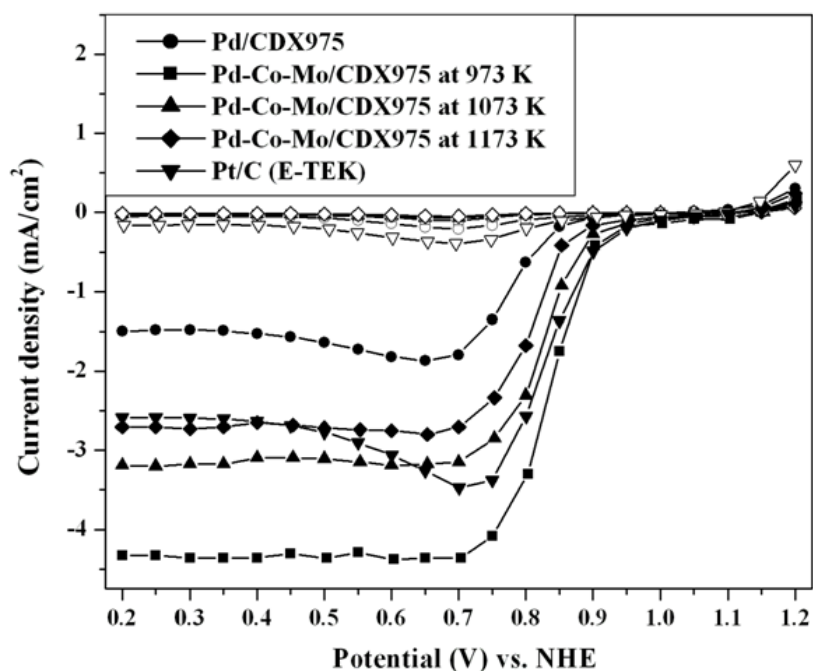


Fig. 5.7 Linear sweep voltammograms (LSVs) of  $O_2$  reduction on carbon supported Pd, Pd-Co-Mo and commercial Pt/C (E-TEK) catalysts in 0.5 M  $H_2SO_4$ ; Scan rate -  $5 \text{ mV s}^{-1}$  (Empty and full symbols corresponding to the LSVs in Ar- and  $O_2$ - saturated 0.5 M  $H_2SO_4$ )

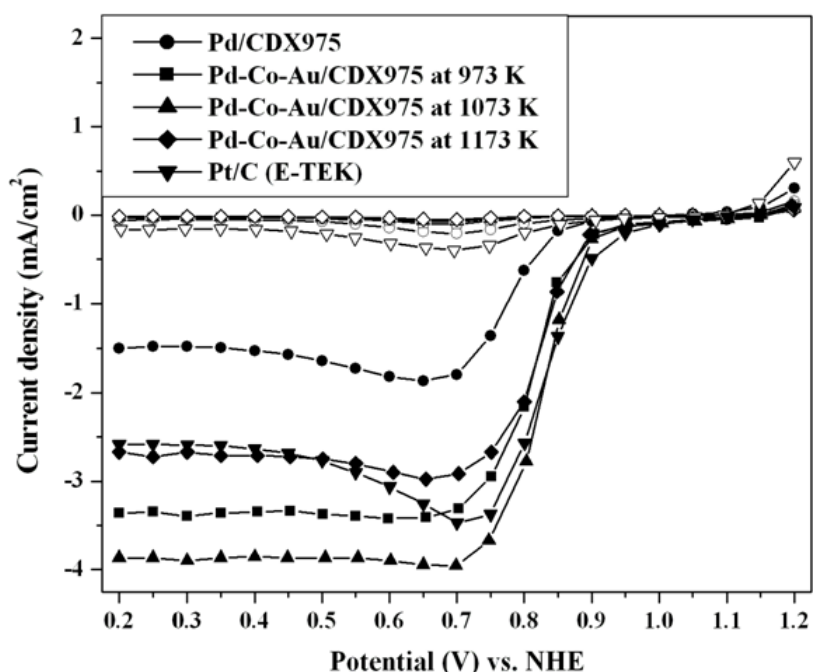


Fig. 5.8 Linear sweep voltammograms (LSVs) of  $O_2$  reduction on carbon supported Pd, Pd-Co-Au and commercial Pt/C (E-TEK) catalysts in 0.5 M  $H_2SO_4$ ; Scan rate -  $5 \text{ mV s}^{-1}$  (Empty and full symbols corresponding to the LSVs in Ar- and  $O_2$ - saturated 0.5 M  $H_2SO_4$ )

Table 5.3 EDX composition, onset potential for oxygen reduction and ORR activity of Pd/CDX975, Pd-Co-M/CDX975 (M = Mo and Au) and commercial Pt/C catalysts

Catalyst	EDX composition Pd:Co:M	Onset potential (mV vs. NHE)	ORR activity at +0.7 V vs NHE (mA cm <sup>-2</sup> )
Pd/CDX975	100 :- :-	+840	1.6
Pd-Co-Mo(7:2:1)/CDX975 at 973 K	77.7:12.3:10.0	+875	3.3
Pd-Co-Mo(7:2:1)/CDX975 at 1073 K	78.3:12.6:9.1	+910	3.9
Pd-Co-Mo(7:2:1)/CDX975 at 1173 K	78.7:12.5:8.8	+880	2.9
Pd-Co-Au(7:2:1)/CDX975 at 973 K	70.2:11.2:18.6	+920	4.1
Pd-Co-Au(7:2:1)/CDX975 at 1073 K	71.3:11.6:17.1	+905	3.0
Pd-Co-Au(7:2:1)/CDX975 at 1173 K	71.8:11.3:16.9	+865	2.6
Commercial Pt/C (E-TEK)	Pt – 19.8	+915	3.1

Among the heat-treated Pd-Co-M/CDX975 catalysts (M = Mo and Au), maximum ORR activity is observed for the heat-treated Pd-Co-Mo/CDX975 at 973 K and Pd-Co-Au/CDX975 at 1073 K. Moreover, their activity is higher than that of commercial Pt/C catalyst. (ii) Oxygen reduction proceeded in a relatively positive potential region for the Pd-Co-M/CDX975 (M = Mo and Au) catalysts compared to the Pd/CDX975. The overpotential for ORR of the Pd alloys is about 50 mV less compared to that of Pd. This is due to the modification of electronic structure and alteration of redox energy levels of Pd by the presence of Co and Mo/Au. The differences in the onset potential for oxygen reduction at various heat-treated Pd-Co-M/CDX975 (M = Mo and Au) catalysts may be due to differences in the surface activation, which are related to the size and distribution of the metallic nanoparticles. (iii) Onset potential for oxygen reduction (around +910 mV vs. NHE) and shape of LSVs indicate that the ORR pathway and rate-determining step are the same on Pd-Co-M/CDX975 (M = Mo and Au) and Pt/C catalysts.

It is known that both the electronic factors arising from the alloy content and geometric factors arising from particle size are known to influence the chemisorption behavior of oxygenated species and consequently the catalytic activity for ORR (Mukerjee *et al.*, 1995b; Toda *et al.*, 1999; Xiong and Manthiram, 2005b). Fig. 5.9 shows the effect of heat-treatment temperature on the surface area and on the catalytic activity for ORR of the Pd–Co–Mo/CDX975 catalysts prepared by the reverse microemulsion method. A nearly linear correlation is observed between ORR current density and the surface area as a function of the heat-treatment temperature. The high ORR activity observed for Pd-Co-Mo/CDX975 catalyst obtained at a heat-treatment temperature of 973 K is due to the small crystallite size and high surface area.

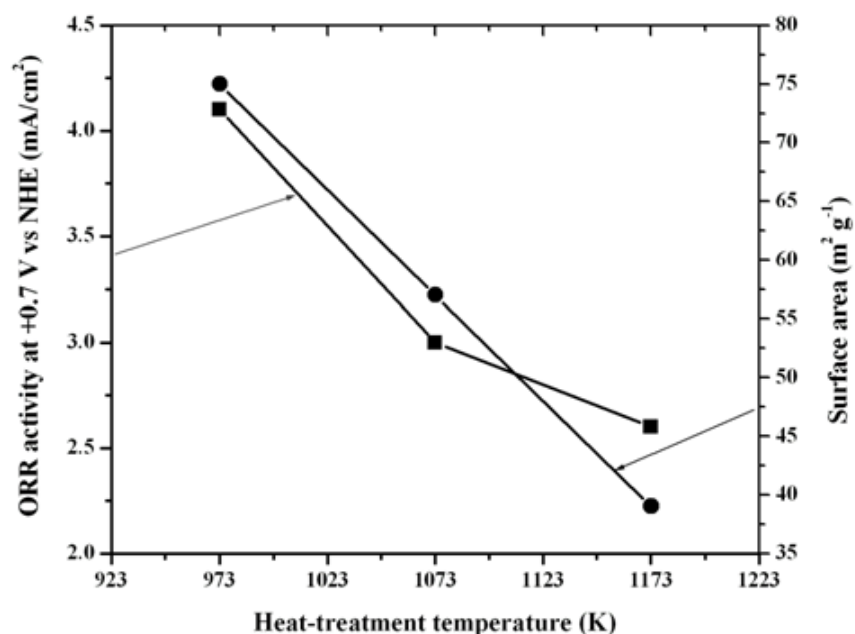


Fig. 5.9 Effect of heat-treatment temperature on the ORR activity and surface area of the carbon supported Pd–Co–Mo (Pd:Co:Mo = 70:20:10 atom%) catalysts prepared by the reverse microemulsion method

Fig. 5.10(a) shows the effect of heat-treatment temperature on the degree of alloying and on the surface area of the Pd–Co–Au/CDX975 catalysts, derived from XRD. It



shows that the degree of alloying ( $D_A$ ) increases while the surface area decreases with increasing heat-treatment temperature. The decrease in the surface area is due to an increase in the crystallite size (Table 5.2). The ORR activity of the catalysts at +0.7 V as a function of heat-treatment temperature is presented in Fig. 5.10(b).

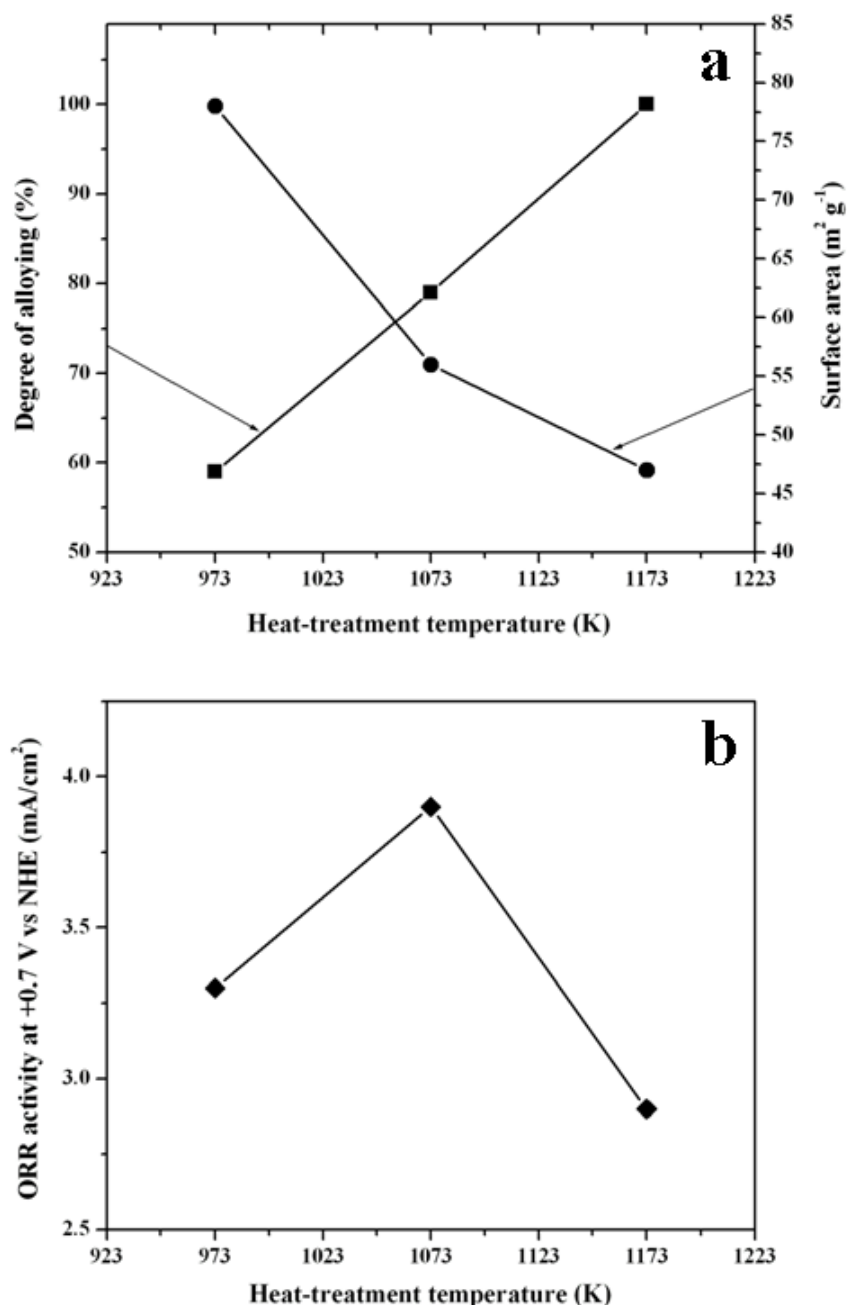


Fig. 5.10 Effect of heat treatment temperature on the (a) degree of alloying and surface area and (b) catalytic activity for ORR of the carbon supported Pd–Co–Au (Pd:Co:Au = 70:20:10 atom%) catalysts prepared by the reverse microemulsion method

The ORR catalytic activity increases with increasing heat-treatment temperature reaches a maximum at 1073 K and then decreases on going to 1173 K. The initial increase is due to an increase in the degree of alloying while the decrease at higher temperatures is due to an increase in particle size and a decrease in surface area.

### 5.4.3 Chronoamperometric Response

The performance of Pd and Pd-Co-M alloy electrocatalysts is examined at +0.7 V vs NHE in O<sub>2</sub>-saturated 0.5 M H<sub>2</sub>SO<sub>4</sub> solution for 3 h. The corresponding current density-time plots are shown in Fig. 5.11 and 5.12. During the test, oxygen gas is bubbled continuously into the solution.

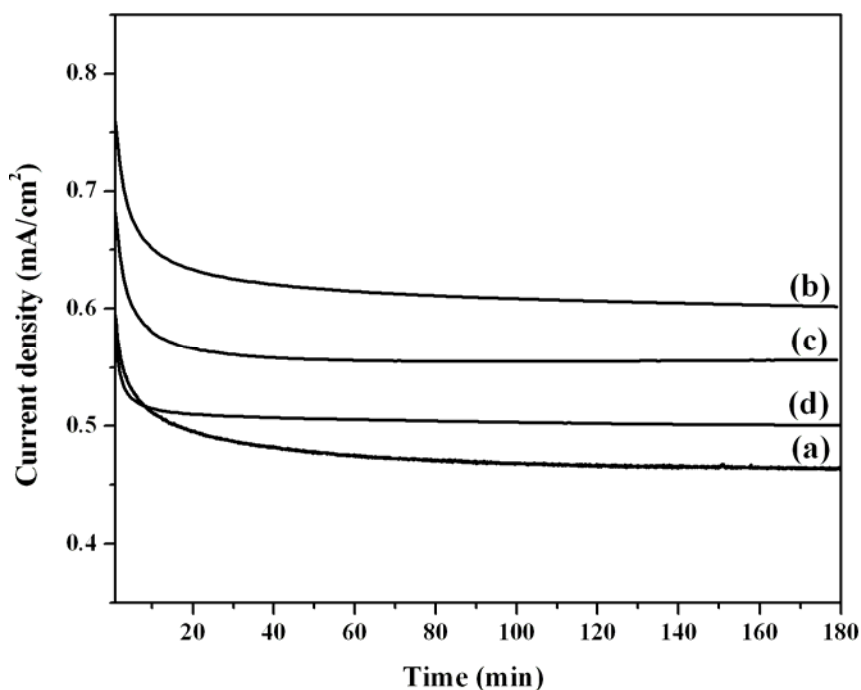


Fig. 5.11 Current density-time plot of (a) Pd/CDX975; heat-treated Pd-Co-Mo(7:2:1)/CDX975 at (b) 973 K (c) 1073 K and (d) 1173 K respectively in oxygen saturated 0.5 M H<sub>2</sub>SO<sub>4</sub> at +0.7 V vs NHE for 3 h

It can be seen that the performance of Pd-Co-M/CDX975 catalysts is better than the Pd/CDX975. In the case of heat-treated Pd-Co-M/CDX975 catalysts at 973 K, current

density declines slowly by the dissolution of alloying components. This may be due to the poor degree of alloying. Among all the carbon supported Pd-Co-M alloy catalysts, heat-treated Pd-Co-M/CDX975 (M = Mo and Au) obtained at 1073 and 1173 K exhibited good performance possibly due to high degree of alloying.

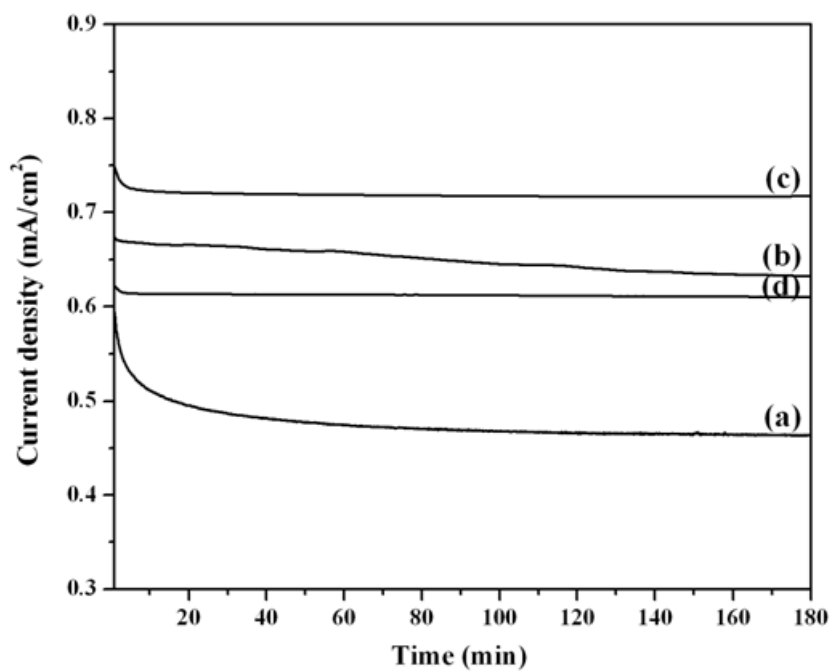


Fig. 5.12 Current density-time plot of (a) Pd/CDX975; heat-treated Pd-Co-Au(7:2:1)/CDX975 at (b) 973 K (c) 1073 K and (d) 1173 K respectively in oxygen saturated 0.5 M H<sub>2</sub>SO<sub>4</sub> at +0.7 V vs NHE for 3 h

## CHAPTER 6

### **Ru<sub>x</sub>Se<sub>y</sub>/C CATALYSTS FOR OXYGEN REDUCTION – A REVERSE MICROEMULSION METHOD OF FABRICATION OF ELECTRODE MATERIAL**

#### **6.1 INTRODUCTION**

Carbon supported Ru<sub>x</sub>Se<sub>y</sub> catalysts constitute one class of materials that show activity for oxygen reduction (Alonso-Vante and Tributsch, 1986; Alonso-Vante *et al.*, 2000). Numerous electrochemical investigations have proven that oxygen reduction occurs on Ru<sub>x</sub>Se<sub>y</sub> catalysts predominantly via four electron reduction path with negligible amount of hydrogen peroxide intermediate compared to the Pt catalysts (Colmenares *et al.*, 2006; Zaikovskii *et al.*, 2006; Colmenares *et al.*, 2007; Fiechter *et al.*, 2007).

Many methods have been reported for carbon supported Ru<sub>x</sub>Se<sub>y</sub> catalysts preparation, including chemical precipitation method (Trapp *et al.*, 1996; Reve *et al.*, 1998), NaBH<sub>4</sub> reduction method (Campbell, 2004), impregnation method (Hilgendorff *et al.*, 2003), colloidal method (Tributsch *et al.*, 2001), decomposition of organometallic precursors (Vogel *et al.*, 2007) and microwave-assisted polyol process (Liu *et al.*, 2007). However, these preparation methods result in the difficulties of controlling chemical composition and particle size regardless of metal content. Trapp *et al.* (1996) proposed a low temperature chemical precipitation method by refluxing metal carbonyls and the corresponding chalcogen in an organic solvent such as xylene or 1,2-dichlorobenzene in Ar atmosphere. The reaction products consist of nano-scale Ru metals and octahedral clusters of Ru, which contain carbon in the centre, surrounded by carbonyl groups. Since this method involved some complex chemical reactions, a mixture containing several polynuclear compounds with amorphous

structures could be produced, depending on the synthesis temperature. It was difficult to separate and characterize this mixture by traditional chemical methods due to their poor solubility, which was probably one of the drawbacks of this synthesis method. Another disadvantage of this method could be that the yield of the final product was 40–60%. Reeve *et al.* (1998) also carried out the synthesis using Ru-based electrocatalysts for oxygen reduction. But the activity of the synthesized catalysts is low compared to Pt. Campbell (2004) disclosed an environment friendly aqueous method for preparing active catalysts such as  $\text{Ru}_x\text{Se}$  by eliminating the carbonyl precursors and toxic solvents like xylene. In this method, the stoichiometric amounts of active carbon, ruthenium (III) chloride and selenium dioxide were taken in a water/propanol solvent and stirred at 353 K for 1 h. The resulting mixed solution was then allowed to cool at room temperature. An aqueous solution of NaOH containing  $\text{NaBH}_4$  was then added to the solution to carry out the chemical reduction. In this way, a carbon-supported catalyst, which has a chemical formula of  $\text{Ru}_x\text{Se}$ , was produced. They claimed that the electrocatalytic ORR activity of prepared catalysts was very close to that of carbon-supported platinum catalysts. Even then, the onset potential is 100 mV less compared to that of commercial Pt/C catalyst. Hilgendorff *et al.* (2003) attempted to synthesize  $\text{Ru}_x\text{Se}_y$  by impregnation process. One possible drawback of this method is that the temperature used to sinter the catalyst particles is relatively high, which could reduce the catalyst active surface area. In this process, a solution of ruthenium oxalate or carbonyl complex was mixed with a carbon support to form slurry, which was then dried to remove the solvent. The formed solid was then heated to decompose the salt, in order to produce the desired form of solid carbon-Ru salt. For selenium incorporation, the solid was dispersed in a solution containing  $\text{H}_2\text{SeO}_3$ . After the chemical reaction between the carbon-Ru salt and

$\text{H}_2\text{SeO}_3$ , a  $\text{Ru}_x\text{Se}_y$  catalyst was produced. The low temperature chemical precipitation method described has the advantage of allowing the reaction performed in a solution to form bimetallic catalysts at low temperature and the prepared catalysts normally have a higher active area. However, this method was limited to those reactants with similar precipitation chemistry or property, which are easily reduced chemically to metals. In order to minimize this limitation, Tributsch *et al.* (2001) followed the colloidal method described by Bönemann *et al.* in 1996. But the reproducibility was relatively low. The first step for the catalyst synthesis was to make colloidal Ru nanoparticles through  $\text{RuCl}_3$  reduction in a solution of tetrahydrofuran (THF) containing  $\text{N}(\text{C}_8\text{H}_{17})_4\text{BEt}_3\text{H}$ , followed by addition of absolute ethanol. After that, the mixture was centrifuged (4500 rpm, 15 min) to obtain the solid powder. After the incorporation of selenium,  $\text{Ru}_x\text{Se}_y\text{O}_z$  nanoparticles were prepared. The produced catalyst was tested for  $\text{O}_2$  reduction and a fairly high electrocatalytic activity was observed. The high catalytic activity has been attributed to its large surface area, narrow particle size distribution, and ability to prevent particle aggregation. All the methods described involve the difficulty in the control of the composition. As a result, various authors obtained  $\text{Ru}_x\text{Se}_y$  catalysts of different Ru and Se compositions with different sizes. So the oxygen reduction activities observed were not comparable. Recently, Colmenares *et al.* (2007) synthesized Se-modified Ru/C catalysts of controllable compositions by two steps process: synthesis of Ru/C by borate route followed by adding controllable amounts of selenium via reductive annealing of the  $\text{H}_2\text{SeO}_3$  impregnated catalysts at 473 K in a  $\text{H}_2$  gas flow. This method results in  $\text{Ru}_x\text{Se}_y/\text{C}$  catalysts with a mean Ru particle diameter of 4 nm with varying amounts of Se and small amount of oxygen content. Even though they were able to control the composition, particle size was not the same in all the catalysts. The results obtained

by various authors were encouraging, but the ORR activity was not comparable with that of commercial Pt/C. All the electrochemical studies indicate that there is optimum Ru:Se composition for the maximum ORR activity. If one is able to control composition and size of  $\text{Ru}_x\text{Se}_y/\text{C}$  catalysts and measure ORR activity, it will shorten the path of search of efficient electrocatalysts for oxygen reduction.

In the present study,  $\text{Ru}_x\text{Se}_y/\text{C}$  ( $x = 1$  and  $y = 0-1$ ) catalysts with similar size and controllable composition have been synthesized by a simple and reproducible reverse microemulsion method (RME) at room temperature. The resultant catalysts are characterized by X-ray diffraction (XRD), scanning electron microscopy (SEM), transmission electron microscopy (TEM), and energy-dispersive X-ray analysis (EDX). The as-synthesized catalysts are investigated for oxygen reduction and the activity obtained is compared with that of commercial Pt/C (E-TEK).

## **6.2 SYNTHESIS OF 20 wt% $\text{Ru}_x\text{Se}_y/\text{CDX975}$ CATALYSTS**

Carbon supported  $\text{Ru}_x\text{Se}_y$  catalysts (where  $x = 1$  and  $y = 0-1$ ) with a metal(s) loading of 20 wt% are prepared by the reverse microemulsion method (RME) with the use of sodium bis(2-ethylhexyl) sulfosuccinate (AOT) as the surfactant and heptane as the oil phase. Aqueous solutions of  $\text{RuCl}_3$ ,  $\text{H}_2\text{SeO}_3$  and  $\text{NaBH}_4$  are used to form the reverse micelle. The size of the particles is controlled by adjusting the molar ratio of surfactant to water ( $W = [\text{H}_2\text{O}]:[\text{AOT}]$ ). Microemulsion 1 is prepared by mixing required amounts of  $\text{RuCl}_3$ , selenous acid, AOT, deionized water and heptane under constant stirring followed by ultrasonication for 20 min. Microemulsion 2 is prepared by mixing sodium borohydride with small amount of NaOH, AOT, deionized water and heptane under constant stirring followed by ultrasonication for 20 min. In both the microemulsions, the molar ratio of water to AOT was kept at 10:1. Microemulsions 1

and 2 are then mixed together and ultrasonicated for 2 h. Subsequently, an appropriate amount of carbon (CDX975) is added to the mixture to give a metal(s):C weight ratio of 20:80. The resultant slurry is kept under constant stirring for 2 h, filtered, washed with acetone and deionized water and dried in an air oven at 348 K for 2 h.

### 6.3 CHARACTERIZATION OF THE Ru<sub>x</sub>Se<sub>y</sub>/CDX975 CATALYSTS

#### 6.3.1 X-ray Diffraction Analysis

XRD measurements are performed on all the catalysts at a scan rate of  $0.05^\circ \text{ s}^{-1}$  over the  $2\theta$  range of  $10^\circ$ - $90^\circ$ . Fig. 6.1 shows the powder X-ray diffraction patterns of the Ru<sub>x</sub>Se<sub>y</sub>/CDX975 catalysts. All the as-synthesized Ru<sub>x</sub>Se<sub>y</sub>/CDX975 catalysts show the peaks at  $2\theta$  values around  $38^\circ$ ,  $42^\circ$ ,  $44^\circ$ ,  $58^\circ$ ,  $69^\circ$ ,  $78^\circ$  and  $85^\circ$  corresponding to the (100), (002), (101), (102), (110), (103) and (112) planes of ruthenium respectively. These characteristic peaks can be assigned to *hcp* ruthenium. The positions and intensities of *hcp* ruthenium diffraction lines are in good agreement with that of JCPDS powder diffraction data file no. 89-4903. With increasing the Se to Ru atomic ratio, Ru diffraction lines shift slightly to higher  $2\theta$  values with respect to the corresponding peaks in Ru/CDX975 catalyst.

To check the solubility of Se in Ru lattice, the lattice parameters (*a*, *c*) and cell volumes are calculated from XRD patterns and given in Table 6.1. The variation of lattice parameters and cell volume with Se content in Ru<sub>x</sub>Se<sub>y</sub> catalysts is plotted and is shown in Fig. 6.2. It can be seen that both the lattice parameters (*a*, *c*) and the cell volume of Ru<sub>x</sub>Se<sub>y</sub> decrease linearly with increasing Se content (obeying Vegard's law) indicating the solubility of Se in Ru lattice. The broad peaks indicate that the particles are in nano-crystalline range. The broad diffraction peak observed at around  $2\theta = 25^\circ$  corresponds to the (002) diffraction plane of the hexagonal structure of the carbon support.



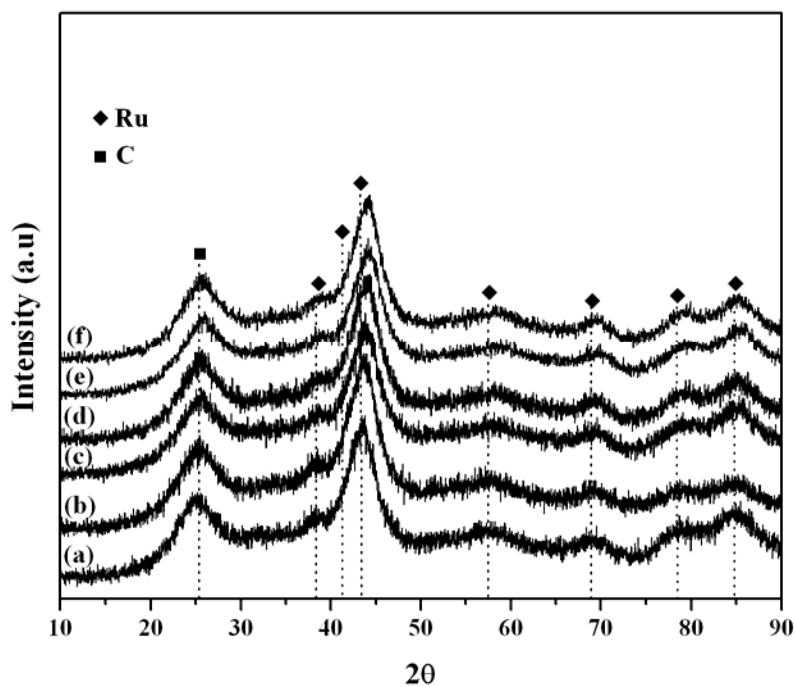


Fig. 6.1 Powder X-ray diffraction patterns of as-synthesized  $\text{Ru}_x\text{Se}_y/\text{CDX975}$  catalysts; (a)  $\text{Ru}/\text{CDX975}$  (b)  $\text{Ru}_1\text{Se}_{0.2}/\text{CDX975}$  (c)  $\text{Ru}_1\text{Se}_{0.4}/\text{CDX975}$  (d)  $\text{Ru}_1\text{Se}_{0.6}/\text{CDX975}$  (e)  $\text{Ru}_1\text{Se}_{0.8}/\text{CDX975}$  and (f)  $\text{Ru}_1\text{Se}_1/\text{CDX975}$

Table 6.1 Lattice parameters (a, c) and cell volume of  $\text{Ru}_x\text{Se}_y/\text{CDX975}$  catalysts

Catalyst	C (Å)	a (Å)	$0.866 a^2 c$ (Å <sup>3</sup> )
$\text{Ru}/\text{CDX975}$	4.27	2.713	27.22
$\text{Ru}_1\text{Se}_{0.2}/\text{CDX975}$	4.263	2.708	27.07
$\text{Ru}_1\text{Se}_{0.4}/\text{CDX975}$	4.257	2.700	26.87
$\text{Ru}_1\text{Se}_{0.6}/\text{CDX975}$	4.251	2.697	26.78
$\text{Ru}_1\text{Se}_{0.8}/\text{CDX975}$	4.245	2.694	26.68
$\text{Ru}_1\text{Se}_1/\text{CDX975}$	4.239	2.687	26.50

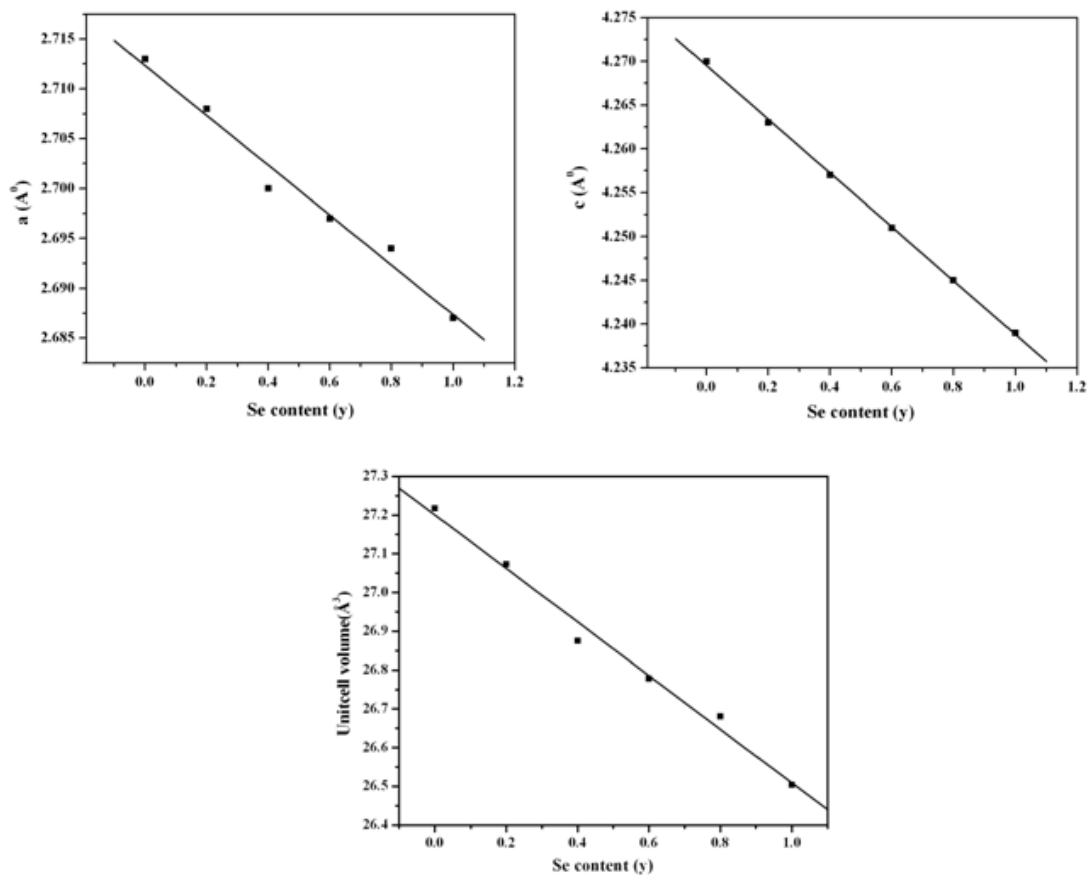


Fig. 6.2 Variation of lattice parameters and cell volume with Se content in  $Ru_xSe_y/CDX975$  catalysts

For crystallite size measurements, XRD spectra are recorded in the  $2\theta$  range of  $63-75^\circ$  at a scan rate of  $0.02^\circ s^{-1}$ . The average crystallite size for the  $Ru_xSe_y/CDX975$  catalysts is calculated from the broadening of the (110) diffraction peak (shown in Fig. 6.3) using Scherrer's equation (Patterson, 1939). The obtained results are given in Table 6.2. The average crystallite size is estimated to be around 3.0 nm in all the  $Ru_xSe_y/CDX975$  catalysts.

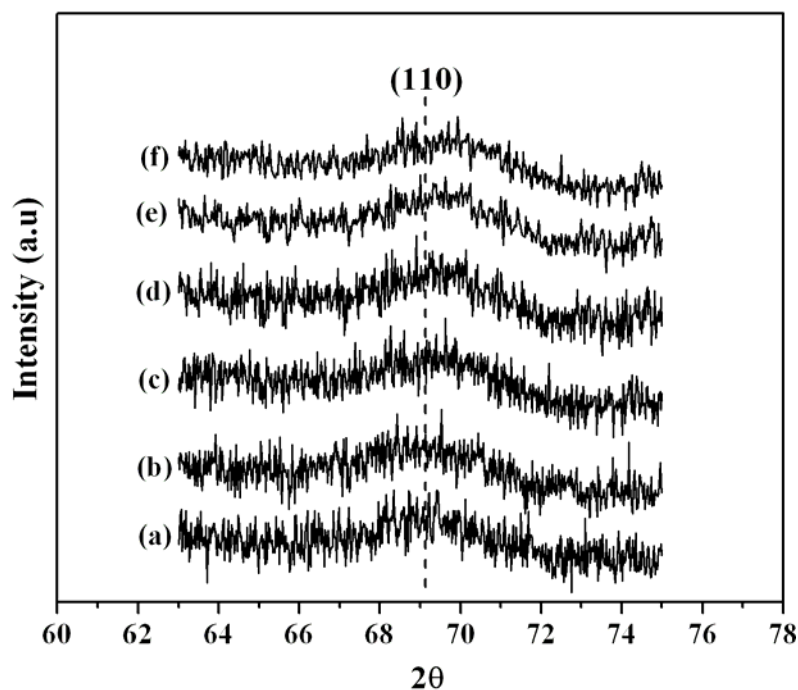


Fig. 6.3 Slow scan XRD spectra for the (110) peak of  $\text{Ru}_x\text{Se}_y/\text{CDX975}$  catalysts; (a)  $\text{Ru}/\text{CDX975}$  (b)  $\text{Ru}_1\text{Se}_{0.2}/\text{CDX975}$  (c)  $\text{Ru}_1\text{Se}_{0.4}/\text{CDX975}$  (d)  $\text{Ru}_1\text{Se}_{0.6}/\text{CDX975}$  (e)  $\text{Ru}_1\text{Se}_{0.8}/\text{CDX975}$  and (f)  $\text{Ru}_1\text{Se}_1/\text{CDX975}$

Table 6.2 Elemental composition, Se/Ru atomic ratio, crystallite size, onset potential for oxygen reduction and ORR activity of 20 wt%  $\text{Ru}_x\text{Se}_y/\text{CDX975}$  ( $x = 1$  and  $y = 0-1$ ) and commercial 20 wt% Pt/C (E-TEK) catalysts

Catalyst	Elemental composition by EDX	Se/Ru atomic ratio	Crystallite size from XRD (nm)	Onset potential (mV vs. NHE) for ORR	ORR activity at +0.65 V vs. NHE ( $\text{mA cm}^{-2}$ )
$\text{Ru}/\text{CDX975}$	100:-	0.0	3.0	+850	1.3
$\text{Ru}_1\text{Se}_{0.2}/\text{CDX975}$	87.7:12.3	0.18	3.0	+875	2.1
$\text{Ru}_1\text{Se}_{0.4}/\text{CDX975}$	76.6:23.4	0.38	3.1	+890	3.0
$\text{Ru}_1\text{Se}_{0.6}/\text{CDX975}$	68.5:31.5	0.59	3.1	+905	4.2
$\text{Ru}_1\text{Se}_{0.8}/\text{CDX975}$	62.2:37.8	0.78	3.1	+885	1.6
$\text{Ru}_1\text{Se}_1/\text{CDX975}$	56.2:43.8	1.00	3.1	+870	1.4
Pt/C (E-TEK)	-	-	-	+930	4.0

### 6.3.2 SEM, EDX and TEM Analysis

Scanning electron microscopy (SEM), transmission electron microscopy (TEM) and energy dispersive X-ray analysis (EDX) are used to observe the morphology, particle size and composition of Ru<sub>1</sub>Se<sub>0.6</sub>/CDX975 catalyst respectively. Fig. 6.4 shows the SEM image and corresponding EDX spectrum of Ru<sub>1</sub>Se<sub>0.6</sub>/CDX975 catalyst. Agglomeration of spherical shaped carbon with metallic particles can be seen from SEM image (Fig. 6.4(a)). Elemental analysis performed by EDX confirms the presence of Ru, Se, C and a very small quantity of oxygen (Fig. 6.4(b)). The calculated elemental composition (Ru:Se) in Ru<sub>1</sub>Se<sub>0.6</sub>/CDX975 is about (wt %) 68.5:31.5 corresponding to Se/Ru atomic ratio of 0.59. Similarly the other catalysts of different Ru and Se composition are analyzed. For each molar ratio of Ru/Se, some regions are chosen randomly to analyze the composition by EDX attached to a SEM. The results are given in Table 6.1. The slight deviation of composition among different particles at each [RuCl<sub>3</sub>]/[H<sub>2</sub>SeO<sub>3</sub>] ratio might result from the detection errors. The deviation could be due to the detection errors and the fact that fewer regions were chosen for analysis. In addition, it is observed that the average compositions were roughly in agreement with those of the initial metal salt solutions.

Fig. 6.5 represents the TEM images of the as-synthesized Ru<sub>1</sub>Se<sub>0.6</sub>/CDX975 and commercial Pt/C catalysts. Well dispersed, uniform size and spherical shaped metallic nanoparticles with an average size of 3.1 nm on the carbon support can be seen from both the low- and high-magnification TEM images (Fig. 6.5(a) and 6.5(b)). The average crystallite size calculated from the XRD peak width was found to be consistent with those obtained from the TEM result. Fig. 6.5(c) shows the narrow size distribution of Ru<sub>1</sub>Se<sub>0.6</sub> nanoparticles on carbon support.

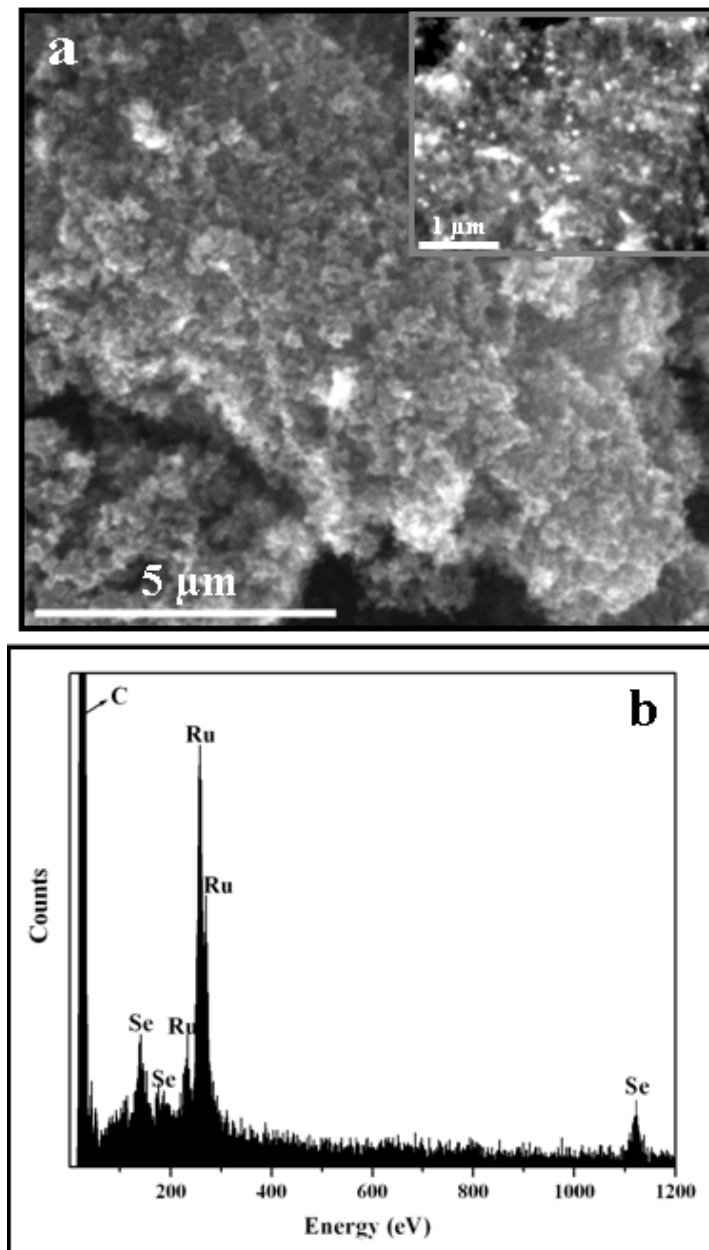


Fig. 6.4 (a) SEM image (inset shows the high magnification image) and (b) EDX spectrum of  $\text{Ru}_1\text{Se}_{0.6}/\text{CDX975}$

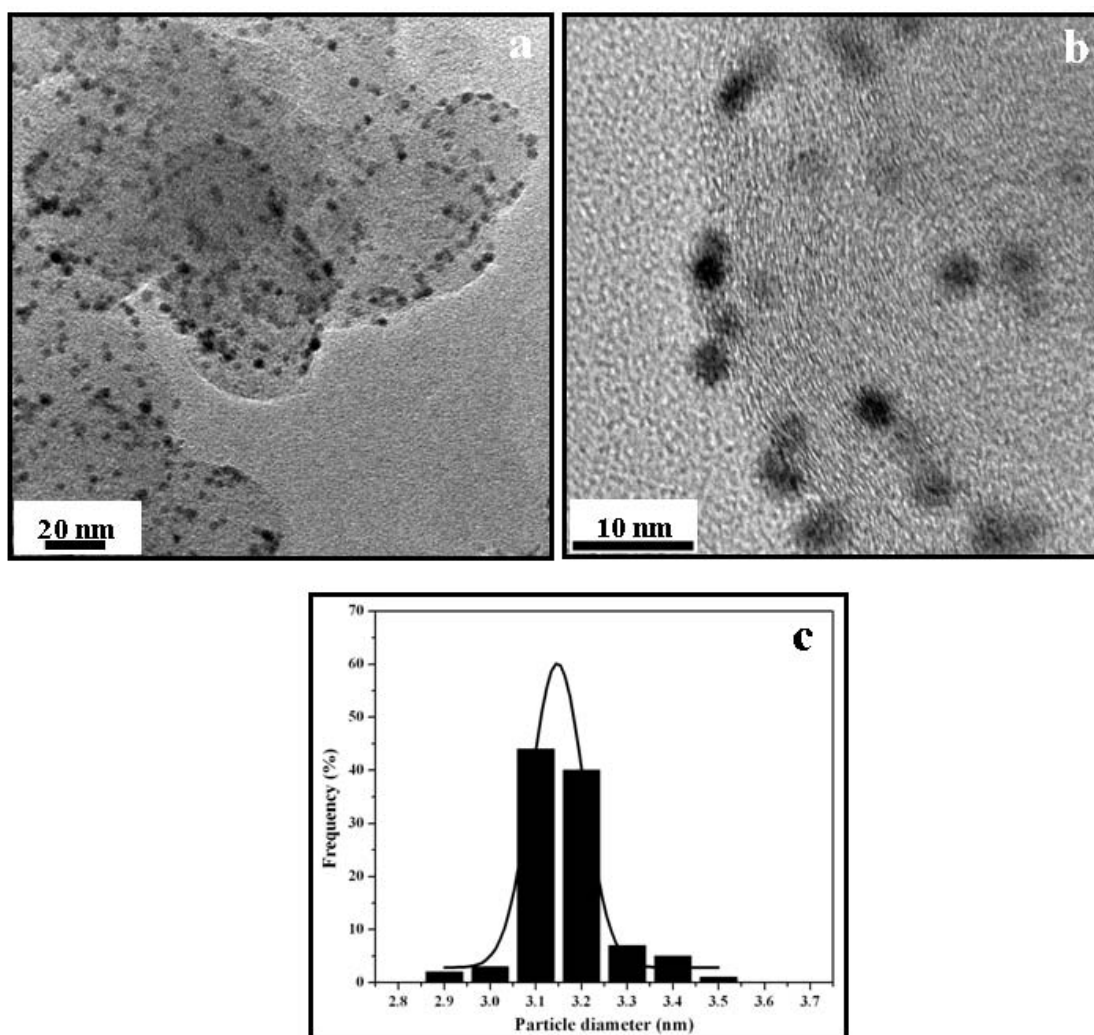


Fig. 6.5 TEM images of (a)  $\text{Ru}_1\text{Se}_{0.6}/\text{CDX975}$  at low magnification (b)  $\text{Ru}_1\text{Se}_{0.6}/\text{CDX975}$  at high magnification. (c) Histogram of  $\text{Ru}_1\text{Se}_{0.6}$  particles on CDX975

## 6.4 ELECTROCHEMICAL PERFORMANCE OF $\text{Ru}_x\text{Se}_y/\text{CDX975}$ CATALYSTS

### 6.4.1 Electrode Fabrication

The electrode is fabricated as follows: 5 mg of the catalyst, 0.5 ml of diluted Nafion® solution (Aldrich, 5 wt.% in 15-20% water/low aliphatic alcohols) and 0.5 ml of isopropanol are ultrasonically blended for 20 min. GC disk ( $0.07 \text{ cm}^2$ ) was polished to a mirror finish with  $0.05 \mu\text{m}$  alumina suspensions before each experiment and served as an underlying substrate of the working electrode. An aliquot of  $5 \mu\text{l}$  catalyst

suspension was pipetted onto the mirror polished glassy carbon substrate, leading to a metal loading of  $70 \mu\text{g}_{\text{metal}} \text{cm}^{-2}$  and dried in flowing argon at room temperature.

#### 6.4.2 Electrochemical Reduction of Oxygen

Activity of the as-synthesized  $\text{Ru}_x\text{Se}_y/\text{CDX975}$  (where  $x = 1$  and  $y = 0-1$ ) and commercial Pt/C catalysts is determined by cyclic voltammetry (CV). All experiments are performed at room temperature in a conventional one-compartment electrochemical glass cell assembled with glassy carbon (GC) disk as the working electrode, Ag/AgCl, 3.5 M KCl (+0.205 V vs. NHE) as the reference and Pt foil as the counter electrodes, respectively. Oxygen saturated 0.5 M  $\text{H}_2\text{SO}_4$  is the electrolyte. Linear sweep voltammetry (LSV) is performed to measure the oxygen reduction activity of as-synthesized  $\text{Ru}_x\text{Se}_y/\text{CDX975}$  and commercial Pt/C (E-TEK) catalysts. For oxygen reduction measurements, linear sweep voltammograms (LSVs) are recorded between +0.2 V and +1.2 V vs. NHE at a scan rate of 5 mV/s in both Ar- and  $\text{O}_2$ -saturated 0.5 M  $\text{H}_2\text{SO}_4$ . The obtained voltammograms are shown in Fig. 6.6. Oxygen reduction activity is calculated by taking the difference in activity at +0.65 V vs. NHE in Ar- and  $\text{O}_2$ - saturated 0.5 M  $\text{H}_2\text{SO}_4$ . Current densities are normalized to the geometric area of the glassy carbon substrate ( $0.07 \text{ cm}^2$ ). The calculated ORR activity of  $\text{Ru}_x\text{Se}_y/\text{CDX975}$  catalysts is given in Table 6.2. It is clear that the electrode fabricated by using as-synthesized  $\text{Ru}_1\text{Se}_{0.6}/\text{CDX975}$  shows higher oxygen reduction activity than other Ru catalysts. A high oxygen reduction current is paramount for an efficient electrochemical power device.

Fig. 6.6 represents that the ORR kinetics is not the same on all the catalysts. Oxygen reduction is facile in the case of Se to Ru atomic ratios of 0.2, 0.4 and 0.6 compared to the Se to Ru atomic ratios of 0, 0.8 and 1.0. In the case of  $\text{Ru}_x\text{Se}_y/\text{C}$  catalysts with x

= 1 and  $y = 0.2$  to  $0.6$ , ORR is diffusion-controlled at potentials below  $+0.6$  V and diffusion and kinetic controlled in the potential region between  $+0.6$  and  $+0.95$  V vs. NHE. In the case of  $\text{Ru}_x\text{Se}_y/\text{C}$  catalysts with  $x = 1$  and  $y = 0, 0.8$  and  $1.0$ , ORR is diffusion-controlled at potentials below  $+0.4$  V and diffusion and kinetic control in the potential region between  $+0.4$  and  $+0.9$  V vs. NHE. The reason for the different curve shapes for  $\text{Ru}_x\text{Se}_y/\text{C}$  catalysts with different Se/Ru atomic ratio may be due to the variation of geometric and electronic factors like Ru-Ru interatomic distance, Ru-Se distance, Ru coordination number and binding capacity of Se towards Ru active species (Zaikovskii *et al.*, 2006; Fiechter *et al.*, 2007). For all the Ru based catalysts, when the potential was swept from  $+1.2$  to  $+0.2$  V vs. NHE, single oxygen reduction peak is observed in the potential region of ca.  $1.0$ – $0.4$  V. The steep increase in peak current at  $+0.65$  V indicates the facile kinetics of ORR. At the lower amounts of Se to Ru atomic ratio of  $0.2$ , the formation of  $-\text{OH}$  species is inhibited to some extent compared to the Ru/CDX975. As a result both the onset potential and activity are increased. This is more prominent in the case of Se to Ru atomic ratio of  $0.4$  and  $0.6$ . At Se/Ru atomic ratio of  $0.6$ , the formation of  $-\text{OH}$  species on Ru surface was completely inhibited. At the Se/Ru atomic ratio of  $0.6$ , the geometric and electronic factors and Ru-Ru interatomic distance may be optimum so that it favours the dissociation of oxygen molecule and facile transfer of electrons; consequently steep increase of oxygen reduction peak current. At the Se contents beyond  $0.6$ , even though the formation of  $-\text{OH}$  species was inhibited, the Ru active species are blocked by the presence of Se. As a result, oxygen reduction is starts at potentials of  $+0.85$  V vs. NHE and complete reduction took place at potentials of  $+0.4$  V vs. NHE.



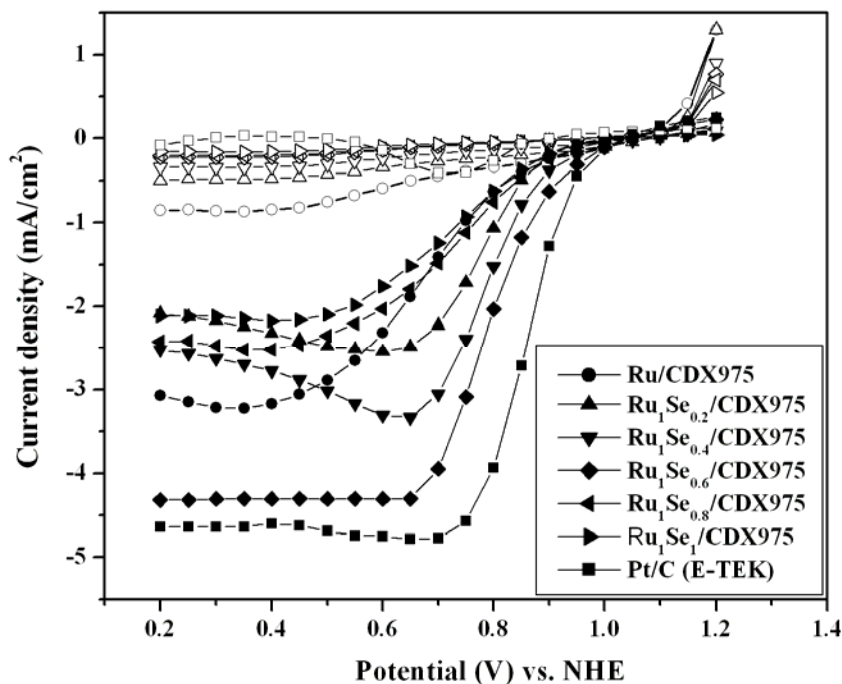


Fig. 6.6 Linear sweep voltammograms (LSVs) of O<sub>2</sub> reduction on 20 wt% Ru<sub>x</sub>Se<sub>y</sub>/CDX975 and commercial Pt/C (E-TEK) catalysts in 0.5 H<sub>2</sub>SO<sub>4</sub>; Scan rate – 5 mV s<sup>-1</sup> (Empty and full symbols corresponding to the LSVs in Ar- and O<sub>2</sub>- saturated 0.5 M H<sub>2</sub>SO<sub>4</sub> respectively)

The obtained oxygen reduction current density is plotted as a function of the Se/Ru atomic ratio in Fig. 6.7. It shows that the current density exhibits a maximum for the Ru<sub>1</sub>Se<sub>0.6</sub>/C catalyst. Further increase in Se content results in a decrease of the ORR activity, which however still exceeds the catalytic activity of the Ru/C catalyst. Recently Fiechter *et al.* (2006) also observed the higher selectivity (98-99%) for oxygen reduction to water at moderate Se loadings ( $y = 0.3-0.6$ ). Moreover, oxygen reduction activity of the as-synthesized Ru<sub>1</sub>Se<sub>0.6</sub>/CDX975 (4.2 mA cm<sup>-2</sup>) was comparable to that of the commercial Pt/C (E-TEK) catalyst (4.0 mA cm<sup>-2</sup>).

Fig. 6.8 represents the cyclic voltammograms (CVs) of Ru/CDX975 and Ru<sub>1</sub>Se<sub>0.6</sub>/CDX975 in de-aerated 0.5 M H<sub>2</sub>SO<sub>4</sub> at a scan rate of 20 mV s<sup>-1</sup>. It is revealed that the commencement of oxide/hydroxide species on the Ru surface at potentials of +0.25 V. The cathodic broad counter peak between +0.15 and +0.45 V can be thus

attributed to the surface oxide/hydroxide reduction and the negative shift of oxide/hydroxide reduction suggests an increased irreversibility of the surface oxidation (Marinkovic *et al.*, 2001; Zaikovskii *et al.*, 2006). It is reported in the literature that the ORR activity decreases with increasing  $\text{OH}_{\text{ad}}$  formation/surface oxidation (Zaikovskii *et al.*, 2006; Colmenares *et al.*, 2006) and also it has been shown that a pure oxide such as  $\text{RuO}_2$  at the metallic ruthenium surface, which would be encountered at potentials of practical oxygen electrodes (0.7-0.9 V vs. NHE) is inactive toward oxygen reduction (Anastasijevic *et al.*, 1986).

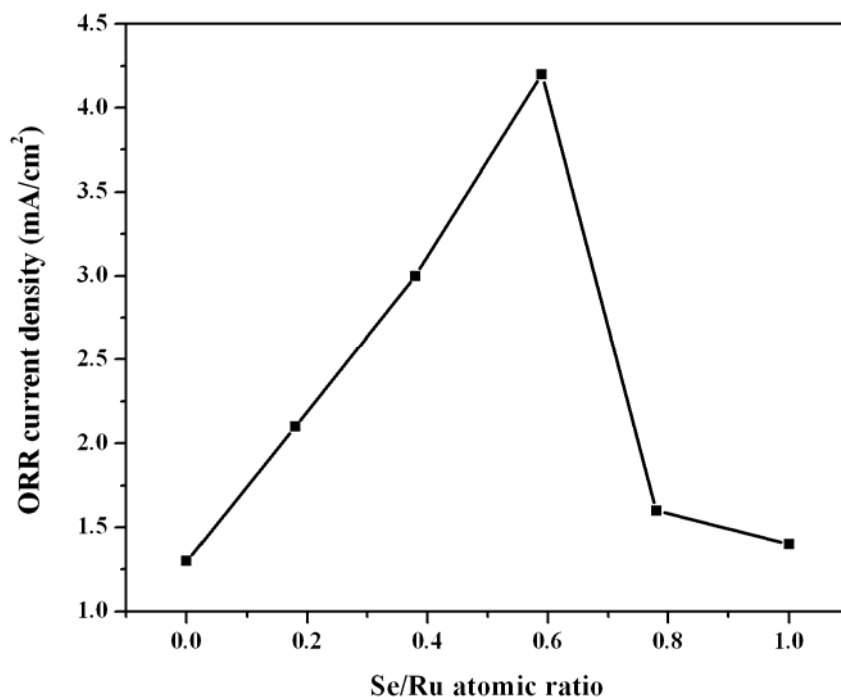


Fig. 6.7 Se/Ru atomic ratio vs. ORR current density of as-synthesized  $\text{Ru}_x\text{Se}_y/\text{CDX975}$  catalysts

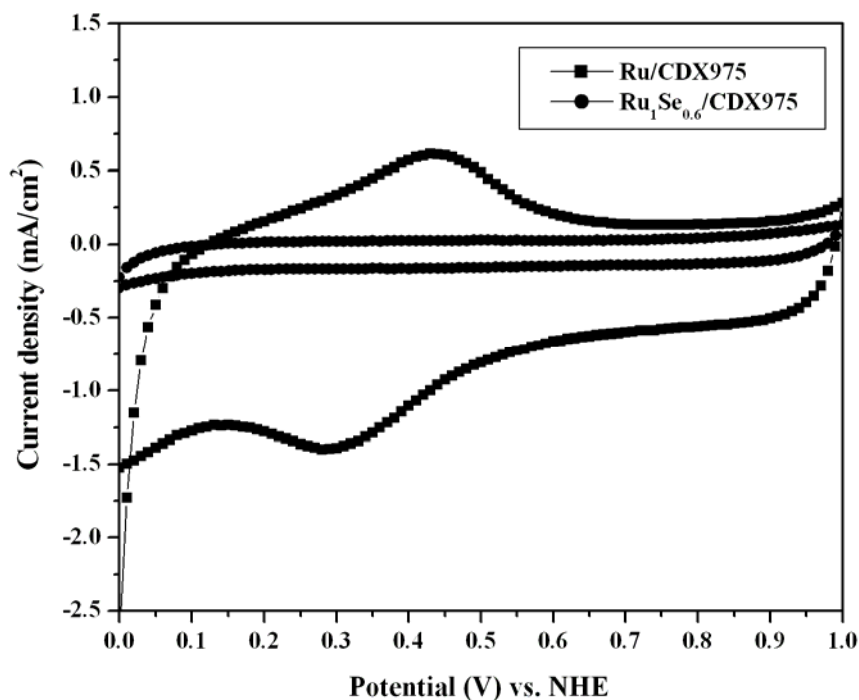


Fig. 6.8 Cyclic voltammograms (CVs) of (■) Ru/CDX975 and (●) Ru<sub>1</sub>Se<sub>0.6</sub>/CDX975 catalysts in Ar-saturated 0.5 H<sub>2</sub>SO<sub>4</sub>; Scan rate – 20 mV s<sup>-1</sup>

In the case of Ru<sub>1</sub>Se<sub>0.6</sub>/CDX975 catalyst, the redox peaks corresponding to the formation and reduction of oxide or hydroxide species was not observed. It indicates that the presence of Se is inhibiting the electrochemical oxidation of Ru and stabilizing the Ru active centers in such a way, it exhibited high ORR activity. Recent studies have shown that similar ORR rate enhancement can be reached by modifying Ru nanoparticles with Se (Colmenares *et al.*, 2006; Zaikovskii *et al.*, 2006; Colmenares *et al.*, 2007; Fiechter *et al.*, 2007). Despite numerous investigations on the structure and electrochemical properties of Ru<sub>x</sub>Se<sub>y</sub> cluster materials (Solorza-Feria *et al.*, 1994; Alonso-Vante and Solorza-Feria, 1995; Dassenoy *et al.*, 2002; Le Rhun and Alonso-Vante, 2002), the role of Se in the enhancement of the catalytic activity is not fully understood yet. Our studies indicate that the presence of selenium in the prepared catalysts is stabilizing the Ru active centers upon electrochemical oxidation

and the optimum selenium content is 0.6. At this optimum Se to Ru atomic ratio, there may be a facile interaction between the metal d-orbitals and adsorbate valence states so that electron transfer takes place from the metal d-orbital to the anti-bonding  $2\pi^*$  orbital of molecular oxygen.

In comparison with Pt/C catalyst, the kinetically controlled region of the ORR is shifted negatively by  $\sim 100$  mV on the Ru/CDX975 catalyst. This shift of the ORR is attributed to the onset of  $\text{OH}_{\text{ad}}$  formation and Ru surface oxidation at lower potentials ( $+0.3$  V vs. NHE) than on the Pt electrode ( $+0.68$  V vs. NHE). In the case of  $\text{Ru}_x\text{Se}_y/\text{CDX975}$  catalysts, a noticeable shift of the ORR in the kinetic region to more positive values is observed for moderate amounts of Se (0.4-0.6) to the Ru. For higher Se/Ru ratios, the onset of the ORR is shifted back to lower potentials. Qualitatively similar shifts were also observed in potentiodynamic R(R)DE measurements performed by Zaikovskii *et al.* (2006).

All these measurements indicate that the  $\text{Ru}_1\text{Se}_{0.6}/\text{CDX975}$  catalyst show a significantly comparable ORR activity with that of the Pt/C catalyst in the technically relevant potential regime between  $+0.6$  and  $+0.8$  V. But the overpotential for the  $\text{O}_2$  reduction is about 20-30 mV higher than for the Pt/C catalyst.

### 6.4.3 Chronoamperometric Response

The current density – time plots of as-synthesized 20 wt%  $\text{Ru}_x\text{Se}_y/\text{CDX975}$  and commercial 20 wt% Pt/C catalysts in oxygen saturated 0.5 M  $\text{H}_2\text{SO}_4$  at  $+0.65$  V vs. NHE are shown in Fig. 6.9. It is seen that the performance of  $\text{Ru}_x\text{Se}_y/\text{CDX975}$  catalysts is better than the Ru/CDX975. This is due to the inhibition of (hydr)oxide formation and stabilization of Ru active centers by the addition of Se. Among all the

carbon supported  $Ru_xSe_y$  catalysts,  $Ru_1Se_{0.6}/CDX975$  exhibited high performance and it is quite similar to that of the commercial Pt/C (E-TEK) catalyst. The increasing order of the performance of Ru based electrodes is as follows:  $Ru/CDX975 < Ru_1Se_1/CDX975 < Ru_1Se_{0.8}/CDX975 < Ru_1Se_{0.2}/CDX975 < Ru_1Se_{0.4}/CDX975 < Ru_1Se_{0.6}/CDX975 \approx$  commercial Pt/C (E-TEK).

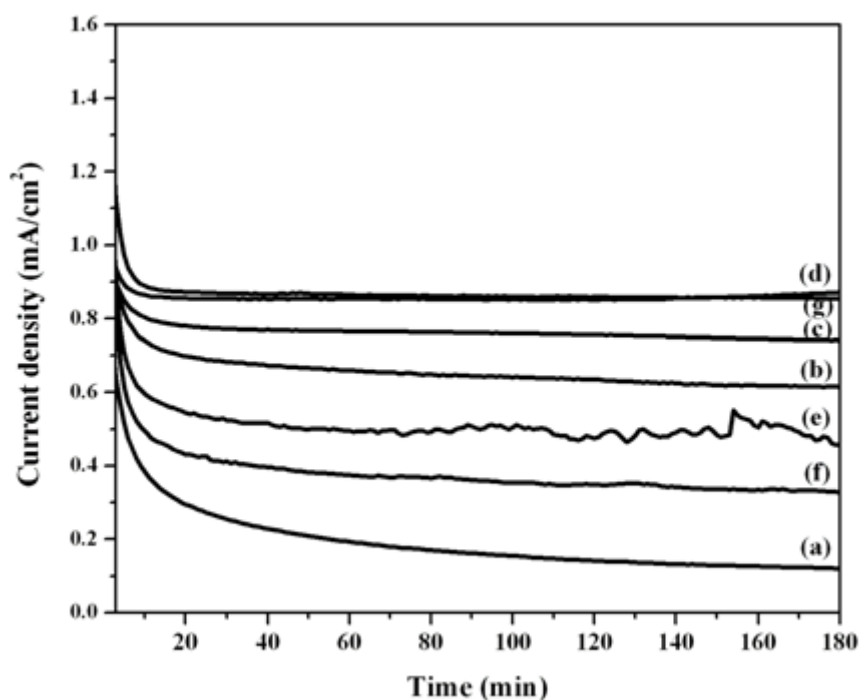


Fig. 6.9 Current density vs. time curves of as-synthesized 20 wt%  $Ru_xSe_y/CDX975$  catalysts; (a)  $Ru/CDX975$  (b)  $Ru_1Se_{0.2}/CDX975$  (c)  $Ru_1Se_{0.4}/CDX975$  (d)  $Ru_1Se_{0.6}/CDX975$  (e)  $Ru_1Se_{0.8}/CDX975$  (f)  $Ru_1Se_1/CDX975$  and (g) commercial Pt/C (E-TEK) measured in oxygen saturated 0.5 M  $H_2SO_4$  at +0.65 V vs. NHE

## CHAPTER 7

### **MN<sub>4</sub>C<sub>x</sub> CLUSTERS (M = Fe and Co) – POTENTIAL OXYGEN REDUCTION ELECTRODES FOR PROTON EXCHANGE MEMBRANE FUEL CELL (PEMFC) APPLICATIONS**

#### **7.1 INTRODUCTION**

Heat-treated transition-metal organic macrocycles (N<sub>4</sub>-metal chelates) adsorbed on carbon which generate MN<sub>4</sub>C<sub>x</sub> clusters, appear to be one of the choices to replace Pt for oxygen reduction. Jasinski (1964) first reported oxygen electrocatalysis with transition metal macrocycle, cobalt(II)phthalocyanine (CoPc) adsorbed on carbon. Shortly thereafter, Jhanke *et al.* (1976), Collman *et al.* (1980), Steiger *et al.* (1994), Zagal *et al.* (1980) and Zagal *et al.* (1992) investigated a variety of macrocyclic complexes as oxygen reduction electrodes for electrochemical devices. All experimental evidences accumulated over the years have demonstrated that macrocyclic complexes of Fe and Co appear to be the best. However, they suffer from low electrochemical stability and decompose either via hydrolysis in the electrolyte or attack of the macrocycle ring by peroxy intermediates generated during oxygen reduction (van Veen *et al.*, 1981). The results were not satisfactory in terms of both the activity and stability of these Co and Fe chelates. Moreover activity was far less compared to the state-of-art Pt electrocatalysts.

Later several research groups (Bagotzky *et al.*, 1977; van Veen *et al.*, 1981; Scherson *et al.*, 1986; Sawaguchi *et al.*, 1990; Widelov and Larson, 1992; Ladouceur *et al.*, 1993; Rongzhong Jiang and Deryn Chu, 2000; Faubert *et al.*, 1996; Lalande *et al.*, 1996; Gojkovic *et al.*, 1998; Schulenburg *et al.*, 2003) have reported that the heat-

treatment of transition metal macrocycles adsorbed on carbon support improves their stability without substantial degradation and, in some instances, enhancing their overall catalytic activity. It was concluded that the optimum temperature for maximum activity depends on the metal, the ligand and nature of support. Although effort has been devoted to determine the composition and the structure of the electrocatalytic center formed upon pyrolysis, some controversies still exist and a number of hypotheses have been put forward to explain the increased activity and stability of the pyrolyzed material. The most widely accepted model to explain the improvement in activity and stability is the creation of M-N<sub>4</sub> moiety on carbon matrix or simply MN<sub>4</sub>C<sub>x</sub> cluster species during the pyrolysis (Joyner *et al.*, 1982; van Wingerden *et al.*, 1988; Choi *et al.*, 2002; Lefèvre *et al.*, 2000, Lefèvre *et al.*, 2002; Lefèvre *et al.*, 2003; Lefèvre *et al.*, 2005; Lalande *et al.*, 1996; Martin Alves *et al.* 1992). Among the various substituted Fe and Co macrocycles, iron and cobalt tetramethoxyphenylporphyrins appear to be best. Their ORR activity is found to be 3/4<sup>th</sup> of commercial Pt/C catalyst and the tests in fuel cell showed that they lack stability (Lefèvre *et al.*, 2000; Lefèvre *et al.*, 2005). This is due to the existence of less number of active sites, large particle size and weak bonding interactions between the carbon and active species responsible for oxygen reduction. These results indicate that there is a possibility of increasing activity by increasing the dispersion of cluster species on carbon support. It is reported in literature that the surface properties of the carbon influences dramatically the degree of dispersion of supported active species and in turns its catalytic activity. Wang *et al.* (1999) showed that pre-treatment of carbon with HNO<sub>3</sub> and/or NH<sub>3</sub> resulted in an improvement in the performance of Fe-based non-precious metal catalysts for oxygen reduction reaction (ORR). Ehrburger *et al.* (1983) reported that the oxygen surface functionalities on carbon improve the

dispersion of iron phthalocyanine (FePc) particles. Gouérec *et al.* (1998) studied the activity and stability of cobalt tetraazaannulene (CoTAA) on two different carbon supports varying in the amount of surface oxygen complexes and concluded that strong interactions between the metal complex and the carbon support are established via the surface oxygen complexes thus increasing the sintering resistance of these particles. Recently, Nalini Subramanian *et al.* (2006) exploited the oxidized carbon as support for cobalt-ethylene diamine complex and observed improved activity and selectivity towards the four electron reduction of oxygen to water.

In the present study, density functional calculations have been carried out to study the facile reduction of oxygen on  $MN_4$  ( $M = Fe$  and  $Co$ ) species. Experimentally,  $MN_4C_x$  clusters have been prepared by the heat-treatment of carbon black (CDX975) supported FeTPP, FePc, FeTMPP and CoTMPP macrocyclic complexes. Optimum conditions for the maximum ORR activity of carbon supported FeTPP and FePc complexes have been investigated by cyclic voltammetry. In order to investigate the role of surface functionalities created on carbon support toward ORR activity of macrocyclic complexes, both untreated and heat-treated metal tetramethoxyphenyl porphyrins (M-TMPP;  $M = Fe$  and  $Co$ ) supported on as-received as well as  $HNO_3$  treated carbon black have been prepared and investigated. Finally, single-cell PEMFC tests are performed on the as-synthesized catalysts and compared with that of the commercial Pt/C (E-TEK) catalyst.

## **7.2 THEORETICAL STUDIES ON $MN_4$ CLUSTERS FOR OXYGEN REDUCTION**

Cerius2 software is used for Force Field calculations. The optimization of  $MN_4$  ( $M = Fe$  and  $Co$ ) and  $O_2$  geometries have been obtained by using Universal Force Field

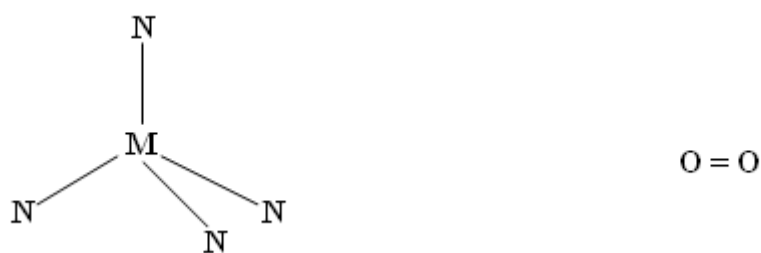


approach (UFF1.02). Using Force Field optimized parameters, DFT single point energy calculations are carried out by Becke's three-parameter hybrid function with LYP correlation function (B3LYP) (Becke, 1988) and an effective core potential basis set LanL2DZ (Hay and Wadt, 1985). This basis set utilizes a double zeta description and an effective core potential (ECP) for atoms. ECP approach is simple and calculates by considering the relativistic effects of inner shell electrons so that one can hope to obtain accurate and reliable values. Calculations for energy levels are carried out using the Gaussian 98 program (Frisch *et al.*, 1998). A singlet state is chosen for  $MN_4$  and a triplet state for  $O_2$ . The frontier orbitals are visualized by using MOLDEEN software.

In the study of chemical reactivity, Klopman (1968) classified electron transfer reactions as a charge-controlled reaction when little transfer occurs and a frontier orbital-controlled reaction when an extensive electron transfer occurs. The first type of reaction is characterized by a large difference in energy between the frontier orbitals of the donor and acceptor molecules. The second type reaction occurs when the two frontier orbitals of the donor and acceptor have energy values close to each other. The reactivity in the latter case is essentially determined by the electron density and/or symmetry. Based on this description, the essential criteria for the reduction of oxygen by  $MN_4$  species are: (i) energies of frontier orbitals should match, (ii) symmetry of frontier orbitals should be similar, and (iii) the electron transfer should be facile.

When  $O_2$  is adsorbed on  $MN_4$  ( $M = Fe$  and  $Co$ ) electrode, the surface may contain different geometries of  $MN_4$  with different bond lengths and bond angles between  $M$  and  $N$ . Hence, the geometry of  $MN_4$  may not be an important parameter in the case of

O<sub>2</sub> adsorption and reduction by electron transfer. Since there can be a number of possibilities, the calculations have been restricted for tetrahedral geometry with the hope that the trends for other geometries may be similar. MN<sub>4</sub> (M = Fe and Co) species alone is considered in the present calculations. The geometries of MN<sub>4</sub> (M = Fe and Co) and O<sub>2</sub> are shown with bond distance and bond angle in Fig. 7.1.



where M = Fe and Co

Co-ordinates: Fe – N distance: 2.00 Å

O – O distance: 1.26 Å

Co – N distance: 2.01 Å

∠N-M-N: 109°47'

Fig. 7.1 Model systems with geometric parameters

Since the O<sub>2</sub> molecule in its ground state possesses two unpaired electrons in a doubly degenerate π\* anti-bonding orbital (HOMO), reduction takes place by the transfer of electrons from the HOMO of MN<sub>4</sub> (M = Fe and Co) species. This can be possible only when the symmetry and energy of these frontier orbitals match with those of oxygen orbital wave functions. The calculated energies of orbitals with percentage atomic orbital contributions are given in Table 7.1. The results suggest that the (i) HOMO energy of FeN<sub>4</sub> is at -7.56 eV and main contribution to its wave function is from d-orbital of Fe (30.8%) and p-orbital of N (69.1%) and (ii) HOMO energy of CoN<sub>4</sub> is at -7.78 eV and main contribution to its wave function is from d-orbital of Co (21.1%) and p-orbital of N (75.4%). The acceptor orbital energy of oxygen is at -8.18

eV and main contribution to its wave function is from p-orbital of each oxygen atom (50%). It shows that the energy of HOMO of MN<sub>4</sub> (M = Fe and Co) is nearly equal to the π\* orbital of O<sub>2</sub>. So the electron transfer can take place easily from the HOMO of MN<sub>4</sub> (M = Fe and Co) to the π\* orbital of O<sub>2</sub> as compared to the HOMO of metal alone. This indicates that the presence of nitrogen atoms around metal in MN<sub>4</sub> plays an important role in attaining the same energy with the π\* orbital of O<sub>2</sub> molecule.

Table 7.1 Percentage atomic orbital contributions to HOMO and LUMO of MN<sub>4</sub> and O<sub>2</sub> by DFT method using Gaussian 98

Model System	Energy (eV)	M (Fe or Co)			N	
		<u>s</u>	<u>p</u>	<u>d</u>	<u>s</u>	<u>p</u>
FeN <sub>4</sub>	HOMO: -7.56	0.0	0.0	30.8	0.0	69.1
	LUMO: -7.00	0.0	0.0	0.0	0.0	100.0
CoN <sub>4</sub>	HOMO: -7.78	2.3	0.0	21.1	1.1	75.4
	LUMO: -7.01	0.0	1.6	3.2	1.6	93.4
O <sub>2</sub>	HOMO: -8.18 LUMO: +6.41	O			O	
		<u>s</u>	<u>p</u>		<u>s</u>	<u>p</u>
		0.0 28.3	50.0 21.7		0.0 28.3	50.0 21.7

The situation considered here is a surface phenomenon. Activation of molecules on surfaces has to be treated in many ways. Individual bonding and overlap may not be sufficient. Frontier orbital wave functions energy and symmetry are the main criteria. It is proposed that in this model all the surface atoms participate in giving rise to a certain molecular wave functions with a particular shape and charge distribution in space. The total wave function of the surface especially involved in bonding with the gaseous molecules can have special charge densities concentrated at particular locations (which are usually termed as active center) and also geometries accounting for the generation of certain type of species. This favoured situation in terms of

frontier orbital wave functions with respect to charge density distribution may be responsible for the bonding. As a result, electron transfer takes place from the HOMO wave function of  $MN_4$  ( $M = Fe$  and  $Co$ ) to the  $\pi^*$  orbital wave function of  $O_2$ . The electron density maps of the frontier orbitals of  $MN_4$  ( $M = Fe$  and  $Co$ ) and  $O_2$  are shown in Fig. 7.2, which indicate that the HOMO of  $MN_4$  have the right symmetry to interact with the  $\pi^*$  orbital of  $O_2$ .

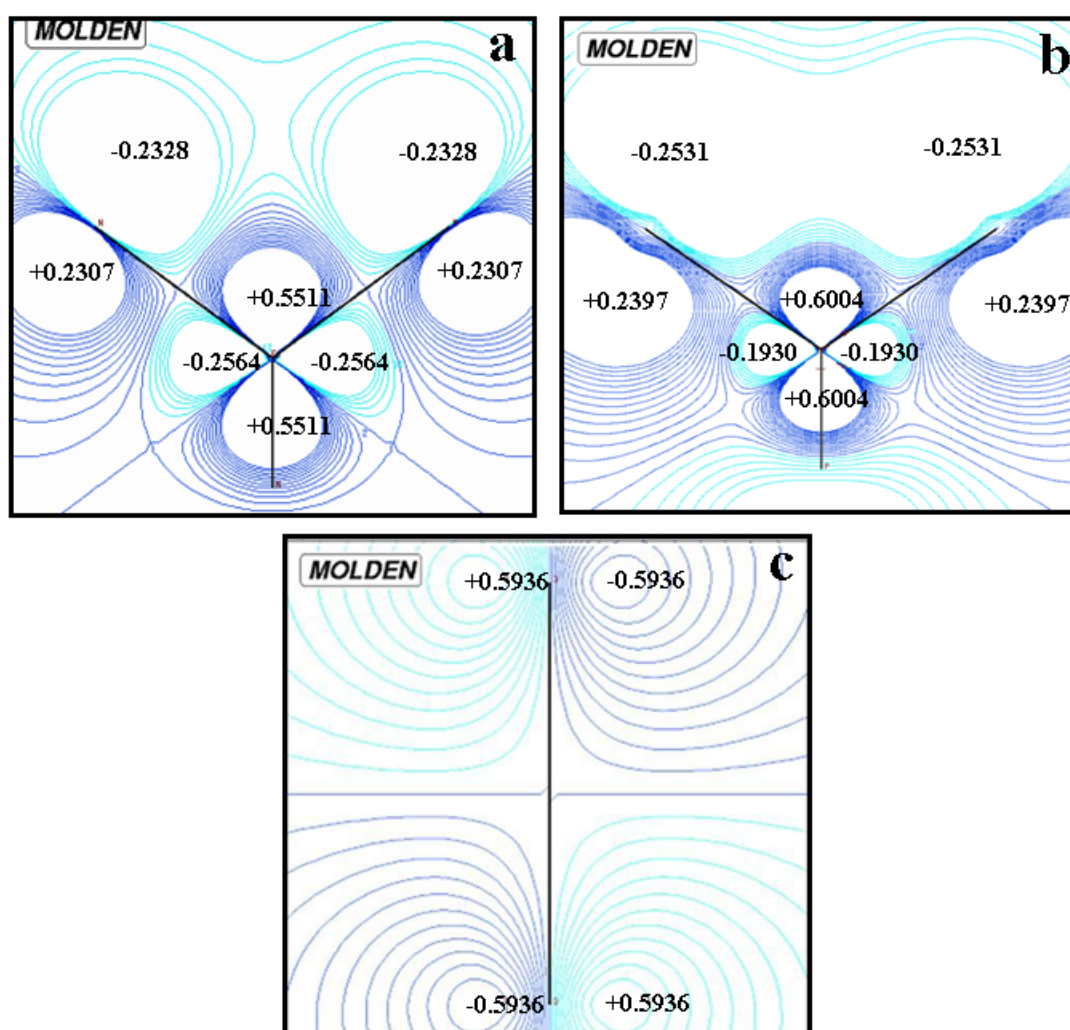


Fig. 7.2 Electron density maps of (a) HOMO of  $FeN_4$  (b) HOMO of  $CoN_4$  and (c)  $\pi^*$  orbital of  $O_2$

The mode of activation of oxygen on  $MN_4$  (Fig. 7.3) shows the directional nature of the HOMO wave function and interaction with the  $\pi^*$  orbital wave function of  $O_2$ . As

a result, facile electron transfer takes place and the adsorbed  $O_2$  leaves the electrode as free oxide species but not incorporated into the  $MN_4$  ( $M = Fe$  and  $Co$ ) lattice. Since the charge transfer to the oxygen has to be first through the  $\pi^*$  orbital and hence this alone has been considered in this study. It is considered that the electron transfer to the  $\sigma^*$  orbital of  $O_2$  may be the crucial step and subsequent rearrangement of electrons and dissociation of oxygen can be a facile process.

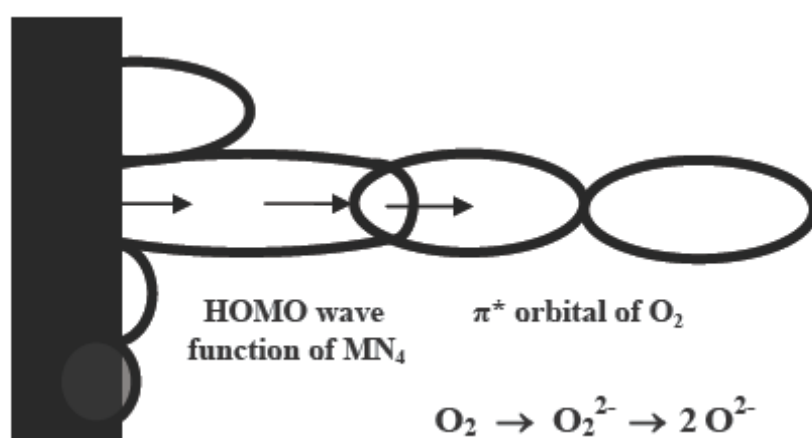


Fig. 7.3 Mode of activation of  $O_2$  on  $MN_4$  ( $M = Fe$  and  $Co$ ) species

## 7.3 EXPERIMENTAL SECTION

### 7.3.1 Synthesis of Iron Tetraphenylporphyrin (FeTPP)

Iron and cobalt tetraphenylporphyrin complexes are synthesized and purified according to the method described by Adler *et al.* (1970). Metal-free tetraphenylporphyrin ( $H_2TPP$ ) is synthesized by refluxing benzaldehyde (0.5 mole) and pyrrole (0.5 mole) in propionic acid (1 l) for 30 min. Then it is filtered, washed with methanol and dried at 373 K for 4 h. Finally, it is purified by column chromatography by employing benzene-chloroform mixture (1:1 v/v) as the eluant. FeTPP was synthesized by adding  $10^{-2}$  moles of anhydrous  $FeCl_2$  and  $5 \times 10^{-3}$  moles of

H<sub>2</sub>TPP to a solution composed of 40 ml of anhydrous pyridine, 5 ml of triethylamine and 0.5 ml of tributylphosphine (added to remove oxygen from the solution) and then refluxed under argon for 2 h. The FeTPP is precipitated by adding 60 ml of distilled water. The precipitate is filtered, washed twice with distilled water and then dried at 348 K for 3 h. Finally, FeTPP is purified by vacuum sublimation at 643 K.

### **7.3.2 Synthesis of Iron Phthalocyanine (FePc)**

Iron phthalocyanine (FePc) is synthesized and purified according to the literature procedure (Lalande *et al.*, 1996). The reaction is carried out under Ar. Briefly, FeCl<sub>2</sub> (2.54 g), phthalonitrile (10.2 g) and tributylphosphine (5 ml) are dissolved in 100 ml of anhydrous ethylene glycol. The solution is refluxed for 30 min and cooled down to room temperature. The crystalline solid is filtered and rinsed with methanol. It is then suspended in a mixture of 150 ml of methanol and 8 ml of formic acid (96%) to be refluxed for 30 min before being hot filtered, rinsed and dried in air at 343 K. Finally, FePc is purified by vacuum sublimation at 793 K.

### **7.3.3 Synthesis of Iron and Cobalt Tetramethoxyphenylporphyrin Complexes (FeTMPP-Cl and CoTMPP)**

Iron and cobalt tetramethoxyphenylporphyrin complexes are synthesized according to the method described by Adler *et al.* (1970). At first, metal free tetramethoxyphenylporphyrin (H<sub>2</sub>TMPP) is synthesized by refluxing *p*-anisaldehyde (0.4 mole) and pyrrole (0.4 mole) in propionic acid (500 ml) for 30 min. Then it is filtered, washed with methanol and dried at 383 K for 72 h. It is purified by column chromatography by employing benzene-chloroform mixture (1:1 v/v) as the eluant. Metal tetramethoxyphenylporphyrin complexes are synthesized by refluxing 56 ml of N,N'-DMF containing 0.67 g H<sub>2</sub>TMPP and 0.25 g metal salt (10% extra) under Ar

atm for 2 h. Then it is cooled in ice bath and a portion of ice-water mixture was added. Finally it is filtered, washed with deionized water and dried at 383 K for 24 h. The complexes are purified by dissolving the porphyrin crystals in a minimum amount of chloroform followed by chromatography in a silica column using a benzene-chloroform mixture (1:1 v/v) as the eluant.

#### **7.3.4 Preparation of FeTPP/CDX975 and FePc/CDX975**

FeTPP is adsorbed onto carbon black (CDX-975) according to the following procedure: 0.17 g of FeTPP is dissolved in 40 ml of anhydrous pyridine. To this solution, 0.54 g of carbon black is added and refluxed for 12 h under Ar. FeTPP is precipitated onto the carbon black by pouring the suspension into 1 l of distilled water. The resulting material was then filtered, rinsed with distilled water and dried overnight at 348 K in air. FePc/CDX-975 is also prepared in the same manner. The catalysts are then heat-treated under Ar for 2 h at temperatures ranging from 373 to 1273 K. The nominal iron loading on the carbon black was 2 wt%.

#### **7.3.5 Modification of Carbon Black (CDX975) Support**

The HNO<sub>3</sub> treatment of the carbon support consists of mixing 0.5 g of carbon black with 20 ml of 70 wt % HNO<sub>3</sub> solution. The suspension is refluxed for 7 h until the colour of the gas in the reflux column became very light. Then the suspension is filtered, washed with deionized water and methanol, dried in an oven at 348 K and finally ground into fine powder. For convenience, as-received carbon (CDX975) and modified (oxidized) carbon are designated as CDX1 and CDX2 respectively. The purpose of the modification is to increase the quinone/hydroquinone groups which will increase the dispersion of metal complexes.

### **7.3.6 Preparation of FeTMPP/CDX975, CoTMPP/CDX975 and MN<sub>4</sub>C<sub>x</sub> Clusters**

The synthesized Fe and Co tetramethoxyphenylporphyrin complexes are adsorbed on both the as-received (CDX1) as well as modified (CDX2) carbon black by dissolving the suitable amount of metal complex (FeTMPPCl or CoTMPP) in chloroform followed by impregnation. Then the resultant suspension was filtered, washed with distilled water and dried at 348 K. Finally it is ground into fine powder and heat treated at 1073 K under Ar atm for 2 h to generate MN<sub>4</sub>C<sub>x</sub> (M = Fe or Co) cluster species responsible for oxygen reduction (Lefèvre *et al.*, 2000; Lefèvre *et al.*, 2005). The nominal metal content in the catalysts is 2 wt%. For brevity, the untreated M-TMPP complexes adsorbed on as-received (CDX1) and oxidized (CDX2) carbon are designated as CDX1-MTMPP(UT) and CDX2-MTMPP(UT) respectively. The heat-treated M-TMPP adsorbed on as-received (CDX1) and oxidized (CDX2) carbon are designated as CDX1-MTMPP(HT) and CDX2-MTMPP(HT) respectively. In these designations, 'M' represents Fe and Co.

### **7.3.7 Estimation of Iron in the Catalysts**

The presence of iron in the catalysts is estimated by following a standard redox titration procedure (Vogel, 1985) described in section 4.4.4.

### **7.3.8 Estimation of Cobalt in the Catalysts**

Co determination is performed using absorption spectroscopy (Faubert *et al.*, 1996) described in section 4.4.5.

### **7.3.9 Estimation of Nitrogen in the Catalysts**

Nitrogen content in the catalysts is determined by CHN analyzer.



## 7.4 CHARACTERIZATION OF THE IRON AND COBALT BASED CATALYSTS

The elemental composition of the synthesized complexes is given in Table 7.2. The good agreement of the calculated and experimentally determined values indicates the purity of the synthesized complexes.

Table 7.2 Elemental composition of the synthesized complexes

Complex	Elemental composition	
	calculated (wt.%)	found (wt.%)
H <sub>2</sub> TPP (C <sub>44</sub> H <sub>30</sub> N <sub>4</sub> )	C, 85.95; H, 4.92; N, 9.12	C, 84.8; H, 4.85; N, 9.07
FeTPP (C <sub>44</sub> H <sub>28</sub> N <sub>4</sub> Fe)	C, 79.05; H, 4.22; N, 8.38; Fe, 8.35	C, 78.12; H, 4.31; N, 8.57; Fe, 8.49
FePc (C <sub>32</sub> H <sub>16</sub> N <sub>8</sub> Fe)	C, 67.56; H, 2.83; N, 19.7, Fe, 9.82	C, 62.88; H, 2.54; N, 19.8, Fe, 9.71
H <sub>2</sub> TMPP (C <sub>48</sub> H <sub>38</sub> N <sub>4</sub> O <sub>4</sub> )	C, 78.47; H, 5.18; N, 7.63	C, 78.13; H, 5.07; N, 7.54
FeTMPPCl (C <sub>48</sub> H <sub>36</sub> N <sub>4</sub> O <sub>4</sub> FeCl)	C, 66.95; H, 4.18; N, 6.51; Fe, 6.49	C, 66.81; H, 4.07; N, 6.43; Fe, 6.57
CoTMPP (C <sub>48</sub> H <sub>36</sub> N <sub>4</sub> O <sub>4</sub> Co)	C, 72.82; H, 4.55; N, 7.08; Co, 7.46	C, 71.90; H, 4.41; N, 6.97; Co, 7.49

Bulk Fe and N concentrations in untreated and heat-treated FeTPP/CDX975 and FePc/CDX975 catalysts are given in Table 7.3 and 7.4 respectively. It indicates that the Fe content of the FeTPP/CDX975 and FePc/CDX975 catalysts remains about 2.0 and 1.85 wt%, respectively for the entire range of temperatures investigated. Contrary to the bulk metal behaviour, the bulk nitrogen content in the FeTPP/CDX975 and FePc/CDX975 catalysts gradually decrease with heat-treatment temperature. This is due to the decomposition of the macrocyclic complexes and release of nitrogen

containing fragments from the carbon surface as a function of heat-treatment temperature.

Bulk metal (Fe or Co) and N concentrations in the untreated and heat-treated M-TMPP/CDX975 (M = Fe and Co) catalysts are given in Table 7.5. Within the error limits, the calculated composition of metal (Fe or Co) and N in the catalysts is found to be around  $MN_{3.7\pm 0.2}$ . To check the effect of oxidized carbon towards the dispersion of  $MN_4$  clusters, TEM images are recorded and are shown in Fig. 7.4.

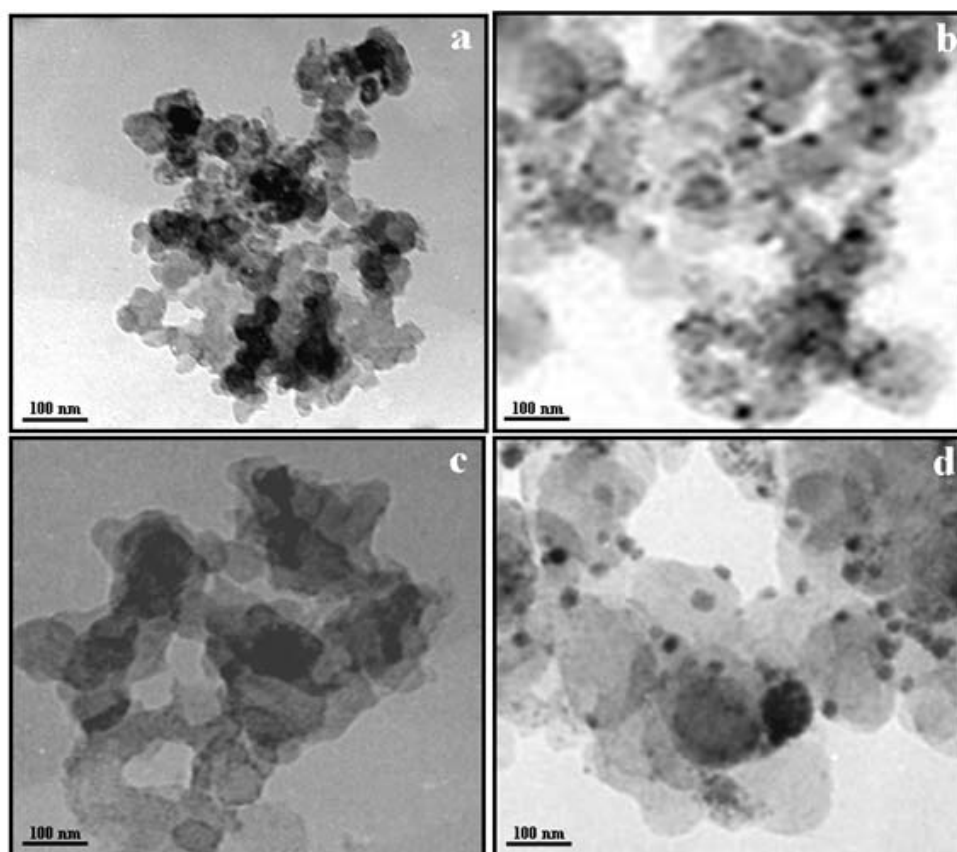


Fig. 7.4 TEM images of (a) CDX1-FeTMPPCl(HT), (b) CDX2-FeTMPPCl(HT), (c) CDX1-CoTMPP(HT) and (d) CDX2-CoTMPP(HT)

Well dispersed  $MN_4$  cluster species are observed in the case of oxidized carbon compared to that of as-received carbon supported catalysts. The average size of cluster species in CDX2-FeTMPPCl(HT) is 11 nm compared to 32 nm for CDX1-

FeTMPPCl(HT). Similarly, The average size of cluster species in CDX2-CoTMPP(HT) is 15 nm compared to 38 nm for CDX1-CoTMPP(HT). These catalysts are characterized qualitatively by EDX and are shown in Fig. 7.5. EDX patterns confirmed the presence of Fe, N and C in CDX1-FeTMPPCl(HT) and CDX2-FeTMPPCl(HT) catalysts (Fig. 7.5(a) and 7.5(b)) and Co, N and C in CDX1-CoTMPP(HT) and CDX2-CoTMPP(HT) catalysts (Fig. 7.5(c) and 7.5(d)).

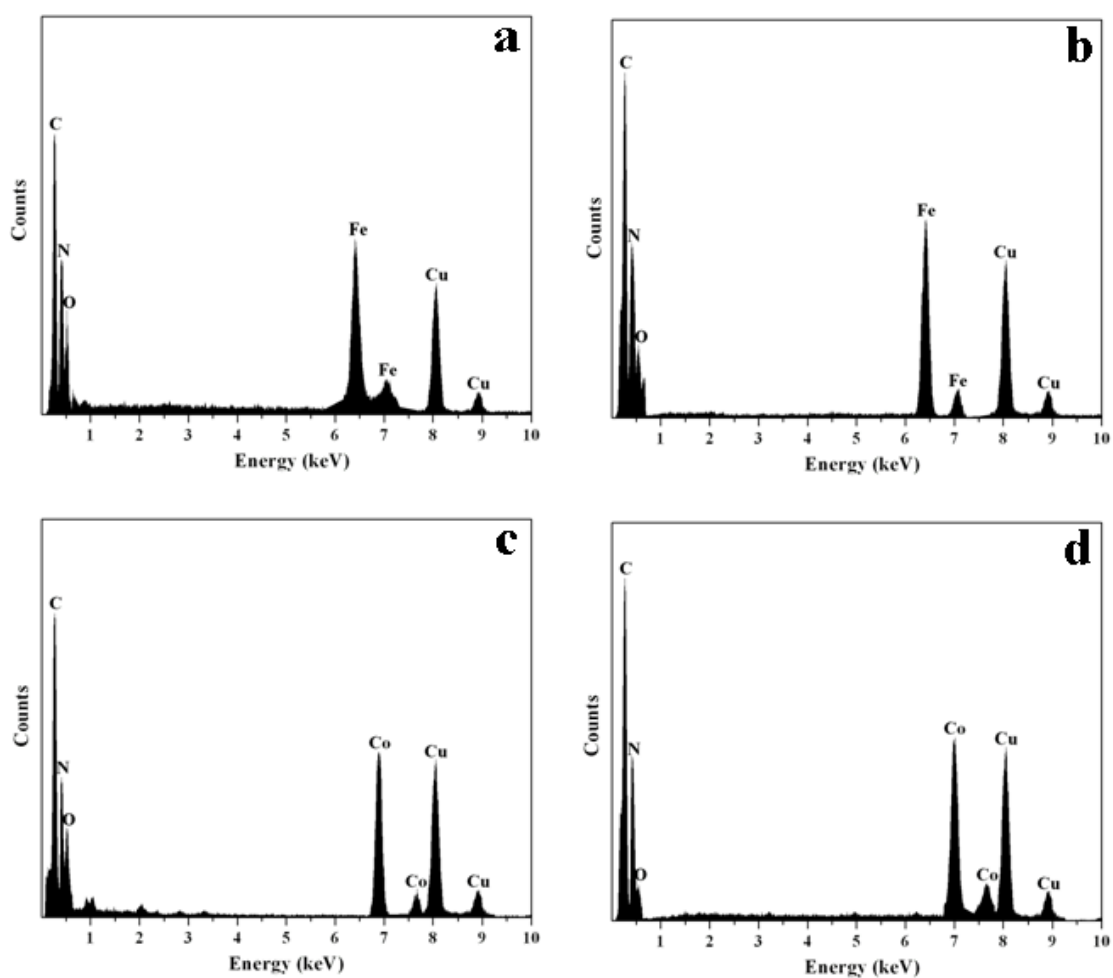


Fig. 7.5 EDX spectra of (a) CDX1-FeTMPPCl(HT), (b) CDX2-FeTMPPCl(HT), (c) CDX1-CoTMPP(HT) and (d) CDX2-CoTMPP(HT)

## 7.5 ELECTROCHEMICAL PERFORMANCE OF IRON AND COBALT BASED CATALYSTS

### 7.5.1 Electrode Fabrication

The working electrode is fabricated as follows: Briefly, 16 mg of finely ground catalyst, 0.4 ml of H<sub>2</sub>O and 0.4 ml of a 5 wt % Nafion in alcohol-water solution (Aldrich) are ultrasonically blended for 10 min. Then 10  $\mu$ l of this suspension was pipetted onto the glassy carbon disk and dried under Ar atmosphere. Current densities are normalized to the geometric area of the glassy carbon substrate (0.07 cm<sup>2</sup>) and the potentials are represented with respect to normal hydrogen electrode (NHE).

### 7.5.2 Electrochemical Reduction of Oxygen

The electrochemical ORR activity of the untreated and heat-treated FeTPP/CDX975 and FePc/CDX975 catalysts is investigated by linear sweep voltammetry and the calculated ORR activity at +0.7 V vs NHE is given in Table 7.3 and 7.4 respectively. It shows that the heat-treated FeTPP/CDX975 at 873 K and FePc/CDX975 at 773 K exhibited good activity for oxygen reduction. The calculated compositions of Fe and N in the heat-treated FeTPP/CDX975 at 873 K and FePc/CDX975 at 773 K are FeN<sub>3.5</sub> and FeN<sub>2.6</sub> respectively. But the activity is less compared to that of commercial Pt/C catalyst.

It is reported that the heat-treatment of M-TMPP/C (M = Fe and Co) at 1073 K generates MN<sub>4</sub>C<sub>x</sub> cluster species based on ToF-SIMS measurements (Lefèvre *et al.*, 2000; Lefèvre *et al.*, 2005). The ORR activity of those MN<sub>4</sub>C<sub>x</sub> (M = Fe and Co) clusters was found to be slightly less compared to that of commercial Pt/C catalyst. In order to improve the ORR activity and study the role of surface functionalities on carbon, untreated and heat-treated MTMPP complexes supported on as-received and oxidized carbons are prepared and oxygen reduction studies are performed.

Table 7.3 Estimated iron loading, nitrogen content and ORR activity of untreated and heat-treated FeTPP/CDX975 catalysts

Heat-treatment temp (K)	Iron loading (wt.%)	Nitrogen content (wt.%)	ORR activity at +0.7 V vs NHE (mA cm <sup>-2</sup> )
Untreated	1.96	2.3	0.0
373	n. m	2.2	0.0
473	n. m	2.1	0.0
573	n. m	2.1	0.1
673	n. m	1.9	1.1
773	n. m	1.7	1.8
873	1.97	1.7	3.8
973	n. m	1.6	2.7
1073	n. m	1.3	1.6
1173	n. m	1.1	1.2
Pt	-	-	4.9

(n. m = not measured)

Table 7.4 Estimated iron loading, nitrogen content and ORR activity of untreated and heat-treated FePc/CDX975 catalysts

Heat-treatment temp (K)	Iron loading (wt.%)	Nitrogen content (wt.%)	ORR activity at +0.7 V vs NHE (mA cm <sup>-2</sup> )
Untreated	1.86	2.0	0.0
373	n. m	1.6	0.0
473	n. m	1.6	0.0
573	n. m	1.5	0.1
673	n. m	1.5	0.4
773	n. m	1.4	2.4
873	1.85	1.2	2.2
973	n. m	1.1	0.4
1073	n. m	0.4	0.3
1173	n. m	0.2	0.2

(n. m = not measured)

As-received, CDX1 and modified (oxidized), CDX2 carbon black supports are electrochemically analyzed to check the nature of the surface functional groups present. Cyclic voltammograms obtained for carbons, CDX1 and CDX2 in Ar-saturated 0.5 M H<sub>2</sub>SO<sub>4</sub> are shown in Fig. 7.6. It can be seen that the as-received carbon (CDX1) and oxidized carbon (CDX2) exhibit well-defined redox peaks at ~0.55 V vs. NHE. These redox peaks are characteristic of the quinone/hydroquinone groups present on the carbon surface (Kinoshita and Bett, 1973). The higher electrochemical activity of the carbon sample treated with HNO<sub>3</sub> (CDX2) compared to the as-received carbon (CDX1) indicates the presence of more number of quinone groups.

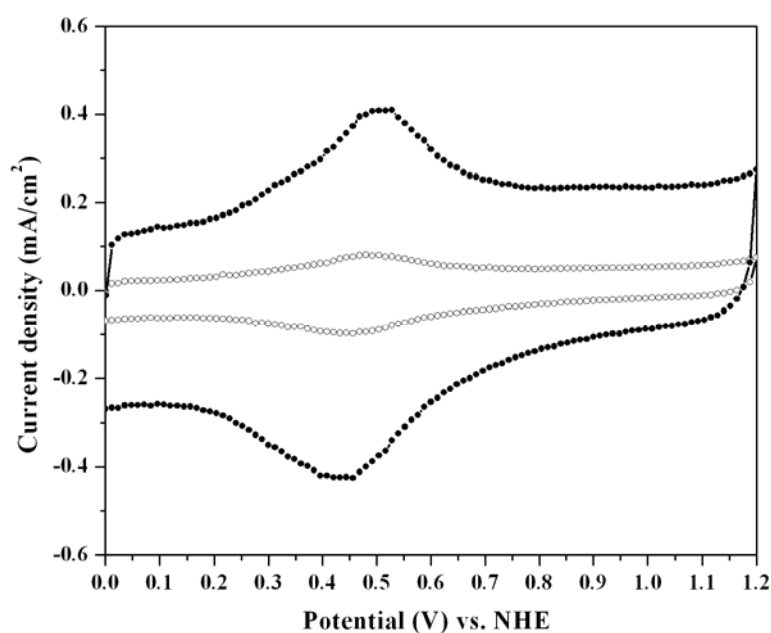


Fig. 7.6 Cyclic voltammograms of (○) CDX1 and (●) CDX2 in Ar- saturated 0.5 M H<sub>2</sub>SO<sub>4</sub>; Scan rate - 10 mV s<sup>-1</sup>

The electrocatalytic ORR activity of untreated and heat-treated Fe(III)TMPP-Cl supported on as-received and oxidized carbons is investigated by linear sweep voltammetry (LSV). Fig. 7.7(a) represents the LSV profile of CDX1-FeTMPPCl(UT)

recorded in Ar- and O<sub>2</sub>- saturated 0.5 M H<sub>2</sub>SO<sub>4</sub> solution in the negative sweep direction at a scan rate of 10 mV s<sup>-1</sup>. At first, the CDX1-FeTMPPCl(UT) electrode is placed in an Ar- saturated 0.5 M H<sub>2</sub>SO<sub>4</sub> electrolyte and the linear sweep voltammogram is recorded at a scan rate of 10 mV s<sup>-1</sup> ranging from +1.0 to +0.0 V. Then pure oxygen gas is purged for 2 h and linear sweep voltammogram is recorded at a scan rate of 10 mV s<sup>-1</sup> ranging from +1.0 to +0.0 V. The steep increase in peak current at +0.7 V vs. NHE represents the electrochemical reduction of oxygen. Oxygen reduction activity is calculated by taking the difference in activity at +0.7 V vs. NHE in Ar- and O<sub>2</sub>- saturated 0.5 M H<sub>2</sub>SO<sub>4</sub> where the oxygen reduction kinetics is more favourable. The same procedure is followed for CDX2-FeTMPPCl(UT) to calculate the ORR activity (Fig. 7.7(b)). The results obtained are given in Table 7.5. It is clear that the electrode, CDX2-FeTMPPCl(UT) exhibited higher specific electrocatalytic activity than CDX1-FeTMPPCl(UT) towards the ORR. Fig. 7.7(c) and 7.7(d) illustrate the LSVs of heat treated Fe(III)TMPP-Cl adsorbed on as-received and oxidized carbons at 1073 K, namely CDX1-FeTMPPCl(HT) and CDX2-FeTMPPCl(HT) in Ar- and O<sub>2</sub>- saturated 0.5 M H<sub>2</sub>SO<sub>4</sub> at a scan rate of 10 mV s<sup>-1</sup>. The electrocatalyst CDX2-FeTMPPCl(HT) exhibited good activity than CDX1-FeTMPPCl(HT). In the case of Co-based catalysts also, a similar trend is observed. The corresponding LSVs are shown in Fig. 7.8. Linear sweep voltammograms show an increase in ORR activity of oxidized carbon supported catalysts compared to the as-received carbon supported catalysts. All these results indicate that the presence of oxygen functionalities (quinone groups) on carbon is playing an important role in generating active sites thereby increasing the ORR activity.

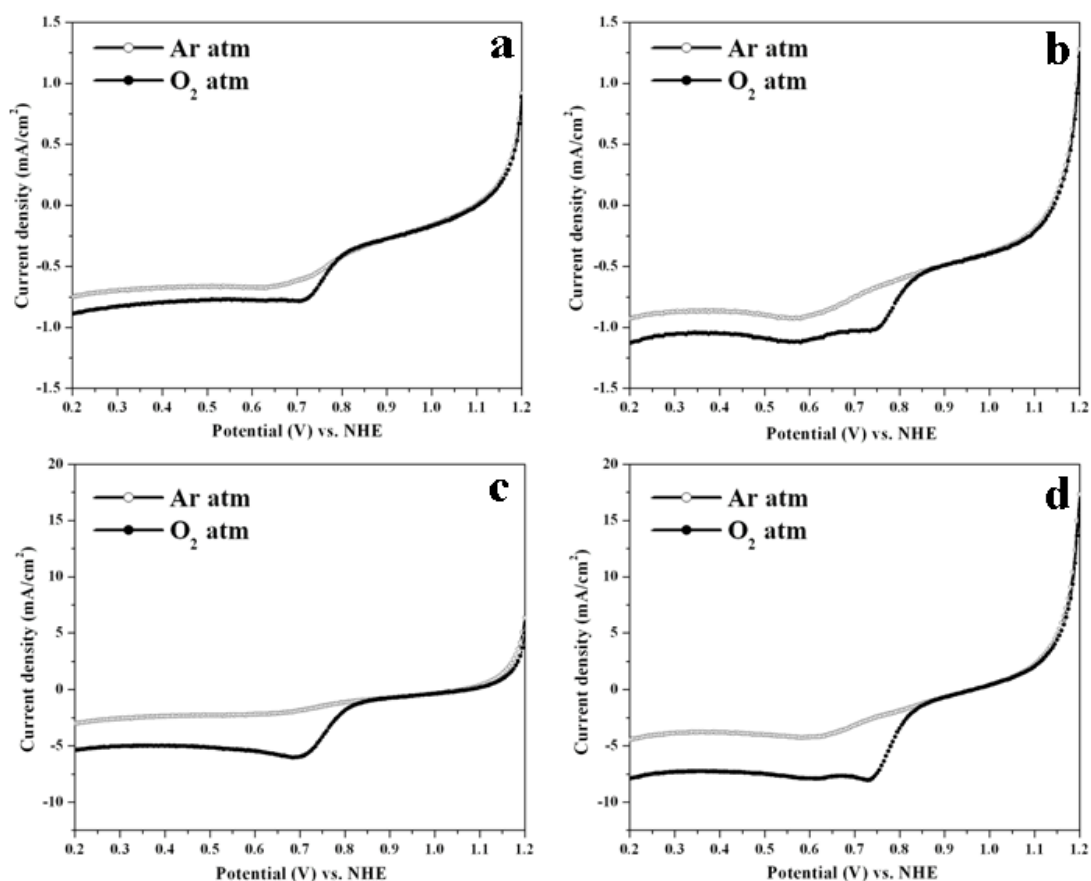


Fig. 7.7 Linear sweep voltammograms (LSVs) of untreated and heat-treated Fe(III)TMPP-Cl supported on as-received and oxidized carbon catalysts (a) CDX1-FeTMPPCl(UT), (b) CDX2-FeTMPPCl(UT), (c) CDX1-FeTMPPCl(HT) and (d) CDX2-FeTMPPCl(HT) in Ar- and O<sub>2</sub>- saturated 0.5 M H<sub>2</sub>SO<sub>4</sub>; Scan rate – 10 mV s<sup>-1</sup>

Compared to the untreated catalysts, a drastic increase in activity towards oxygen reduction is observed with the catalysts obtained by heat-treatment. This observation is in agreement with that of the previous literature reports (Gojkovic *et al.*, 1998; Gouérec *et al.*, 1998). The ORR activity of untreated catalysts, CDX1-MTMPP(UT) is 15-20 times less compared to that heat-treated catalyst, CDX1-MTMPP(HT). Similar situation is observed in the case of oxidized carbon supported catalysts. It means that the active species generated by the heat-treatment are the reason for the high selectivity to the four electron reduction of oxygen to water.



Table 7.5 Estimated metal loading, nitrogen content, onset potential for oxygen reduction and ORR activity of Fe- and Co-based catalysts as well as commercial Pt catalysts

Catalyst	Metal (Fe or Co or Pt) loading (wt.%)	Nitrogen content (wt.%)	Onset potential for oxygen reduction (mV vs. NHE)	ORR activity at +0.7 V vs. NHE (mA cm <sup>-2</sup> )
CDX1-FeTMPPCl(UT)	2.01	2.0	+810	0.2
CDX2-FeTMPPCl(UT)	2.03	2.0	+830	0.4
CDX1-FeTMPPCl(HT)	1.96	1.9	+840	4.2
CDX2-FeTMPPCl(HT)	1.97	1.9	+870	4.9
CDX1-CoTMPP(UT)	1.98	2.0	+740	0.2
CDX2-CoTMPP(UT)	1.97	2.0	+760	0.3
CDX1-CoTMPP(HT)	1.89	1.9	+795	3.2
CDX2-CoTMPP(HT)	1.93	1.8	+860	4.5
Pt/Vulcan XC72R (E-TEK)	2.07	-	+910	4.9

(UT = untreated and HT = heat-treated)

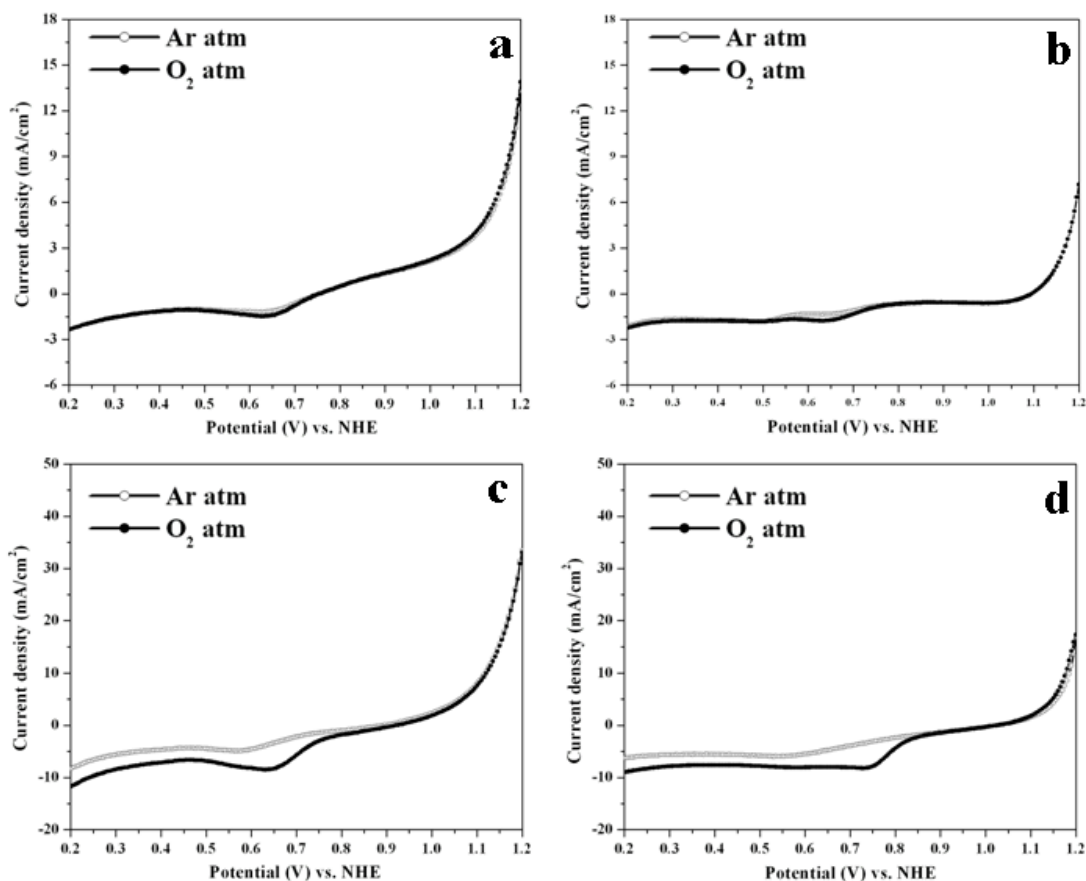


Fig. 7.8 Linear sweep voltammograms (LSVs) of untreated and heat-treated CoTMPP supported on as-received and oxidized carbon catalysts (a) CDX1-CoTMPP(UT), (b) CDX2-CoTMPP(UT), (c) CDX1-CoTMPP(HT) and (d) CDX2-CoTMPP(HT) in Ar- and O<sub>2</sub>- saturated 0.5 M H<sub>2</sub>SO<sub>4</sub>; Scan rate -10 mV s<sup>-1</sup>

One more important observation is that the shift of oxygen reduction onset potential to positive values in the case of oxidized carbon samples compared to the as-received carbon samples. In both Fe and Co based catalysts, there is approximately +30 mV or more positive shift of onset potential for oxygen reduction in the case of oxidized carbon containing electrocatalysts compared to that of the as-received carbon containing electrocatalysts. It implies that the overpotential for oxygen reduction is reduced by means of oxidized carbon support. Even though the onset potential for oxygen reduction on untreated and heat-treated catalysts is almost comparable, ORR activity is high in heat-treated catalysts. The diffusion-limited plateau of the

polarization curve for carbon supported catalysts is shown in Fig. 7.9. A similar shape of polarization curves was reported for O<sub>2</sub> reduction on ink-type electrodes using different supported macrocycles (Zagal, 1992). The model proposed by Jiang and Anson (1991) shows that the plateau is more inclined when the distribution of active sites is less uniform and the reaction is slower. However, with the use of HNO<sub>3</sub> treated oxidized carbon based catalysts, activity towards oxygen reduction increases. A single step reduction wave with a well-developed limiting plateau similar to that of Pt catalysts is observed. The activation overpotential for oxygen reduction on CDX2-FeTMPPCl(HT) decreases by 30 mV compared to CDX1-FeTMPPCl(HT).

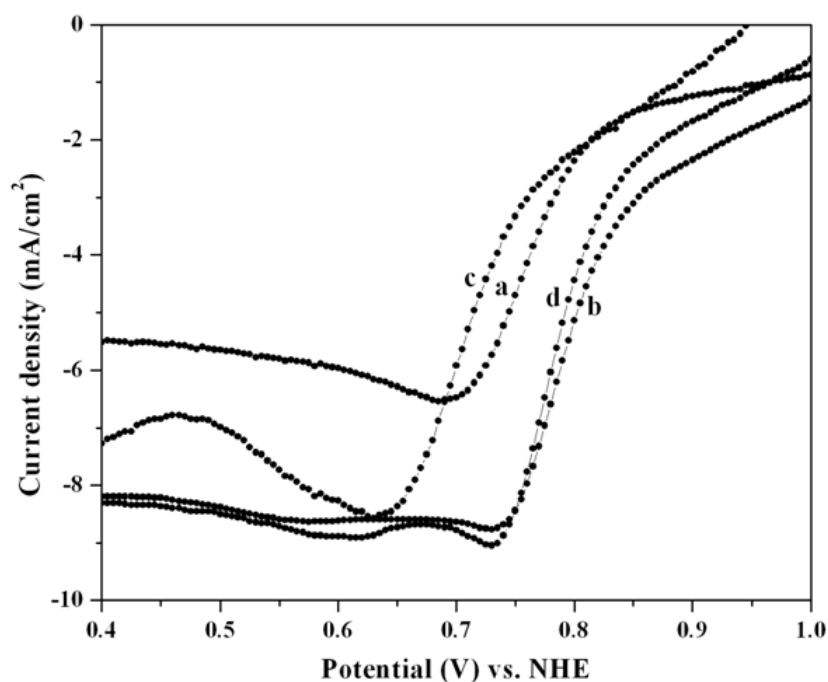


Fig. 7.9 Polarization curve of heat-treated MTMPP (M = Fe and Co) supported on as-received and oxidized carbon catalysts: (a) CDX1-FeTMPPCl(HT), (b) CDX2-FeTMPPCl(HT), (c) CDX1-CoTMPP(HT) and (d) CDX2-CoTMPP(HT) in O<sub>2</sub>- saturated 0.5 M H<sub>2</sub>SO<sub>4</sub>; Scan rate – 10 mV s<sup>-1</sup>

Similarly, the activation overpotential for oxygen reduction on CDX2-CoTMPP(HT) decreases by 65 mV compared to CDX1-CoTMPP(HT). A comparison of the oxygen

reduction activity of the prepared catalysts indicates that the activity increases with the increase of the amount of quinone groups. TEM images also show the higher dispersion of  $MN_4$  clusters in the case of oxidized carbon (CDX2) support compared to the as-received carbon support (CDX1). It means that the presence of quinone groups on carbon increased the dispersion of  $MN_4$  ( $M = Fe$  and  $Co$ ) clusters and causes the enhancement of ORR activity. It is reported that the carbon will be usually covered with oxygen complexes mainly carbonyl and hydroxyl groups by means of nitric acid treatment (Ehrburger *et al.* 1983; Nalini Subramanian *et al.*, 2005). Higher dispersion of the  $MN_4$  clusters on the oxidized carbon may originate from interfacial bonds with the oxygen complexes of the carbon surfaces. Thus the migration and the coalescence of the active species are considerably lowered by the presence of oxygenated groups which act as anchors for the supported clusters. Therefore by increasing the number of oxygen groups on the carbon support by nitric acid treatment, the dispersion of the active species as well as their performance is increased.

For comparison, a commercial Pt/C of same metal content is investigated for oxygen reduction under the same conditions. The corresponding LSVs are shown in Fig. 7.10. The oxygen reduction activity calculated at +0.7 V vs. NHE is  $4.9 \text{ mA cm}^{-2}$ . The heat-treated metal tetramethoxyphenylporphyrin complexes supported on oxidized carbon, CDX2-FeTMPPCl(HT) and CDX2-CoTMPP(HT) electrocatalysts also exhibited comparable ORR activities,  $4.9$  and  $4.5 \text{ mA cm}^{-2}$  respectively. Moreover, the onset potential for oxygen reduction on CDX2-FeTMPPCl(HT) and CDX2-CoTMPP(HT) catalysts are +870 and +860 mV vs. NHE respectively whereas for commercial Pt/C, the onset potential is +910 mV vs. NHE. It implies that the  $MN_4C_x$  active species shows less than 50 mV higher overpotential for oxygen reduction in comparison to

the commercial Pt/C catalyst. These results suggest that these  $MN_4C_x$  species are better alternative to Pt catalysts for oxygen reduction.

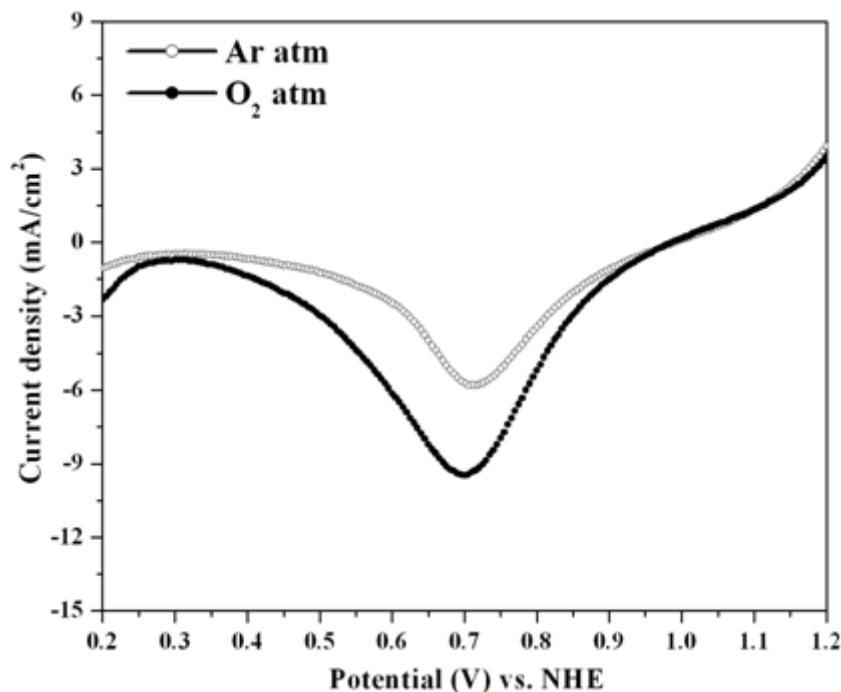


Fig. 7.10 Linear sweep Voltammograms (LSVs) of commercial 2 wt.% Pt/Vulcan XC72R (E-TEK) in Ar- and O<sub>2</sub>- saturated 0.5 M H<sub>2</sub>SO<sub>4</sub>; Scan rate - 10 mV s<sup>-1</sup>

### 7.5.3 Chronoamperometric Response

The current density – time plots of Fe- and Co- based catalysts in oxygen saturated 0.5 M H<sub>2</sub>SO<sub>4</sub> at +0.7 V vs. NHE are shown in Fig. 7.11 and 7.12 respectively. The performance of heat-treated metal tetramethoxyphenylporphyrin complexes supported on oxidized carbon, CDX2-FeTMPPCl(HT) and CDX2-CoTMPP(HT) electrodes is found to be better compared to the as-received carbon supported catalysts, CDX1-FeTMPPCl(HT) and CDX1-CoTMPP(HT). Strong bonding interactions between the active species and oxidized carbon may be the possible reason for this behaviour. Moreover, their performance is comparable to that of commercial Pt/C (E-TEK) electrode.

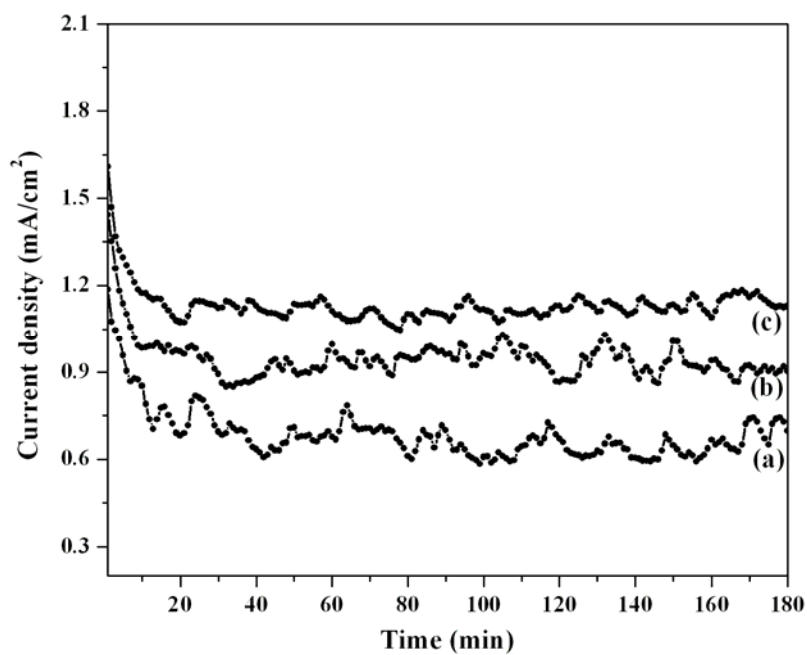


Fig. 7.11 Current density vs. time plots of (a) CDX1-FeTMPPCl(HT), (b) CDX2-FeTMPPCl(HT) and (c) commercial Pt/C (E-TEK) measured in oxygen saturated 0.5 M  $\text{H}_2\text{SO}_4$  at +0.7 V vs. NHE

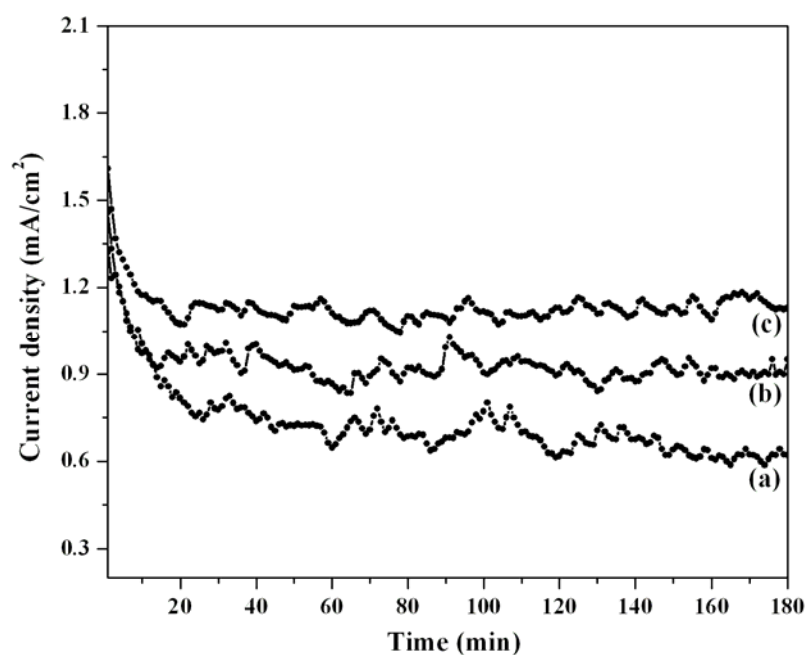


Fig. 7.12 Current density vs. time plots of (a) CDX1-CoTMPP(HT) and (b) CDX2-CoTMPP(HT) and (c) commercial Pt/C (E-TEK) measured in oxygen saturated 0.5 M  $\text{H}_2\text{SO}_4$  at +0.7 V vs. NHE

#### 7.5.4 Single-Cell PEMFC Measurements

The measurements in PEM fuel cells are obtained in a fuel cell test station. The procedure for the preparation of gas diffusion electrode (GDE) and single cell assembly was followed according to the literature (Lefèvre *et al.*, 2000). Gas diffusion electrodes are prepared by a combined filtration/brushing procedure using the commercial Pt/C catalysts, prepared catalysts, a carbon cloth substrate (PWB-3, Stackpole), a PTFE suspension (Teflon 306A, DuPont) and a Nafion® solution. The anode (20 wt% Pt/C from E-TEK) consists of  $0.4 \text{ mg Pt cm}^{-2}$ . The cathode (prepared Fe and Co catalyst) consists of  $0.2 \text{ mg metal cm}^{-2}$ . A homogeneous catalyst suspension consisted of 12.9 mg of catalyst, 0.5 ml of H<sub>2</sub>O and 0.3 ml of 5 wt % Nafion solution blended ultrasonically for 1 h was applied on the teflonized carbon cloth substrate by layer wise. Each layer is applied by pipetting 60  $\mu\text{l}$  of the catalyst suspension and then spreading it uniformly over the entire surface. A hot plate is used to accelerate the drying of the catalyst suspension between each application. Both anode and cathode electrodes are then placed in a vacuum oven at 348 K for 1 h. The single cell membrane-electrode assembly (MEA) is fabricated by sandwiching the Nafion 115 membrane between the cathode and anode by hot pressing at 413 K and  $50 \text{ kg cm}^{-2}$  for 1 min. The geometric area of the electrodes is  $6.25 \text{ cm}^2$ . The same procedure is followed to fabricate the reference membrane-electrode assembly (MEA) using 2 wt % Pt from E-TEK at the cathode. The cathode Pt loading for the reference MEA is  $0.2 \text{ mg Pt cm}^{-2}$ . All fuel cell measurements are performed at 353 K. The O<sub>2</sub> and H<sub>2</sub> gas back pressures are 60 and 30 psi respectively. The two gases are humidified prior to admission into the fuel cell by passing them through stainless steel containers filled with H<sub>2</sub>O kept at 373 K. Before the steady-state polarization curves are recorded, the cell was left under open circuit conditions for 30 min (MEA

conditioning). Then a polarization curve is recorded by varying the applied potential from 0.9 to 0 V vs NHE.

Fig. 7.13 compares the electrochemical performances in a single-cell PEMFC at 353 K using the heat-treated M-TMPP (M = Fe and Co) supported on as-received and oxidized carbons and the commercial 2 wt.% Pt/C (E-TEK) catalyst with same metal loading as the cathode under the identical test conditions. The current densities obtained at 0.7 V vs. NHE are given in Table 7.6.

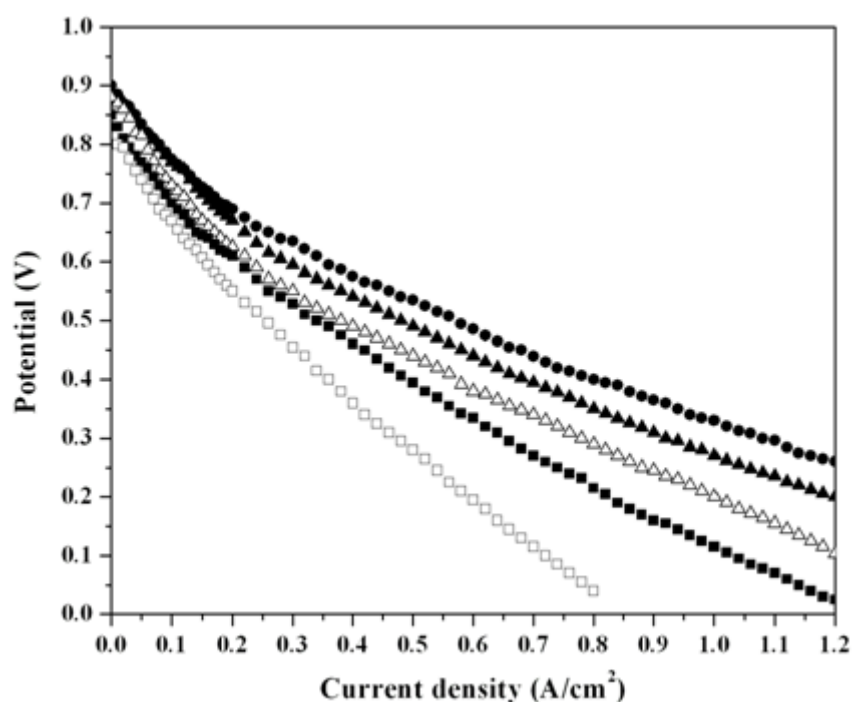


Fig. 7.13  $H_2/O_2$  PEM fuel cell polarization curves with ( $\Delta$ ) CDX1-FeTMPPCl(HT), ( $\blacktriangle$ ) CDX2-FeTMPPCl(HT), ( $\square$ ) CDX1-CoTMPP(HT) and ( $\blacksquare$ ) CDX2-CoTMPP(HT) and ( $\bullet$ ) commercial Pt/C (E-TEK) for oxygen reduction at 353 K

The performance of the heat treated M-TMPP (M = Fe and Co) supported on oxidized carbon is better compared to that of the heat-treated M-TMPP (M = Fe and Co) supported on as-received carbon. The increased order of performance in terms of current densities at 0.7 V is, CDX1-CoTMPP(HT) < CDX2-CoTMPP(HT)  $\approx$  CDX1-



FeTMPPCl(HT) < CDX2-FeTMPPCl(HT)  $\approx$  Pt/C (E-TEK). At 0.7 V, CDX2-FeTMMCl(HT) and CDX2-CoTMPP(HT) catalysts yielded a current densities of  $\sim$ 171 and  $\sim$ 104 mA cm<sup>-2</sup> respectively while the commercial Pt/C (E-TEK) catalyst gave a current density of  $\sim$ 180 mA cm<sup>-2</sup>. The CDX2-FeTMMCl(HT) and CDX2-CoTMPP(HT) catalysts show an open circuit voltage of  $\sim$ 0.89 and  $\sim$ 0.85 V respectively, which is close to that found with the commercial Pt catalyst ( $\sim$ 0.9 V).

Table 7.6 Single-cell PEM fuel cell performance of Fe- and Co-based catalysts as well as commercial Pt catalysts at +0.7 V vs. NHE

Catalyst	Performance at +0.7 V vs NHE (mA cm <sup>-2</sup> )
CDX1-FeTMPPCl(HT)	125
CDX2-FeTMPPCl(HT)	171
CDX1-CoTMPP(HT)	82
CDX2-CoTMPP(HT)	104
Pt/Vulcan XC72R (E-TEK)	180

## CHAPTER 8

### SUMMARY AND CONCLUSIONS

The search for an efficient electrocatalysts for oxygen reduction reaction (ORR) has been a topic of current interest. At present, conventional carbon supported Pt is the successful and commercially exploited electrocatalyst for ORR in various electrochemical devices. But the sluggish kinetics of ORR, high overpotential and cost of Pt catalysts hinder the commercialization of the devices. These difficulties can be overcome by either preparing Pt particles of desirable size on carbon or alloying Pt with a suitable element and supported on carbon. In recent years, significant research has been focused on various non-Pt based electrocatalysts such as Pd, Pd alloys,  $\text{Ru}_x\text{Se}_y$  and  $\text{MN}_4\text{C}_x$  clusters. But the ORR activity and performance is less compared to that of the state-of-art commercial Pt/C catalysts. Literature reports indicate that the composition and size of the particles play an important role in the enhancement of the activity. Thus, attempts were made to prepare the electrocatalysts in nano-size range with suitable composition and electrochemical measurements have been performed to investigate the oxygen reduction activity.

The conclusions drawn from this study are:

- Monodispersed Pt nanoparticles of different sizes (2.0, 2.5, 3.5, 4.0, 5.0 and 6.0 nm) were synthesized by reduction of platinum(II)acetylacetonate with 1,2-hexadecanediol in the presence of long chain carboxylic acid and long chain alkyl amine as protecting agents. Particle sizes were varied by changing the refluxing time and combination of protecting agents either oleic acid and oleylamine or nonanoic acid and nonylamine. The purified Pt nanoparticles were loaded onto carbon black (CDX975) under ultrasonic

agitation to achieve 20 wt.% Pt/C. The prepared materials were characterized by XRD, TEM and EDX techniques. Face-centered cubic (fcc) structure of Pt was evident from XRD. TEM images of the as-synthesized catalysts displayed uniform size and shaped Pt nanoparticles on the carbon support. EDX confirms the presence of Pt and C in the catalysts. Steady-state linear sweep voltammetric measurements showed that the optimum size of Pt for oxygen reduction is 3-4 nm. This is due to the alteration of energy levels associated with the particle size of Pt. As-synthesized Pt nanoparticles of sizes, 3.5 and 4.0 nm loaded on carbon catalysts exhibited comparable activity with that of commercial Pt/C (E-TEK) catalyst.

- Monodispersed Pt-M alloy (M = Fe, Co and Cr) nanoparticles prepared by polyol reduction method were loaded onto carbon black and characterized by XRD, TEM and EDX. Spherical shaped Pt-M alloy (50:50 atom%) nanoparticles with narrow size distribution were observed on carbon support. Electrochemical measurements indicate the formation of Pt (hydr)oxy species is lowered in the case of Pt-M alloys compared to that of Pt. Pt alloys exhibited 1.5 times higher ORR activity than that of commercial Pt/C (E-TEK). The higher ORR activity, low overpotential and low degradation of activity of the Pt-M/CDX975 (M = Fe, Co and Cr) compared to that of commercial Pt/C (E-TEK) make them more appropriate cathodes for electrochemical device applications.
- Carbon black (CDX975) supported Pd and Pd-Co-M (M = Mo and Au) alloy nanoparticles with 70:20:10 atom% were prepared by the reduction of metal precursor(s) with hydrazine in reverse microemulsion of water/Triton X-

100/propanol-2/cyclohexane. The as-synthesized Pd-Co-M/CDX975 (M = Mo and Au) catalysts were heat-treated at 973, 1073 and 1173 K to promote alloy formation. These materials were characterized by powder XRD, TEM and EDX. Single phase face-centered cubic structure of Pd in the catalysts was observed from XRD pattern. TEM and EDX analysis revealed the nano-sized metallic particles with exact composition. Electrochemical measurements indicated that the Pd alloys exhibit higher ORR activity than Pd. This is attributed to the suppression of oxy species on Pd surface in the presence of alloying elements. Comparable ORR activity of heat-treated Pd-Co-Mo/CDX975 at 973 K and Pd-Co-Au/CDX975 at 1073 K catalysts with that of Pt/C (E-TEK) makes them as viable oxygen reduction electrodes for electrochemical device applications.

- Reverse microemulsion method (RME) has been used to synthesize 20 wt% Ru<sub>x</sub>Se<sub>y</sub>/CDX975 catalysts. XRD patterns showed the presence of Ru in *hcp* phase and the similar particle size (around 3 nm) in all the as-synthesized catalysts. As evident from EDX, the composition obtained for the as-synthesized catalysts was nearly in agreement with those of the starting metal content. TEM image of Ru<sub>1</sub>Se<sub>0.6</sub>/CDX975 showed the high dispersion of metallic particles on carbon (CDX975) support. A series of Ru<sub>x</sub>Se<sub>y</sub>/CDX975 catalysts for the O<sub>2</sub> reduction were evaluated by linear sweep voltammetry. The improvement of ORR activity by the presence of Se with a maximum activity (geometric area-normalized current density) for the Ru<sub>1</sub>Se<sub>0.6</sub>/CDX975 catalyst were observed. The reason for the improved activity is the stabilization of Ru active sites by Se, against blocking as a result of (hydr)oxide formation. The comparable ORR activity and stability of

Ru<sub>1</sub>Se<sub>0.6</sub>/CDX975 with that of commercial Pt/C (E-TEK) catalyst makes it as an alternative to Pt for oxygen reduction.

- Density functional calculations showed that, same symmetry and energy of the HOMO of MN<sub>4</sub> (M = Fe and Co) and  $\pi^*$  orbital of O<sub>2</sub> make the reduction feasible. The presence of 'N' in the active site MN<sub>4</sub> (M = Fe and Co) plays an important role in attaining directional wave function there by leading to a facile electron transfer.
- The optimum conditions for the maximum ORR activity of FeTPP/CDX975 and FePc/CDX975 catalysts were investigated. Electrochemical measurements showed that the heat-treated FeTPP/CDX975 at 873 K and FePc/CDX975 at 773 K exhibited good activity for oxygen reduction. But, the activity was less compared to the commercial Pt/C catalyst.
- The role exerted by the oxygenated surface groups in the dispersion of active species (generated from the heat-treatment of FeTMPP-Cl and CoTMPP), responsible for oxygen reduction was studied. The results indicated that, introduction of surface oxygen functionalities (quinones) on carbon support increases the dispersion of active species and enhances the ORR activity. Comparable ORR activity and single-cell PEMFC performance of MN<sub>4</sub>C<sub>x</sub> (M = Fe and Co) clusters with that of commercial Pt/C (E-TEK) make them as the potential candidates to replace Pt for oxygen reduction.

## REFERENCES

1. **Adler, A.D., F. R. Longo, F. Kampas, and J. Kim** (1970) On the preparation of metalloporphyrins. *J. Inorg. Nucl. Chem.* **32**, 2443-2445.
2. **Alonso-Vante, N.** *Chevrel phases and chalcogenides*. pp. 534-543. In Wolf Vielstich, Hubert A. Gasteiger, Anold Lamm. (eds.) *Hand book of Fuel Cells – Fundamentals, Technology and applications, Vol. 2: Electrocatalysis*, John Wiley & Sons, 2003.
3. **Alonso-Vante, N., P. Bogdanoff, and H. Tributsch** (2000) On the origin of the selectivity of oxygen reduction of ruthenium-containing electrocatalysts in methanol-containing electrolyte. *J. Catal.* **190**, 240-246.
4. **Alonso-Vante, N., W. Jaegermann, H. Tributsch, W. Honle, and K. Yvon** (1987) Electrocatalysis of oxygen reduction by chalcogenides containing mixed transition metal clusters. *J. Am. Chem. Soc.*, **109**, 3251-3257.
5. **Alonso-Vante, N., I.V. Malakhov, S.G. Nikitenko, E.R. Savinova, and D.I. Kochubey** (2002) The structure analysis of the active centers of Ru-containing electrocatalysts for the oxygen reduction. An in situ EXAFS study. *Electrochim. Acta*, **47**, 3807-3814.
6. **Alonso-Vante, N., B. Schubert, and H. Tributsch** (1989) Transition metal cluster materials for multi-electron transfer catalysis. *Mater. Chem. Phys.*, **22**, 281-307.
7. **Alonso-Vante, N. and O. Solorza-Feria** (1995) Kinetics studies of oxygen reduction in acid medium on novel semiconducting transition metal chalcogenides. *Electrochim. Acta*, **40**, 567-576.
8. **Alonso-Vante, N. and H. Tributsch** (1986) Energy conversion catalysis using semiconducting transition metal cluster compounds. *Nature*, **323**, 431-432.
9. **Anastasijevic, N.A., M. Dimitruevic, and R. R. Adzic** (1986) Oxygen reduction on a ruthenium electrode in acid electrolyte. *Electrochim. acta*, **31**, 1125-1130.
10. **Anastasijevic, N.A., V. Vesovic, and R.R. Adzic** (1987) Determination of the kinetic parameters of the oxygen reduction reaction using the rotating ring-disk electrode : Part I. Theory. *J. Electroanal. Chem.*, **229**, 305-316.
11. **Antoine, O., Y. Bultel, and R. Durand** (2001) Oxygen reduction reaction kinetics and mechanism on platinum nanoparticles inside Nafion<sup>®</sup>. *J. Electroanal. Chem.* **499**, 85-94.
12. **Antolini, E.** (2003) Formation of carbon-supported PtM alloys for low temperature fuel cells: A review. *Mater. Chem.Phys.*, **78**, 563-573.

13. **Antolini, E., R.R. Passos, and E.A. Ticianelli** (2002) Electrocatalysis of oxygen reduction on a carbon supported platinum-vanadium alloy in polymer electrolyte fuel cells. *Electrochim. Acta*, **48**, 263-270.
14. **Antolini, E., J.R.C. Salgado, M.J. Giz, and E.R. Gonzalez** (2005a) Effects of geometric and electronic factors on ORR activity of carbon supported Pt–Co electrocatalysts in PEM fuel cells. *Int. J. Hydrogen Energy*, **30**, 1213-1220.
15. **Antolini, E., J.R.C. Salgado, and E.R. Gonzalez** (2005b) Carbon supported Pt<sub>75</sub>M<sub>25</sub> (M = Co, Ni) alloys as anode and cathode electrocatalysts for direct methanol fuel cells. *J. Electroanal. Chem.*, **580**, 145-154.
16. **Antolini, E., J.R.C. Salgado, and E.R. Gonzalez** (2005c) Oxygen reduction on a Pt<sub>70</sub>Ni<sub>30</sub>/C electrocatalyst prepared by the borohydride method in H<sub>2</sub>SO<sub>4</sub>/CH<sub>3</sub>OH solutions. *J. Power Sources*, **155**, 161-166.
17. **Antolini, E., J.R.C. Salgado, L.G.R.A. Santos, G. Garcia, E.A. Ticianelli, E. Pastor and E.R. Gonzalez** (2006) Carbon supported Pt–Cr alloys as oxygen-reduction catalysts for direct methanol fuel cells. *J. Appl. Electrochem.* **36**, 355-362.
18. **Appleby, A.J.** (1986) Phosphoric acid fuel cells (PAFCs). *Energy*, **11**, 13-94.
19. **Appleby, A.J.** (1993) Electrocatalysis of aqueous dioxygen reduction. *J. Electroanal. Chem.* **357**, 117-179.
20. **Baglio, V., A. Stassi, A. Di Blasi, C.D. Urso, V. Antonucci, and A.S. Arico** (2007) Investigation of bimetallic Pt–M/C as DMFC cathode catalysts. *Electrochim. Acta*, **53**, 1360-1364.
21. **Bagotzky, V.S., M.R. Tarasevich, K.A. Radyushkina, O.A. Levina, and S.I. Andrusova** (1978) Electrocatalysis of the oxygen reduction process on metal chelates in acid electrolyte. *J. Power Sources*, **13**, 233-240.
22. **Balcerzak, M., E. Świącicka, and E. Balukiewicz** (1999) Determination of platinum and ruthenium in Pt and Pt–Ru catalysts with carbon support by direct and derivative spectrophotometry. *Talanta*, **48**, 39-47.
23. **Bard, A.J** *Electroanalytical Chemistry*. Marcel Dekker Inc., New York, 1976.
24. **Bayrakceken, A., A. Smirnova, U. Kitkamthorn, M. Aindow, L. Türker, I. Eröglu, and C. Erkey** (2008) Pt-based electrocatalysts for polymer electrolyte membrane fuel cells prepared by supercritical deposition technique. *J. Power Sources*, **179**, 532-540.
25. **Beard, B.C. and P.N. Ross** (1990) The structure and activity of Pt-Co alloys as oxygen reduction electrocatalysts. *J. Electrochem. Soc.* **137**, 3368-3374.
26. **Beck, F.** (1977) The redox mechanism of the chelate-catalysed oxygen cathode. *J. Appl. Electrochem.* **7**, 239-245.

27. **Becke, A.D.** (1988) Density-functional exchange-energy approximation with correct asymptotic behaviour. *Phys. Rev. A* **38**, 3098-3100.
28. **Bell, A.T.** (2003) The impact of nanoscience on heterogeneous catalysis. *Science*, **299**, 1688-1691.
29. **Bett, J., J. Lundquist, E. Washington, and P. Stonehart** (1973) Platinum crystallite size considerations for electrocatalytic oxygen reduction-I. *Electrochim. Acta*, **18**, 343-348.
30. **Bettelheim, A., D. Ozer, R. Harth, and R. Ydgar** (1990) Dioxygen reduction and hydrogen peroxide dismutation using electropolymerized bilayers of cobalt + manganese tetrakis(*o*-aminophenyl)porphyrins. *J. Electroanal. Chem.* **281**, 147-161.
31. **Biloul, A., O. Contamin, G. Scarbeck, M. Savy, B. Palys, J. Riga, and J. Verbist** (1994) Oxygen reduction in acid media: influence of the activity of CoNPc(1,2) bilayer deposits in relation to their attachment to the carbon black support and role of surface groups as a function of heat treatment. *J. Electroanal. Chem.*, **365**, 239-246.
32. **Blurton, KF., P. Greenberg, H.G. Oswin, and D.R. Putt** (1972) The electrochemical activity of dispersed platinum. *J. Electrochem. Soc.*, **119**, 559-564.
33. **Bockris J. O'M. and A. K. N. Reddy** *Modern Electrochemistry: Vol. 2*. Plenum Press, New York, 1970.
34. **Bönnemann, H., G. Braun, W. Brijoux, R. Brinkmann, S. Tilling, K. Seevogel, and K. Siepen** (1996) Nanoscale colloidal metals and alloys stabilized by solvents and surfactants: Preparation and use as catalyst precursors. *J. Organometallic Chem.*, **520**, 143-162.
35. **Bouwkamp-Wijnoltz, A.L., W. Visscher, and J.A.R. van Veen** (1998) The selectivity of oxygen reduction by pyrolysed iron porphyrin supported on carbon. *Electrochim. Acta*. **43**, 3141-3152.
36. **Bregoli, J.** (1978) The influence of platinum crystallite size on the electrochemical reduction of oxygen in phosphoric acid. *Electrochim. Acta*, **23**, 489-492.
37. **Bron, M., P. Bogdanoff, S. Fiechter, I. Dorbandt, M. Hilgendorff, H. Schulenburg, and H. Tributsch** (2001) Influence of selenium on the catalytic properties of ruthenium-based cluster catalysts for oxygen reduction. *J. Electroanal. Chem.* **500**, 510-517.
38. **Bron, M., S. Fiechter, M. Hilgendorff, P. Bogdanoff, and S. Fiechter** (2002) Catalysts for oxygen reduction from heat-treated carbon-supported iron phenantroline complexes. *J. Appl. Electrochem.*, **32**, 211-216.



39. **Campbell, S.A.** (2004) Non-noble metal catalysts for the oxygen reduction reaction. *US Patent* 0096728 A1.
40. **Cao G,** Nano structures and nano materials Synthesis properties and applications. Imperial College Press, London, 2004.
41. **Capek, I.** (2004) Preparation of metal nanoparticles in water-in-oil (w/o) microemulsions. *Adv. Colloid and Interface Science*, **110**, 49-74.
42. **Chang, C.K., H.Y. Liu, and I. Abdalmuhdi** (1984) Electroreduction of oxygen by pillared cobalt(II) cofacial diporphyrin catalysts. *J. Am. Chem. Soc.*, **106**, 2725-2726.
43. **Chang, C-C., T-C Wen, and H-J Tien** (1997) Kinetics of oxygen reduction at oxide-derived Pd electrodes in alkaline solution. *Electrochim. Acta*, **42**, 557-565.
44. **Chevrel, R., M. Sergent, and J. Pringent** (1971) Sur de nouvelles phases sulfurées ternaires du molybdène. *J. Solid State Chem.*, **3**, 515-519.
45. **Choi, H.J., G. Kwag, and S. Kim** (2002) Electrochemical and XAFS investigation of nitrite reduction by heat-treated  $\mu$ -oxo derivative of iron phthalocyanine supported on high area carbon. *J. Electroanal. Chem.* **508**, 105-114.
46. **Collman, J.P., P. Denisevich, Y. Konai, M. Marocco, C. Koval, and F.C. Anson** (1980) Electrode catalysis of the four-electron reduction of oxygen to water by dicobalt face-to-face porphyrins. *J. Am. Chem. Soc.*, **102**, 6027-6036.
47. **Collman, J.P., M. Marocco, P. Denisevich, C. Koval, and F.C. Anson** (1979) Potent catalysis of the electroreduction of oxygen to water by dicobalt porphyrin dimers adsorbed on graphite electrodes. *J. Electroanal. Chem.* **101**, 117-122.
48. **Colmenares, L., Z. Jusys, and R.J. Behm** (2006) Electrochemical surface characterization and O<sub>2</sub> reduction kinetics of Se surface-modified Ru nanoparticle-based RuSe<sub>y</sub>/C catalysts. *Langmuir*, **22**, 10437-10445.
49. **Colmenares, L., Z. Jusys, and R.J. Behm** (2007) Activity, selectivity, and methanol tolerance of Se-modified Ru/C cathode catalysts. *J. Phys. Chem. C*, **111**, 1273-1283.
50. **Convert, P., C. Coutanceau, P. Crouigneau, F. Gloagen, and C. Lamy** (2001) Electrodes modified by electrodeposition of CoTAA complexes as selective oxygen cathodes in a direct methanol fuel cell. *J. Appl. Electrochem.*, **31**, 945-952.
51. **Cui, H.-F., J.-S. Ye, W.-D. Zhang, J. Wang, and F.-S. Sheu** (2005) Electrocatalytic reduction of oxygen by a platinum nanoparticle/carbon nanotube composite electrode. *J. Electroanal. Chem.*, **577**, 295-302.

52. **Cullity, B.D.** *Elements of X-ray Diffraction*. Addison-Wesley, Massachusetts, 1978.
53. **Cushing, B.L., V.L. Kolesnichenko, and C.J. O'Connor** (2004) Recent advances in the liquid-phase syntheses of inorganic nanoparticles, *Chem. Rev.*, **104**, 3893-3946.
54. **Damjanovic, A.** (1991) On the kinetics and mechanism of oxygen reduction at oxide film-covered Pt electrodes in acid solutions. *J. Electrochem. Soc.*, **138**, 2315-2320.
55. **Damjanovic, A. and J. O'M. Bockris** (1966) The rate constants for oxygen dissolution on bare and oxide-covered platinum. *Electrochim. Acta*, **11**, 376-377.
56. **Damjanovic, A., M.A. Gensaw, and J. O'M. Bockris** (1966) Distinction between intermediates produced in main and side electroodic reactions. *J. Chem. Phys.*, **45**, 4057-4059.
57. **Dassenoy, F., W. Vogel, and N. Alonso-Vante** (2002) Structural studies and stability of cluster-like Ru<sub>x</sub>Se<sub>y</sub> electrocatalysts. *J. Phys. Chem. B* **106**, 12152-12157.
58. **Deiss, E., F. Holzer, and O. Haas** (2002) Modeling of an electrically rechargeable alkaline Zn-air battery. *Electrochim. Acta*, **47**, 3995-4010.
59. **Durand, R.R., C.S. Bencosme, J.P. Collman, and F.C. Anson** (1983) Mechanistic aspects of the catalytic reduction of dioxygen by cofacial metalloporphyrins. *J. Am. Chem. Soc.*, **105**, 2710-2718.
60. **Duron, S., R. Rivera-Noriega, M.A. Leyva, P. Nkeng, G. Poillerat, and O. Solorza-Feriz** (2000) Oxygen reduction on a Ru<sub>x</sub>S<sub>y</sub>(CO)<sub>n</sub> cluster electrocatalyst in 0.5 M H<sub>2</sub>SO<sub>4</sub>. *J. Solid State Electrochem.*, **4**, 70-74.
61. **Eastoe, J., M.J. Hollamby, and L. Hudson** (2006) Recent advances in nanoparticle synthesis with reversed micelles. *Adv. in Colloid and Interface Science*, **128-130**, 5-15.
62. **Ehrburger, P., A. Mongilardi, and J.J. Lahaye** (1983) Dispersion of iron phthalocyanine on carbon surfaces, *J. Colloid Interface Sci.* **91**, 151-159.
63. **Elzing, A., A. van der Putten, W. Visscher, and E. Barendrecht** (1987) The cathodic reduction of oxygen at metal tetrasulfonato-phthalocyanines: influence of adsorption conditions on electrocatalysis. *J. Electroanal. Chem.*, **233**, 99-112.
64. **Enyo, M., T. Yamazaki, K. Kai, and K. Suzuki** (1983) Amorphous Pd-Zr alloys for water electrolysis cathode materials. *Electrochim. Acta*, **28**, 1573-1579.

65. **Eriksson, S., Ulf Nylén, S. Rojas, and M. Boutonnet** (2004) Preparation of catalysts from microemulsions and their applications in heterogeneous catalysis. *Appl. Catal. A: General*, **265**, 207-226.
66. **Etcheberry, A., J. Gautron, and J.L. Sculfort** (1988) A study of the mechanisms of O<sub>2</sub> reduction at n- and p-InP in acid aqueous electrolyte. *J. Electroanal. Chem.*, **247**, 265-276.
67. **Faubert, G., G. Lalande, R. Cote, D. Guay, J.P. Dodelet, L.T. Weng, P. Bertrand, and G. Denes** (1996) Heat-treated iron and cobalt tetraphenylporphyrins adsorbed on carbon black: Physical characterization and catalytic properties of these materials for the reduction of oxygen in polymer electrolyte fuel cells. *Electrochim. Acta*, **41**, 1689-1701.
68. **Fernández, J.L., D.A. Walsh, and A.J. Bard** (2005a) Thermodynamic guidelines for the design of bimetallic catalysts for oxygen electroreduction and rapid screening by scanning electrochemical microscopy. M-Co (M: Pd, Ag, Au). *J. Am. Chem. Soc.* **127**, 357-365.
69. **Fernández, J.L., V. Raghuvver A. Manthiram, and A. J. Bard** (2005b) Pd-Ti and Pd-Co-Au electrocatalysts as a replacement for platinum for oxygen reduction in proton exchange membrane fuel cells. *J. Am. Chem. Soc.* **127**, 13100-13101.
70. **Fernández, J.L., J.M. White, Y. Sun, W. Tang, G. Henkelman, and A.J. Bard** (2006) Characterization and theory of electrocatalysts based on scanning electrochemical microscopy screening methods. *Langmuir*, **22**, 10426.
71. **Fiechter, S., I. Dorbandt, P. Bogdanoff, G. Zehl, H. Schulenburg, H. Tributsch, M. Bron, J. Radnik, and M. Fieber-Erdmann** (2007) Surface modified ruthenium nanoparticles: Structural investigation and surface analysis of a novel catalyst for oxygen reduction. *J. Phys. Chem. C*, **111**, 477-487.
72. **Fischer, C., N. Alonso- Vante, S. Fiechter, and H. Tributsch** (1995) Electrocatalytic properties of mixed transition metal tellurides (Chevrephases) for oxygen reduction. *J. Appl. Electrochem.*, **24**, 1004-1008.
73. **Frisch, M.J., G.W. Trucks, H.B. Schlegel, P.M.W. Gill, B.G. Johnson, M.A. Robb, J.R. Cheeseman, T.A. Keith, G.A. Petersson, J.A. Montgomery, K. Raghavachari, M.A. Al-Laham, V.G. Zakrzewski, J.V. Ortiz, J.B. Foresman, J. Cioslowski, B.B. Stefanov, A. Nanayakkara, M. Challacombe, C.Y. Peng, P.Y. Ayala, W. Chen, M.W. Wong, J.L. Andres, E.S. Replogle, R. Gomperts, R.L. Martin, D.J. Fox, J.S. Binkley, D.J. Defrees, J. Baker, J.P. Stewart, M. Head-Gordan, C. Gonzalez, and J.A. Pople** (1998) *GAUSSIAN98W*, Gaussian Inc, Pittsburgh.
74. **Gamez, A., D. Richard, and P. Gallezot** (1996) Oxygen reduction on well-defined platinum nanoparticles inside recast ionomer. *Electrochim. Acta*, **41**, 307-314.

75. **Gasteiger, H.A., S.K. Shyam, B. Sompalli, and F.T. Wagner** (2005) Activity benchmarks and requirements for Pt, Pt-alloy, and non-Pt oxygen reduction catalysts for PEMFCs. *Appl. Catal. B: Environmental*, **56**, 9-35.
76. **Geins, L., R. Faure and R. Durand** (1998) Electrochemical reduction of oxygen on platinum nanoparticles in alkaline media. *Electrochim. Acta.*, **44**, 1317-1327.
77. **Giner, J. and L. Swette** (1966) Oxygen reduction on titanium nitride in alkaline electrolyte. *Nature*, **211**, 1291-1292.
78. **Giordano, N., E. Passalacqua, L. Pino, A.S. Arico, V. Antonucci, M. Vivaldi, and K. Kinoshita** (1991) Analysis of platinum particle size and oxygen reduction in phosphoric acid. *Electrochim Acta*, **36**, 1979-1984.
79. **Giordano, N., P.L. Antonucci, E. Passalacqua, L. Pino, A.S. Arico, V. Antonucci, V. Alderucci, and V. Recupero** (1994) Effect of particle size on the performance of PAFC O<sub>2</sub> reduction electrocatalysis. *Int. J. Hydrogen Energy*, **19**, 165-168.
80. **Glass, J.T., G.L. Cahen, G.E. Stoner, and E.J. Taylor** (1987) The effect of metallurgical variables on the electrocatalytic properties of PtCr alloys. *J. Electrochem. Soc.*, **134**, 58-65.
81. **Gojkovic, S. Lj., S. Gupta, and R.F. Savinell** (1998a) Heat-treated iron(III) tetramethoxyphenyl porphyrin supported on high-area carbon as an electrocatalyst for oxygen reduction. I. Characterization of the electrocatalyst. *J. Electrochem. Soc.*, **145**, 3493-3499.
82. **Gojkovic, S.L., S.K. Zecevic, and R.F. Savinell** (1998b) O<sub>2</sub> reduction on an ink-type disk electrode using Pt supported on high-area carbons. *J. Electrochem. Soc.*, **145**, 3713-3720.
83. **Gojkovic, S. Lj., S. Gupta, and R. F. Savinell** (1999) Heat-treated iron(III) tetramethoxyphenyl porphyrin chloride supported on high-area carbon as an electrocatalyst for oxygen reduction: Part II. Kinetics of oxygen reduction. *J. Electroanal. Chem.*, **462**, 63-72.
84. **Gong, Y, Y.D. Yeboah, S.N. Lvov, V. Balashov, and Z. Wang** (2007) Fe-modified, Pt-based cathodic electrocatalysts for oxygen reduction reaction with enhanced methanol tolerance. *J. Electrochem. Soc.*, **154**, B560-B565.
85. **Gonzalez-Cruz, R. and O. Solorza-Feria** (2003) Oxygen reduction in acid media by a Ru<sub>x</sub>Fe<sub>y</sub>Se<sub>z</sub>(CO)<sub>n</sub> cluster catalyst dispersed on a glassy carbon-supported Nafion film. *J. Solid State Electrochem.*, **7**, 289-295.
86. **Gouérec, P., M. Savy, and J. Riga** (1998) Oxygen reduction in acidic media catalyzed by pyrolyzed cobalt macrocycles dispersed on an active carbon: The importance of the content of oxygen surface groups on the evolution of the chelate structure during the heat treatment. *Electrochim. Acta*, **43**, 743-753.

87. **Grgur, B.N., N.M. Markovic, and P.N. Ross** (1997) Temperature-dependent oxygen electrochemistry on platinum low-index single crystal surfaces in acid solutions. *Can. J. Chem.*, **75**, 1465-1471.
88. **Griffith, J.S.** (1956) On the magnetic properties of some haemoglobin complexes. *Proc. R. Soc. London Ser. A* **235**, 23-36.
89. **Grinberg, V.A., T.L. Kulova, N.A. Maiorova, Zh.V. Dobrokhotova, A.A. Pasynskii, A.M. Skundin, and O.A. Khazova** (2007) Nanostructured catalysts for cathodes of oxygen-hydrogen fuel cells, *Russ. J. Electrochem.*, **43**, 75-84.
90. **Guo, J.W., T.S. Zhao, J. Prabhuram, and C.W. Wong** (2005) Preparation and the physical/electrochemical properties of a Pt/C nanocatalyst stabilized by citric acid for polymer electrolyte fuel cells. *Electrochim. Acta*, **50**, 1973-1983.
91. **Guo, Y., L. Zhuang, and J. Lu** (2007) First-principles considerations in the design of Pd-alloy catalysts for oxygen reduction. *Angew. Chem. Int. Ed.* **46**, 2862-2864.
92. **Gupta, S., D. Tryk, I. Bae, W. Aldred, and E. Yeager** (1989) Heat-treated polyacrylonitrile-based catalysts for oxygen electroreduction. *J. Appl. Electrochem.*, **19**, 19-27.
93. **Gupta, S., D. Tryk, S.K. Zecevic, W. Aldred, D. Guo, and R.F. Savinell** (1998) Methanol-tolerant electrocatalysts for oxygen reduction in a polymer electrolyte membrane fuel cell. *J. Appl. Electrochem.*, **28**, 673-682.
94. **Hammer, B. and J.K. Nørskov** (2000) Theoretical surface science and catalysis - calculations and concepts. *Adv. Catal.* **45**, 71-129.
95. **Haram, S.K., A.R. Mahadeshwar, and S.G. Dixit** (1996) Synthesis and characterization of copper sulfide nanoparticles in Triton-X-100 water-in-oil microemulsions. *J. Phys. Chem.*, **100**, 5868-5873.
96. **Hay, P.J. and W.R. Wadt** (1985) *Ab initio* effective core potentials for molecular calculations. Potentials for the transition metal atoms Sc to Hg. *J. Chem. Phys.* **82**, 270-283.
97. **Hays, C.C., R. Manoharan, and J.B. Goodenough** (1993) Methanol oxidation and hydrogen reactions on NiZr in acid solution. *J. Power Sources*, **45**, 291-301.
98. **Heiz, U., A. Sanchez, S. Abbet, and W.-D. Schneider** (1999) Catalytic oxidation of carbon monoxide on monodispersed platinum clusters: each atom counts. *J. Am. Chem. Soc.*, **121**, 3214-3217.
99. **Hernández-Fernández, P., S. Rojas, P. Ocon, J.L. Gomez de la Fuente, J. San Fabian, J. Sanza, M.A. Pena, F.J. Garcia-Garcia, P. Terreros, and J.L.G. Fierro** (2007) Influence of the preparation route of bimetallic Pt-Au

- nanoparticle electrocatalysts for the oxygen reduction reaction. *J. Phys. Chem. C*, **111**, 2913-2923.
100. **Hilgendorff, M., P. Bogdanoff, and M. Bron** (2003) Preparation, structure and performance of Ru-based oxygen reduction catalysts in PEM fuel cells. *Proceedings of the Fuel cell systems of the world renewable energy congress VII*, Köln, July, 227-230.
  101. **Hoar, T.P. and J.H. Schulman** (1943) Transparent water in oil dispersions: the oleopathic. Hydromicelle. *Nature*, **152**, 102-103.
  102. **Hoare, J.P.** *The Electrochemistry of Oxygen*. Wiley, New York, 1968.
  103. **Hoare, J.P. and S. Schuldiner** (1958) An electrochemical investigation of hydrogen producing reactions catalyzed by nickel and nickel-palladium cathodes. *J. Phys. Chem.* **62**, 229-233.
  104. **Horowitz, H.S., J.M. Longo, and H.H. Horowitz** (1983) Oxygen electrocatalysis on some oxide pyrochlores. *J. Electrochem. Soc.*, **130**, 1851-1859.
  105. **Hou, Z., B. Yi, and H. Zhang** (2003) Preparing high loading Pt/C by modifying the carbon support. *Electrochemical and Solid-State Lett.*, **6**, A232-A235.
  106. **Hwang, J.T. and J.S. Chung** (1993) The morphological and surface properties and their relationship with oxygen reduction activity for platinum-iron electrocatalysts. *Electrochim. Acta*, **38**, 2715-2723.
  107. **Huang, Q., H. Yang, Y. Tang, T. Lu, and D.L. Akins** (2006) Carbon-supported Pt-Co alloy nanoparticles for oxygen reduction reaction. *Electrochem. Commun.* **8**, 220-224.
  108. **Hufner, S. and G.K. Wertheim** (1975) Core-line asymmetries in the X-ray photoemission spectra of metals. *Phy. Rev. B*, **11**, 678-683.
  109. **Hwang, B.J., S.M. Senthil Kumar, C.-H. Chen, Monalisa, M.-Y. Cheng, D.-G. Liu, and J.-F. Lee** (2007) An Investigation of structure-catalytic activity relationship for Pt-Co/C bimetallic nanoparticles toward the oxygen reduction reaction. *J. Phys. Chem. C*, **111**, 15267-15276.
  110. **Hyeon, T., S.S. Lee, J. Park, Y. Chung, and H.B. Na** (2001) Synthesis of highly crystalline and monodisperse maghemite nanocrystallites without a size-selection process. *J. Am. Chem. Soc.*, **123**, 12798-12801.
  111. **Ioroi, T. and K. Yasuda** (2005) Platinum-Iridium alloys as oxygen reduction electrocatalysts for polymer electrolyte fuel cells. *J. Electrochem. Soc.* **152**, A1917-A1924.

112. **Ishihara, A., K. Lee, S. Doi, S. Mitsushima, N. Kamiya, M. Hara, K. Domen, K. Fukuda, and K. Ota** (2005) Tantalum oxynitride for a novel cathode of PEFC. *Electrochemical and Solid-State Lett.*, **8**, A201-A203.
113. **Jahnke, H., M. Schönborn, and G. Zimmermann** (1976) Organic dyestuffs as catalysts for fuel cells. *Top. Curr. Chem.* **61**, 133-181.
114. **Jalan, V. and E.J. Taylor** (1983) Importance of interatomic spacing in catalytic reduction of oxygen in phosphoric acid. *J. Electrochem. Soc.* **130**, 2299-2302.
115. **Jasinski, R.** (1964) A new fuel cell cathode catalyst. *Nature*, **201**, 1212-1213.
116. **Jiang, R. and F.C. Anson** (1991) The origin of inclined plateau currents in steady-state voltammograms for electrode processes involving electrocatalysis. *J. Electroanal. Chem.* **305**, 171-184.
117. **Jiang, R. and D. Chu** (2000) Remarkably active catalysts for the electroreduction of O<sub>2</sub> to H<sub>2</sub>O for use in an acidic electrolyte containing concentrated methanol. *J. Electrochem. Soc.* **147**, 4605-4609.
118. **Joyner, R.W., J.A.R van Veen, and W.M.H. Sachtler** (1982) Extended X-ray absorption fine structure (EXAFS) study of cobalt-porphyrin catalysts supported on active carbon. *J. Chem. Soc. Faraday. Trans. I*, **78**, 1021-1028.
119. **Kim, J.-H., A. Ishihara, S. Mitsushima, N. Kamiya, and K. Ota** (2007) Catalytic activity of titanium oxide for oxygen reduction reaction as a non-platinum catalyst for PEFC. *Electrochim. Acta*, **52**, 2492-2497.
120. **King, F., M.J. Quinn, and C.D. Litke** (1995) Oxygen reduction on copper in neutral NaCl solution. *J. Electroanal. Chem.*, **385**, 45-55.
121. **Kinoshita, K.** (1990) Particle size effects for oxygen reduction on highly dispersed platinum in acid electrolytes. *J. Electrochem. Soc.*, **137**, 845-848.
122. **Kinoshita, K.** *Electrochemical Oxygen Technology*. John Wiley & Sons, New York, 1992.
123. **Kinoshita, K. and J.A.S. Bett** (1973) Potentiodynamic analysis of surface oxides on carbon blacks. *Carbon*, **11**, 403-411.
124. **Klabunde, K.J., J. Stark, O. Koper, C. Mohs, D.G. Park, S. Decker, Y. Jiang, I. Lagadic, and D. Zhang** (1996) Nanocrystals as stoichiometric reagents with unique surface chemistry. *J. Phys. Chem.*, **100**, 12142-12153.
125. **Klopman, G.** (1968) Chemical reactivity and the concept of charge- and frontier-controlled reactions. *J. Am. Chem. Soc.* **90**, 223-234.
126. **Koffi, R.C., C. Coutanceau, E. Garnier, J.-M. Léger, and C. Lamy** (2005) Synthesis, characterization and electrocatalytic behaviour of non-alloyed PtCr

- methanol tolerant nanoelectrocatalysts for the oxygen reduction reaction (ORR). *Electrochim. Acta*, **50**, 4117-4127.
127. **Kozawa, A., V.E. Zilinois, and R.J. Brodd** (1970) Oxygen and hydrogen peroxide reduction at a ferric phthalocyanine-catalyzed graphite electrode. *J. Electrochem. Soc.*, **117**, 1470-1474.
  128. **Kunz., H.R. and G.A. Gruver** (1975) The catalytic activity of platinum supported on carbon for electrochemical oxygen reduction in phosphoric acid. *J. Electrochem. Soc.*, **112**, 1279- 1287.
  129. **Ladouceur, M., G. Lalonde, L. Dignard-Bailey, M.L. Trudeau, R. Schulz, D. Guay, and J.P. Dodelet** (1993) Pyrolyzed cobalt phthalocyanine as electrocatalyst for oxygen reduction. *J. Electrochem. Soc.* **140**, 1974-1981.
  130. **Lalonde, G., R. Cote, D. Guay, J.P. Dodelet, L.T. Weng, and P. Bertrand** (1997) Is nitrogen important in the formulation of Fe-based catalysts for oxygen reduction in solid polymer fuel cells? *Electrochim. Acta.*, **42**, 1379-1388.
  131. **Lalonde, G., R. Cote, G. Tamizhmani, D. Guay, J.P. Dodelet, L. Dignard-Baley, L.T. Weng, and P. Bertrand** (1995) Physical, chemical and electrochemical characterization of heat-treated tetracarboxylic cobalt phthalocyanine adsorbed on carbon black as electrocatalyst for oxygen reduction in polymer electrolyte fuel cells. *Electrochim. Acta.*, **40**, 2635-2646.
  132. **Lalonde, G., G. Faubert, R. Cote, D. Guay, J.P. Dodelet, L.T. Weng, and P. Bertrand** (1996) Catalytic activity and stability of heat-treated iron phthalocyanines for the electroreduction of oxygen in polymer electrolyte fuel cells. *J. Power Sources*, **61**, 227-237.
  133. **Le Rhun, V. and N. Alonso-Vante** (2000) Tailoring of nanodivided electrocatalyst materials based on transition metal. *J. New Mater. Electrochem. Syst.* **3**, 333-338.
  134. **Lee, K., A. Ishihara, S. Mitsushima, N. Kamiya, and K. Ota** (2004) Stability and electrocatalytic activity for oxygen reduction in WC+Ta catalyst. *Electrochim. Acta*, **49**, 3479-3485.
  135. **Lee, K., J. Zhang, H. Wang, and D.P. Wilkinson** (2006) Progress in the synthesis of carbon nanotube- and nanofiber-supported Pt electrocatalysts for PEM fuel cell catalysis. *J. Appl. Electrochem.*, **36**, 507-522.
  136. **Lee, K., O. Savadogo, A. Ishihara, S. Mitsushima, N. Kamiya, and K.-I. Ota** (2006) Methanol-tolerant oxygen reduction electrocatalysts based on Pd-3d transition metal alloys for direct methanol fuel cells. *J. Electrochem. Soc.* **153**, A20-A24.
  137. **Leela Mohana Reddy, A. and S. Ramaprabhu** (2007) Pt/SWNT-Pt/C nanocomposite electrocatalysts for proton-exchange membrane fuel cells. *J. Phys. Chem. C*, **111**, 16138-16146.



138. **Lefèvre, M., P. Bertrand, and J.P. Dodelet** (2000) O<sub>2</sub> reduction in PEM fuel cells: Activity and active site structural information for catalysts obtained by the pyrolysis at high temperature of Fe precursors. *J. Phys. Chem B* **104**, 11238-11247.
139. **Lefèvre, M., P. Bertrand, and J.P. Dodelet** (2002) Molecular oxygen reduction in PEM fuel cells: Evidence for the simultaneous presence of two active sites in Fe-based catalysts, *J. Phys. Chem. B* **106**, 8705-8713.
140. **Lefèvre, M., P. Bertrand, and J.P. Dodelet** (2003) Fe-based catalysts for the reduction of oxygen in polymer electrolyte membrane fuel cell conditions: determination of the amount of peroxide released during electroreduction and its influence on the stability of the catalysts. *Electrochim. Acta*, **48**, 2749-2760.
141. **Lefèvre, M., J.P. Dodelet, and P. Bertrand** (2005) Molecular oxygen reduction in PEM fuel cell conditions: ToF-SIMS analysis of Co-based electrocatalysts. *J. Phys. Chem. B* **109**, 16718-16724.
142. **Li, Y., J. Liu, Y. Wang, and Z.L. Wang** (2001) Preparation of monodispersed Fe-Mo nanoparticles as the catalyst for CVD synthesis of carbon nanotubes. *Chem. Mater.*, **13**, 1008-1014.
143. **Li, H., G. Sun, N. Li, S. Sun, D. Su, and Q. Xin** (2007) Design and preparation of highly active Pt-Pd/C catalyst for the oxygen reduction reaction. *J. Phys. Chem. C* **111**, 5605-5617
144. **Li, W., W. Zhou, H. Li, Z. Zhou, B. Zhou, G. Sun, and Q. Xin** (2004) Nano-structured Pt-Fe/C as cathode catalyst in direct methanol fuel cell, *Electrochim. Acta*, **49**, 1045-1055.
145. **Liang, C.C. and A.L. Juliard** (1965) The overpotential of oxygen reduction at platinum electrodes. *J. Electroanal. Chem.* **9**, 390-394.
146. **Lipkowski, J. and P. N. Ross** *Electrocatalysis*. Wiley-VCH, New York 1998.
147. **Lima, F.H.B., J. Zhang, M.H. Shao, K. Sasaki, M.B. Vukmirovic, E.A. Ticianelli, and R.R. Adzic** (2007) Catalytic activity-d-band center correlation for the O<sub>2</sub> reduction reaction on platinum in alkaline solutions. *J. Phys. Chem. C*, **111**, 404-410.
148. **Liu, Z., L.M. Gan, L. Hong, W. Chen, and J.Y. Lee** (2005) Carbon-supported Pt nanoparticles for proton exchange membrane fuel cells. *J. Power Sources*, **139**, 73-78.
149. **Liu, Y., A. Ishihara, S. Mitsushima, N. Kamiya, and K. Ota** (2005) Zirconium oxide for PEFC cathodes. *Electrochemical and Solid-State Lett.* **8**, A400-A402.

150. **Li, X., S. Ge, C.L. Hui, and I.-M. Hsing** (2004) Well-dispersed multiwalled carbon nanotubes supported platinum nanocatalysts for oxygen reduction. *Electrochemical and Solid-State Lett.*, **7**, A286-A289.
151. **Li, H., G. Sun, N. Li, S. Sun, D. Su, and Q. Xin** (2007) Design and preparation of highly active Pt-Pd/C catalyst for the oxygen reduction reaction. *J. Phys. Chem. C*, **111**, 5605-5617.
152. **Li, H., Q. Xin, W. Li, Z. Zhou, L. Jiang, S. Yang, and G. Sun** (2004) An improved palladium-based DMFCs cathode catalyst. *Chem. Commun.* 2776-2777.
153. **Li, W., W. Zhou, H. Li, Z. Zhou, B. Zhou, G. Suna, and Q. Xin** (2004) Nano-structured Pt-Fe/C as cathode catalyst in direct methanol fuel cell. *Electrochim. Acta*, **49**, 1045-1055.
154. **Liu, Z., L.M. Gan, L. Hong, W. Chen, and J.Y. Lee** (2005) Carbon-supported Pt nanoparticles as catalysts for proton exchange membrane fuel cells. *J. Power Sources*, **139**, 73-78.
155. **Liu, Z., M. Shamsuzzoha, E.T. Adab, W. Matthew Reichert, and D.E. Nikles** (2007) Synthesis and activation of Pt nanoparticles with controlled size for fuel cell electrocatalysts. *J. Power Sources*, **164**, 472-480.
156. **Liu, C., X. Wu, T. Klemmer, N. Shukla, X. Yang, D. Weller, A. G. Roy, M. Tanase, and D. Laughlin** (2004) Polyol process synthesis of monodispersed FePt nanoparticles. *J. Phys. Chem. B*, **108**, 6121-6123.
157. **Liu, G., H. Zhang, and J. Hu** (2007) Novel synthesis of a highly active carbon-supported Ru<sub>85</sub>Se<sub>15</sub> chalcogenide catalyst for the oxygen reduction reaction. *Electrochem. Commun.* **9**, 2643-2648.
158. **Liu, G., H. Zhang, M. Wang, H. Zhong, and J. Chen** (2007) Preparation, characterization of ZrO<sub>x</sub>N<sub>y</sub>/C and its application in PEMFC as an electrocatalyst for oxygen reduction. *J. Power Sources*, **172**, 503-510.
159. **Luczak, F.J. and D.A. Landsman** (1984) Ternary fuel cell catalysts containing platinum, cobalt and chromium. *US Patent 447 506*.
160. **Luczak, F.J. and D.A. Landsman** (1987) Ordered ternary fuel cell catalysts containing platinum and cobalt and method for making the catalysts. *US Patent 4 677 092*.
161. **Luo, J., N. Kariuki, L. Hana, L. Wang, C.-J. Zhong, and T. Heb** (2006) Preparation and characterization of carbon-supported PtVFe electrocatalysts. *Electrochim. Acta*, **51**, 4821-4827.
162. **Ma, H., X.-Z. Xue, J.-H. Liao, C.P. Liu, and W. Xing** (2006) Effect of borohydride as reducing agent on the structures and electrochemical properties of Pt/C catalyst. *App. Surf. Sci.*, **252**, 8593-8597.

163. **Maillard, F., M. Martin, F. Gloaguen, and J.-M. Léger** (2002) Oxygen electroreduction on carbon-supported platinum catalysts. Particle-size effect on the tolerance to methanol competition. *Electrochim. Acta*, **47**, 3431-3440.
164. **Maja, M., C. Orecchia, M. Strano, P. Tosco, and M. Vanni** (2000) Effect of structure of the electrical performance of gas diffusion electrodes for metal air batteries. *Electrochim. Acta*, **46**, 423-432.
165. **Makino, K., K. Furukawa, K. Okajima, and M. Sudoh** (2005) Optimization of the sputter-deposited platinum cathode for a direct methanol fuel cell. *Electrochim. Acta*, **51**, 961-965.
166. **Malakhov, I.V., S.G. Nikitenko, E.R. Savinova, D.I. Kochubey, and N. Alonso-Vante** (2002) In situ EXAFS study to probe active centers of Ru chalcogenide electrocatalysts during oxygen reduction reaction. *J. Phys. Chem. B*, **106**, 1670-1676.
167. **Malik, W.U. and B. Ramesh** (1973) Spectrophotometric determination of chromium(III) using potassium hexacyanoferrate(II). *Mikrochim. Acta*, **1**, 681-684.
168. **Manoharan, R. and J.B. Goodenough** (1995) Oxygen reduction on CrO<sub>2</sub> bonded to a proton-exchange membrane. *Electrochim. Acta*, **40**, 303-307.
169. **Marinkovic, N.S., J.X. Wang, H. Zajonz, and R.R. Adzic** (2001) Adsorption of bisulfate on the Ru(0001) single crystal electrode surface. *J. Electroanal. Chem.* **500**, 388-394.
170. **Markovic, N.M., H.A. Gasteiger, and P.N. Ross** (1995) Oxygen reduction on platinum low-index single-crystal surfaces in sulfuric acid: Rotating ring-Pt(hkl) disk studies. *J. Phys. Chem.*, **99**, 3411-3415.
171. **Markovic, N.M., H.A. Gasteiger, and P.N. Ross** (1997) Kinetics of oxygen reduction on Pt(hkl) electrodes: Implications for the crystallite size effect with supported Pt electrocatalysts. *J. Electrochem. Soc.*, **144**, 1591-1597.
172. **Martin, J., J. Hollamby, and Laura Hudson** (2006) Recent advances in nanoparticle synthesis with reversed micelles. *Adv. Colloid and Interface Science* **128-130**, 5-15.
173. **Martins Alves, M.C., J. P. Dodelet, D. Guay, M. Ladouceur, and G. Tourillon** (1992) Origin of the electrocatalytic properties for oxygen reduction of some heat-treated polyacrylonitrile and phthalocyanine cobalt compounds adsorbed on carbon black as probed by electrochemistry and X-ray absorption spectroscopy. *J. Phys. Chem.*, **96**, 10898-10905.
174. **Mathiyarasu, J. and K.L.N. Phani** (2007) Carbon-supported palladium-cobalt-noble metal (Au, Ag, Pt) nanocatalysts as methanol tolerant oxygen-reduction cathode materials in DMFCs. *J. Electrochem. Soc.*, **154**, B1100-B1105.

175. **Matsumoto, Y., H. Yoneyama, and H.J. Tamura** (1977) Influence of the nature of the conduction band of transition metal oxides on catalytic activity for oxygen reduction. *J. Electroanal. Chem.*, **83**, 237-243.
176. **Matsuki, K. and H. Kamada** (1986) Oxygen reduction electrocatalysis on some manganese oxides. *Electrochim. Acta*, **31**, 13-18.
177. **Mazza, F. and S. Trasatti** (1963) Tungsten, titanium, and tantalum carbides and titanium nitrides as electrodes in redox systems. *J. Electrochem. Soc.*, **110**, 847-849.
178. **Min, M., J. Cho, K. Cho, and H. Kim** (2000) Particle size and alloying effects of Pt-based alloy catalysts for fuel cell applications. *Electrochim. Acta*, **45**, 4211-4217.
179. **Mukerjee, S. and J. McBreen** (1999) Effect of particle size on the electrocatalysis by carbon-supported Pt electrocatalysts: an in situ XAS investigation. *J. Electroanal. Chem.*, **45**, 163-171.
180. **Mukerjee, S. and S. Srinivasan** (1993) Enhanced electrocatalysis of oxygen reduction on platinum alloys in proton exchange membrane fuel cells. *J. Electroanal. Chem.* **357**, 201-224.
181. **Mukerjee, S., S. Srinivasan, M.P. Soriaga, and J. McBreen** (1995a) Effect of preparation conditions of Pt alloys on their electronic, structural and electrocatalytic activities for oxygen reduction: XRD, XAS and electrochemical studies. *J. Phys. Chem.* **99**, 4577-4589.
182. **Mukerjee, S., S. Srinivasan, M.P. Soriaga, and J. McBreen** (1995b) Role of structural and electrolytic properties of Pt and Pt alloys on electrocatalysis of oxygen reduction: An in situ XANES and EXAFS investigation. *J. Electrochem. Soc.* **142**, 1409-1422.
183. **Murthi, V.S., R. Craig Urian, and S. Mukerjee** (2004) Oxygen reduction kinetics in low and medium temperature acid environment: correlation of water activation and surface properties in supported Pt and Pt alloy electrocatalysts. *J. Phys. Chem. B* **108**, 11011-11023.
184. **Nalini Subramanian, P., P. Swaminatha Kumaraguru, H. Colon-Mercado, H. Kim, N. Branko Popov, T. Black, and A.D. Chen** (2006) Studies on Co-based catalysts supported on modified carbon substrates for PEMFC cathodes. *J. Power Sources*, **157**, 56-63.
185. **Nath, A., N. Kopelev, S.D. Tyagi, V. Chechersky, and Y. Wei** (1993) A novel class of ferromagnetic materials. *Materials Lett.*, **16**, 39-44.
186. **Nisha Shukla, Erik. B. Svedberg, and J. Eii** (2006) Surfactant isomerization and dehydrogenation on FePt nanoparticles. *Colloids and Surfaces A: Physicochem. Eng. Aspects*, **301**, 113-116.

187. **Nissinen, T., T. Valo, M. Gasik, J. Rantanen, and M. Lampinen** (2002) Microwave synthesis of catalyst spinel  $\text{MnCo}_2\text{O}_4$  for alkaline fuel cell. *J. Power sources*, **106**, 109-115.
188. **Nørskov, J.K., J. Rossmeisl, A. Logadottir, L. Lindqvist, J.R. Kitchin, T. Bligaard, and H. Jonsson** (2004) Origin of the overpotential for oxygen reduction at a fuel-cell cathode. *J. Phys. Chem. B*, **108**, 17886-17892.
189. **Paffet, M.T., G.J. Beery, and S. Gottesfeld** (1988) Oxygen Reduction at  $\text{Pt}_{0.65}\text{Cr}_{0.35}$ ,  $\text{Pt}_{0.2}\text{Cr}_{0.8}$  and roughened platinum. *J. Electrochem. Soc.* **135**, 1431-1436.
190. **Panchenko, A., M.T.M. Koper, T.E. Shubina, S.J. Mitchell, and E. Roduner** (2004) Ab-initio calculations of intermediates of oxygen reduction on low-index platinum surfaces. *J. Electrochem. Soc.*, **151**, A2016-A2027.
191. **Patterson, A.L.**, (1939) The Scherrer formula for X-ray particle size determination. *Phy. Rev.* **56**, 978-982.
192. **Pauling, L.** (1964) Nature of the iron-oxygen bond in oxyhæmoglobin. *Nature*, **203**, 182-183.
193. **Paulus, U.A., T.J. Schmidt, H.A. Gasteiger, and R.J. Behm** (2001) Oxygen reduction on a high-surface area Pt/Vulcan carbon catalyst: a thin-film rotating ring-disk electrode study. *J. Electroanal. Chem.* **495**, 134-145.
194. **Paulus, U.A., A. Wokaun, G.G. Scherer, T.J. Schmidt, V. Stamenkovic, N.M. Markovic, and P.N. Ross** (2002a) Oxygen reduction on high surface area Pt-based alloy catalysts in comparison to well defined smooth bulk alloy electrodes. *Electrochim. Acta*, **47**, 3787-3798.
195. **Paulus, U.A., A. Wokaun, G.G. Scherer, T.J. Schmidt, V. Stamenkovic, V. Radmilovic, N.M. Markovic, and P.N. Ross** (2002b) Oxygen reduction on carbon-supported Pt-Ni and Pt-Co alloy catalysts. *J. Phys. Chem. B* **106**, 4181-4191.
196. **Perez, J., H.M. Villulas, and E.R. Gonzalez** (1997) Structure sensitivity of oxygen reduction on platinum single crystal electrodes in acid solutions. *J. Electroanal. Chem.*, **435**, 179-187.
197. **Peuckert, M., T. Yoneda, R.A. Dalla Betta, and M. Boudart** (1986) Oxygen reduction on small supported platinum particles. *J. Electrochem. Soc.*, **133**, 944-947.
198. **Pietron, J.J., R.M. Stroud, and D.R. Rolison** (2002) Using three dimensions in catalytic mesoporous nanoarchitectures. *Nano Lett.* **2**, 545-549.
199. **Prabhuram, J., X. Wang, C.L. Hui, and I.-M. Hsing** (2003) Synthesis and characterization of surfactant-stabilized Pt/C nanocatalysts for fuel cell applications. *J. Phys. Chem. B*, **107**, 1057-11064.

200. **Qi, Z. and P.G. Pickup** (1998) High performance conducting polymer supported oxygen reduction catalysts. *Chem. Commun.*, 2299-2300.
201. **Qian, Y., W. Wen, P.A. Adcock, Z. Jiang, N. Hakim, M.S. Saha, and S. Mukerjee** (2008) PtM/C catalyst prepared using reverse micelle method for oxygen reduction reaction in PEM fuel cells. *J. Phys. Chem. C* **112**, 1146-1157.
202. **Raghuveer, V., Keshav Kumar, and B. Viswanathan** (2002) Nanocrystalline lead ruthenium pyrochlore as oxygen reduction electrode. *Indian. J. Eng. Mater. Sci.* **9**, 137-140.
203. **Raghuveer, V., A. Manthiram, and A.J. Bard** (2005) Pd-Co-Mo electrocatalyst for the oxygen reduction reaction in proton exchange membrane fuel cells. *J. Phys. Chem. B* **109**, 22909-22912.
204. **Raghuveer, V., P.J. Ferreira, and A. Manthiram** (2006) Comparison of Pd-Co-Au electrocatalysts prepared by conventional borohydride and microemulsion methods for oxygen reduction in fuel cells. *Electrochem. Commun.* **8**, 807-814.
205. **Rajesh, B., K. Ravindranathan Thampi, J.-M. Bonard, N. Xanthopoulos, H.J. Mathieu, and B. Viswanathan** (2003) Carbon nanotubes generated from template carbonization of polyphenyl acetylene as the support for electrooxidation of methanol, *J. Phys. Chem. B*, **107**, 2701-2708.
206. **Rajesh, B., K. Ravindranathan Thampi, J.-M. Bonard, N. Xanthopoulos, H.J. Mathieu, and B. Viswanathan** (2004) Nanostructured conducting polyaniline tubules as catalyst support for Pt particles for possible fuel cell applications. *Electrochemical and Solid-State Lett.*, **7**, A404-A407.
207. **Ralph, T.R. and M.P. Hogarth** (2002) Catalysis for low temperature fuel cells. Part I: The cathode challenges. *Platinum Met. Rev.*, **46**, 3-14.
208. **Reeve, R. W., P.A. Christensen, A.J. Dickinson, A. Hamnett, S.A. Haydock, and S.C. Roy** (1998a) Methanol-tolerant oxygen reduction catalysts based on transition metal sulfides and their application to the study of methanol permeation. *Electrochim. Acta*, **45**, 4237-4250.
209. **Reeve, R. W., P.A. Christensen, A. Hamnett, S.A. Haydock, and S.C. Roy** (1998b) Methanol tolerant oxygen reduction catalysts based on transition metal sulfides. *J. Electrochem. Soc.* **145**, 3463-3471.
210. **Saha, M.S., R. Li, and X. Sun** (2008) High loading and monodispersed Pt nanoparticles on multiwalled carbon nanotubes for high performance proton exchange membrane fuel cells. *J. Power Sources*, **177**, 314-322.
211. **Salgado, J.R.C., E. Antolini, and E.R. Gonzalez** (2005a) Carbon supported Pt<sub>70</sub>Co<sub>30</sub> electrocatalyst prepared by the formic acid method for the oxygen reduction reaction in polymer electrolyte fuel cells. *J. Power Sources*, 141, 13-18.

212. **Salgado, J.R.C., E. Antolini, and E.R. Gonzalez** (2005b) Carbon supported Pt–Co alloys as methanol-resistant oxygen-reduction electrocatalysts for direct methanol fuel cells. *Appl. Catal. B: Environmental*, **57**, 283-290.
213. **Salvador-Pascual, J.J., S. Citalán-Cigarroa, and O. Solorza-Feria** (2007) Kinetics of oxygen reduction reaction on nanosized Pd electrocatalyst in acid media. *J. Power Sources*, **172**, 229-234.
214. **Santos, L.G.R.A., C.H.F. Oliveira, I.R. Moraes, and E.A. Ticianelli** (2006) Oxygen reduction reaction in acid medium on Pt–Ni/C prepared by a microemulsion method. *J. Electroanal. Chem.*, **596**, 141-148.
215. **Sattler, M.L. and P.N. Ross** (1986) The surface structure of Pt crystallites supported on carbon black. *Ultramicroscopy* **20**, 21-28.
216. **Savadogo, O., K. Lee, K. Oishi, S. Mitsushima, N. Kamiya, and K.-I. Ota** (2004) New palladium alloys catalyst for the oxygen reduction reaction in an acid medium. *Electrochem. Commun.*, **6**, 105-109.
217. **Sawaguchi, T., T. Itabashi, T. Matsue, and I. Uchida** (1990) Electrochemical reduction of oxygen by metalloporphyrin ion-complexes with heat treatment. *J. Electroanal. Chem.* **279**, 219-230.
218. **Scherson, D., S.L. Gupta, C. Fierro, E.B. Yeager, M.E. Kordesch, J. Eldridge, R.W. Hoffman, and J. Blue** (1983) Cobalt tetramethoxyphenyl porphyrin-emission Mossbauer spectroscopy and O<sub>2</sub> reduction electrochemical studies. *Electrochim. Acta*, **28**, 1205-1209.
219. **Scherson, D., A.A. Tanaka, S.L. Gupta, D. Tryk, C. Fierro, R. Holze, and E.B. Yeager** (1986) Transition metal macrocycles supported on high area carbon: Pyrolysis-mass spectrometry studies. *Electrochim. Acta*, **31**, 1247-1258.
220. **Schmidt, T.J., H.A. Gasteiger, G.D. Stab, P.M. Urban, D.M. Kolb, and R.J. Behm** (1998) Characterization of high-surface area electrocatalysts using a rotating disk electrode configuration. *J. Electrochem. Soc.*, **145**, 2354-2358.
221. **Schmidt, T.J., U.A. Paulaus, H.A. Gasteiger, N. Alonso-Vante, and R.J. Behm** (2000) Oxygen reduction on Ru<sub>1.92</sub>Mo<sub>0.08</sub>SeO<sub>4</sub>, Ru/Carbon, and Pt/Carbon in pure and methanol-containing electrolytes. *J. Electrochem. Soc.*, **147**, 2620-2624.
222. **Schmidt, T.J., U.A. Paulaus, H.A. Gasteiger, and R.J. Behm** (2001) The oxygen reduction reaction on a Pt/carbon fuel cell catalyst in the presence of chloride anions *J. Electroanal. Chem.* **508**, 41-47.
223. **Schubert, B., E. gocke, R. Schoellhorn, and H. Tributsch** (1996) *In situ* X-ray-electrochemical studies on the origin of H<sub>2</sub>O<sub>2</sub> production during oxygen reduction at transition metal cluster materials. *Electrochim. Acta*, **41**, 1471-1478.

224. **Schulenburg, H., S. Stankov, V. Schunemann, J. Radnik, I. Dorbandt, S. Fiechter, P. Bogdanoff, and H. Tributsch** (2003) Catalysts for the oxygen reduction from heat-treated iron(III) tetramethoxyphenylporphyrin chloride: Structure and stability of active sites. *J. Phys. Chem. B* **107**, 9034-9041.
225. **Scott, K., A.K. Shukla, C.L. Jackson, and W.R.A. Meuleman** (2004) A mixed-reactants solid-polymer-electrolyte direct methanol fuel cell. *J. Power Sources*, **126**, 67-75.
226. **Sepa, D.B., M.V. Vojnovic, and A. Damjanovic** (1981) Reaction intermediates as a controlling factor in the kinetics and mechanism of oxygen reduction at platinum electrodes. *Electrochim. Acta*, **26**, 781-793.
227. **Shao, M.H., K. Sasaki, and R.R. Adzic** (2006) Pd-Fe nanoparticles as electrocatalysts for oxygen reduction. *J. Am. Chem. Soc.* **128**, 3526-3527.
228. **Shao, M.H., P. Liu, J. Zhang, and R.R. Adzic** (2007) Origin of enhanced activity in palladium alloy electrocatalysts for oxygen reduction reaction. *J. Phys. Chem B* **111**, 6772-6775.
229. **Shevchenko, E.V., D.V. Talapin, H. Schnablegger, A. Kornowski, O. Festin, P. Svedlindh, M. Haase, and H. Weller** (2003) Study of nucleation and growth in the organometallic synthesis of magnetic alloy nanocrystals: the role of nucleation rate in size control of CoPt<sub>3</sub> nanocrystals. *J. Am. Chem. Soc.*, **125**, 9090-9101.
230. **Shukla, A.K., C.L. Jackson, K. Scott, and G. Murgia** (2002) A solid-polymer electrolyte direct methanol fuel cell with a mixed reactant and air anode. *J. Power Sources*, **111**, 43-51.
231. **Shukla, A.K., R.K. Raman, N.A. Choudhury, K.R. Priolkar, P.R. Sarode, S. Emura, and R. Kumashiro** (2004) Carbon-supported Pt-Fe alloy as a methanol-resistant oxygen-reduction catalyst for direct methanol fuel cells. *J. Electroanal. Chem.* **563**, 181-190.
232. **Sidik, R.A. and A.B. Anderson** (2002) Density functional theory study of O<sub>2</sub> electroreduction when bonded to a Pt dual site. *J. Electroanal. Chem.*, **528**, 69-76.
233. **Smith, T.D. and J.R. Pilbrow** (1981) Calculations of the electronic structures of organometallic compounds and homogeneous catalytic processes. Part I. main group organometallic compounds. *Coord. Chem. Rev.*, **39**, 295-383.
234. **Sode, A., W. Li, Y. Yang, P.C. Wong, E. Gyenge, K.A.R. Mitchell, and D. Bizzotto** (2006) Electrochemical formation of a Pt/Zn Alloy and its use as a catalyst for oxygen reduction reaction in fuel cells. *J. Phys. Chem. B* **110**, 8715-8722.
235. **Solorza-Feria, O., K. Ellmer, M. Gierstig, and N. Alonso-Vante** (1994) Novel low-temperature synthesis of semiconducting transition metal



- chalcogenide electrocatalyst for multielectron charge transfer: molecular oxygen reduction. *Electrochim. Acta*, **39**, 1647-1653.
236. **Solorza-Feria, O., S. Citalan-Cigarroa, R. Rivera-Noriega, and S.M. Fernandez-Valverde** (1999) Oxygen reduction in acid media at the amorphous Mo–Os–Se carbonyl cluster coated glassy carbon electrodes. *Electrochem. Commun.*, **1**, 585-589.
  237. **Solorza-Feria, O., S. Ramirez-Raya, R. Rivera-Noriega, E. Ordonez-Regil, and S.M. Fernandez-Valverde** (1997) Kinetic studies of molecular oxygen reduction on  $W_{0.013}Ru_{1.27}Se$  thin films chemically synthesized. *Thin Solid Films*, **311**, 164-170.
  238. **Song, S., Y. Wang, P. Tsiakaras, and P.K. Shen** (2008) Direct alcohol fuel cells: A novel non-platinum and alcohol inert ORR electrocatalyst, *Applied Catal. B: Environmental*, **78**, 381-387.
  239. **Steiger, B. and F.C. Anson** (1994) New electrocatalysts for the four-electron reduction of dioxygen based on (5,10,15-Tris(pentaammineruthenium(II)-4-cyanophenyl)-20-(1-methylpyridinium-4-yl)porphyrinato)cobalt(II) immobilized on graphite electrodes, *Inorg. Chem.* **33**, 5767-5779.
  240. **Steiger, B., C. Chi, and F.C. Anson** (1993) Electrocatalysis of the reduction of dioxygen by adsorbed cobalt 5,10,15,20-tetraarylporphyrins to which one, two, or three pentaammineruthenium(2+) centers are coordinated. *Inorg. Chem.*, **32**, 2107-2113.
  241. **Sun, S., C.B. Murray, D. Weller, L. Folks, and A. Moser** (2000) Monodisperse FePt nanoparticles and ferromagnetic FePt nanocrystal superlattices. *Science*, **287**, 1989-1991.
  242. **Sun, G.-Q., J.-T. Wang, S. Gupta, and R.F. Savinell** (2001) Iron(III) tetramethoxyphenylporphyrin (FeTMPP-C1) as electrocatalyst for oxygen reduction in direct methanol fuel. *J. Appl. Electrochem.*, **31**, 1025-1031.
  243. **Takasu, Y., N. Ohashi, X.G. Zhang, and Y. Murakami** (1996) Size effects of platinum particles on the electroreduction of oxygen. *Electrochim. Acta*, **41**, 2595-2600.
  244. **Taleb, A, C. Petit, and M.-P. Pileni** (1997) Synthesis of highly monodisperse silver nanoparticles from AOT reverse micelles: A way to 2D and 3D self-organization, *Chem. Mater.*, **9**, 950-959.
  245. **Tamizhmani, G. and G.A. Capuano** (1994) Improved electrocatalytic oxygen reduction performance of platinum ternary alloy-oxide in solid-polymer-electrolyte fuel cells. *J. Electrochem. Soc.*, **141**, 968-975.
  246. **Tamizhmani, G., J.P. Dodelet, and D. Guay** (1996) Crystallite size effects of carbon-supported platinum on oxygen reduction in liquid acids. *J. Electrochem. Soc.*, **143**, 18-23.

247. **Tanaka, A.A., C. Fierro, D.A. Scherson, and E.B. Yeager** (1989) Oxygen reduction on adsorbed iron tetrapyrrolineporphyrine. *Mater. Chem. Phys.*, **22**, 431-456.
248. **Tatsumi, K. and R. Hoffman** (1981) Metalloporphyrins with unusual geometries. 1. Mono-, di-, triatom-bridged porphyrin dimers. *J. Am. Chem. Soc.*, **103**, 3328-3341.
249. **Taube, H.** (1965) Mechanisms of oxidation with oxygen. *J. Gen. Physiol.*, **49**, 29-50.
250. **Teliska, M., V.S. Murthi, S. Mukerjee, and D.E. Ramaker** (2005) Correlation of water activation, surface properties, and oxygen reduction reactivity of supported Pt-M/C bimetallic electrocatalysts using XAS. *J. Electrochem. Soc.*, **152**, A2159-A2169.
251. **Toda, T., H. Igarashi, H. Uchida, and M. Watanabe** (1999) Enhancement of the electroreduction of oxygen on Pt alloys with Fe, Ni, and Co. *J. Electrochem. Soc.* **146**, 3750-3756.
252. **Toda, T., H. Igarashi, and M. Watanabe** (1998) Role of electronic property of Pt and Pt alloys on electrocatalytic reduction of oxygen. *J. Electrochem. Soc.* **145**, 4185-4188.
253. **Tominaka, S., T. Momma, and T. Osaka** (2008) Electrodeposited Pd-Co catalyst for direct methanol fuel cell electrodes: Preparation and characterization. *Electrochim. Acta*, **53**, 4679-4686.
254. **Trapp, V., P.A. Christensen, and A. Hamnett** (1996) New catalysts for oxygen reduction based on transition-metal sulfides. *J. Chem. Soc. Faraday Trans.*, **92**, 4311-4319.
255. **Trasatti, S.** (1971) Work function, electronegativity, and electrochemical behaviour of metals: II. Potentials of zero charge and "electrochemical" work functions *J. Electroanal. Chem.*, **33**, 351-378.
256. **Trasatti, S.** (1980) *Electrodes of conductive metallic oxides part A, B*; Elsevier Scientific Publishing Co., Amsterdam, 1980.
257. **Tributsch, H., M. Bron, M. Hilgendorff, H. Schulenburg, I. Dorbandt, V. Eyert, P. Bogdanoff, and S. Fiechter** (2001). Methanol-resistant cathodic oxygen reduction catalysts for methanol fuel cell. *J. Appl. Electrochem.* **31**, 739-748.
258. **Tse, Y., P. Janda, H. Lam, J. Zhang, W.J. Pietro, and A.B.P. Lever** (1997) Monomeric and polymeric tetra-aminophthalocyanatocobalt(II) modified electrodes: electrocatalytic reduction of oxygen. *J. Porph. Phthal.*, **3**, 16-21.
259. **Ulstrup, J.** (1977) Catalysis of the electrochemical reduction of molecular dioxygen by metal phthalocyanines. *J. Electroanal. Chem.*, **79**, 191-197.

260. **Vago, E.R. and E.J. Calvo** (1995) Oxygen electro-reduction on iron oxide electrodes: III. Heterogeneous catalytic H<sub>2</sub>O<sub>2</sub> decomposition. *J. Electroanal. Chem.*, **388**, 161-165.
261. **Valentine, J.S.** (1973) Dioxygen ligand in mononuclear Group VIII transition metal complexes. *Chem. Rev.*, **73**, 235-245.
262. **van Bokhoven, J.A. and J.T. Miller** (2007) d-electron density and reactivity of the d band as a function of particle size in supported gold catalysts. *J. Phys. Chem. C*, **111**, 9245-9249.
263. **Van Der Putten, A., A. Elzing, W. Visscher E. Barendrecht, and R.D. Harcourt** (1988) Increased valence theory and the four electron reduction of O<sub>2</sub> to H<sub>2</sub>O. *J. Mol. Struct. (Theochem)* **180**, 309-318.
264. **van Veen, J.A.R., J.F. van Baar, and K.J. Kroese** (1981) Effect of heat treatment on the performance of carbon-supported transition-metal chelates in the electrochemical reduction of oxygen. *J. Chem. Soc. Faraday. Trans. I*, **77**, 2827-2843.
265. **van Wingerden, B., J.A.R. van Veen, and C.T.J. Mensch** (1988) An extended X-ray absorption fine structure study of heat-treated cobalt porphyrin catalysts supported on active carbon. *J. Chem. Soc. Faraday. Trans. I*, **84**, 65-74.
266. **Vaska, L.** (1976) Dioxygen-metal complexes: toward a unified view. *Acc. Chem. Res.*, **9**, 175-183.
267. **Vasudevan, P., N. Santosh, N. Mann, and S. Tyagi** (1990) Transition metal complexes of porphyrins and phthalocyanines as electrocatalysts for dioxygen reduction. *Transition Met. Chem.*, **15**, 81-90.
268. **Vielstitch, W.** *Fuel Cells*, Wiley/Interscience, London, 1965.
269. **Viswanathan, B. and M. Aulice Scibioh** *Fuel cells - Principles and Applications*. Universities Press (India) Private Limited, 2006.
270. **Viswanathan, B., V. Chidambaram and S. Chandravathanam** (2004) On the nature of noble metal electrodes prepared using formaldehyde as reducing agent. *Indian Journal of Chemistry Section A*, **43A**, 706-709.
271. **Vogel, A.I.** *A Text Book of Quantitative Inorganic Analysis*. ELBS and Longman, London, 1985.
272. **Vogel, W.M. and J.M. Baris** (1977) The reduction of oxygen on platinum black in acid electrolytes. *Electrochim. Acta*, **22**, 1259-1263.
273. **Vogel, W., P. Kaghazchi, T. Jacob, and N. Alonso-Vante** (2007) Genesis of Ru<sub>x</sub>Se<sub>y</sub> nanoparticles by pyrolysis of Ru<sub>4</sub>Se<sub>2</sub>(CO)<sub>11</sub>: A combined X-ray in situ and DFT study. *J. Phys. Chem. C* **111**, 3908-3913.

274. **Voinov, M., D. Buehler, and H. Tannenberger** (1971) Oxygen reduction on tungsten carbide. *J. Electrochem. Soc.* **118**, 1137-1138.
275. **Vračar, Lj.M., N.V. Krstajić, V.R. Radmilović, and M.M. Jakšić** (2006) Electrocatalysis by nanoparticles - oxygen reduction on Ebonex/Pt electrode, *J. Electroanal. Chem.*, **587**, 99-107.
276. **Vračar, Lj.M., D.B. Sepa, and A. Damjanovic** (1987) Pd electrode in oxygen saturated solutions: rest potentials in solutions of different pH. *J. Electrochem. Soc.* **134**, 1695-1697.
277. **Vračar, Lj.M. D.B. Sepa, and A. Damjanovic** (1989) Pd electrode in oxygen saturated aqueous solutions: potential dependent adsorption of oxygen containing species and their effect on oxygen reduction. *J. Electrochem. Soc.* **136**, 1973-1977.
278. **Wang, Y.X. and P.B. Balbuena** (2005) Design of oxygen reduction bimetallic catalysts: ab-initio-derived thermodynamic guidelines. *J. Phys. Chem. B* **109**, 18902-18906.
279. **Wang, C., H. Daimon, Y. Lee, J. Kim, and S. Sun** (2007) Synthesis of monodisperse Pt nanocubes and their enhanced catalysis for oxygen reduction. *J. Am. Chem. Soc.*, **129**, 6974-6975.
280. **Wang, H., R. Cote, G. Faubert, D. Guay, and J.P. Dodelet** (1999) Effect of the pre-treatment of carbon black supports on the activity of Fe-based electrocatalysts for the reduction of oxygen. *J. Phys. Chem. B* **103**, 2042-49.
281. **Wang, R., S. Liao, Z. Fu, and S. Ji** (2008) Platinum free ternary electrocatalysts prepared via organic colloidal method for oxygen reduction. *Electrochem. Commun.*, **10**, 503-506.
282. **Wang, W., D. Zheng, C. Du, Z. Zou, X. Zhang, B. Xia, H. Yang and D.L. Akins** (2007) Carbon-supported Pd-Co bimetallic nanoparticles as electrocatalysts for the oxygen reduction reaction. *J. Power Sources*, **167**, 243-249.
283. **Watanabe, M., K. Tsurumi, T. Mizukami, T. Nakamura, and P. Stonehart** (1994) Activity and stability of ordered and disordered Co-Pt alloys for phosphoric acid fuel cells. *J. Electrochem. Soc.* **141**, 2659-2668.
284. **Wei, Z.D., S.H. Chan, L.L. Li, H.F. Cai, Z.T. Xia, and C.X. Sun** (2005) Electrodepositing Pt on a Nafion-bonded carbon electrode as a catalyzed electrode for oxygen reduction reaction. *Electrochim. Acta*, **50**, 2279-2287.
285. **Widelov, A. and R.Larson** (1992) ESCA and electrochemical studies on pyrolysed iron and cobalt tetraphenylporphyrins. *Electrochim. Acta*, **37**, 187-197.

286. **Will, F.G. and C.A. Knorr** (1960a) Investigation of adsorption phenomena on rhodium, iridium, palladium, and gold with the potentiostatic triangle method. *Z. Electrochem.* **64**, 220-275.
287. **Will, F.G. and C.A. Knorr** (1960b) Investigation of formation and removal of hydrogen and oxygen coverage on platinum by a new, nonstationary method. *Z. Electrochem.* **64**, 258-269.
288. **Wroblowa, H.S., Y.C. Pan, and G. Razumney** (1976) Electroreduction of oxygen a new mechanistic criterion. *J. Electroanal. Chem.*, **69**, 195-201.
289. **Xiong, L., A.M. Kannan, and A. Manthiram** (2002) Pt–M (M = Fe, Co, Ni and Cu) electrocatalysts synthesized by an aqueous route for proton exchange membrane fuel cells. *Electrochem. Commun.* **4**, 898-903.
290. **Xiong, L. and A. Manthiram** (2005a) Nanostructured Pt–M/C (M = Fe and Co) catalysts prepared by a microemulsion method for oxygen reduction in proton exchange membrane fuel cells. *Electrochim. Acta*, **50**, 2323-2329.
291. **Xiong, L. and A. Manthiram** (2005b) Effect of atomic ordering on the catalytic activity of carbon supported PtM (M = Fe, Co, Ni, and Cu) alloys for oxygen reduction in PEMFCs. *J. Electrochem. Soc.* **152**, A697-A703.
292. **Xu, Y., W.A. Shelton, and W.F. Schneider** (2006) Effect of particle size on the oxidizability of platinum clusters. *J. Phys. Chem. A*, **110**, 5839-5846.
293. **Yang, H., N. Alonso-Vante, C. Lamy, and D.L. Akins** (2005) High methanol tolerance of carbon-supported Pt-Cr alloy nanoparticle electrocatalysts for oxygen reduction, *J. Electrochem. Soc.* **152**, A704-A709.
294. **Yang, H., N. Alonso-Vante, J.-M. Lèger, and C. Lamy** (2004) Tailoring, structure, and activity of carbon-supported nanosized Pt-Cr alloy electrocatalysts for oxygen reduction in pure and methanol-containing electrolytes. *J. Phys. Chem. B* **108**, 1938-1947.
295. **Yang, H., C. Coutanceau, J.-M. Lèger, N. Alonso-Vante, and C. Lamy** (2005) Methanol tolerant oxygen reduction on carbon-supported Pt–Ni alloy nanoparticles. *J. Electroanal. Chem.*, **576**, 305-313.
296. **Yang, H., W. Vogel, C. Lamy, and N. Alonso-Vante** (2004) Structure and electrocatalytic activity of carbon-supported Pt-Ni alloy nanoparticles toward the oxygen reduction reaction. *J. Phys. Chem. B*, **108**, 11024-11034.
297. **Yang, J. and J. Xu** (2003) Nanoporous amorphous manganese oxide as electrocatalyst for oxygen reduction in alkaline solutions. *Electrochem. Commun.* **5**, 306-311.
298. **Yeager, E.** (1981) Recent advances in the science of electrocatalysis. *J. Electrochem. Soc.* **128**, 160C-171C.

299. **Zagal, J.** (1992) Metallophthalocyanines as catalysts in electrochemical reactions. *Coord. Chem. Rev.* **119**, 89-136.
300. **Zagal, J., P. Bindra, and E. Yeager** (1980) A mechanistic study of oxygen reduction on water soluble phthalocyanines adsorbed on graphite electrodes. *J. Electrochem. Soc.* **127**, 1506-1517.
301. **Zagal, J., M. Paez, A.A. Tanaka, J.R. dos Santos, and C.A. Linkous** (1992) Electrocatalytic activity of metal phthalocyanines for oxygen reduction. *J. Electroanal. Chem.* **339**, 13-30.
302. **Zaikovskii, V.I., K.S. Nagabhushana, V.V. Kriventsov, K.N. Loponov, S.V. Cherepanova, R.I. Kvon, H. Bönemann, D.I. Kochubey, and E.R. Savinova** (2006) Synthesis and structural characterization of Se-modified carbon-supported Ru nanoparticles for the oxygen reduction reaction. *J. Phys. Chem. B* **110**, 6881-6890.
303. **Zeliger., H.** (1967) Fuel cell performance as a function of catalyst surface area. *J. Electrochem. Soc.*, **114**, 144-145.
304. **Zhang, L., K. Lee, and J. Zhang** (2007a) The effect of heat-treatment on nanoparticle size and ORR activity for carbon-supported Pd-Co alloy electrocatalysts. *Electrochim. Acta*, **52**, 3088-3094.
305. **Zhang, L., K. Lee, and J. Zhang** (2007b) Effect of synthetic reducing agents on morphology and ORR activity of carbon-supported nano-Pd-Co alloy electrocatalysts. *Electrochim Acta*, **52**, 7964-7971.
306. **Zhang, J., X. Wang, C. Wu, H. Wang, B. Yi, and H. Zhang** (2004) Preparation and characterization of Pt/C catalysts for PEMFC cathode: effect of different reduction methods. *React. Kinet. Catal. Lett.*, **83**, 229-236.
307. **Zheng, J., M. Wang, X. Zhang, Y. Wu, P. Li, X. Zhou, and W. Yuan** (2008) Platinum/carbon nanofiber nanocomposite synthesized by electrophoretic deposition as electrocatalyst for oxygen reduction. *J. Power Sources*, **175**, 211-216.
308. **Zhong, H., H. Zhang, Y. Liang, J. Zhang, M. Wang, and X. Wang** (2007) A novel non-noble electrocatalyst for oxygen reduction in proton exchange membrane fuel cells. *J. Power Sources*, **164**, 572-577.
309. **Zhong, H., H. Zhang, G. Liu, Y. Liang, J. Hu, and B. Yi** (2006) A novel non-noble electrocatalyst for PEM fuel cell based on molybdenum nitride. *Electrochem. Commun.*, **8**, 707-712.
310. **Zhou, D.B. and H. Vander Poorten** (1995) Electrochemical characterization of oxygen reduction on Teflon-bonded gad diffusion electrodes. *Electrochim. Acta*, **40**, 1819-1826.

## LIST OF PUBLICATIONS BASED ON RESEARCH WORK

### I REFEREED JOURNALS

1. **Ch. Venkateswara Rao** and **B. Viswanathan** (2004) Oxygen reduction by  $\text{FeN}_4$  – A DFT study. *Indian Journal of Chemistry Section A: Inorganic, Physical, Theoretical and Analytical Chemistry*, **43A**, 2333-2335.
2. **B. Viswanathan, Ch. Venkateswara Rao** and **U.V. Varadaraju** (2006) On the search for non-noble metal based electrodes for oxygen reduction reaction. *Photo/Electrochemistry & Photobiology in the Environment, Energy and Fuel*, **5**, 43-101.
3. **Ch. Venkateswara Rao** and **B. Viswanathan** (2007)  $\text{Ru}_x\text{Se}_y/\text{C}$  electrodes for oxygen reduction – A reverse microemulsion method of fabrication of electrode material, *Journal of Physical Chemistry C*, **111**, 16538-16543.

### II NATIONAL/INTERNATIONAL CONFERENCE

1. **Ch. Venkateswara Rao** and **B. Viswanathan** (2004) ‘Oxygen reduction by  $\text{FeN}_4$  – as seen by Density Functional Approach, *National workshop on the Advances in Catalysis*, January 6 - 7<sup>th</sup> 2004, Loyola college, Chennai, India.
2. **Ch. Venkateswara Rao, B. Viswanathan** and **U.V. Varadaraju** (2006) Nanoparticle Pt loaded carbon materials as cathodes for possible fuel cell applications, *Indo-Australian Symposium on Nanoscience and Nanotechnology*, March 31<sup>st</sup> - April 1<sup>st</sup> 2006, Indian Institute of Science, Bangalore, India.
3. **Ch. Venkateswara Rao, B. Viswanathan** and **U.V. Varadaraju** (2006) The ORR activity of polyol reduced platinum on carbon electrodes – Role of crystal planes on activity, *Taiwan-India Conference on Nanomaterials*, Dec 11-12<sup>th</sup> 2006, Lunghwa University of Science and Technology, Taouyen, Taiwan. (Received best poster award)
4. **B. Viswanathan** and **Ch. Venkateswara Rao** (2006) Metallic nanomaterials decorated on carbon nanotubes as electrodes for Fuel cell applications, *Indo-Japan workshop on Nanomaterials*, Dec 4-5<sup>th</sup> 2006, Indian Institute of Chemical Technology, Hyderabad, India.
5. **Ch. Venkateswara Rao, B. Viswanathan** and **U.V. Varadaraju** (2007)  $\text{MN}_4\text{C}_x$  clusters – are they potential oxygen reduction electrode materials?, *18<sup>th</sup> National Symposium on Catalysis*, April 16-18<sup>th</sup> 2007, Indian Institute of Petroleum, Dehradun, India.

# CURRICULUM VITAE

1. NAME : CH. VENKATESWARA RAO
2. ADDRESS : Research Scholar  
National Centre for Catalysis Research  
Department of Chemistry  
Indian Institute of Technology Madras  
*E-mail:* [venkatpmr2000@yahoo.com](mailto:venkatpmr2000@yahoo.com)
2. DATE OF BIRTH : 03-03-1978
3. EDUCATIONAL QUALIFICATIONS
- 1995-1998 Bachelor of Science (B.Sc)
- Institution : A.G & S.G. College, Vuyyuru
- 1998-2000 Master of Science (M.Sc. Chemistry)
- Institution : Andhra University, Visakhapatnam
- Doctor of Philosophy (Ph.D)
- Institution : Indian Institute of Technology Madras
- Registration Date : 29-07-2002



## DOCTORAL COMMITTEE

**CHAIR PERSON** : **Prof. R. Dhamodharan**  
Head, Department of Chemistry  
Indian Institute of Technology Madras

**GUIDE** : **Prof. B. Viswanathan**  
Department of Chemistry  
Indian Institute of Technology Madras

**CO-GUIDE** : **Prof. U.V.Varadaraju**  
Department of Chemistry  
Indian Institute of Technology Madras

**MEMBERS** : **Prof. T. K. Varadarajan**  
Department of Chemistry  
Indian Institute of Technology Madras

**Prof. M.V.S. Sangaranarayanan**  
Department of Chemistry  
Indian Institute of Technology Madras

**Prof. A. Subrahmanyam**  
Department of Physics  
Indian Institute of Technology Madras

**Prof. S.K. Seshadri**  
Department of Metallurgical and Materials Engineering  
Indian Institute of Technology Madras